Synthesis of Functional Water-Soluble Polymers

by

Muxiu Li

A thesis submitted in partial fulfilment of the requirements for the degree of

Doctor of Philosophy in Chemistry

Department of Chemistry

University of Warwick

THE UNIVERSITY OF WARWICK

September 2013

“路漫漫其修远兮，吾将上下而求索”

屈原

“非淡泊无以明志，非宁静无以致远”

诸葛亮

Table of Contents

List of Figures

Acknowledgements

I would like to thank my supervisor, Professor Haddleton, first for giving me the opportunity to work in Haddleton group from my master project and continuing my PhD, and also for all his help and advice throughout my studies. Secondly, I would like to thank my industrial supervisor, Ezat Khoshdel, for supporting all the work has done in Unilever, and I can still remember the great tour in Port Sunlight.

My thanks go to Dr Eleni Bitziou, Dr Julien Rosselgong and Rajan Randev whom I started working with and helped me a lot during my master project. Dr Julien Rosselgong and Dr Florence Gayet who have been a great help to me on the chemistry in the early stages of my PhD. I still remember the first initiator and column chromatography I have made. Great appreciation also goes to Dr Nicole Jagielski, and we had a great time in Bristol, Bath, Cardiff, and London. Thank you for visiting me back in Coventry after you left for work in Zurich, and also other post-docs: Remzi, Paul, and Ronan, thank you for helping me and giving me various advices.

It has been great opportunity and experience for becoming a member of Haddleton group. Although I am a quiet person and do not talk too much in group, there are still so many fantastic memories I won't forget in my whole life. Thank you for Stacy and Mat, I have enjoyed my first camping nights with both of you, Qiang, Kay, Jamie, and James. It is very difficult to thank everyone has come and gone from the group over the past three years. My thanks go to these ex-group members: Ant, George, Guangzhao, Jasmin, Yanzi, and Claudia; and also people now in the group: Athina, Chris Summers, Chris Waldron, Alex, Vasiliki, Zaidong, and Jenny.

I also want to thank my friends outside the group, all the people in Chinese Society from Chemistry Department. I can't remember how many Chinese Festivals we have spent together. There were many more people who made my life in UK memorable,

and I really appreciated that your guys have come and gone in my life: Ofelia, Jeong-Hee, Kaihui, Yibo, Rehab, Jin, Kasra, and Tim.

Finally, I want to thank my mum and my whole family who support my study in UK for so many years. Without your love and motivation throughout the years this would not have been done. I also want to say a special thank you to Yunhua for your love, patience, and support throughout my PhD!

Declaration

Experimental work contained in this thesis is original research carried out by the author, unless otherwise stated, in the Department of Chemistry at the University of Warwick, between October 2010 and September 2013. No material contained herein has been submitted for any other degree, or at any other institution.

Results from other authors are referenced in the usual manner throughout the text.

Signature: Date:

Muxiu Li

Abbreviations

AIBN – 2,2’-azobis(2-cyaopropane)

APA – 3-azidopropylacrylate

ATRP – atom transfer radical polymerisation

BFEC – benzyl ferrocenecarbodithioxylate

BzMA – benzyl methacrylate

CD – β-cyclodextrin

CE – capillary electrophoresis

CPDN – 2-cyanoprop-2-yl α-dithionaphthalate

CRP – controlled/living radical polymerisation

CuAAC – Cu(I)-catalysed alkyne-azide cycloaddition

CuPc – copper phthalocyanine

DBU – 1,8-diazabicyclo[4.3.0]non-5-ene

DCC – 1,3-dicyclohexylcarbodiimide

DCM – dichloromethane

DEAEMA – 2-(diethylamino)ethyl methacrylate

DEGEEA – di(ethylene glycol) ethyl ether acrylate

DIAD – diisopropyl azodicarboxylate

DiPAEMA – 2-(di-isopropylamino)ethyl methacrylate

DIPEA – diisopropylethylamine

DMAE(M)A – *N*,*N*-dimethlaminoethyl (methy)acrylate

DMAP – 4-dimethylaminopyridine

DMF – *N,N'*-dimethylforamide

DMSO – dimethylsulfoxide

DP – degree of polymerisation

DSC – differential scanning calorimetry

EBiB – ethyl 2-bromoisobutyrate

EDC – 1-ethyl-3-[3-(dimethylamino)propyl]carbodiimide

EE(M)A – 1-ethoxyethyl (meth)acrylate

EO – ethylene oxide

ESI-MS – electrospray ionization-mass spectrometry

fcGE – ferrocenyl glycidyl ether

FEB – (ferrocen-1-yl)ethyl benzodithioate

FRP – free radical polymerisation

GPC – gel permeation chromatography

GTP – group transfer polymerisation

HeLa – human cervical cancer cell line

HEMA – 2-hydroxyethyl methacrylate

HMDS – hexamethyldisilazane

HMTETA – 1,1,4,7,10,10-hexamethyltriethylenetetramine

HPLC – high performance liquid chromatography

IR – infrared

LCST – lower critical solution temperature

MALDI-ToF – matrix assisted laser desorption/ionisation-time of flight

MEMA – 2-(*N*-morpholino)ethyl methacrylate

Me_6-TREN – tris[2-(dimethylamino)ethyl]amine

MLCT – metal to ligand charge-transfer

M_n – number average molecular weight

MWCO – molecular weight cut-off

NMP – nitroxide-mediated polymerisation/ *N*-methyl-2-pyrrolidone

NMR – nuclear magnetic resonance

NIPAAm – *N*-isopropylacrylamide

NLO – nonlinear optical

O(pGal) – protected galactose oligomer

PAA – poly(acrylic acid)

PAMAM – poly(amidoamines)

Pc – phthalocyanine

PDA – photo diode array

PDI (Đ) – dipersity index

PDT – photodynamic therapy

PEG – poly(ethylene glycol)

PEO – poly(ethylene oxide)

P(Gal) – poly(galactose)

PMAA – poly(methacrylic acid)

PMDETA – *N,N,N',N'',N''*-pentamethyldiethylenetriamine

$PMEO_2MA$ – di(ethylene glycol)methyl ether methacrylate

$PMEO_3MA$ – tri(ethylene glycol)methyl ether methacrylate

PMEDSAH – poly{[2-(methacryloyloxy)ehthyl]dimethyl(3-sulfopropyl)ammonium hydroxide}

PMETAI – poly{[2-(methacryloyloxy)ethyl] trimethylammonium iodide}

PNPMA – *p*-nitrophenyl methacrylate

POEGMA - poly(oligo(ethylene glycol) methacrylates)

P(pGal) – protected poly(galactose)

P*t*BuA – poly(*tert*-butyl acrylate)

PVFc – poly(vinylferrocene)

PVP – poly(vinylpyrrolidone)

PYP – 4-pyrrolidinopyridine

RAFT – reversible addition-fragmentation chain transfer polymerisation

RI – refractive index

ROMP – ring-opening metathesis polymerisation

ROP – ring-opening polymerisation

RP-HPLC – reversible-phase high-performance liquid chromatography

SET-LRP – single electron transfer living radical polymerisation

SiPc – silicon phthalocyanine

SPR – surface plasmon resonance

SWNT – single-wall carbon nanotubes

TBAB – tetrabutylammonium bromide

TBAF – tetrabutylammonium fluoride

TBTA – tris((1-benzyl-1*H*-1,2,3-triazol-4-yl)methyl)amine

TEA – triethyl amine

TEMPO – 2,2,6,6-tetramethylpiperidynyl-*N*-oxyl

*t*Bu(M)A – *tert*-butyl (meth)acrylate

TFA – trifluoroacetic acid

THF – tetrahydrofuran

THPMA – 2-tetrahydropyranyl methacrylate

TMSMA – trimethylsilyl methacrylate

UCST – upper critical solution temperature

UV-Vis – ultraviolet-visible

ZnPc – zinc phthalocyanine

Abstract

The objective of this work was to synthesise water-soluble polymers bearing desirable functionality, particularly to improve water-solubility of phthalocyanines by incorporation of hydrophilic polymers for personal oral care applications.

Prior to preparation of water-soluble polymers containing phthalocyanine, the second chapter described the synthesis of ferrocenyl initiator for polymerisation of *tert*-butyl acrylate by SET-LRP, followed by acidolysis of *tert*-butyl group yielding poly(acrylic acid) containing ferrocenyl end group. The resulting polymer could be used as the scale inhibitor for a potential oil drilling application, and further detected by cyclic voltammetry due to the presence of the ferrocene end group.

The majority of the thesis is focussed on an investigation of novel approaches for covalently attachment of water-soluble polymers to (copper or zinc) phthalocyanines. The initial PEGylated *CuPc* complexes were obtained via DCC/EDC coupling reactions, and the resulting blue powder showed excellent solubility in water; however, it revealed a broad molecular weight distribution due to the presence of mono-, di-, and tri- substitutions of PEG chains as confirmed by GPC analysis.

PEGylation of phthalocyanines were further improved via a combination of Mitsunobu reaction and CuAAC "click" reaction. In this approach, the substituted macrocycles were prepared from 4,5-bis-(4-hydroxyphenoxy)phthalonitrile as a precursor. The final PEGylated *CuPcs* or metal-free *Pcs* with different PEG chain lengths were prepared by two different routes. The incorporation of the *(Cu)Pc* core with the polymer chain was confirmed and distinguished by THF-GPC equipped with a PDA detector, and also showed an increase in hydrodynamic volume with increasing the PEG chain length with a narrow dispersity remained.

PDMAEMA, as a dual responsive polymer was also introduced to *ZnPc* using a core-first approach by a combination of ATRP and CuAAC reaction with sharing the same CuBr/PMDETA catalyst, yielding the star-shaped water-soluble polymer. The polymer solution represented tuneable LCSTs in range between 83 and 33 ^{o}C with increasing the pH of the buffer solution from 7 to 10. The polymer was further transformed into highly polyelectrolyte stars with *ZnPc* core by quaternization of the

pendant amino groups with either methyl iodide or 1,3-propanesultone. The resulting zwitterionic star after quaternized with propanesultone, *ZnPc*-PMEDSAH, exhibited a UCST value 17 ^{o}C, compared with the quaternized salt, *ZnPc*-PMETAI with no obvious phase transition observed. In addition, their optical properties and aggregation behaviour in water were investigated by UV-Vis spectroscopy.

The final study involved the synthesis of water-soluble zinc phthalocyanines conjugated to poly(galactose) by an arm-first approach. The well-defined protected galactose oligomer arm was synthesised by SET-LRP with a desirable ω-chain end as confirmed by MALDI-ToF MS analysis which were ready for post-functionalisation. Following a click reaction and deprotection of the acetal groups, the isolated green powder achieved good water-solubility and emitted a sharp fluorescent band at approximate 695 nm via excitation at 610 nm in DMF. The GPC analysis also showed that a narrow molecular weight distribution remained after deprotection and confirmed the presence of *ZnPc* core by the PDA detector.

Chapter 1 Introduction

1.1 Polymerisation techniques: a brief overview

1.1.1 Free radical polymerisation

Free radical polymerisation is a type of chain-growth polymerisation, which is one of the most common methods for obtaining a wide variety of polymers and material composites. Free radicals are independently-existing species, usually generated by homolytic dissociation of an initiator. Therefore, an active centre is introduced to attack one monomer, and the electron migrates to another part of the molecule, followed by the addition of another monomer to that centre by a chain-type kinetic mechanism[1] and the process is repeated. The active centre is ultimately destructed or transferred by termination or chain transfer reactions stopping the chain growth. At least four types of distinct reactions describe the whole polymerisation process, including *initiation*, *propagation*, *termination*, and *chain transfer*.

The initiation step involves creation of the free radical active centre, and addition of one of these free radicals to the less substituted end of carbon-carbon double bond of the monomer would be expected to be predominated, **Figure 1.1.1**. The radicals have very short lifetimes and transfer their activity to monomers efficiently. Peroxides (e.g. benzoyl peroxide) or azo compounds (e.g. 2,2'-azobis(2-cyaopropane), AIBN) are commonly used as initiators, **Figure 1.1.2**, which undergo thermolysis in the convenient temperature range of 50-100 ^{o}C.

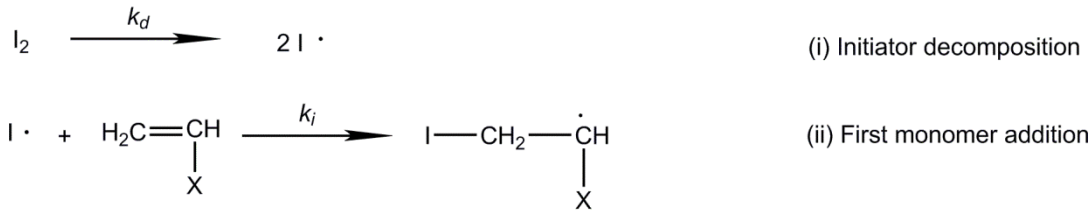

Figure 1.1.1 Initiation step of free radical polymerisation

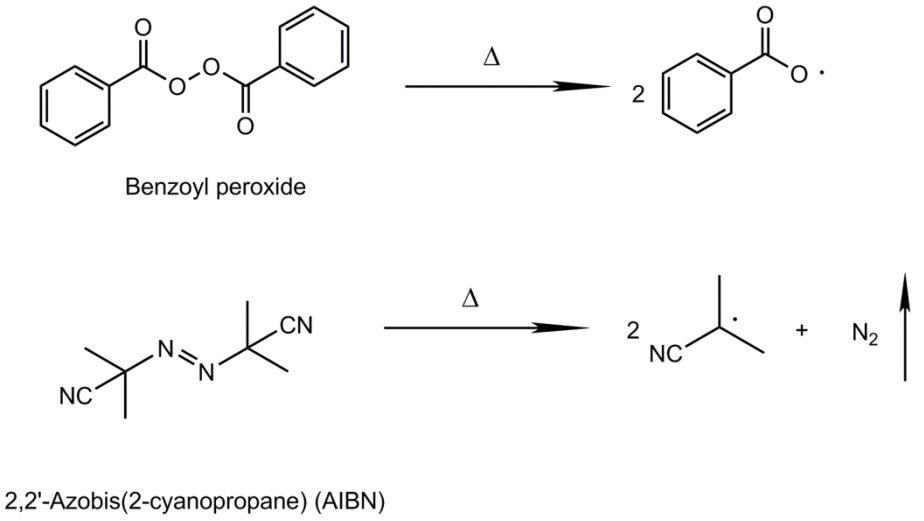

Figure 1.1.2 Formation of radicals using benzoyl peroxide or AIBN

The propagation step (**Figure 1.1.3**) involves the growth of the polymer chain by the sequential addition of the monomer to the propagating radical. In theory, the process is repeated until all monomers consumed, or most often until a side reaction irreversibly terminates the reaction.

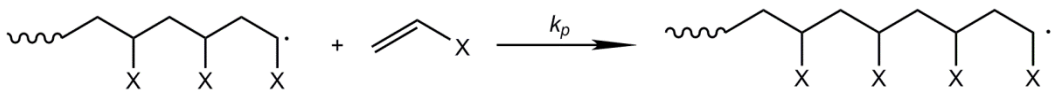

Figure 1.1.3 Propagation step of free radical polymerisation

In this stage, the termination of the polymer chain leads to removal of two radicals from the system. There are two reactions involved in termination: *combination* and

disproportionation, **Figure 1.1.4**. Termination by combination is the simplest way to halt the polymerisation, in which the two unpaired electrons couple together to form a new polymer chain. Therefore, the molecular weight of the polymeric product will be considerably higher on average, and the polymer chain contains two initiator fragments per molecule by this type of termination. Disproportionation is another way to stop the propagation reaction when an atom, usually hydrogen, is transferred from an active chain to another. This mode of termination produces an insignificant effect on the average molecular weight, but yields a terminal unsaturation in one of the dead polymer chains.

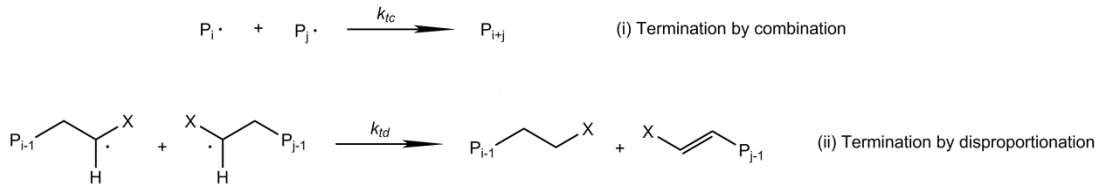

Figure 1.1.4 Termination step of free radical polymerisation

Chain transfer is another type of free radical reaction which may also occur in the polymerisation process. Chain transfer arises (**Figure 1.1.5**) when hydrogen or some other atom is transferred from a molecule in the system including initiator, monomer, solvent, and polymer, to the polymer radical. This results in the termination of the original polymer radical but also the creation of a new one; therefore, chain transfer reactions reduce the average molecular weight of the final product. In many cases, a chain transfer agent is typically added to the reaction system to restrict the molecular weight, e.g. thiols.

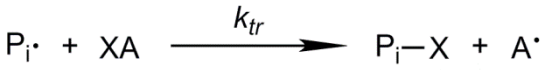

Figure 1.1.5 Chain transfer of free radical polymerisation

1.1.2 Living polymerisation

Living polymerisation is a chain-growth process for which proceeds in the absence of termination or transfer reactions.[1] In living polymerisation, initiation is effectively instantaneous relative to propagation, which means the rate of initiation needs to be much more rapid than the rate of propagation, and all active centres must be quantitatively reactive with a monomer at the same time. Compared with free radical polymerisation which leads to rather broad molecular weight distributions, living polymerisations can lead to much narrower distributions, and also enables the synthesis of block copolymers with controlled architecture via sequential monomer addition.

1.1.2.1 Ionic polymerisation

There are two modes of ionic living polymerisations: anionic and cationic polymerisations. Szwarc *et al.*[2, 3] first demonstrated and reported the living polymerisation in 1956 in the anionic polymerisation of styrene initiated with an alkali metal/naphthalene system in tetrahydrofuran (THF) at low temperature (-80 ^{o}C). The precursor to the initiator was prepared by the reaction of sodium metal with naphthalene resulting in the formation of green coloured naphthalene radical-anion which instantaneously changed onto deep red/orange upon addition of styrene. As the propagating centre is anionic, termination by combination of chain-ends does not occur. Propagation repeats with complete consumption of monomers. Despite the continuing development of new methods for the synthesis of well-defined (co)polymers, anionic polymerisation is still one of the most reliable and versatile method for the preparation of various polymers, **Figure 1.1.6** illustrating the mechanism of living anionic polymerisation. In the case of vinyl monomers CH_2=CHR, the R group requires some electron withdrawing character to stabilise the resulting carbanion, including styrene and substituted styrenes, alkyl methacrylates and acrylates, and conjugated dienes, etc. The broad utility of living anionic polymerisation is mainly due to the efficient generation of polyanions that do not undergo termination or chain transfer reactions.[4] However, the growing polymer chain can be terminated by impurities or deliberate addition of chain-transfer agent.

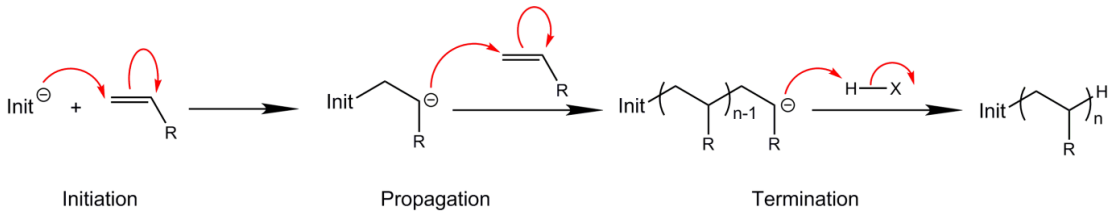

Figure 1.1.6 Mechanism of living anionic polymerisation

In cationic polymerisation, the initiator systems are generally Lewis acids, such as BF_3, $AlCl_3$, and $TiCl_4$ with a proton-donating co-initiator including water or methanol, or protonic acids. Compared with anionic polymerisation, the substituents on vinyl monomers that promote cationic polymerisation are electron-donating to stabilise the propagating carbocations, including alkyl, 1,1-dialkyl, and alkoxy, etc. The counterion should not be highly nucleophilic as this will terminate the propagating cation by covalent bond formation. Therefore, living cationic polymerisation is much less versatile than living anionic polymerisation, partially due to termination of chain growth and various chain transfer reactions.

1.1.2.2 Controlled radical polymerisation

Nowadays, conventional FRP still has many advantages over other polymerisation processes, and nearly 50% of all commercial synthetic polymers are produced using this method.[5] However, a major limitation of FRP is poor control over the molecular weight with broader distribution. To overcome these issues, controlled and living radical polymerisations (CRP) have been developed and widely studied in the last decades.[5, 6] Compared with FRP, CRP enables the synthesis of well-defined polymers with predetermined molecular weights and more uniform distributions. It also provides precise control over the polymeric architecture and desirable functionalities. The development of several promising CRP systems relies on the establishment of a dynamic equilibrium between the active propagating radicals and various dormant chains. There are generally two modes of equilibria: radicals may be reversibly terminated in a deactivation/activation process, or they can be involved in a "reversible transfer", degenerative exchange process, **Figure 1.1.7**.[6]

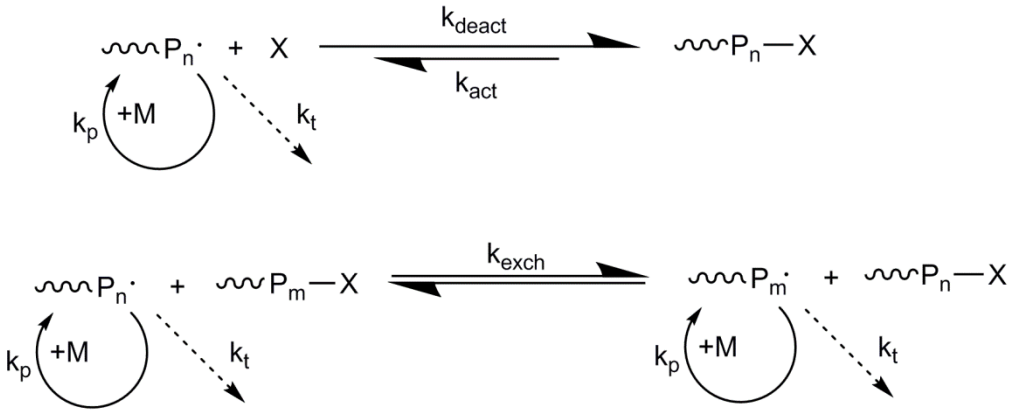

Figure 1.1.7 Dynamic equilibria of CRP systems

These controlled polymerisations proceed in such a manner that the contribution of termination and chain transfer is minimised and the apparent simultaneous growth of all chains can be achieved via almost instantaneous initiation. A combination of fast initiation and negligible chain transfer reactions or termination result in a constant rate of propagation. In addition, all the chains should retain their active centres after the full consumption of the monomer, which enables the preparation of block copolymers by following monomer addition.

1.1.2.2.1 Nitroxide mediated radical polymerisation

The first system that led to successful living and controlled radical polymerisation was patented by Solomon *et al.*,[7] and further reported by Georges *et al.* in 1993.[8] Controlled radical polymerisation of styrene was reported by using a stable nitroxide radical, 2,2,6,6-tetramethylpiperidynyl-*N*-oxyl (TEMPO) as a control agent, and a (macro)alkoxyamine as the predominant species, **Figure 1.1.8**. Nitroxide-mediated polymerisation (NMP) is based on the establishment of an equilibrium between active and dormant species, and the dormant functionality generates back the propagating radical and the free nitroxide by homolytic cleavage of the C-ON bond at elevated temperature. In addition, numerous nitroxides have been designed and reviewed for controlled polymerisation of various vinyl monomers.[9]

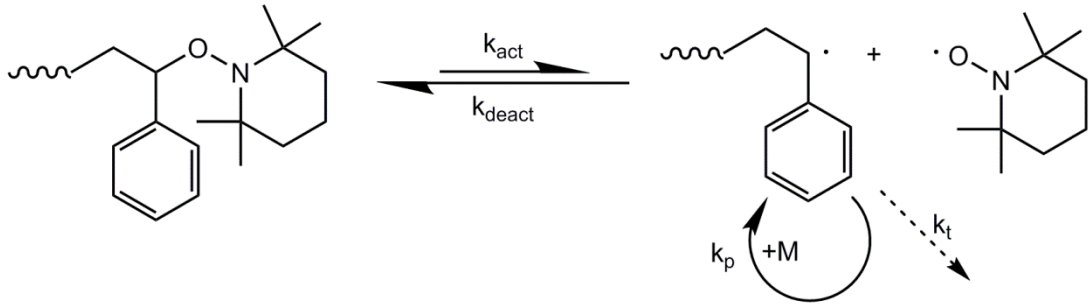

Figure 1.1.8 Nitroxide-mediated polymerisation using TEMPO as a mediator.

1.1.2.2.2 Reversible addition-fragmentation chain transfer polymerisation

Reversible addition-fragmentation chain transfer polymerisation (RAFT) is currently one of the most popular CRP processes since it has been discovered by Moad, Rizzardo and Thang in 1998.[10] The key feature of RAFT process is the chain transfer agent, thiocarbonylthio RAFT agents,[11-13] which control a sequence of addition-fragmentation equilibria as shown in **Figure 1.1.9**. Initiation of the polymerisation starts with a conventional free radical initiator, and addition of a propagating radical ($P_n^{\cdot}$) to the dithioester compounds followed by fragmentation of the intermediate radical results in a polymeric dithioester compound and a new active radical ($R^{\cdot}$). Reaction of this new radical with monomer forms a new propagating radical ($P_m^{\cdot}$). Rapid equilibrium between the active propagating radicals ($P_n^{\cdot}$ and $P_m^{\cdot}$) and the dormant polymeric thiocarbonylthio compounds provides equal probability for all chains to grow and produce polymers with low dispersity. Until the completion of the polymerisation, most of chains are dormant and terminated with the thiocarbonylthio groups which can be reinitiated upon addition another monomer.[14-17]

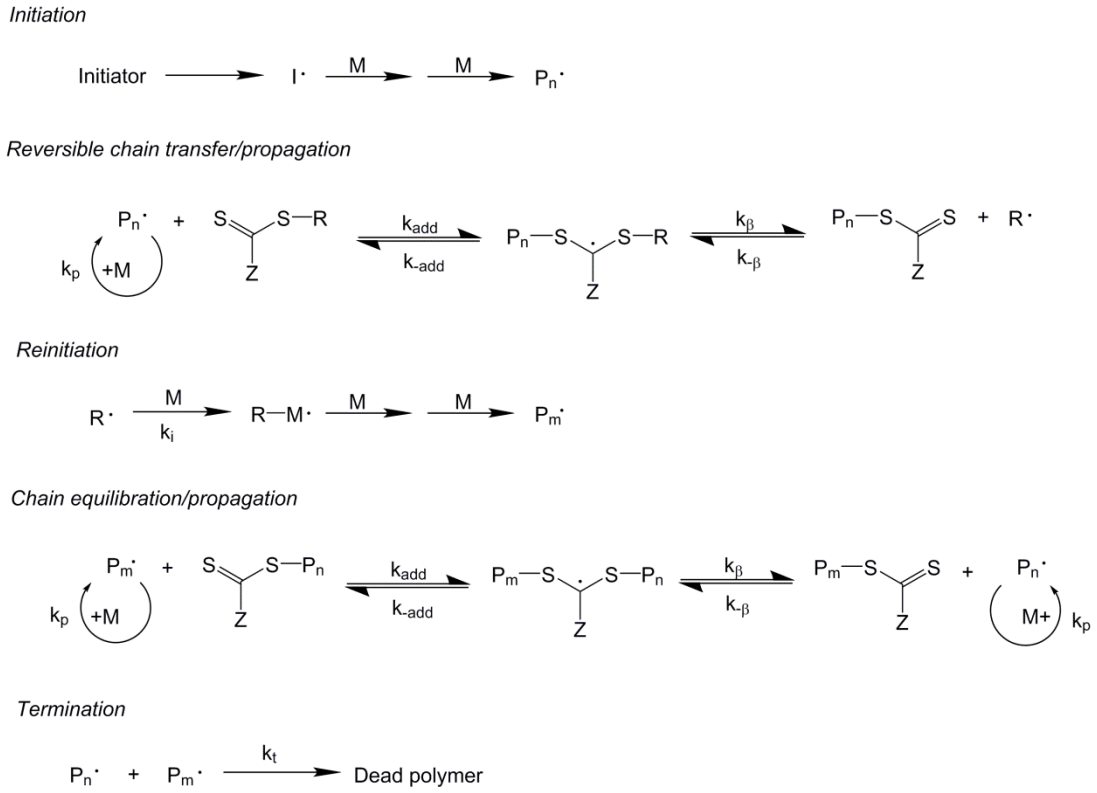

Figure 1.1.9 Mechanism of RAFT polymerisation

1.1.2.2.3 Atom transfer radical polymerisation

Atom transfer radical polymerisation (ATRP) was developed in 1995 simultaneously by Sawamoto and Matyjaszewski.[18, 19] Both systems employ a leaving group X, normally a halide, such as chloride or bromide in reaction. The activation-deactivation equilibrium is based on a rapid exchange of the halogen atom between the dormant propagating chain (P_n-X) and a transition metal complex in the lower oxidation state (TM^n-Y/Ligand), resulting in the formation of propagating radical ($P_n^{\cdot}$) and the metal complex in the higher oxidation state with a coordinated halide ligand (X-TM^{n+1}-Y/Ligand), **Figure 1.1.10**.[20] Copper-(I) is by far the most widely used transition metal for synthesis of well-defined polymers by ATRP, numerous other metals including ruthenium, iron, nickel, molybdenum, rhodium and rhenium have also been investigated.[21] The metal is chelated by ligands such as bipyridines,[19] aliphatic amines,[22] *N*-alkyl-2-pyridylmethanimine,[23] or aryl phosphines[24] that can stabilize the metal in different oxidation states and facilitate solubility of the halide salts. ATRP has been successfully employed for preparation of a variety of monomer

including styrene, substituted styrene, acrylates, methacrylates and other vinyl monomers with controlled molecular weight and architecture.

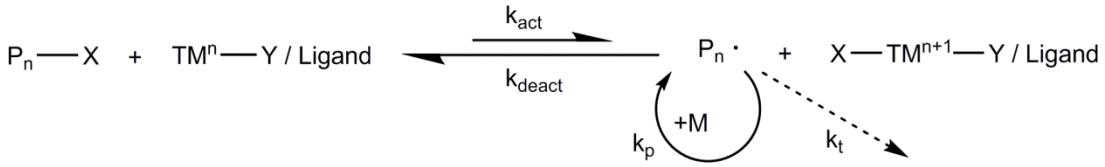

Figure 1.1.10 General mechanism of ATRP process

1.1.2.2.4 Single electron transfer living radical polymerisation

Single electron transfer living radical polymerisation (SET-LRP) has been drawing increasing attention since the Percec group described the "ultrafast synthesis of ultrahigh molar mass polymers from vinyl monomers", such as (meth)acrylate and vinyl chloride at ambient temperature.[25] Unlike ATRP process, the active catalyst is Cu(0) rather than Cu(I)X species. The polymerisation proceeds by an outer-sphere SET mechanism in which Cu(0) acts as electron donors, and the dormant initiator and propagating chain P_n-X act as electron acceptors.[25] The equilibrium between the dormant chains and the propagating radicals relies on the rapid disproportionation of in situ produced Cu(I)X by activating Cu(0) and deactivating Cu(II)X_2 in presence of appropriate nitrogen containing ligands and polar solvents, as shown in **Figure 1.1.11**.[26, 27] More recently, this approach has been modified by Haddleton group, performing SET-LRP in water.[28] The key step in this new process is to allow full disproportionation of CuBr/Me_6-TREN to Cu(0) powder and Cu(II)Br in pure water prior to addition of both monomer and initiator. Percec *et al.* has previously investigated for polymerisation of vinyl chloride in water and THF mixture under similar condition.[29] However, the new technique provides an extremely powerful tool for the synthesis of functional water-soluble polymers with controlled molecular weight and narrow molecular weight distributions. In addition, the present high chain end fidelity is capable of undergoing chain extensions or multi-block copolymerisation via iterative monomer addition to full conversion.

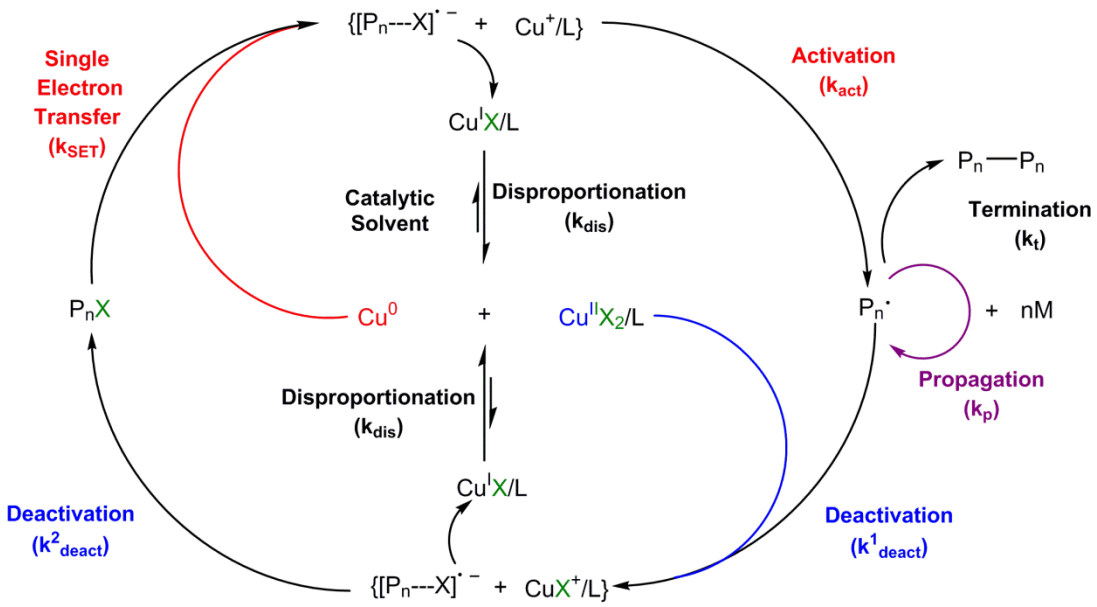

Figure 1.1.11 Proposed mechanism for SET-LRP process[27]

1.2 The discovery of ferrocene

Ferrocene was first reported in the literature by two different groups, Pauson *et al.* and Miller *et al*., in December 1951 and February 1952 respectively.[30, 31] Although both teams noted that the unusual high stability of the compound melted at 173 ^{o}C without decomposition and easily sublimed, they were not the ones that recognized its structure, **Figure 1.2.1**. The correct structure, **Figure 1.2.2**, was soon afterward proposed independently by Wilkinson *et al.* and Fisher *et al.*, according to the diamagnetism of $[Fe(C_5H_5)_2]$ and the IR spectrum of the compound.[32, 33] Fisher concluded that the whole set of the six π-electrons of each cyclopentadienyl anion participated in the bonding of iron(II), and that each five-membered ring formally acts as a tridentate ligand.[34] The structural proposals were at first not generally accepted; however, Eiland and co-workers proved by X-ray crystallography that the structure proposed by Wilkinson and Fisher was correct.[35] In addition, the term "molecular sandwich" which like ferrocene published by Dunitz *et al.* was accepted almost immediately.[36]

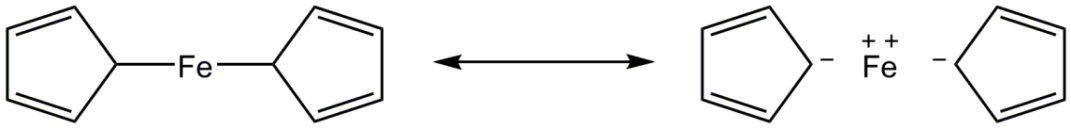

Figure 1.2.1 Structure of ferrocene (incorrect) predicted by Pauson and Kealy[30]

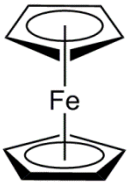

Figure 1.2.2 Correct structure of ferrocene discovered by Fisher and Wilkinson[32,33]

After the discovery of ferrocene and its structural characterisation, ferrocene has been rapidly recognised as having great potential in organometallic materials including nonlinear optical (NLO) devices,[37] electrochemical sensors,[38] and molecular biotechnology,[39] etc. The incorporation of ferrocene units into polymeric architectures probably is a good strategy to enhance the material properties due to its electron donating ability, reversible redox chemistry, steric properties and ready functionalisation of this stable fragment.[40] Examples of polymers containing ferrocene will be discussed in greater details in Chapter **2.1**.

1.3 Phthalocyanines

1.3.1 History and structure of phthalocyanines[41, 42]

Phthalocyanine (*Pc*) was firstly discovered by Braun and Tcherniac as a highly coloured by-product during the preparation of *ortho*-cyanobenzamide from phthalimide and acetic acid in 1907. Similarly, Swiss researchers, de Diesbach and von der Weid, accidentally obtained a 23% yield of an exceptionally stable blue materials, copper(II) phthalocyanine (*CuPc*), in an attempted conversion of *ortho*-dibromobenzene into phthalonitrile in 1927. Later, the Grangemouth plant of Scottish Dyes Ltd. (later ICI) formed a blue-green material during the industrial

preparation of phthalimide from phthalic anhydride. Due to the business and academic interests in this novel coloured substance, collaboration between Reginald P. Linstead from Imperial College, London, and ICI was initiated and a series of papers were published for describing the structure of *Pc* and the synthesis of some of its metal derivatives,[43-48] and their structures were further confirmed by X-ray diffraction techniques.

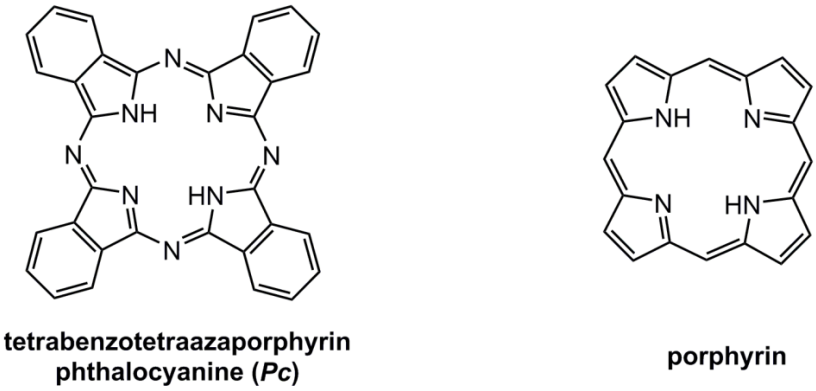

Figure 1.3.1 Structures of phthalocyanine and porphyrin macrocycles

Pc is a symmetrical macrocycle composed of four iminoisoindoline units with a central cavity of sufficient size that can be replaced by more than 70 metal ions such as Cu^{2+}, Fe^{2+}, Zn^{2+}, Al^{3+}, Si^{4+} and etc., and a variety of substituents can be incorporated either at the peripheral position or at the axial position. As shown in **Figure 1.3.1**, *Pc* is closely related to the naturally occurring porphyrin ring system with four benzo-subunits and the nitrogen atom at each of the four *meso* positions, and occasionally is referred to as *tetrabenzotetraazaporphyrin*. Like the porphyrin macrocycle, *Pc* is a planar aromatic macrocycle presenting an 18 π-electron aromatic cloud delocalized over an arrangement of alternated carbon and nitrogen atoms, which is also contributed to the intense blue-green colour. The absorption spectra of *Pcs* show intense Q-bands in the visible region, usually centred at 620-700 nm; therefore, *Pcs* have been utilized industrially as dyes or pigments in various fields. However, the planar aromatic structure of these macrocycles often results in unsubstituted *Pcs* possessing very poor solubility in almost all solvents due to π-π stacking. Therefore, efforts have been devoted for the synthetic strategies of

functionalised *Pcs* to improve the solubility and increase the number of applications using the relevant properties.

1.3.2 Synthesis of phthalocyanines[41, 42]

Different methods of organic chemical synthesis have been applied to prepare novel derivatives of metal or metal-free *Pcs* designed to possess desirable properties. A number of *ortho*-disubstituted benzene derivatives (**Figure 1.3.2**) can be used as precursors by cyclotetramerisation reaction for preparation of metal *Pcs* with addition of different metal salts; however, Linstead's initial papers described the experimental details for the preparation of *Pcs* from phthalonitrile (ortho-dicyanobenzene), which is still considered as the best precursor for synthesis of *Pcs* on a laboratory scale.

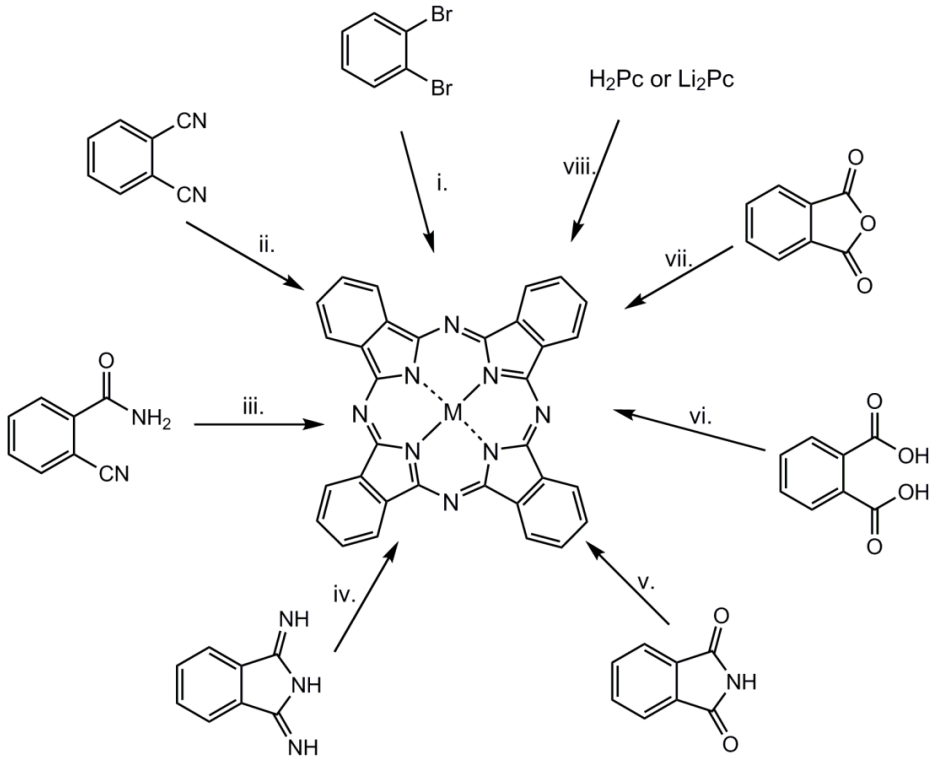

Figure 1.3.2 Synthetic routes to metal *Pcs*: i.) Large excess of Cu(I)CN in conc. solution of refluxed DMF;[49] ii.) solution of refluxed DMF with metal salt;[50] iii.) high boiling-point solvent (e.g. quinoline) with metal salt at 205 ^{o}C;[51] iv.) in 2-ethoxyethanol with metal salt at 50 ^{o}C;[52] v.) solvent free, in fused urea with metal salt at 160 ^{o}C;[53] vi.) high boiling-point solvent (e.g. nitrobenzene) with urea, metal salt, NH_4Cl, and $(NH_4)_6Mo_7O_{24}$ at 180 ^{o}C;[54] vii.) in nitrobenzene with urea, metal salt and $(NH_4)_6Mo_7O_{24}$ at 190 ^{o}C;[55] or in hexamethyldisilazane (HMDS) and DMF with metal salt and *p*-TsOH at 130 ^{o}C;[56] viii.) in refluxed quinoline with metal salt[57]

As described above, symmetrical phthalocyanines are readily available by cyclotetramerisation of phthalonitrile or diiminoisoindolines; however, unsymmetrically substituted *Pcs* of the $\mathbf{A_3B}$ type are usually difficult to obtain. The most common method is the statistical condensation of two different phthalonitriles or diiminoisoindolines **A** and **B**, following by complex chromatographical purification. The ring expansion reaction of subphthalocyanines[58] as shown in **Figure 1.3.3** is one of the most elegant synthetic strategies, reported by Kobayashi *et al.*[59] for obtaining unsymmetrically substituted *Pcs* of the $\mathbf{A_3B}$ type. Substituted Sub*Pc* ($\mathbf{A_3}$) and diiminoisoindoline analogues (**B**) were reacted at 80-90 ^{o}C in a

mixture of DMSO/chlorobenzene, or 1-chloronaphthalene (1:4 to 4:1 v/v) for 5-27 hours. This method was claimed to have several advantages over the conventional statistical cyclotetramerisation: (i) high yields (8-20%), (ii) selectivity, and (iii) simple purification procedures as there are no byproducts.

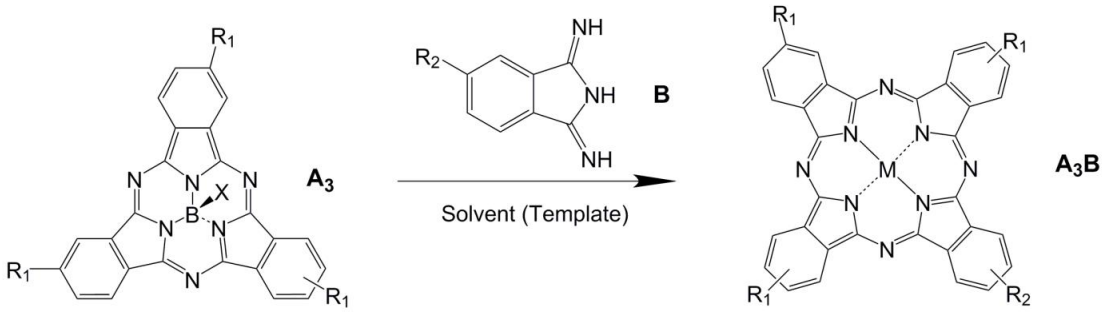

Figure 1.3.3 Synthesis of unsymmetrical phthalocyanine analogues by ring expansion reaction of subphthalocyanines[58-60]

Many phthalocyanines are thermally and chemically stable, do not melt but can be sublimed, and support intense electromagnetic radiation and play an exceptional role in material science due to their versatile synthetic routes.[61] More interestingly free *Pcs* and *Pc* metal ion complexes find diverse applications in numerous advanced technologies due to other unique properties, including electronic conductivity,[62, 63] nonlinear optical behaviour,[64, 65] liquid crystallinity,[66-68] singlet oxygen generation,[69-71] and photovoltaic properties.[72, 73]

1.4 Whitening toothpastes[74]

1.4.1 Introduction

Some recent studies have shown that consumers and patients have always had a strong desire for white teeth and many individuals ranging from 17.9 to 52.6 % are dissatisfied with their current teeth colour, depending on the population examined.[75-77] The desire for whiter teeth has given rise to a growing trend in the increased use of tooth whitening products;[78] therefore, manufactures of oral care products are

constantly developing improvements and new strategies for teeth whitening in order to meet the demanding expectations of patients and consumers.

The colour of the teeth is influenced by a combination of their intrinsic colour and the presence of any extrinsic stains that can form on the teeth surface.[79, 80] Intrinsic tooth colour is greatly influenced by the light absorption and scattering properties of the enamel and dentin, and dentin plays a significant role in determining the overall tooth colour;[81] however, any extrinsic stains due to poor tooth brushing technique, smoking, dietary of coloured food and the use of certain cationic agents, which can be absorbed into the acquired pellicle on the surface of enamel have a great effect on the extrinsic colour.[82] The majority of the teeth whitening products work in one of two ways, either by bleaching of the teeth, or by the removal and control of extrinsic stain. Bleaching usually involves hydrogen peroxide or carbamide peroxide containing gel applied onto the teeth via various formats including a mouth guard or strip or even painting directly on. The peroxide causes decolourisation or bleaching of the coloured materials found within the teeth resulting in whiter teeth.[83] As for the removal and control of the extrinsic stain, specific abrasives and/or chemical agents can be added to toothpaste. These improved stain removal/prevention products are termed whitening toothpastes.

1.4.2 Tooth whitening agents

Most of the whitening toothpastes contain the same basic functional ingredient, all of which play a specific role within the formulation, including solid cleansing abrasive materials, humectants for solubilisation of other ingredients and to prevent the formulation from drying out; thickening agents to define the rheological properties; surfactants to generate foam and deliver the desirable properties during use, active agents such as fluoride to provide health benefits, flavour, sweetener, opacifying agents; colours for characteristic taste and appearance; and buffering agents and preservatives to maintain formulation stability.

1.4.2.1 Abrasives

In general, whitening toothpastes are specially formulated to provide this benefit by removing and preventing formation of extrinsic stain. It is widely accepted that toothpastes require a certain amount of abrasive to remove or prevent extrinsic stains from forming, and the evidence to date stills suggests that the primary stain removal ingredient in tooth paste is the abrasive.[84] Abrasives are the insoluble components added to toothpaste in order to aid the physical removal of stains, plaque and food debris. Nowadays, the abrasives used include hydrated silica, calcium pyrophosphate, alumina, perlite and sodium bicarbonate. Abrasives have been shown to effectively remove extrinsic stains but also can help in preventing tooth stains from reforming. In addition, the abrasive particles can become trapped between the toothbrush and the stained tooth surface during tooth brushing. As the abrasive is physically harder than the stain, the stain can be removed, leaving a cleaned tooth surface. However, abrasive cleaning primarily influences only extrinsic stains and has insignificant effect on the intrinsic discoloration or the natural shade of the teeth. Abrasive cleaning may be further limited by the accessibility of the toothbrush to stained areas of the teeth, particularly in interproximal areas, gingival areas and malocclusion sites.

1.4.2.2 Chemical agents

Whitening toothpaste may contain additional chemical agents which enhance the abrasive cleaning by aiding the removal and/or prevention of extrinsic stains. The intrinsic tooth whitening efficacy of peroxide is well established in certain delivery formats, whereas the application of peroxide in toothpaste is much more challenging in terms of formulation factors and the relatively shortened exposure times.[85] However, despite these challenges, toothpastes containing certain amount of oxidative chemicals such as peroxide, peroxide sources and sodium chlorite have been shown to significantly decrease tooth yellowness and increase lightness of tooth samples in a series of in vitro studies.[86-88]

Owing to the incorporation of extrinsic stain into the pellicle, a salivary protein film that forms on the tooth surface, it is possible that enzymes such as proteases could help degrade the stained films and potentiate their removal. Recently, a toothpaste

containing a mixture of the protease enzyme papain, alumina and sodium citrate have been demonstrated to be effective at removing established stains.[89-91]

Moreover, a few of synthetic and natural polymers and copolymers widely used in pharmaceutical and personal care industries, and their unique properties make them especially effective in variety of oral care products.[92] Copolymers of maleic acid and methyl vinylether with high molecular weight can help control the formation and growth of tartar in the mouth. Due to the strong bioadhesive functionality of the maleic acid group combined with high molecular weight, the products create a greater number of adhesive contacts per polymer chain. Other polymers, like linear and crosslinked poly(vinylpyrrolidone) (PVP) homopolymers and copolymers, have been recently added to toothpaste formulations as stain prevention and removal ingredients.

Other chemical agents, such as phosphate materials including pyrophosphate, tripolyphosphate and hexametaphosphate, tend to have a strong binding affinity for enamel, dentin and tartar, and they have shown to desorb stain components during adsorption.[93, 94]

1.4.3 Optical routes

Reduction on the yellowness of the tooth colour was reported in a number of *in vivo* and *in vitro* whitening studies to be important in aiding the overall self-perception of tooth whiteness.[95] This observation has been applied in the development of a silica whitening toothpaste containing copper phthalocyanine (also named blue covarine). Following brushing extracted teeth *in vitro*, the blue covarine has been shown to be deposited onto the tooth surface and to give a yellow to blue colour shift with an overall improvement in measurable and perceivable tooth whitening.[96] Moreover, this toothpaste has shown to act as an effective abrasive system for removal of extrinsic stain compared to other clinically proven silica-based whitening toothpastes.[97] Collins *et al.*[98] also demonstrated in a clinical study that brushing once with the toothpaste containing blue covarine can give as significant and immediate reduction in tooth yellowness and an increase in tooth whiteness, as measured by image analysis of digital photographs of the teeth. Thus, it can be concluded that the

silica-based toothpaste containing blue covarine is not only effective in the removal of extrinsic stains but also in significantly whitening the intrinsic colour of teeth.

1.4.4 Evaluation of whitening toothpaste

A number of tooth whitening *in vitro* models evaluating the effects of toothpaste have been reported in the literature, and one of the most commonly used methods for assessing the stain removal is developed by Stookey *et al*.[84] In this model, square bovine enamel blocks were used and mounted in poly(methyl methacrylate) blocks. The specimens were polished and lightly acid etched in order to facilitate stain accumulation and adherence. Following immersion into a staining media and air drying at 37 ^{o}C, the colour of the stained specimens can be measured with a colorimeter. The test toothpastes were dispersed in an aqueous diluent and the stained specimens were then mounted in a mechanical brushing machine and brushed for a set number of brush strokes. The colour of the specimens was remeasured and the amount of stain removed can be calculated. Extracted human teeth have also been used as the substrate in the evaluation of tooth whitening where the toothpaste has been designed to have an effect on the average intrinsic tooth colour. The teeth were first cleaned with a prophylaxis paste to remove any traces of surface extrinsic stain, followed by a brushing protocol with test toothpaste. The changes in intrinsic tooth colour can be measured with a colorimeter, spectrophotometer or by comparison with a Vita shade guide under controlled lighting conditions.[96, 99-101]

The clinical evaluations of whitening toothpaste on the measurement of extrinsic stains include subjective clinician determinations and objective instrumental methods. In terms of determining the overall average tooth colour or shade change after the use of whitening toothpastes, a number of techniques have been described including the use of Vita shade guides,[88] colorimeters,[102] and image analysis of digital photographs of teeth.[98] Regardless of the methodology employed, important factors in stain assessments include the calibration and standardisation of objective measures and/or the demonstration of reproducibility and sensitivity in subjective indices.[103]

1.5 Click chemistry

1.5.1 A general concept

The concept of "click chemistry" was first introduced by Kolb, Finn, and Sharpless in 2001[104] and concerned reactions to generate substances by joining small units together with carbon-heteroatom links (C-X-C). A desirable click reaction must be high-yielding, stereospecific, wide in scope and easy to perform, and create only byproducts that can be removed by non-chromatographic methods. Several types of reactions have been identified that fulfil these criteria with a high thermodynamic driving force that lead specifically to one product, such as cycloadditions of unsaturated species (and also Diels-Alder reactions), nucleophilic ring-opening reaction (particularly strained heterocyclic electrophiles such as epoxides and aziridines), "non-aldol" type carbonyl reactions (formation of hydrazones and oxime ethers) and additions to carbon-carbon multiple bonds (oxidative cases such as epoxidation, dihydroxylation, aziridination and Michael additions of Nu-H reactants).

Among these reactions, Huisgen's 1,3-dipolar cycloaddition[105] of organic azides and alkynes has been receiving increasing interest and is the most direct route to formation of 1,2,3-triazoles. The traditional Huisgen cycloaddition reaction usually requires high temperatures (often more than 100 ^{o}C for at least several hours) and results in a mixture of 1,4- and 1,5-regioisomers, **Figure 1.5.1**-(a).[106, 107]

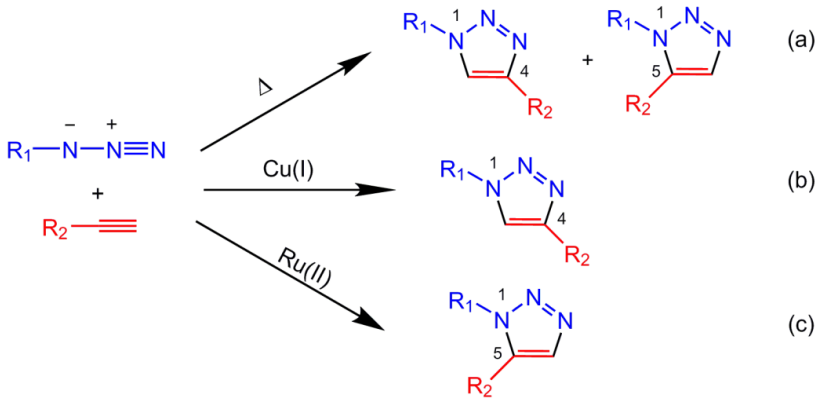

Figure 1.5.1 Huisgen's 1,3-dipolar cycloaddition of alkynes and azides under different reaction conditions

This major drawback of the azide-alkyne cycloaddition was successfully overcome in 2002 by two independent groups, Meldal and Sharpless with their co-workers, using Cu(I)-based catalysts.[108, 109] This Cu(I)-catalysed azide-alkyne cycloaddition (CuAAC) process (**Figure 1.5.1**-b) is very robust, tolerates a number of unprotected functional groups, and affording quantitatively and regioselectively 1,4-disubstituted-1,2,3-trazoles under aqueous condition at ambient temperature. By contrast, a ruthenium(II)-catalysed reaction was further developed for regioselective formation of 1,5-disubstituted triazoles, **Figure 1.5.1**-(c).[110]

1.5.2 Cu(I)-catalysed azide-alkyne cycloaddition

Following the discovery of the Cu(I)-catalysed transformation to give 1,4-disubstituted 1,2,3-triazoles, Fokin and Sharpless proposed a mechanism as shown in **Figure 1.5.2**, supported both by experimental evidence and density functional theory (DFT) studies.[111, 112] The catalytic sequence begins with the coordination of the alkyne (1) to the Cu(I) species and conversion into a Cu-acetylide species (2). This conversion is very likely to happen in aqueous solutions without addition of amine base which is required when the reaction is performed in organic solvents. The azide then replaces one of ligands and binds to the copper atom via the nitrogen proximal to carbon, forming intermediate (3). Sequentially, the distal nitrogen of the azide in intermediate (3) attacks the C-2 carbon of the acetylide, forming the unusual six-membered copper-(III) metallacycle (4) followed by ring contraction and proteolysis of triazolyl-copper derivative (5) affording the final 1,4-disubstituted 1,2,3-triazole product.

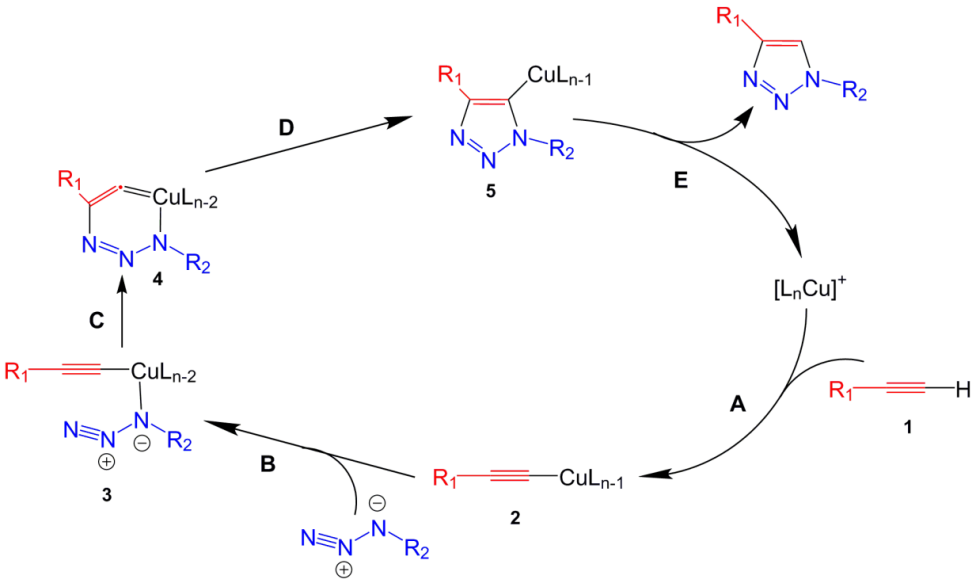

Figure 1.5.2 Proposed mechanism for Cu(I)-catalysed ligation by Fokin and Sharpless[111]

In addition, a wide variety of catalysts have been tested and reported for promotion of the CuAAC processes. A common strategy is to introduce the Cu(I) salt *in situ* by reducing $CuSO_4$ with ascorbic acid and/or sodium ascorbate; other Cu(I) salts, for example, CuI, $CuOTf{\cdot}C_6H_6$, and $[Cu(NCCH_3)_4][PF_6]$ can also be used directly in the absence of a reducing agent.[108] The most commonly used accelerating ligand, tris((1-benzyl-1*H*-1,2,3-triazol-4-yl)methyl)amine (TBTA), has been discovered by Fokin and co-workers and could dramatically accelerate the CuAAC reactions resulting in Cu(I) complexes with improved stability in the presence of oxygen.[113] The CuAAC reaction responds to changes in ligands, buffer salts, and substrates in a complex manner;[114] furthermore, Fokin and Finn reported that tris(2-benzimidazolymethyl)amines have been found to be the most promising family of accelerating ligands among more than 100 mono-, bi-, and polydentate candidates. The benzimidazole derivatives are easy to prepare and give substantial improvements in rate and yields with convenient workup to remove residual Cu and ligand.[115]

1.5.2.1 CuAAC in polymer and material science

Following the development of Cu(I) catalysis of Huisgen 1,3-dipolar cycloaddition, this CuAAC provides the ideal "click" reaction for highly defined polymeric architectures with novel properties and shows an enormous potential in material science. The first report of click chemistry applied to polymer science was described by Hawker, Fokin, Sharpless and co-workers.[116] They demonstrated the preparation of a large number of diverse dendrimers with high purity and almost quantitative yield by the CuAAC click chemistry. Afterwards, the application of CuAAC click chemistry in polymer chemistry has grown considerably and been reviewed in a range of excellent papers.[117-121]

Hoogenboom, Becer, Schubert and co-workers have summarised at least four common ways that combine controlled radical polymerisation techniques (ATRP, SET-LRP, RAFT, and NMP) and click chemistry to construct various clicked polymeric architectures, **Figure 1.5.3**.[121] The post-click strategy represents that well-defined polymers with versatile clickable functionalities synthesised from functional initiators or clickable monomers can be achieved to construct various architectures by clicking post to the polymerisation. By contrast, if the functional initiator or monomers with clickable moieties interfere with the radical process, clicked polymeric architectures can be obtained by using functional units that are clicked prior to the polymerisation, which is the so-called "pre-click" route. Moreover, in many cases CRP and click reaction occur simultaneously during the polymer synthesis. CuBr/PMDETA, for example, is one of the most commonly used catalytic systems in CuAAC process for polymer chemistry, and the same as for the ATRP polymerisation that allows a simultaneous/one-pot process of click reaction and polymerisation. In addition, the pre-functional polymers with high end-group fidelity prepared by CRP can be modified with clickable moiety to achieve clickable polymers for further desired architectures. Therefore, the combination of click reactions with suitable CRP techniques via an appropriate strategy has been widely used for building novel polymeric structures with defined composition, preparing polymer bioconjugates, functionalising or cross-linking colloidal objects such as polymer, lipid or inorganic nanoparticles, etc.[117]

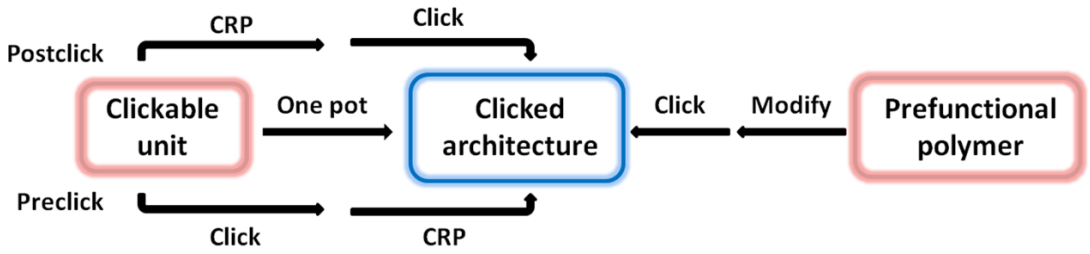

Figure 1.5.3 Schematic representation of the strategies towards clicked architectures[121]

1.5.2.2 CuAAC in phthalocyanine modification

The Cu(I)-catalysed 1,3-dipolar cycloaddition of alkynes and azides has been also becoming a successful synthetic tool for functionalisation and modification phthalocyanine related materials with improved properties.[122-126] Functionalisation of single-wall carbon nanotubes (SWNTs) with 4-(2-trimethylsilyl)ethynylaniline and the subsequent attachment of a zinc phthalocyanine (*ZnPc*) bearing an azide group by CuAAC reaction (**Figure 1.5.4**) was described by Bourgoin *et al.*.[126] The resulting SWNT-*ZnPc* nanotube derivatives were fully characterised and integrated into photoactive electrodes which revealed stable and reproducible photocurrents.

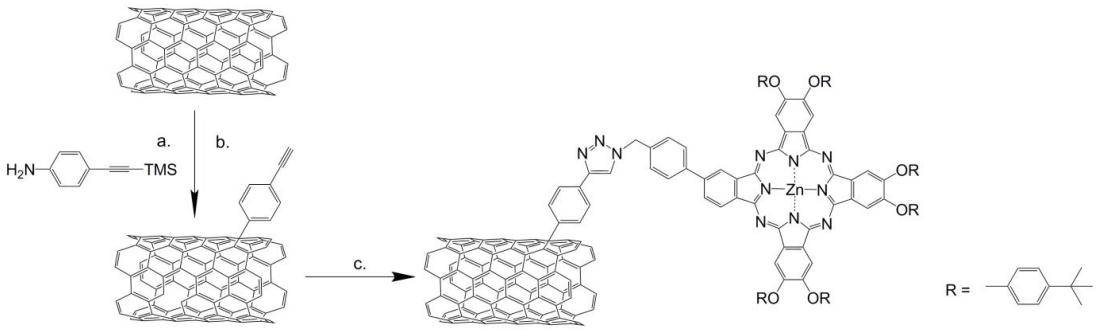

Figure 1.5.4 SWCT-*ZnPc* conjugates:[126] (a) Isoamyl nitrite, NMP, 60 ^{o}C, 48 h; (b) NBu_4F, THF/NMP, rt, 1h; (c) $CuSO_4{\cdot}5H_2O$, sodium ascorbate, NMP, 70 ^{o}C, 48 h

A further novel and significantly improved protocol for functionalised *Pcs* was demonstrated by Rowan *et al.* in 2009.[122] The synthesis of *tert*-butyldimethylsilyl-protected octaactylene phthalocyanine was described, and followed by *in situ*

deprotection and CuAAC clicking approach leading to a highly efficient and quantitative route to a novel class of octatriazole-functionalised phthalocyanines, **Figure 1.5.5**. Due to the versatility of click chemistry, this method provides great potential for the highly efficient, mild, and easy construction of novel functionalised *Pcs*, in particular those bearing sensitive groups.

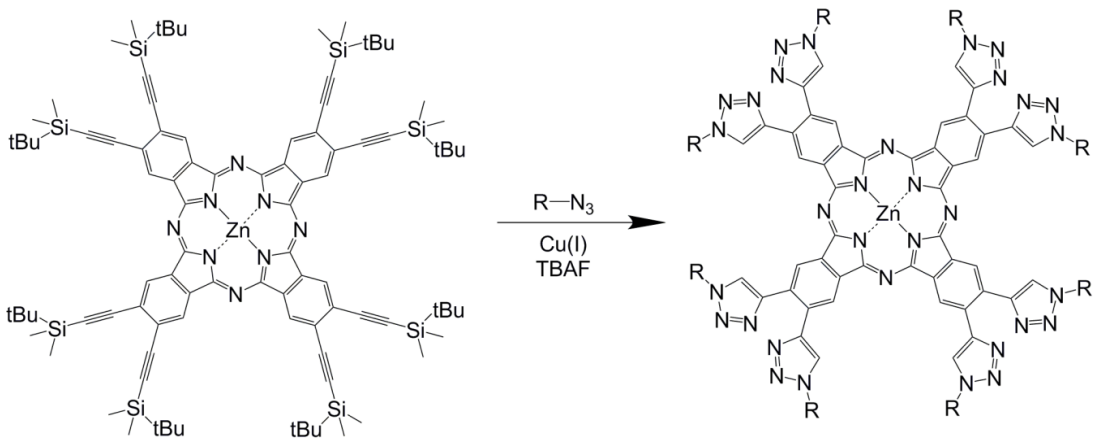

Figure 1.5.5 Post-modification of octaaceylene via *in situ* deprotection and click chemistry[122]

In addition, several carbohydrate-phthalocyanine conjugates via 1,3-dipolar cycloaddition reaction have been reported recently.[123, 124] Schotten *et al.*[123] demonstrated for the first time, ex post substitution of a full-fledged octa-propargyloxy *ZnPc* derivative with carbohydrates; Lafont and co-workers[121] reported the synthesis of asymmetrical amphiphilic carbohydrate-phthalocyanine conjugates via CuAAC click chemistry of propargylic glycosides on a novel azido-phthalocyanine. These phthalocyanines bearing carbohydrate moieties enhance the amphiphilicity of the hydrophobic phthalocyanine and have attracted attention as potential cell specific agents. Therefore, the click modification of phthalocyanine derivatives not only will provide a rapid and effective synthetic route towards highly diverse *Pcs* for biological tests but also deliver *Pcs* into functional supramolecular biological matrices.

1.6 References

1. P. C. Heimenz and T. P. Lodge, eds., *Polymer Chemistry, Second Edition*, CRC Press, 2007.
2. M. Szwarc, *Nature*, 1956, **178**, 1168-1169.
3. M. Szwarc, M. Levy and R. Milkovich, *Journal of the American Chemical Society*, 1956, **78**, 2656-2657.
4. K. Hong, D. Uhrig and J. W. Mays, *Current Opinion in Solid State and Materials Science*, 1999, **4**, 531-538.
5. K. Matyjaszewski and J. Spanswick, *Materials Today*, 2005, **8**, 26-33.
6. W. A. Braunecker and K. Matyjaszewski, *Progress in Polymer Science*, 2007, **32**, 93-146.
7. D. H. Solomon, E. Rizzardo and P. Caciolo, 1986, **4581429**.
8. M. K. Georges, R. P. N. Veregin, P. M. Kazmaier and G. K. Hamer, *Macromolecules*, 1993, **26**, 2987-2988.
9. J. Nicolas, Y. Guillaneuf, C. Lefay, D. Bertin, D. Gigmes and B. Charleux, *Progress in Polymer Science*, 2013, **38**, 63-235.
10. J. Chiefari, Y. K. Chong, F. Ercole, J. Krstina, J. Jeffery, T. P. T. Le, R. T. A. Mayadunne, G. F. Meijs, C. L. Moad, G. Moad, E. Rizzardo and S. H. Thang, *Macromolecules*, 1998, **31**, 5559-5562.
11. Y. K. Chong, J. Krstina, T. P. T. Le, G. Moad, A. Postma, E. Rizzardo and S. H. Thang, *Macromolecules*, 2003, **36**, 2256-2272.
12. J. Skey and R. K. O'Reilly, *Chemical Communications*, 2008, **0**, 4183-4185.
13. D. J. Keddie, G. Moad, E. Rizzardo and S. H. Thang, *Macromolecules*, 2012, **45**, 5321-5342.
14. G. Moad, E. Rizzardo and S. H. Thang, *Australian Journal of Chemistry*, 2005, **58**, 379-410.
15. G. Moad, E. Rizzardo and S. H. Thang, *Australian Journal of Chemistry*, 2006, **59**, 669-692.
16. G. Moad, E. Rizzardo and S. H. Thang, *Australian Journal of Chemistry*, 2009, **62**, 1402-1472.
17. G. Moad, E. Rizzardo and S. H. Thang, *Australian Journal of Chemistry*, 2012, **65**, 985-1076.

18. M. Kato, M. Kamigaito, M. Sawamoto and T. Higashimura, *Macromolecules*, 1995, **28**, 1721-1723.
19. J.-S. Wang and K. Matyjaszewski, *Journal of the American Chemical Society*, 1995, **117**, 5614-5615.
20. K. Matyjaszewski and J. Xia, *Chemical Reviews*, 2001, **101**, 2921-2990.
21. M. Kamigaito, T. Ando and M. Sawamoto, *Chemical Reviews*, 2001, **101**, 3689-3746.
22. J. Xia and K. Matyjaszewski, *Macromolecules*, 1997, **30**, 7697-7700.
23. D. M. Haddleton, C. B. Jasieczek, M. J. Hannon and A. J. Shooter, *Macromolecules*, 1997, **30**, 2190-2193.
24. A. Hirao, K. Kato and S. Nakahama, *Macromolecules*, 1992, **25**, 535-540.
25. V. Percec, T. Guliashvili, J. S. Ladislaw, A. Wistrand, A. Stjerndahl, M. J. Sienkowska, M. J. Monteiro and S. Sahoo, *Journal of the American Chemical Society*, 2006, **128**, 14156-14165.
26. T. Guliashvili and V. Percec, *Journal of Polymer Science Part A: Polymer Chemistry*, 2007, **45**, 1607-1618.
27. B. M. Rosen and V. Percec, *Chemical Reviews*, 2009, **109**, 5069-5119.
28. Q. Zhang, P. Wilson, Z. Li, R. McHale, J. Godfrey, A. Anastasaki, C. Waldron and D. M. Haddleton, *Journal of the American Chemical Society*, 2013, **135**, 7355-7363.
29. V. Percec, A. V. Popov, E. Ramirez-Castillo, M. Monteiro, B. Barboiu, O. Weichold, A. D. Asandei and C. M. Mitchell, *Journal of the American Chemical Society*, 2002, **124**, 4940-4941.
30. T. J. Kealy and P. L. Pauson, *Nature*, 1951, **168**, 1039-1040.
31. S. A. Miller, J. A. Tebboth and J. F. Tremaine, *Journal of the Chemical Society (Resumed)*, 1952, **0**, 632-635.
32. G. Wilkinson, M. Rosenblum, M. C. Whiting and R. B. Woodward, *Journal of the American Chemical Society*, 1952, **74**, 2125-2126.
33. E. O. Fisher and W. Z. Pfab, *Naturforsch*, 1952, **7b**, 377-379.
34. H. Werner, *Angewandte Chemie International Edition*, 2012, **51**, 6052-6058.
35. P. F. Eiland and R. Pepinsky, *Journal of the American Chemical Society*, 1952, **74**, 4971-4971.
36. J. D. Dunitz and L. E. Orgel, *Nature*, 1953, **171**, 121-122.

37. N. Tsuboya, R. Hamasaki, M. Ito, M. Mitsuishi, T. Miyashita and Y. Yamamoto, *Journal of Materials Chemistry*, 2003, **13**, 511-513.
38. S.-J. Choi, B.-G. Choi and S.-M. Park, *Analytical Chemistry*, 2002, **74**, 1998-2002.
39. D. R. van Staveren and N. Metzler-Nolte, *Chemical Reviews*, 2004, **104**, 5931-5986.
40. R. D. A. Hudson, *Journal of Organometallic Chemistry*, 2001, **637–639**, 47-69.
41. A. B. P. L. C.C.Leznoff, ed., *Phthalocyanine: Properties and Applications*, VCH Publishers, New York, 1989-1996.
42. N. B. McKeown, ed., *Phthaloyanine Materials*, Cambridge University Press, Cambridge, 1998.
43. G. T. Byrne, R. P. Linstead and A. R. Lowe, *Journal of the Chemical Society (Resumed)*, 1934, **0**, 1017-1022.
44. C. E. Dent and R. P. Linstead, *Journal of the Chemical Society (Resumed)*, 1934, **0**, 1027-1031.
45. C. E. Dent, R. P. Linstead and A. R. Lowe, *Journal of the Chemical Society (Resumed)*, 1934, **0**, 1033-1039.
46. R. P. Linstead, *Journal of the Chemical Society (Resumed)*, 1934, **0**, 1016-1017.
47. R. P. Linstead and A. R. Lowe, *Journal of the Chemical Society (Resumed)*, 1934, **0**, 1022-1027.
48. R. P. Linstead and A. R. Lowe, *Journal of the Chemical Society (Resumed)*, 1934, **0**, 1031-1033.
49. G. Pawlowski and M. Hanack, *Synthesis*, 1980, **1980**, 287-289.
50. S. Zeki Yldz and Y. Gok, *New Journal of Chemistry*, 1998, **22**, 1365-1369.
51. M. K. Lowery, A. J. Starshak, J. N. Esposito, P. C. Krueger and M. E. Kenney, *Inorganic Chemistry*, 1965, **4**, 128-128.
52. B. Cabezón, E. Quesada, S. Esperanza and T. Torres, *European Journal of Organic Chemistry*, 2000, **2000**, 2767-2775.
53. F.-D. Cong, B. Ning, X.-G. Du, C.-Y. Ma, H.-F. Yu and B. Chen, *Dyes and Pigments*, 2005, **66**, 149-154.
54. K. R. Venugopala Reddy and J. Keshavayya, *Dyes and Pigments*, 2002, **53**, 187-194.

55. J. Metz, O. Schneider and M. Hanack, *Inorganic Chemistry*, 1984, **23**, 1065-1071.

56. H. Uchida, H. Yoshiyama, P. Y. Reddy, S. Nakamura and T. Toru, *Synlett*, 2003, **2003**, 2083-2085.

57. R. D. Joyner and M. E. Kenney, *Journal of the American Chemical Society*, 1960, **82**, 5790-5791.

58. C. G. Claessens, D. González-Rodríguez and T. Torres, *Chemical Reviews*, 2002, **102**, 835-854.

59. N. Kobayashi, R. Kondo, S. Nakajima and T. Osa, *Journal of the American Chemical Society*, 1990, **112**, 9640-9641.

60. N. Kobayashi, *Journal of Porphyrins and Phthalocyanines*, 1999, **3**, 453-467.

61. G. de la Torre, C. G. Claessens and T. Torres, *Chemical Communications*, 2007, **0**, 2000-2015.

62. M. F. Craciun, S. Rogge, M. J. L. den Boer, S. Margadonna, K. Prassides, Y. Iwasa and A. F. Morpurgo, *Advanced Materials*, 2006, **18**, 320-324.

63. G. Givaja, P. Amo-Ochoa, C. J. Gomez-Garcia and F. Zamora, *Chemical Society Reviews*, 2012, **41**, 115-147.

64. J. Andzelm, A. M. Rawlett, J. A. Orlicki, J. F. Snyder and K. K. Baldridge, *Journal of Chemical Theory and Computation*, 2007, **3**, 870-877.

65. M. O. Senge, M. Fazekas, E. G. A. Notaras, W. J. Blau, M. Zawadzka, O. B. Locos and E. M. Ni Mhuircheartaigh, *Advanced Materials*, 2007, **19**, 2737-2774.

66. D. M. Knawby and T. M. Swager, *Chemistry of Materials*, 1997, **9**, 535-538.

67. E. Venuti, R. G. Della Valle, I. Bilotti, A. Brillante, M. Cavallini, A. Calò and Y. H. Geerts, *Journal of Physical Chemistry C*, 2011, **115**, 12150-12157.

68. H. Hayashi, W. Nihashi, T. Umeyama, Y. Matano, S. Seki, Y. Shimizu and H. Imahori, *Journal of the American Chemical Society*, 2011, **133**, 10736-10739.

69. K. T. de Oliveira, F. F. de Assis, A. O. Ribeiro, C. R. Neri, A. U. Fernandes, M. S. Baptista, N. P. Lopes, O. A. Serra and Y. Iamamoto, *Journal of Organic Chemistry*, 2009, **74**, 7962-7965.

70. J.-W. Hofman, F. van Zeeland, S. Turker, H. Talsma, S. A. G. Lambrechts, D. V. Sakharov, W. E. Hennink and C. F. van Nostrum, *Journal of Medicinal Chemistry*, 2007, **50**, 1485-1494.

71. H. Ali and J. E. van Lier, *Chemical Reviews*, 1999, **99**, 2379-2450.

72. Q. H. Cui, L. Jiang, C. Zhang, Y. S. Zhao, W. Hu and J. Yao, *Advanced Materials*, 2012, **24**, 2332-2336.
73. G. Mattioli, C. Melis, G. Malloci, F. Filippone, P. Alippi, P. Giannozzi, A. Mattoni and A. Amore Bonapasta, *Journal of Physical Chemistry C*, 2012, **116**, 15439-15448.
74. A. Joiner, *Journal of Dentistry*, 2010, **38**, E17-E24.
75. M. N. Alkhatib, R. Holt and R. Bedi, *Journal of Dentistry*, 2004, **32**, 561-566.
76. M. N. Alkhatib, R. Holt and R. Bedi, *Gerodontology*, 2005, **22**, 32-36.
77. J. Xiao, X. D. Zhou, W. C. Zhu, B. Zhang, J. Y. Li and X. Xu, *Journal of Oral Rehabilitation*, 2007, **34**, 351-360.
78. M. J. Pickles, M. Evans, C. J. Philpotts, A. Joiner, R. J. Lynch, N. Noel and M. Laucello, *Int Dent J*, 2005, **55**, 197-202.
79. A. Watts and M. Addy, *Br Dent J*, 2001, **190**, 309-316.
80. A. Joiner, *Journal of Dentistry*, 2004, **32**, 3-12.
81. J. J. ten Bosch and J. C. Coops, *Journal of Dental Research*, 1995, **74**, 374-380.
82. A. Joiner, N. M. Jones and S. J. Raven, *Advances in Dental Research*, 1995, **9**, 471-476.
83. A. Joiner, *Journal of Dentistry*, 2006, **34**, 412-419.
84. G. K. Stookey, T. A. Burkhard and B. R. Schemehorn, *J Dent Res*, 1982, **61**, 1236-1239.
85. A. Baig, T. He, J. Buisson, L. Sagel, E. Suszcynsky-Meister and D. J. White, *Compend Contin Educ Dent*, 2005, **26**, 47-53.
86. F. Ayad, H. Arcuri, E. Brevilieri, S. Laffi, A. M. Lemos, M. Yoshioka, E. Baines, J. Sheth and W. DeVizio, *Am J Dent*, 1999, **12**, 164-166.
87. D. Hoic, N. Dixit, M. Prencipe, R. Subramanyam, R. Cameron, R. Abdel Malak, L. Lagman, T. Xu and R. Richter, *J Clin Dent*, 2004, **15**, 37-40.
88. A. Kakar, K. Rustogi, Y. P. Zhang, M. E. Petrone, W. DeVizio and H. M. Proskin, *J Clin Dent*, 2004, **15**, 41-45.
89. T. C. Lyon, Jr., W. A. Parker and G. P. Barnes, *J Esthet Dent*, 1991, **3**, 51-53.
90. R. C. Emling, S. Levin, X. Shi, S. Weinberg and S. L. Yankell, *J Clin Dent*, 1992, **3**, 59-65.
91. R. C. Emling, X. Shi and S. L. Yankell, *J Clin Dent*, 1992, **3**, 66-69.

92. I. S. P. Brouchers, *Polymers For Oral Care: Product and Application Guide*, 2003.
93. D. J. White, *J Clin Dent*, 2002, **13**, 1-5.
94. R. P. Shellis, M. Addy and G. D. Rees, *Journal of Dentistry*, 2005, **33**, 313-324.
95. A. Joiner, I. Hopkinson, Y. Deng and S. Westland, *Journal of Dentistry*, 2008, **36, Supplement 1**, 2-7.
96. A. Joiner, C. J. Philpotts, C. Alonso, A. T. Ashcroft and N. J. Sygrove, *J Dent*, 2008, **36**, S8-14.
97. A. Joiner, C. J. Philpotts, A. T. Ashcroft, M. Laucello and A. Salvaderi, *J Dent*, 2008, **36**, S32-37.
98. L. Z. Collins, M. Naeeni and S. M. Platten, *J Dent*, 2008, **36**, S21-25.
99. C. J. Kleber, M. H. Moore and B. J. Nelson, *J Clin Dent*, 1998, **9**, 72-75.
100. C. J. Kleber, M. S. Putt and B. J. Nelson, *J Clin Dent*, 1998, **9**, 16-21.
101. M. S. Putt, M. H. Moore, J. L. Milleman, K. R. Milleman, S. H. Thong, L. M. Vorwerk, A. J. Charig, B. J. Nelson and A. E. Winston, *J Clin Dent*, 2009, **20**, 79-86.
102. T. F. Walsh, A. Rawlinson, D. Wildgoose, I. Marlow, J. Haywood and J. M. Ward, *J Dent*, 2005, **33**, 413-418.
103. D. J. White, *J Clin Dent*, 2001, **12**, 25-29.
104. H. C. Kolb, M. G. Finn and K. B. Sharpless, *Angewandte Chemie International Edition*, 2001, **40**, 2004-2021.
105. R. Huisgen, *In 1,3-Dipolar Cycloaddition Chemistry*, Wiley: New York, 1984.
106. R. Huisgen, B. A. Davis and M. Morikawa, *Angewandte Chemie International Edition in English*, 1968, **7**, 826-827.
107. K. V. Gothelf and K. A. Jørgensen, *Chemical Reviews*, 1998, **98**, 863-910.
108. V. V. Rostovtsev, L. G. Green, V. V. Fokin and K. B. Sharpless, *Angewandte Chemie International Edition*, 2002, **41**, 2596-2599.
109. C. W. Tornøe, C. Christensen and M. Meldal, *The Journal of Organic Chemistry*, 2002, **67**, 3057-3064.
110. L. Zhang, X. Chen, P. Xue, H. H. Y. Sun, I. D. Williams, K. B. Sharpless, V. V. Fokin and G. Jia, *Journal of the American Chemical Society*, 2005, **127**, 15998-15999.

111. F. Himo, T. Lovell, R. Hilgraf, V. V. Rostovtsev, L. Noodleman, K. B. Sharpless and V. V. Fokin, *Journal of the American Chemical Society*, 2004, **127**, 210-216.

112. V. O. Rodionov, V. V. Fokin and M. G. Finn, *Angewandte Chemie International Edition*, 2005, **44**, 2210-2215.

113. T. R. Chan, R. Hilgraf, K. B. Sharpless and V. V. Fokin, *Organic Letters*, 2004, **6**, 2853-2855.

114. V. O. Rodionov, S. I. Presolski, D. D íaz D íaz, V. V. Fokin and M. G. Finn, *Journal of the American Chemical Society*, 2007, **129**, 12705-12712.

115. V. O. Rodionov, S. I. Presolski, S. Gardinier, Y.-H. Lim and M. G. Finn, *Journal of the American Chemical Society*, 2007, **129**, 12696-12704.

116. P. Wu, A. K. Feldman, A. K. Nugent, C. J. Hawker, A. Scheel, B. Voit, J. Pyun, J. M. J. Fr échet, K. B. Sharpless and V. V. Fokin, *Angewandte Chemie International Edition*, 2004, **43**, 3928-3932.

117. J.-F. Lutz, *Angewandte Chemie International Edition*, 2007, **46**, 1018-1025.

118. W. H. Binder and R. Sachsenhofer, *Macromolecular Rapid Communications*, 2008, **29**, 952-981.

119. P. Lundberg, C. J. Hawker, A. Hult and M. Malkoch, *Macromolecular Rapid Communications*, 2008, **29**, 998-1015.

120. M. Meldal, *Macromolecular Rapid Communications*, 2008, **29**, 1016-1051.

121. U. Mansfeld, C. Pietsch, R. Hoogenboom, C. R. Becer and U. S. Schubert, *Polymer Chemistry*, 2010, **1**, 1560-1598.

122. M. Juríček, P. H. J. Kouwer, J. Rehák, J. Sly and A. E. Rowan, *The Journal of Organic Chemistry*, 2008, **74**, 21-25.

123. H. J. Berthold, S. Franke, J. Thiem and T. Schotten, *The Journal of Organic Chemistry*, 2010, **75**, 3859-3862.

124. M. A. Ermeydan, F. Dumoulin, T. V. Basova, D. Bouchu, A. G. Gurek, V. Ahsen and D. Lafont, *New Journal of Chemistry*, 2010, **34**, 1153-1162.

125. I. L ópez-Duarte, M. V. Mart ínez-D íaz, E. Schwartz, M. Koepf, P. H. J. Kouwer, A. E. Rowan, R. J. M. Nolte and T. Torres, *ChemPlusChem*, 2012, **77**, 700-706.

126. S. p. Campidelli, B. Ballesteros, A. Filoramo, D. D. a. Díaz, G. de la Torre, T. s. Torres, G. M. A. Rahman, C. Ehli, D. Kiessling, F. Werner, V. Sgobba, D.

M. Guldi, C. Cioffi, M. Prato and J.-P. Bourgoin, *Journal of the American Chemical Society*, 2008, **130**, 11503-11509.

Chapter 2 Synthesis of Water-Soluble Polymer Containing Ferrocenyl End Group

2.1 Polymers containing ferrocene

Metal-containing polymers are considered as an important category of polymeric materials due to their unusual and attractive properties. Among these materials, polymers with a ferrocene moiety attract a number of academic and industrial researchers due to the significantly different properties including electrical conductivity, magnetic behaviour, thermal stability, and redox reversibility, and nonlinear optical properties.[1] Generally, ferrocene can be appended to the polymer chain in two ways, either side-chain ferrocene-containing polymers with the ferrocene unit as a pendant group, or main chain containing polymers with ferrocene as an integral part of polymer backbone.[2]

The first known metal-containing polymer, poly(vinylferrocene) (PVFc), made from vinyl ferrocene monomer by a radical-initiated polymerization, was reported as early as 1955.[3] During the 1970s and 1980s, some ferrocene-containing acrylate and methacrylate monomers were first prepared by Pittman *et al.*,[4] and polymerised by conventional free radical, cationic and anionic polymerization; however, most of these polymers lacked control of molecular weight.[4-9] Deschenaux and co-workers first reported the synthesis of ferrocene-containing side-chain liquid-crystalline polymers,[10] obtained by grafting vinyl-containing ferrocene monomers onto commercially available polyhydrosiloxanes. Subsequently, the preparation and mesomorphic properties of a similar ferrocene-containing methacrylate monomer (with methacrylate) by free-radical polymerisation (or copolymerisation) were reported by the same group.[6]

Recently, a series of side-chain ferrocene-containing polymers that differ in the linkers between the ferrocene unit and the backbone were prepared via ATRP.[11] The kinetic studies indicated that polymerisation of most monomers (**Figure 2.1.1**) followed a "controlled"/living manner. The polymerisation rates were affected by the

vinyl monomer structures and decreased with an increase of the linker length due to the steric effect of the alkyl linkers. It was also found that methacrylate polymerisation was much faster than acrylate polymerisation under the ATRP condition using CuCl/bipyridine catalytic system. The thermal properties of all homopolymers showed a tuneable glass transition temperature from over 100 to -20 ^{o}C depending on the length of linkers.

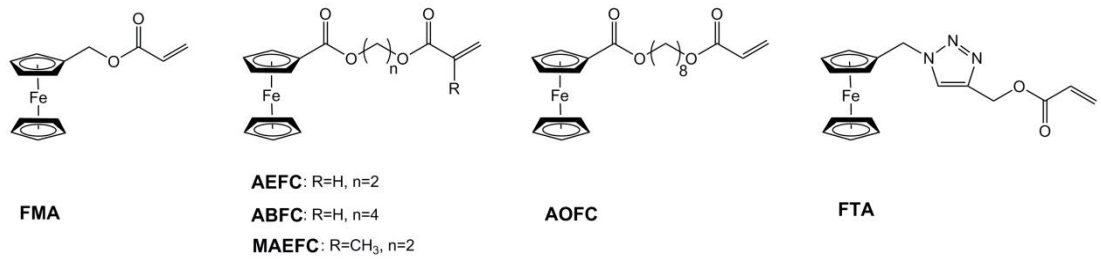

Figure 2.1.1 A series of ferrocene-containing (meth)acrylate monomers prepared by Hardy *et al.*[11]

In early 1990s, Manners and co-workers reported the discovery of the first example of high molecular weight poly(ferrocenylsilanes) by ring opening polymerization (ROP) at high temperatures, possessing a highly unusual main chain comprising ferrocene units and silicon atoms,[12] which opened a new route for synthesis of organometallic polymers. Although the thermal ROP method is very convenient, the molecular weight of the polymer is out of control and the molecular weight distribution is usually broad. It is also difficult to prepare block copolymers due to significant termination. Therefore, alternative routes have been explored by the same group,[13] and it was found that oligo or poly(ferrocenylsilanes) was obtained by addition of various quantities of anionic initiators via anionic ROP.[14, 15]

Later on, the first living polymerisation of a metal-containing monomer to afford polymers with transition metal atoms in the main chain was demonstrated, and the preparation and characterisation of a variety of unprecedented block copolymer structures were also represented. [16] Anionic ROP of silaferrocenophane with different initiators (FcLi, PhLi and *n*-BuLi) was carried out in THF at 25 ^{o}C with different monomer to initiator ratios, followed by quenching of the living polymer

with either H_2O or Me_3SiCl, **Figure 2.1.2**. The block copolymer was synthesised from the living poly(ferrocenylsilane) by ROP of cyclic siloxane $[Me_2SiO]_3$ with addition of Me_3SiCl. Manners group were further demonstrated that by controlling the diblock ratio of poly(ferrocenyldimethylsilane-*b*-dimethylsiloxane) (PFDMS-*b*-PDMS), the organometallic-inorganic copolymers were self-assembled to form cylindrical micelles or nanotubes in selective *n*-alkane solvents. [17-20]

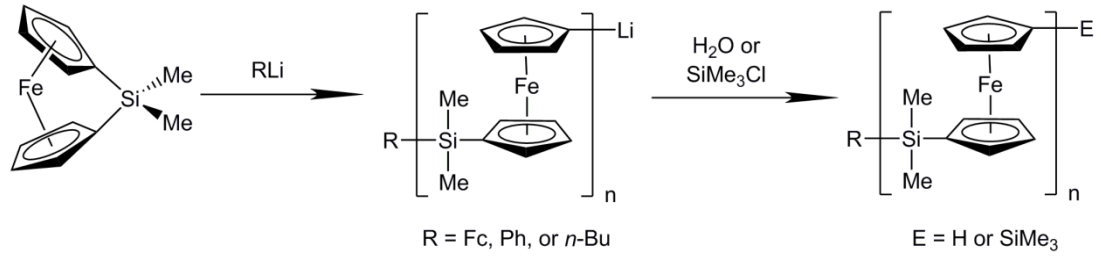

Figure 2.1.2 Anionic ROP of silaferrocenophane with different initiators[16]

The incorporation of a ferrocenyl moiety into the polymer chain ends has been first reported by Zhou *et al.* in 2009.[21] Two novel RAFT agents, (ferrocen-1-yl)ethyl benzodithioate (FEB) bearing ferrocenyl moiety in the R group and benzyl ferrocenecarbodithioxylate (BFEC) bearing ferrocenyl moiety in the Z group, were designed and synthesised (**Figure 2.1.3**) for controlled polymerisation of styrene (PS). The electrochemical behaviours of the polymers were similar to that of ferrocene, and the stability of thiocarbonyl-thio group in common organic solvents were also investigated. The result showed that FEB-PS had better stability than BFEC-PS, e.g. FEB-PS was little affected according UV-Vis analysis but BFEC-PS was affected at different degree by some organic solvents, and the stability was in the order of CH_2Cl_2 > THF > acetone > $CHCl_3$ > DMF.

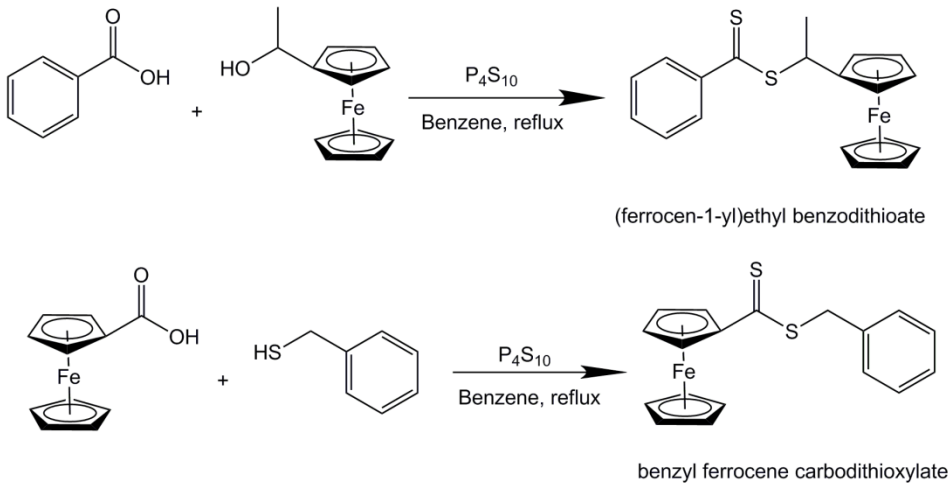

Figure 2.1.3 Synthetic routes of two novel RAFT agents containing ferrocene group[21]

More recently, the first ferrocene-containing epoxide monomer, ferrocenyl glycidyl ether (fcGE), was introduced by Tonhauser and co-workers.[22] The monomer was homo-polymerised and also copolymerised with ethylene oxide (EO) via anionic ROP with varying molecular weights, **Figure 2.1.4**, which lead to electroactive, water-soluble, and thermoresponsive poly(ethylene glycol) (PEG) derived copolyethers. All water-soluble copolyethers with ferrocene side chains revealed a lower critical solution temperature (LCST) in the range 7.2 – 82.2 ^{o}C, which was further tuneable by oxidation/reduction of ferrocene demonstrated by cyclic voltammetry. Moreover, the copolymers were evaluated for potential biomedical application on a human cervical cancer cell line (HeLa), exhibiting good biocompatibility in the case of low amounts fcGE incorporated (below 5%), which were promising for novel redox sensors.

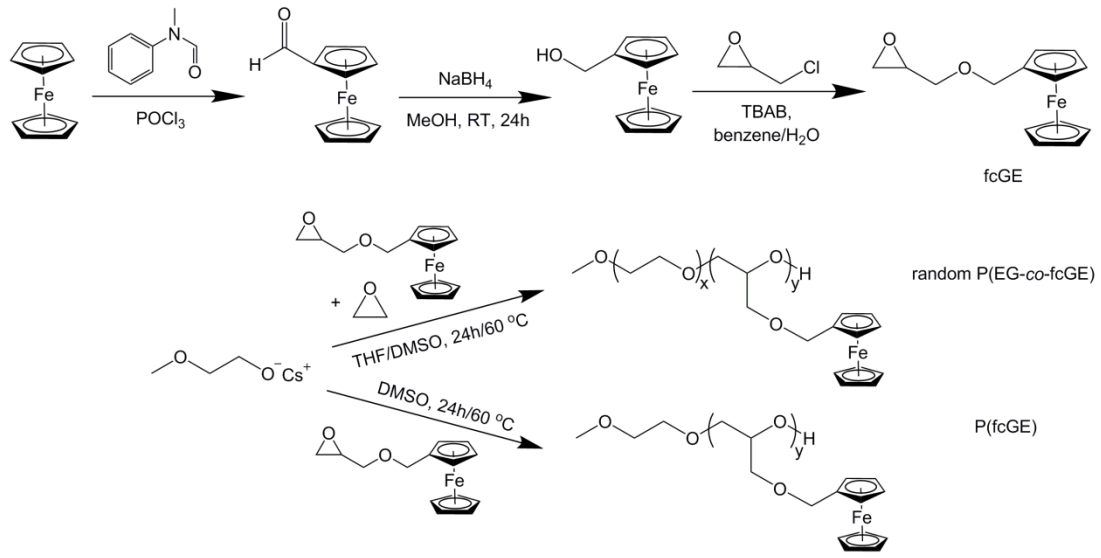

Figure 2.1.4 Synthesis of epoxide monomer ferrocenyl glycidyl ether (fcGE), and of poly(ferrcenyl glycidyl ether) and poly(ethylene glycol-co-ferrocenyl glycidyl ether) by anionic ROP[22]

2.2 Preparation of poly((meth)acrylic acid) by controlled radical polymerisation

Poly(methacrylic acid) (PMAA) and poly(acrylic acid) (PAA) are polyelectrolytes, in which the degree of ionization is dependent upon the pH and ionic strength of the aqueous media. PAA is virtually undissociated at low pH (pH ≤ 4), whereas a fully charged chain results at pH ≥ 8.[23] Study showed that the interactions of hardness ions with anionic polymers containing different functional groups suggested PAA widely used as scale inhibitor and as dispersant for removal of mineral scales, e.g. $CaCO_3$.[24] Moreover, much interest has been received by the self-assembly of block copolymers containing (meth)acrylic acid segments, due to their feasibility to obtain nanostructured materials and various potential applications in separation technology, controlled drug delivery and release.[25-28] Owing to the successful development in controlled radical polymerisation methods including ATRP, NMP and RAFT, such controlled polymerisation techniques have become key tools for synthesis of complex polymers with well-defined structures.

2.2.1 Direct polymerisations of acrylic acid

Although CRP methods are more tolerant of functional groups and impurities, difficulties were encountered to obtain well-defined homopolymers or copolymers from its direct (co)polymerisation. To the best of my knowledge, only RAFT and NMP have been reported for controlled homo-polymerisation of AA without the need for the use of protecting groups.

Chiefari *et al.* was the first to describe the controlled polymerisation of AA using RAFT in dimethylformamide solution at 60 ^{o}C with slow polymerisation rate (18% yield in 4 hours).[29] Furthermore, Ladavière *et al.* investigated a series of RAFT agents to control the polymerisation in alcohol or water, especially with phenoxyxanthates or with trithiocarbonates.[30] With NMP, Couvreur and co-workers have reported the first example of controlled PAA homopolymers.[31] The polymerisations were performed in 1,4-dioxane solution at 120 ^{o}C, using an alkoxyamine initiator based on the *N*-*tert*-butyl-*N*-(1-diethyl phosphono-2,2-dimethyl propyl) nitroxide, SG1, **Figure 2.2.1**.

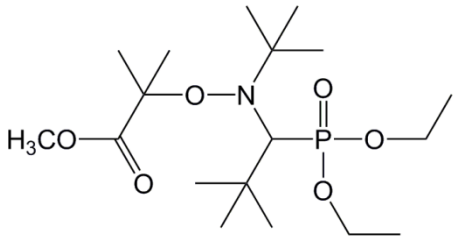

Figure 2.2.1 Structure of SG1-based alkoxyamine initiator[31]

ATRP was even less successful for controlled (co)polymerisation of acrylic and methacrylic acid based monomers, due to the rapid reaction between monomers with the metal complexes.[32] Armes *et al.* reported the first example of the polymerisation of an acidic monomer, sodium methacrylate directly via ATRP in aqueous media, using CuBr/2,2'-bipyridine catalyst with a poly(ethylene oxide) (PEO)-based macroinitiator.[33] The resulting copolymers revealed that the choice of initiator and pH is critical for successful ATRP, and the optimum pH lies between 8 and 9. It was concluded that there appears to a balance between reduced propagation at high pH and competing protonation of the ligand at low pH.

2.2.2 Polymerisations from protected monomers

Due to the limitations of direct controlled polymerisation of (meth)acrylic acid monomer, protected monomers are still widely used to obtain well-defined polymers with (meth)acrylic acid segments. Protected monomers include *tert*-butyl (meth)acrylate (*t*Bu(M)A), trimethylsilyl methacrylate (TMSMA), benzyl methacrylate (BzMA), 2-tetrahydropyranyl methacrylate (THPMA), and *p*-nitrophenyl methacrylate (PNPMA), which can be successful polymerised by anionic polymerisation,[34-36] group transfer polymerisation,[37, 38] and controlled radical polymerisation[39, 40] with controlled structure and uniform molecular weight distribution. Following acid hydrolysis, thermolysis, or catalytic hydrogenolysis, these masked acid groups liberate their original acid functionality.

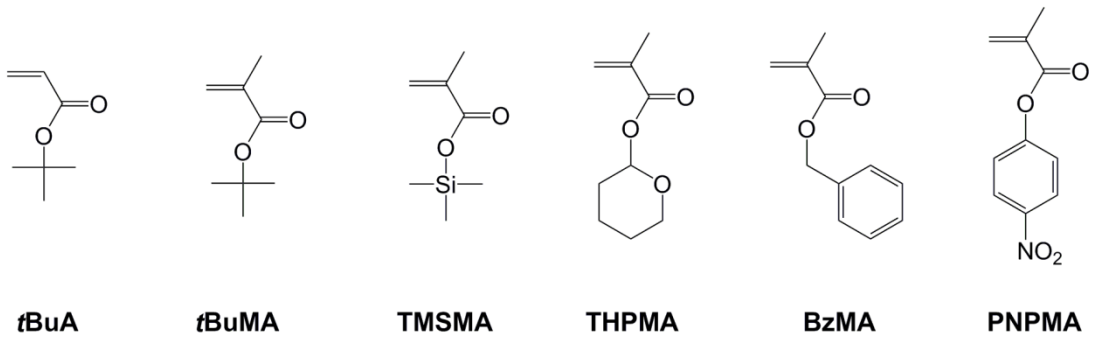

Figure 2.2.2 Structures of protected (meth)acrylic acid monomers

Davis *et al.*[39] reported controlled polymerisation of *t*BuA under ATRP conditions using CuBr/*N,N,N',N'',N''*-pentamethyldiethylenetriamine (PMDETA) as catalyst with both monofunctional and difunctional alkyl halide initiators. Subsequent hydrolysis of the polymer in refluxing dioxane with addition of HCl afforded poly(acrylic acid). Several block copolymers were further prepared by using both monofunctional and difunctional P*t*BuA as macroinitiator, and amphiphilic block copolymers were obtained upon hydrolysis.

Methacrylate monomers containing hemiacetal ester moieties were designed as a new protection technique by Nakane *et al.*.[41] 1-Alkoxyethyl methacrylates were synthesised by acid-catalysed addition of methacrylic acid to alkyl vinyl ethers, and further copolymerised with butyl methacrylate by radical copolymerisation using AIBN. The monomers, 1-ethoxyethyl (meth)acrylate (EE(M)A), were further

proved to be well-synthesised under ATRP conditions, giving polymers with good control of average molar mass and uniform distribution.[42] The hemiacetal ester moieties can be easily transformed into carboxylic acid group with elimination of the vinyl ether by simple thermal treatment without the need for an additional purification step.

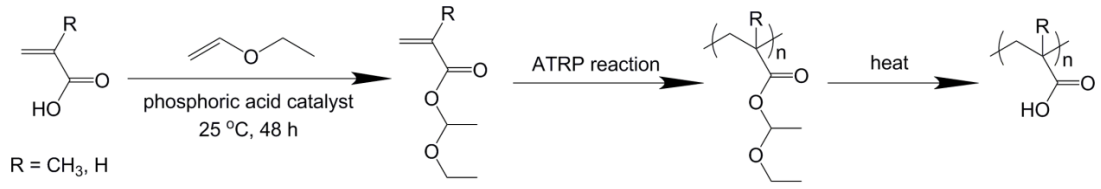

Figure 2.2.3 Reagents and conditions for the synthesis of P(M)AA from PEE(M)A[42]

2.3 Results and discussion

This work focuses on the design and synthesis of water-soluble polymers, poly(acrylic acid) containing ferrocenyl end group, which could be further detected by cyclic voltammetry and used as a scale inhibitor for a potential oil well drilling application. The initial attempt (**Figure 2.3.1**) was based on the preparation of ferrocenyl ester initiator by one-step esterification of 1-(ferrocenyl)ethanol with 2-bromopropionyl bromide. Following the purification by flash chromatography, the product was isolated as an orange solid, and directly used as an initiator for successful polymerisation of *tert*-butyl acrylate (*t*BuA) by SET-LRP. However, it was found that the ester bond present in the ferrocenyl end group was not strong enough to resist acidolysis of the *tert*-butyl group, probably due to the secondary alcohol of ferrocene derivative used for initiator synthesis. Therefore, a further ferrocenyl initiator with an amide linker (**Figure 2.3.2**) was designed for synthesis the same polymer under the same conditions. The desired polymers were obtained after lyophilisation with presence of ferrocenyl moiety.

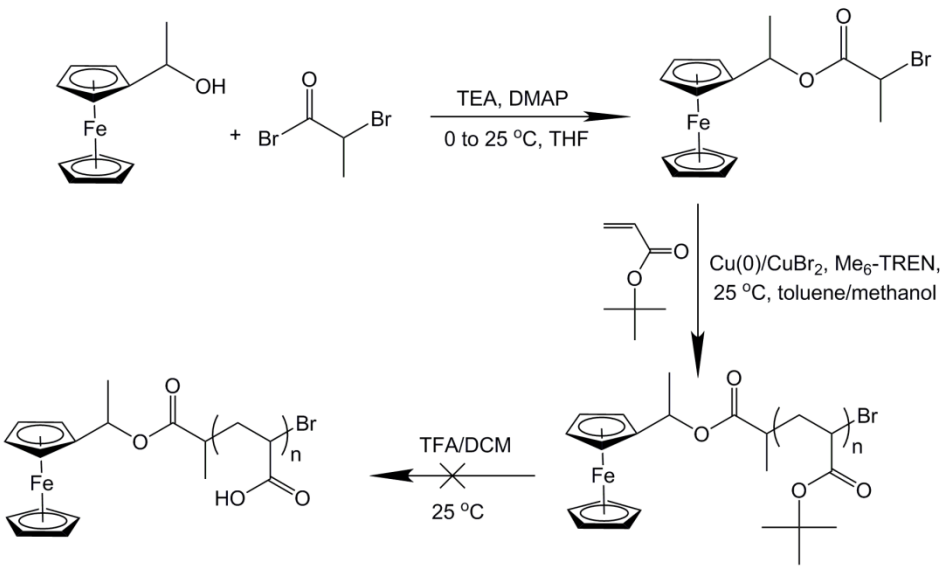

Figure 2.3.1 Overall scheme of synthesis poly(acrylic acid) containing ferrocenyl end group using ferrocenyl ester initiator

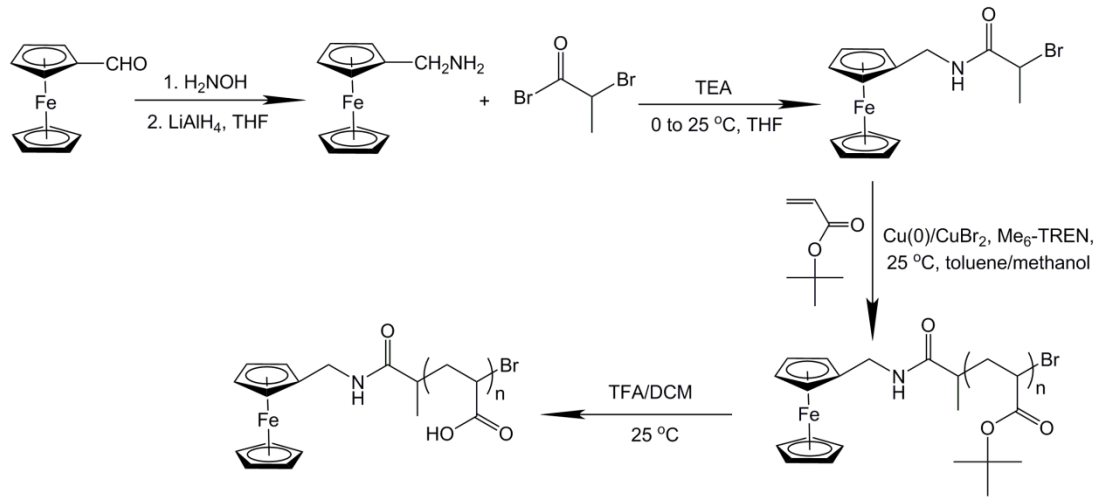

Figure 2.3.2 Overall scheme of synthesis poly(acrylic acid) containing ferrocenyl end group using ferrocenyl amide initiator

2.3.1 Synthesis of ferrocenyl initiator containing amide moiety

The ferrocenyl amide initiator was obtained via a two-step reaction. The ferrocenylmethylamine was first synthesised from ferrocene carboxaldehyde as described in literature.[43] Following by the further amidification with addition of triethylamine (TEA), the final product was purified by flash chromatography and isolated as orange colour crystals in good yield (52%).

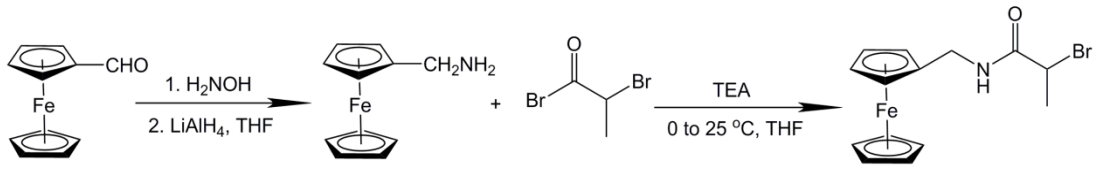

Figure 2.3.3 Synthesis of ferrocenyl amide initiator

Both of ^{1}H and ^{13}C NMR characterisations confirmed the successful synthesis of ferrocenyl amide initiator, **Figure 2.3.4**. It showed that the characteristic chemical shifts of protons and carbons on the cyclopentadiene ring are at δ 4.2 and 68.6 ppm respectively, and the split patterns of the protons on bromopropionate moiety were clearly resolved. The amide carbonyl group can also be found at approximately δ 168 ppm from the ^{13}C NMR spectra.

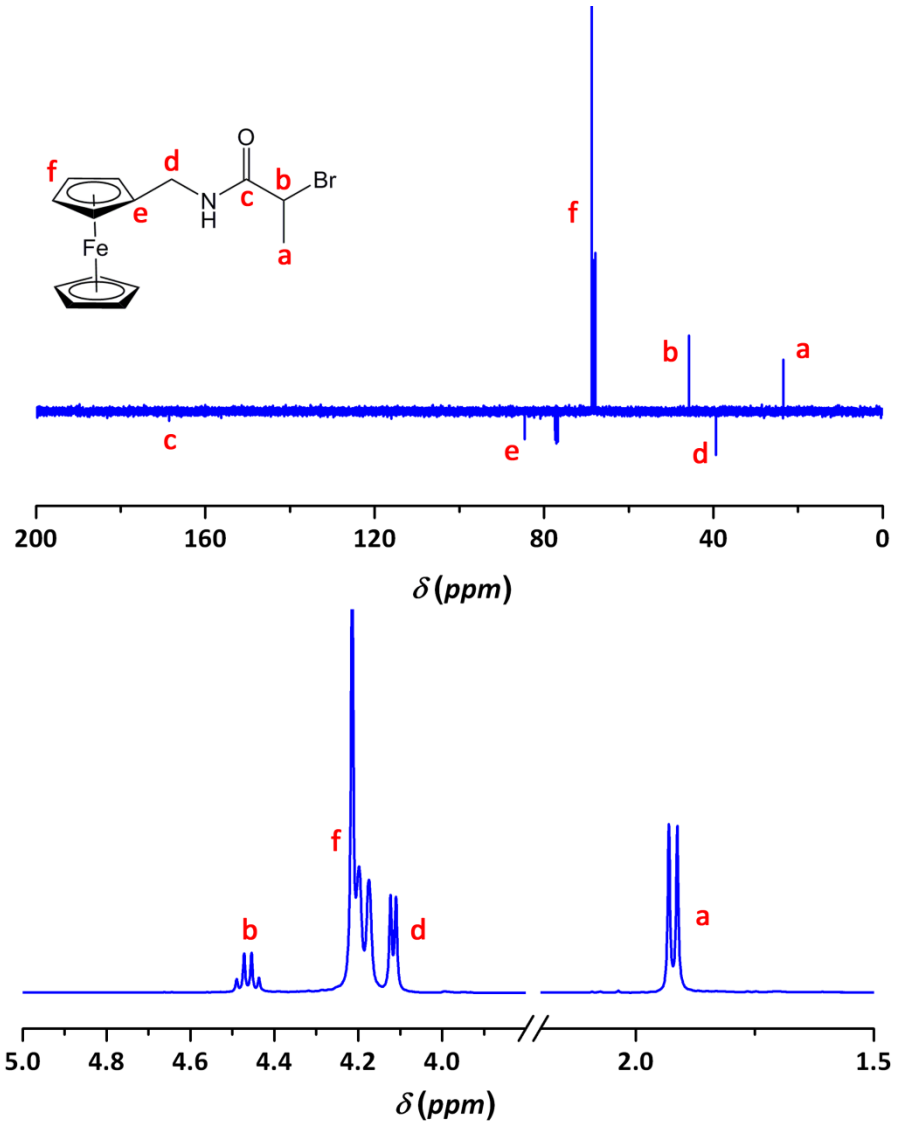

Figure 2.3.4 ^{1}H and ^{13}C NMR characterisations of ferrocenyl amide initiator

Following NMR analysis, the initiator was further analysed by THF-GPC equipped with a photodiode array detector (PDA), **Figure 2.3.5**, which could record the full UV-Vis spectrum at every retention time. The resulting 3D image represented that the distinctive UV-Vis absorption at approximately 440 nm is ascribed to the ferrocene group with the retention time at 18.8 min.

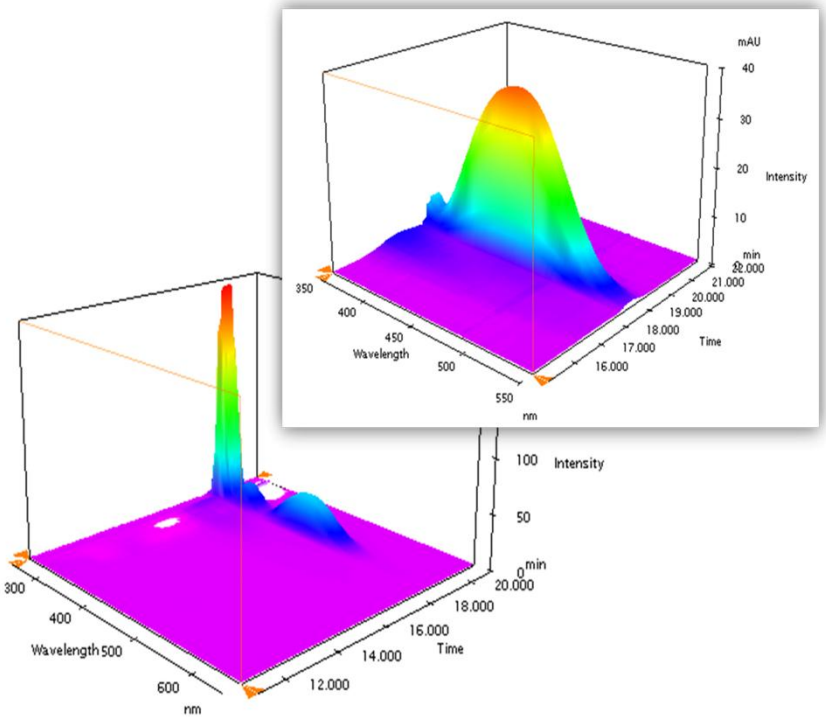

Figure 2.3.5 GPC-PDA 3D image of purified ferrocenyl amide initiator with expansion between 350 and 550 nm region

2.3.2 Synthesis of poly(*tert*-butyl acrylate) using ferrocenyl amide initiator by SET-LRP

It was found that poly(*tert*-butyl acrylate) can be well-synthesised via SET-LRP using Cu(0)/$CuBr_2$ and Me_6-TREN catalytic system in toluene/methanol mixture (14/1, v/v) using ferrocenyl amide initiator.

.

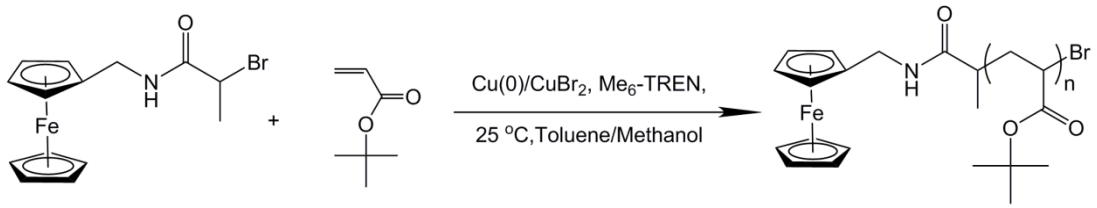

Figure 2.3.6 Synthesis of poly(*tert*-butyl acrylate) using ferrocenyl amide initiator under SET-LRP condition

Kinetics of polymerisation monitored by ^{1}H NMR analysis during 8 hours for ferrocenyl amide tagged P*t*BuA (Targeted DP = 30) is shown in **Figure 2.3.7**. The signals between δ 6.5 and 5.5 ppm resulting from the vinyl protons decreased in intensity in comparison with the internal standard (proton on mesitylene δ 6.8 ppm). Moreover, the shift of the *tert*-butyl protons from δ 1.55 to 1.49 ppm indicated the incorporation of *t*BuA within the polymer chain. It was also noted that the chemical shift of protons on ferrocenyl end group remained at approximately δ 4.18 ppm during the polymerisation. The desired polymer was isolated by precipitation in methanol and water mixture, and the molecular weight of the polymer was estimated by comparing the integration of protons on the ferrocenyl group with those on the *tert*-butyl groups ($M_{n,\,NMR}$ = 5300 g mol^{-1}, DP_{NMR} = 39).

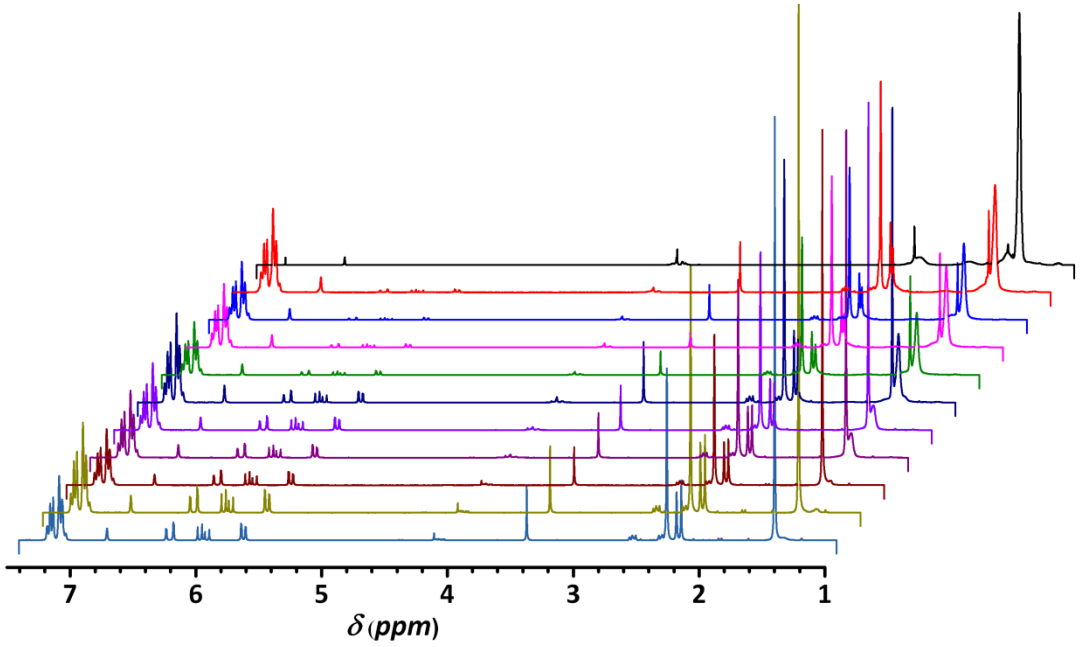

Figure 2.3.7 ^{1}H NMR analysis of ferrocenyl amide tagged P*t*BuA (DP = 30) in 8 hours at different time intervals (light blue to red colour) and final purified polymer (black trace)

GPC aliquots were taken at various times during the polymerisation and subsequently analysed by THF-GPC equipped with both differential refractive index (DRI) and PDA detectors. Monomer conversion was evaluated by NMR over 8 hours and ≥ 90% conversion was achieved, **Figure 2.3.8**-(a). It was also noticed that less than 2 hours induction period was observed, followed by first order kinetics.

Moreover, an increase in molecular weight distribution during the polymerisation was seen in **Figure 2.3.8**-(b), and the dispersity became lower (PDI = 1.14 following precipitation, $M_{n,\,GPC}$ = 6200 g mol^{-1}).

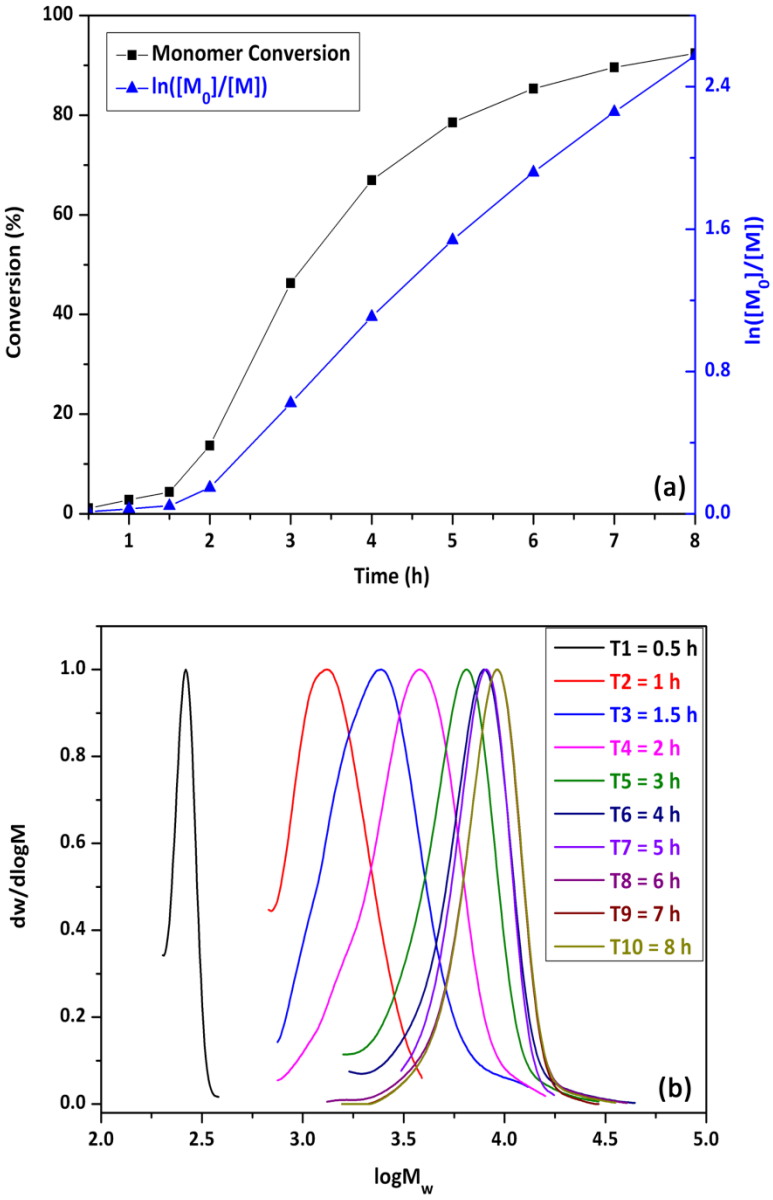

Figure 2.3.8 (a) Schematic linear variation of conversion within 8 hours of polymerisation of *t*BuA (Targeted DP = 30) using ferrocenyl amide initiator; (b) molecular weight distributions of P*t*BuA samples at different time periods

Following the successful polymerisation of P*t*BuA using ferrocenyl amide initiator with targeted DP = 30, ferrocene tagged P*t*BuA with different degrees of

polymerisation (DP = 20 and DP = 50) were synthesised under the same conditions. Aliquots were taken at different time periods during polymerisations and analysed by both NMR and THF-GPC analysis. All ferrocene tagged polymers with different DPs represented a good first order kinetics over 8 hours, **Figure 2.3.9**-(a), and the propagation rate was relatively higher for lower degree of polymerisation (DP = 20) due to the relatively higher concentration of propagating radicals present in the reaction system. During all polymerisation processes, $M_{n,\ GPC}$ increased almost linearly with NMR conversion and PDI became lower, as would be expected for a living radical polymerisations.

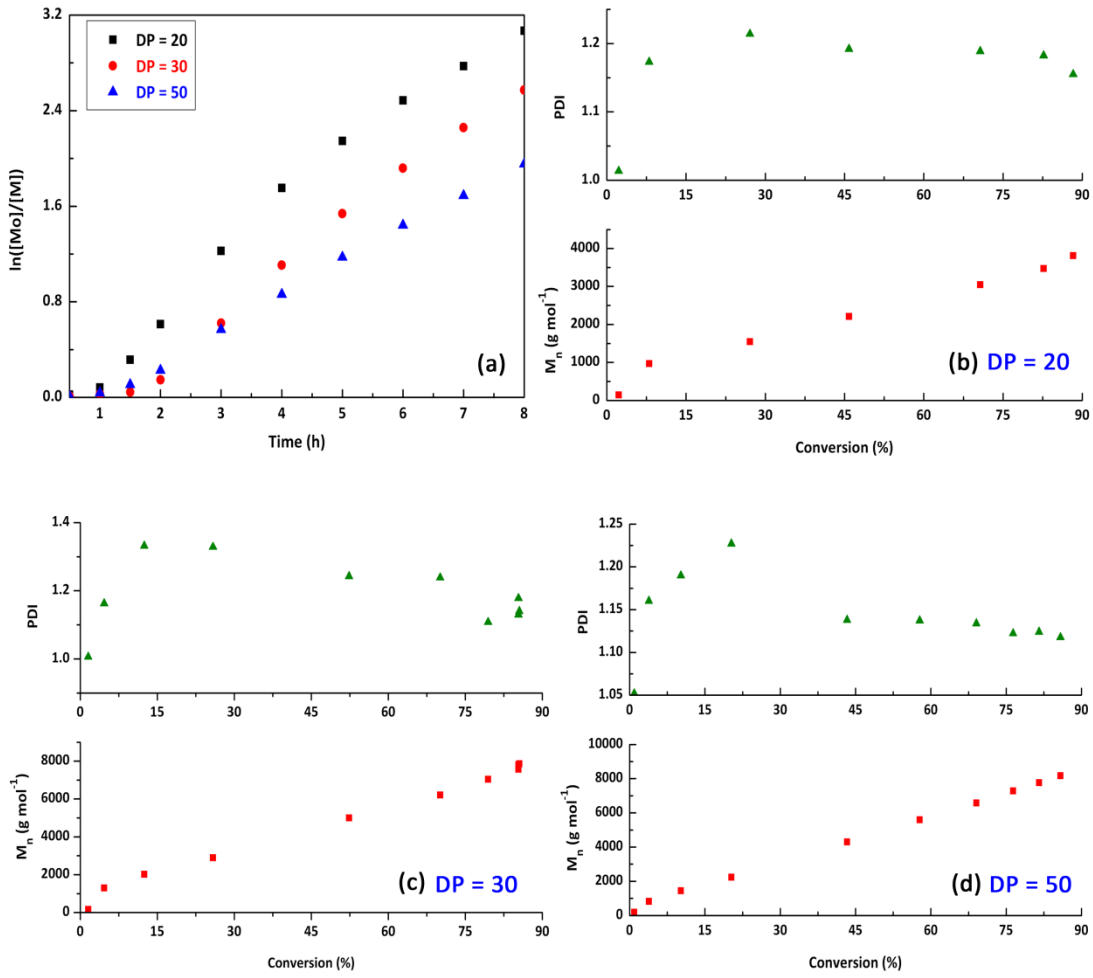

Figure 2.3.9 (a) First order kinetic plots of P*t*BuA with different degrees of polymerisation using a ferrocenyl amide initiator; (b-d) $M_{n,\ GPC}$ and PDI versus NMR conversion for corresponding ferrocenyl amide tagged P*t*BuA

The results from the isolated ferrocene tagged P*t*BuA are summarised in **Table 2.3.1** as obtained from both ^{1}H NMR and GPC analysis. It showed that well-defined polymers with narrow PDIs were obtained for all the cases, and the initiation efficiency was calculated by comparing the targeted DPs with the experimental DPs for each polymer, which was relatively consistent as 76%.

Targeted DP	$M_{n, GPC}$	$M_{n, NMR}$	DP_{NMR}	PDI
20	4300	3700	26	1.12
30	6200	5300	39	1.14
50	9300	8900	67	1.11

Table 2.3.1 Summarised ^{1}H NMR and THF-GPC characterisations of ferrocenyl amide tagged P*t*BuA with different DPs

In order to investigate the incorporation of ferrocenyl moiety into the polymer chain, all kinetics samples were also characterised with THF-GPC coupled with a PDA detector showing 3D images for each state during the polymerisation. **Figure 2.3.10**-(a) represents the UV traces of the purified P*t*BuA (Targeted DP = 30) tagged with ferrocenyl amide end group showing its characteristic UV-Vis absorption at 440 nm. The same UV-Vis spectra were also observed for the other two polymers, as shown in the expanded region between 350 and 600 nm of **Figure 2.3.10**-(b-d). As expected, a shift to earlier retention time and a decrease in UV-Vis intensity can be noticed when the polymer chain becoming longer, which also confirms the incorporation of the ferrocene moiety in each case.

The molecular weight distributions of P*t*BuA performed via RI detector of THF-GPC also revealed the clear increase in the distribution as the polymer chain proceeds longer, **Figure 2.3.11**.

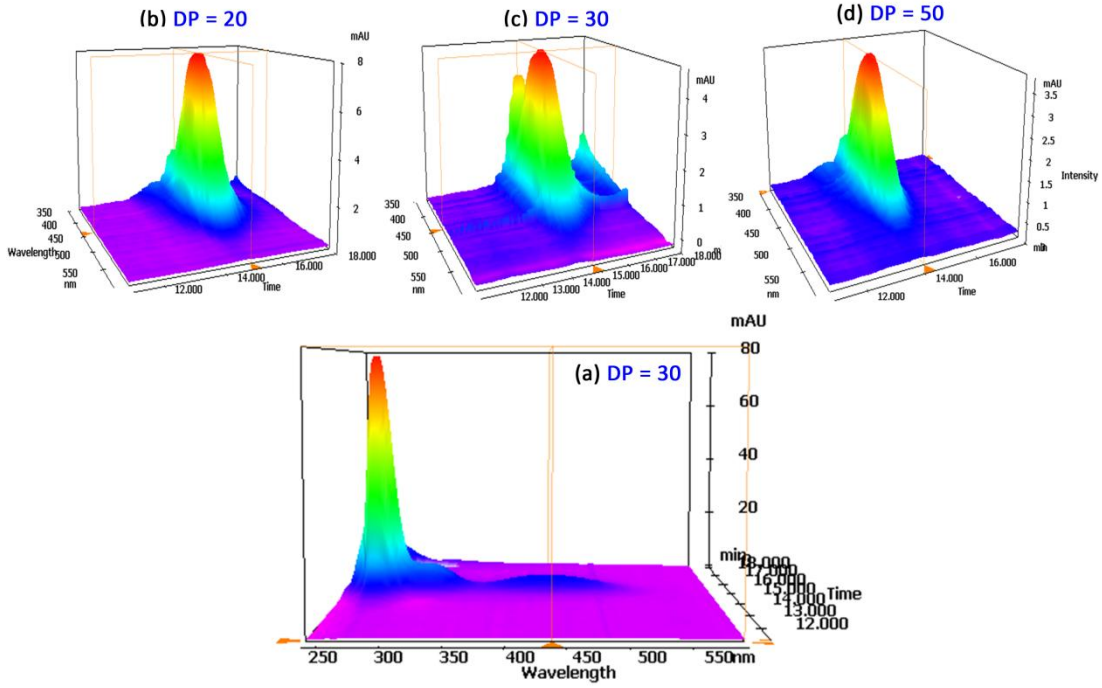

Figure 2.3.10 3D images of purified ferrocenyl amide tagged *t*BuA polymers by THF-GPC equipped with PDA detector: (a) UV-Vis spectra of P*t*BuA (DP = 30); (b-d) expended regions (between 350 and 600 nm) for different DPs

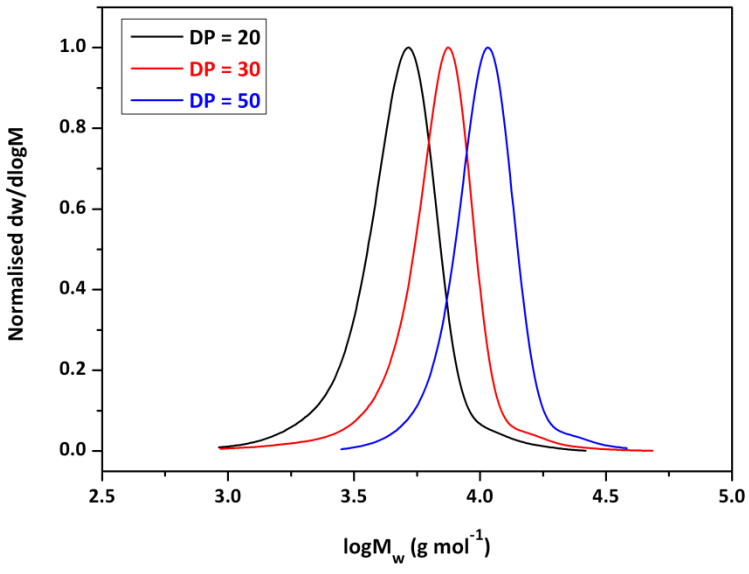

Figure 2.3.11 Molecular weight distributions of P*t*BuA containing ferrocenyl end group with different DPs.

2.3.3 Acidolysis of ferrocenyl amide tagged P*t*BuA

Following synthesis of well-defined P*t*BuAs containing ferrocenyl amide end group with different DPs by SET-LRP, their water-solubility was achieved by acidolysis, **Figure 2.3.12**. The *t*-butyl groups were deprotected by addition of excess of TFA (12 equiv. compared to the amount of *t*-butyl groups) to afford poly(acrylic acid) (PAA).

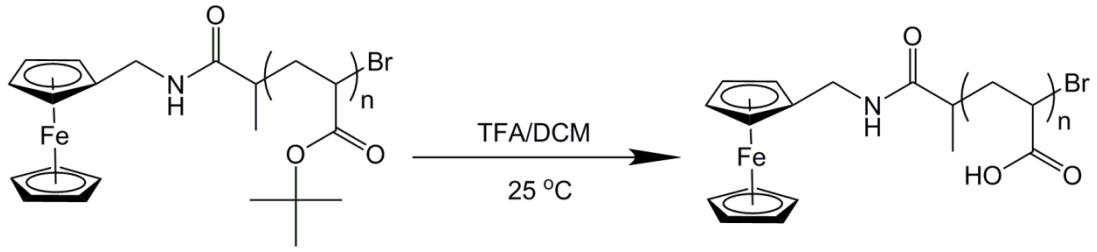

Figure 2.3.12 Acidolysis of ferrocenyl amide tagged P*t*BuA to afford PAA containing ferrocenyl end group

Following the deprotection of all three polymers with different degrees of polymerisation (DP = 20, 30, and 50), their water-solubility was confirmed by NMR analysis in deuterium oxide. ^{1}H NMR analysis of ferrocenyl tagged P*t*BuA (DP = 30) before and after deprotection, **Figure 2.3.13**, represented the disappearance of protons on *t*-butyl groups at δ 1.49 ppm, and also confirmed from the ^{13}C NMR analysis (**Figure 2.3.14**) that the carbons on *t*-butyl groups at δ 28.1 and 80.3 ppm disappeared. Moreover, the signal of carbonyl carbons on *t*-butyl ester groups δ 174.16 ppm for P*t*BuA before deprotection was shifted to δ 178.74 ppm after deprotection presenting the carboxylic acid carbons for PAA. However, it was noticed that evidence of the ferrocenyl group was hard to find either from the ^{1}H or from the ^{13}C NMR spectrum.

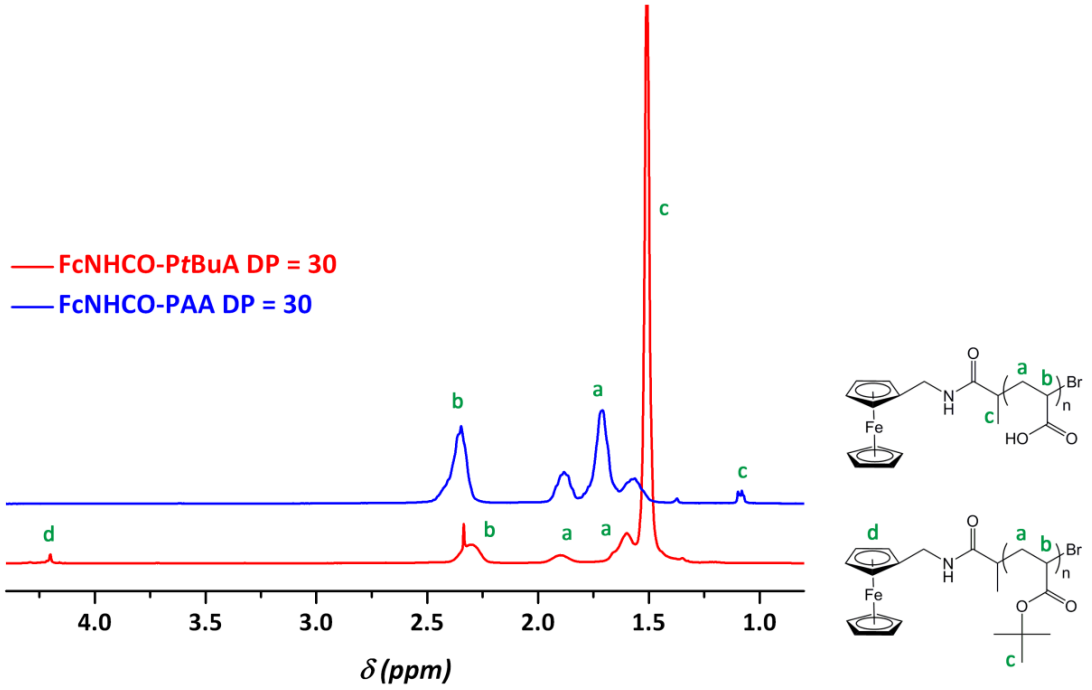

Figure 2.3.13 ^{1}H NMR analysis of ferrocenyl amide tagged P*t*BuA (*$CDCl_3$*, red line) and of ferrocenyl amide tagged PAA (*D_2O*, blue line)

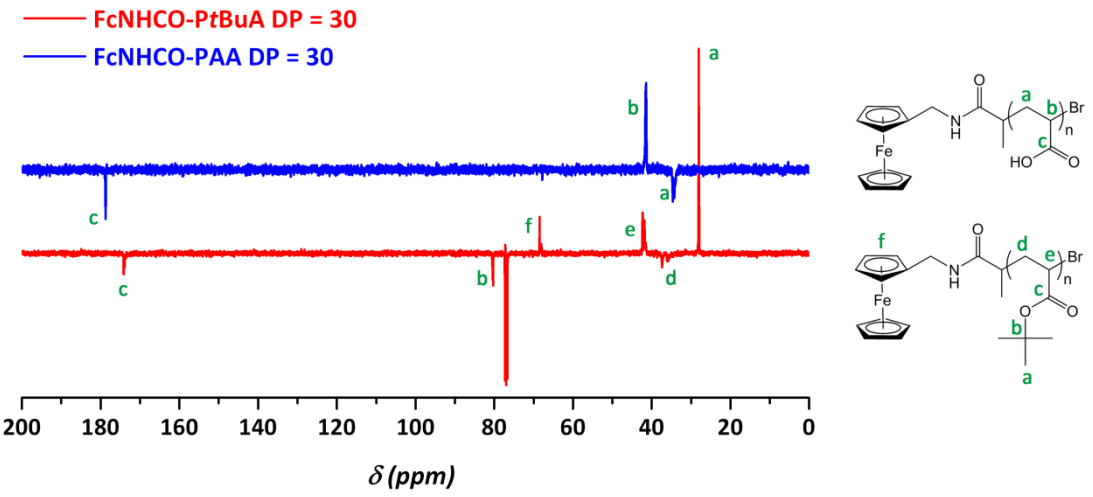

Figure 2.3.14 ^{13}C NMR analysis of ferrocenyl amide tagged P*t*BuA (*$CDCl_3$*, red line) and of ferrocenyl amide tagged PAA (*D_2O*, blue line)

In order to prove the presence of the ferrocene end group, all deprotected polymers were analysed by aqueous GPC equipped with multi-detectors including RI, UV (λ = 440 nm) and Viscometer. The RI chromatograms (**Figure 2.3.15**) from all lyophilized acrylic acid polymers illustrated a shift to earlier retention time with increasing the polymer chain, as expected. Each polymer was then monitored by multi-detector followed by overlapping the chromatograms obtained, **Figure 2.3.16**. It can be observed that both of chromatograms from RI and Viscometer were well-overlapped representing a uniformed distribution for every polymer (from DP = 20 to 50), and the peaks from UV detector with low intensity at 440 nm confirmed the presence of ferrocene group at the polymer chain end.

However, the UV traces was partially overlapped with chromatograms from RI and Viscometer showing significant shoulder peaks at earlier retention time for each case with unknown reasons, **Figure 2.3.16-**(a-c). It was also noticed that the shoulder peak was becoming less intense with increasing the hydrodynamic volume of the polymer; therefore, we assumed that this phenomenon may be due to the hydrophobicity of the ferrocenyl end group which has more effect on the lower DP of the hydrophilic polymer. It was proved by synthesis of longer chain of poly(acrylic acid) containing ferrocene end (DP = 100) as previously described. As shown in **Figure 2.3.16-**(d), the chromatogram from the UV detector was better overlapped with those from RI and Viscometer with insignificant high molecular weight shoulder.

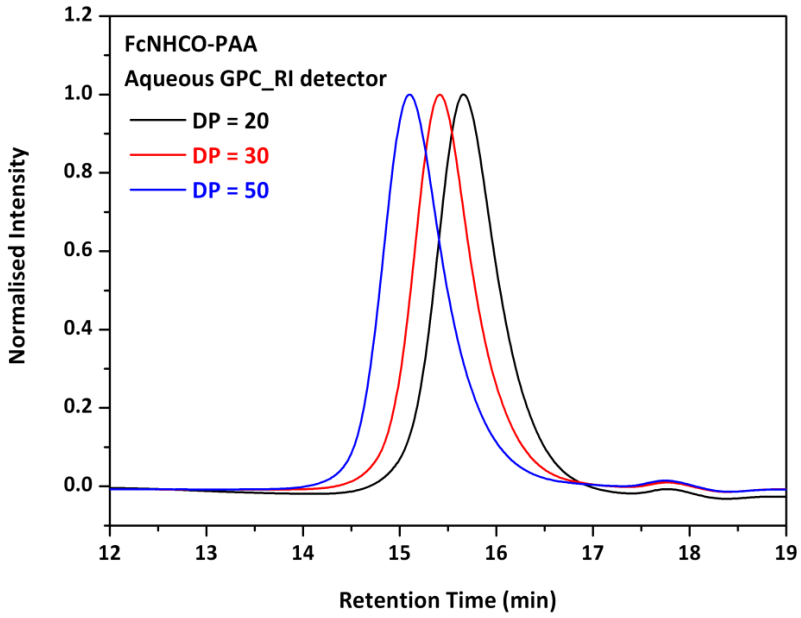

Figure 2.3.15 Aqueous GPC analysis of ferrocenyl tagged poly(acrylic acid) with different degrees of polymerisation by RI detector.

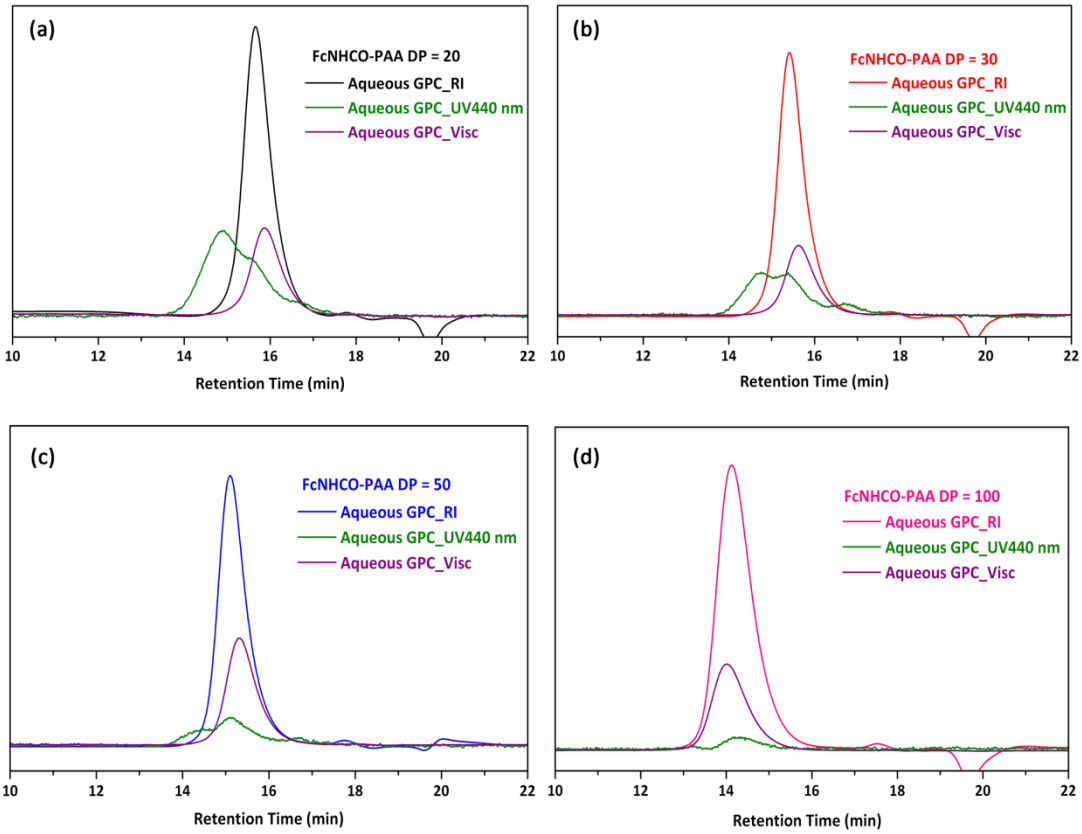

Figure 2.3.16 Aqueous GPC analysis of ferrocenyl tagged PAA with different DPs (DP = 20, 30, 50 and 100) via multi-detector (RI, UV and Viscometer)

The summary from ^{1}H NMR and aqueous GPC analysis of PAA containing ferrocene end group (**Table 2.3.2**) showed a decrease in molecular weight by both characterisations compared with that obtained before deprotection. Moreover, the polymers were becoming more uniform with increasing the polymer chain (DP = 100, PDI = 1.21). The images (**Figure 2.3.17**) exhibited the golden colour of the ferrocene tagged P*t*BuA with different DPs before deprotection, and became less coloured PAA containing ferrocene end group with increasing DPs after deprotection. However, this may suggest that the ferrocenyl end was partially cleaved during acidolysis.

Targeted DP	$M_{n, GPC}$	$M_{n, NMR}$	DP_{NMR}	PDI
20	2700	2200	26	1.65
30	4400	3200	39	1.44
50	7600	5200	67	1.3
100	11,100	8300	110	1.21

Table 2.3.2 Summarised ^{1}H NMR (D_2O) and aqueous GPC characterisations of PAA containing ferrocenyl end group with different DPs

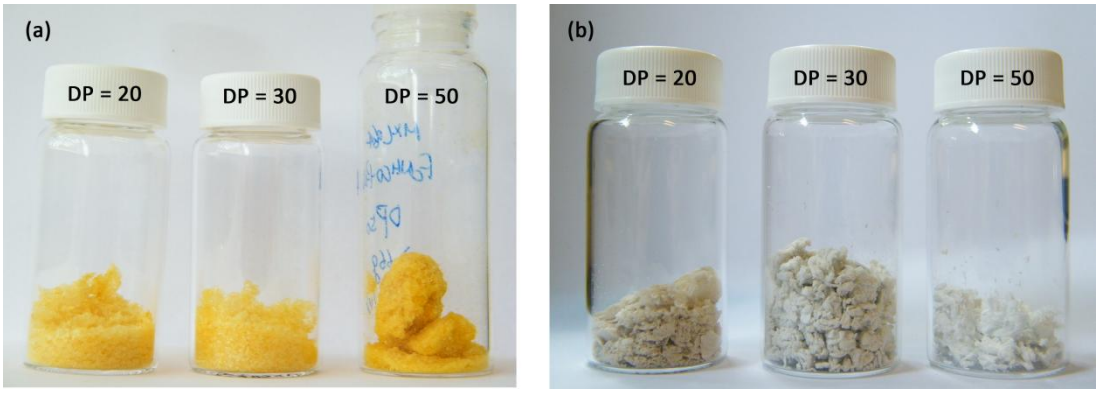

Figure 2.3.17 (a) Images of ferrocenyl tagged P*t*BuA with different DPs before deprotection; (b) images of the obtained ferrocenyl tagged PAA after deprotection

2.4 Conclusions

This chapter has involved the post-polymerisation of poly(acrylic acid)s containing ferrocene end group via preparation of poly(*tert*-butyl acrylate) using a ferrocene amide initiator with different degrees of polymerisation under SET-LRP condition followed by acidolysis.

The ferrocene functionalised initiator was successfully made and used to polymerise *t*BuA using Cu(0)/Cu(II)Br/Me_6-TREN catalytic system in toluene and methanol mixture. It was demonstrated that all polymerisation processes followed first order kinetics, and relatively uniform polymers (PDI $\leq$ 1.15) with different degrees of polymerisation were obtained. The incorporation of the ferrocene end group was monitored by ^{1}H NMR and confirmed by THF-GPC coupled with PDA detector in all cases. The GPC traces from RI detector represented a clear increase in molecular weight distribution with increasing the polymer chain length. The initiator efficiency was estimated as 76% by comparing the targeted DP with the experimental DP.

Following the deprotection of *tert*-butyl groups under acidic conditions, the obtained poly(acrylic acid)s were confirmed by ^{1}H and ^{13}C NMR in deuterium oxide showing the disappearance of *tert*-butyl groups; however, the ferrocene end group was hardly to be seen from NMR analysis. All polymers were further conducted by aqueous GPC analysis by multi-detector. The chromatograms from RI detector of increasing the polymer chain length showed a shift to earlier retention time. The chromatograms overlapped well in both the RI and Viscometer for each case revealed a uniform molecular weight distribution for each polymer after acidolysis, and the signals from UV detector at λ = 440 nm indicated the presence of the ferrocenyl chain end in each polymer. However, the existing shoulder peak at earlier retention time for each polymer from the UV chromatogram exhibited decreased intensity with increasing the polymer chain, which may be explained by the hydrophobicity of the ferrocene end having more effect on the shorter hydrophilic polymer chain. This hypothesis was proved by synthesis of longer poly(acrylic acid) containing ferrocene end (DP = 100) by the same method, representing better overlapped chromatograms from all three detectors.

The summarised results showed a reasonable decrease in molecular weight by both of ^{1}H NMR and aqueous GPC analysis. The polymers appeared less coloured, and the dispersities of polymer samples also revealed a narrower distribution with increasing the polymer chain length. The ferrocenyl tagged poly(acrylic acid)s were designed and used as scale inhibitors for potential oil well drilling application.

2.5 Experimental

Reagents and Conditions

Copper wire (diameter = 1.25 mm) was activated by washing in 35% hydrochloric acid for 15 min, and exhaustively rinsed with MilliQ water and dried under nitrogen. Copper(I) bromide (Aldrich, 98%) was purified according to the method of Keller and Wycoff,[45] and Me_6-TREN was synthesised according to literature procedures[46] and stores under nitrogen prior to use. All the other reagents and solvents were obtained at the highest purity available from Sigma-Aldrich and used without further purification unless otherwise stated. All reactions were carried out using standard Schlenk techniques under an inert atmosphere of nitrogen, unless otherwise stated. TLC performed using pre-coated silica gel 60 F254 and developed in the solvent system indicated. Compounds were visualized by use of UV light (254 or 302 nm) or a basic solution (10 % w/w K_2CO_3 in water) of $KMnO_4$. Merck 60 (230 - 400 mesh) silica gel was used for column chromatography.

Instrumentals and analysis

Nuclear Magnetic Resonance

NMR spectra were obtained on Bruker DPX-300, Bruker DPX-400 and Bruker DRX-500 spectrometers. All chemical shifts are reported in ppm (δ) relative to tetramethylsilane, referenced to the chemical shifts of residual solvent resonance (^1H and ^{13}C). The following abbreviations were used to explain the multiplicities: s = singlet, d = doublet, dd = doublet of doublets, t = triplet, td = triplet of doublets, m = multiplet.

Fourier Transform Infra-Red (FTIR) spectrometry

Infrared absorption spectra were recorder on a Bruker VECTOR-22 FTIR spectrometer using a Golden Gate diamond attenuated total reflection (ATR) cell.

Gel Permeation Chromatography (GPC) Analysis

GPC analysis was performed based on solubility of the polymer or conjugated and on the available detectors of each system.

Tetrahydrofuran

GPC was performed on a Varian 390-LC MDS system equipped with a PL-AS RT/MT autosampler, a PL-gel 3 μm (50 x 7.5 mm) guard column, two PL-gel 5 μm (300 x 7.5 mm) mixed-D columns equipped with a differential refractive index and Shimadzu SPD-M20A diode array detectors, using THF with 2% TEA as the eluent with a flow rate of 1.0 mL min^{-1}. Narrow molecular weight standards of both poly(MMA) (between 200 and 467,400 g mol^{-1}) and polystyrene (between 162 and 24,600 g mol^{-1}) were used to calibrate the SEC and data fitted with a 3rd order polynomial.

Aqueous system

GPC was performed on a Varian 390-LC MDS system equipped with a PL-AS RT/MT autosampler, a PL aquagel-OH 8 μm (50 x 7.5 mm) guard column, two PL aquagel-OH 8 μm (300 x 7.5 mm) mixed-H columns equipped with ultraviolet and differential refractive index detectors, using pH 8.2 phosphate buffer as the eluent with a flow rate of 1.0 mL min^{-1}. Narrow molecular weight standard of PEG (between 110 and 458,500 g mol^{-1}) was used to calibrate the SEC and data fitted with a 3rd order polynomial.

***N*-Methylferrocene-2-bromopropionamide**

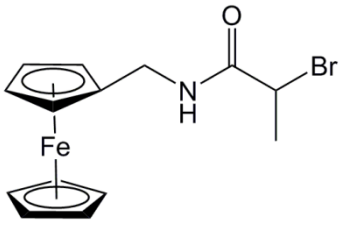

1-(Ferrocenylmethylamide) [43, 44] (2.164 g, 8.69 mmol) was dissolved in 40 mL of anhydrous tetrahydrofuran, followed by addition of distilled triethylamine (4.2 mL, 31.55 mmol) under nitrogen and the reaction mixture was cooled in an ice-water bath. A solution of 2-bromopropionyl bromide (1.58 mL, 15.08 mmol) in 20 mL of

dry tetrahydrofuran was slowly added drop-wise at 0 ℃ upon stirring. At the end of the addition, the flask was warmed to ambient temperature and stirred overnight. After filtration and concentration, the reaction mixture is redissolved in dichloromethane, washed with saturated aqueous $NaHCO_3$ solution (3 x 50 mL), water (3 x 50 mL). The combined organic layers were dried over $MgSO_4$, filtered, and concentrated under vacuum. The product was purified by silica column chromatography (SiO_2, hexane/ethyl acetate: 9/1) to afford a yellow crystalline solid. (Yield: 52 %)

IR (neat): ν = 3296, 3102, 1650, 1533 cm^{-1}.

^{1}H NMR (400.03 MHz, $CDCl_3$, 298 K): δ 4.46 (q, 1H, C*H*Br, J = 7.03 Hz), 4.21 (s, 5H, C*H*Fc), 4.17 (m, 4H, C*H*Fc), 4.12 (d, 2H, CH_2NH, J = 5.27 Hz) 1.93 (d, 3H CH_3Br, J = 7.03 Hz); ^{13}C NMR (100.59 MHz, $CDCl_3$, 298 K): δ 168.50 (NH*C*O), 84.54 (ferrocenyl C connected with CH_2), 68.64 (ferrocenyl C), 45.69 (*C*H_2NH), 39.31 (*C*HBr), 23.4 (*C*H_3Br).

ESI-MS m/z: calcd for $C_{14}H_{16}BrFeNO$ 371.98 $[M+Na]^+$, observed 371.9.

Typical procedure for polymerisation of *t*BuA using ferrocene amide initiator by SET-LRP

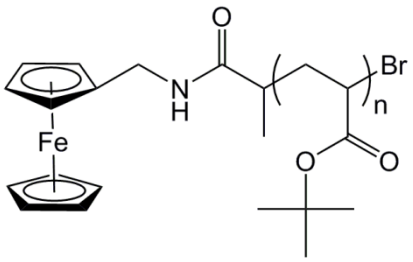

For a typical targeted DP_{30}: 2.56 g of *t*BuA (19.96 mmol) were charged in a Schlenk tube with 0.29 mL of MeOH. The ferrocene amide initiator (0.23 g, 0.67 mmol) dissolved in 4.06 mL toluene and Me_6-TREN (0.18 mL, 0.67 mmol) was injected via a degassed syringe. Mesitylene (0.4 mL) was added as an internal reference in the system. The Schlenk solution was subjected to 3 freeze-pump-thaw cycles and then cannulated under N_2 into a second Schlenk tube, previously evacuated and filled with N_2, containing Cu(0) (0.037 g, 0.58 mmol) and $CuBr_2$ (0.02 g, 0.09 mmol). The temperature was adjusted to 25 ℃ and samples were removed periodically using a

degassed syringe for conversion (t = 0). At the end of the polymerization, the mixture was air bubbled through 2 h, diluted with $CHCl_3$ and passed through a basic alumina column in order to remove copper species. After evaporation the polymer was redissolved in DCM and then precipitated into $MeOH/H_2O$ (1/1, v/v) mixture. After removing the solvents, the polymer sample is redissolved in $CHCl_3$ extracted with water, dried and placed under vacuum to afford golden colour powder. (Yield: 85%)

IR (neat): ν = 2976, 1722 cm^{-1}.

^1H NMR (400.03 MHz, $CDCl_3$, 298 K): δ 4.05-4.3 (m, H on ferrocenyl end group), 2.1-2.35 (br, C*H* of the polymer backbone), 1.80-1.95 (br, meso CH_2 of the polymer backbone), 1.25-1.64 (br, meso and racemo CH_2 of the polymer backbone), 1.25-1.47 [br, (CH_3)$_3$C]; ^{13}C NMR (100.59 MHz, $CDCl_3$, 298 K): δ 174.16 (carbonyl *C*), 80.31 [(CH_3)$_3$*C*], 68.51 (*C* on ferrocenyl end group), 42.31-41.85 (*α* carbon of the polymer backbone), 35.8-37.4 (*β* carbon of the polymer backbone), 28.1-27.9 [(*C*H$_3$)$_3$C].

$M_{n,NMR}$ = 5300 g/mol and $M_{n,GPC}$ = 6200 g/mol, PDI = 1.1

Acidolysis of P*t*BuA containing ferrocene end group to afford ferrocenyl tagged PAA

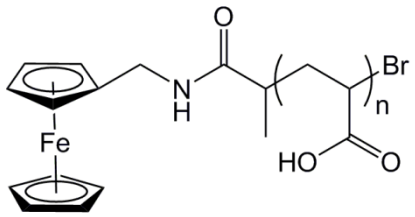

The collected P*t*BuA (0.646 g, ca. 5 mmol of *t*BuA units) was dissolved in 40 mL of DCM for 15 min. Trifluoroacetic acid (TFA, 5 mL, 0.067 mol) was added slowly and the reaction mixture was stirred at 25 ℃ for 24 h. DCM and TFA were then removed under reduced vacuum and the polymer was dissolved in deionised water

with vigorous stirring, followed by dialysis in water for three days and lyophilised. (Yield: 80%)

Warning: ferrocenyl end may be partially cleaved by this approach.

IR (neat): ν = 2932, 1705, 1241 cm^{-1}.

^{1}H NMR (400.03 MHz, D_2O, 298 K): δ 2.2-2.55 (br, C*H* of the polymer backbone), 2.05-1.45 (br, CH_2 of the polymer backbone); ^{13}C NMR (100.59 MHz, $CDCl_3$, 298 K): δ 178.74 (carboxylic acid *C*), 41.46 (α carbon of the polymer backbone), 34.24 (β carbon of the polymer backbone).

2.6 References

1. P. Nguyen, P. Gomez-Elipe and I. Manners, *Chemical Reviews*, 1999, **99**, 1515-1548.
2. R. D. A. Hudson, *Journal of Organometallic Chemistry*, 2001, **637**, 47-69.
3. F. S. Arimoto and A. C. Haven, *Journal of American Chemical Society*, 1955, **77**, 6295-6297.
4. C. U. Pittman, J. C. Lai, D. P. Vanderpool, M. Good and R. Prado, *Macromolecules*, 1970, **3**, 746-754.
5. C. U. Pittman, R. L. Voges and W. R. Jones, *Macromolecules*, 1971, **4**, 291-297.
6. R. Deschenaux, V. Izvolenski, F. Turpin, D. Guillon and B. Heinrich, *Chemical Communications*, 1996, 439-440.
7. C. U. Pittman, O. E. Ayers, S. P. McManus, J. E. Sheats and C. E. Whitten, *Macromolecules*, 1971, **4**, 360-362.
8. C. U. Pittman, R. L. Voges and W. B. Jones, *Macromolecules*, 1971, **4**, 298-302.
9. M. E. Wright, *Organometallics*, 1990, **6**, 853–856.
10. R. Deschenaux, I. Kosztics, U. Scholten, D. Guillon and M. Ibn-Elhaj, *Journal of Materials Chemistry*, 1994, **4**, 1351-1352.
11. C. G. Hardy, L. Ren, T. C. Tamboue and C. Tang, *Journal of Polymer Science Part A: Polymer Chemistry*, 2011, **49**, 1409-1420.

12. D. A. Foucher, B. Z. Tang and I. Manners, *Journal of the American Chemical Society*, 1992, **114**, 6246-6248.
13. Y. Ni, R. Rulkens and I. Manners, *Journal of the American Chemical Society*, 1996, **118**, 4102-4114.
14. R. Rulkens, A. J. Lough and I. Manners, *Journal of the American Chemical Society*, 1994, **116**, 797-798.
15. R. Rulkens, Y. Ni and I. Manners, *Journal of the American Chemical Society*, 1994, **116**, 12121-12122.
16. Y. Ni, R. Rulkens, J. K. Pudelski and I. Manners, *Macromolecular Rapid Communications*, 1995, **16**, 637-641.
17. J. Massey, K. N. Power, I. Manners and M. A. Winnik, *Journal of the American Chemical Society*, 1998, **120**, 9533-9540.
18. J. A. Massey, K. Temple, L. Cao, Y. Rharbi, J. Raez, M. A. Winnik and I. Manners, *Journal of the American Chemical Society*, 2000, **122**, 11577-11584.
19. J. Raez, R. Barjovanu, J. A. Massey, M. A. Winnik and I. Manners, *Angewandte Chemie International Edition*, 2000, **39**, 3862-3865.
20. J. Raez, I. Manners and M. A. Winnik, *Journal of the American Chemical Society*, 2002, **124**, 10381-10395.
21. N. Zhou, Z. Zhang, J. Zhu, Z. Cheng and X. Zhu, *Macromolecules*, 2009, **42**, 3898-3905.
22. C. Tonhauser, A. Alkan, M. Schömer, C. Dingels, S. Ritz, V. Mailänder, H. Frey and F. R. Wurm, *Macromolecules*, 2013, **46**, 647-655.
23. H. Mori and A. H. E. Müller, *Progress in Polymer Science*, 2003, **28**, 1403-1439.
24. F. L. Buchholz, in *Ullmann's Encyclopedia of Industrial Chemistry*, ed. S. Hawkins, Schulz, G., VCH: Weinheim, Germany, 1992, vol. A21, pp. 143-156.
25. S. Förster and M. Antonietti, *Advanced Materials*, 1998, **10**, 195-217.
26. A. Rösler, G. W. M. Vandermeulen and H.-A. Klok, *Advanced Drug Delivery Reviews*, 2001, **53**, 95-108.
27. S. Förster and T. Plantenberg, *Angewandte Chemie International Edition*, 2002, **41**, 688-714.
28. T. Liu, C. Burger and B. Chu, *Progress in Polymer Science*, 2003, **28**, 5-26.

29. J. Chiefari, Y. K. Chong, F. Ercole, J. Krstina, J. Jeffery, T. P. T. Le, R. T. A. Mayadunne, G. F. Meijs, C. L. Moad, G. Moad, E. Rizzardo and S. H. Thang, *Macromolecules*, 1998, **31**, 5559-5562.
30. C. Ladavière, N. Dörr and J. P. Claverie, *Macromolecules*, 2001, **34**, 5370-5372.
31. L. Couvreur, C. Lefay, J. Belleney, B. Charleux, O. Guerret and S. Magnet, *Macromolecules*, 2003, **36**, 8260-8267.
32. T. E. Patten and K. Matyjaszewski, *Advanced Materials*, 1998, **10**, 901-915.
33. E. J. Ashford, V. Naldi, R. O'Dell, N. C. Billingham and S. P. Armes, *Chemical Communications*, 1999, **0**, 1285-1286.
34. A. H. E. Müller, *Die Makromolekulare Chemie*, 1981, **182**, 2863-2871.
35. A. Leon, B. Vincent and N. Cawdery, *Colloid Polym Sci*, 1994, **272**, 427-432.
36. H. S. Kitayama T, Hironaka Y, Iijima T, Hatada K., *Polym J (Tokyo)*, 1995, **27**, 314-318.
37. M. A. Doherty and A. H. E. Müller, *Die Makromolekulare Chemie*, 1989, **190**, 527-539.
38. S. P. Rannard, N. C. Billingham, S. P. Armes and J. Mykytiuk, *European Polymer Journal*, 1993, **29**, 407-414.
39. K. A. Davis and K. Matyjaszewski, *Macromolecules*, 2000, **33**, 4039-4047.
40. Y. Liu, L. Wang and C. Pan, *Macromolecules*, 1999, **32**, 8301-8305.
41. Y. Nakane, M. Ishidoya and T. Endo, *Journal of Polymer Science Part A: Polymer Chemistry*, 1999, **37**, 609-614.
42. W. Van Camp, F. E. Du Prez and S. A. F. Bon, *Macromolecules*, 2004, **37**, 6673-6675.
43. A. Baramee, A. Coppin, M. Mortuaire, L. Pelinski, S. Tomavo and J. Brocard, *Bioorganic & Medicinal Chemistry*, 2006, **14**, 1294-1302.
44. P. D. Beer and D. K. Smith, *Journal of the Chemical Society-Dalton Transactions*, 1998, 417-423.
45. R. N. Keller and H. D. Wycoff, *Inorg. Synth.*, 1946, 1-4.
46. M. Ciampolini and N. Nardi, *Inorganic Chemistry*, 1966, **5**, 41-44.

Chapter 3 Design and Synthesis of Water-soluble PEGylated (Copper) Phthalocyanines

3.1 Introduction

3.1.1 Sulfonated phthalocyanines

Phthalocyanines bearing sulfonate or sulfonic acid groups are one of the most common anionic substituents to achieve water-solubility, which can be strongly pH-dependent. The synthetic strategy can follow different ways, either by using sulfonated phthalocyanine's precursors, or by sulfonation of the macrocycle itself.

The synthetic precursors of the direct cyclotetramerisation of tetrasulfonated phthalocyanines (**Figure 3.1.1**) are either sulfonated phthalic acid or its corresponding sulfonated phthalic anhydride. The first description of sulfonated phthalocyanines can date from 1952 by Baumann,[1] and precursors can be the sulfonic acid or the sodium salt. However, the method leads to variable, but significant amounts of uncomplexed metal ions. The procedures were then modified by Weber and Busch[2] to limit the metallic impurities by washing with 1N hydrochloric acid saturated with sodium chloride, resulting in highly purified tetrasulfonated phthalocyanines with 80% yield. This template assisted synthesis has been utilized as preparation of a wide range of metalated phthalocyanines. Furthermore, the strategy was either modified to be solvent free,[3] or possible to prepare nitrogen-labelled derivatives via using ^{15}N-urea.[4]

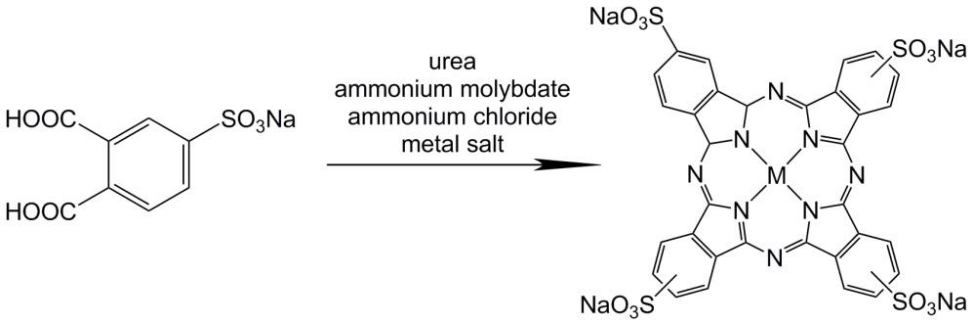

Figure 3.1.1 Weber and Busch's synthesis of tertrasulfonated phthalocyanines[2]

The second widely used approach to synthesise sulfonated derivatives is the sulfonation of the macrocycle itself which is used in a variety of industrial applications. Metalated or metal-free unsubstituted phthalocyanines are sulfonated by treatment with concentrated sulfuric acid (H_2SO_4, 35% SO_3 free) or chlorosulfonic acid at 80 – 140 ^oC. By this way, a mixture of mono-, di-, tri-, and tetrasulfonated phthalocyanines can be obtained. The degree of sulfonation of the phthalocyanines can be determined and products separated by high performance liquid chromatography (HPLC),[5] but the operating parameters must be very tightly controlled. However, capillary electrophoresis (CE) has been found to clearly separate sulfonated phthalocyanine mixtures according to the degree of sulfonation by Schofield.[6] The compounds with the lowest degree of sulfonation have the shortest retention time, and the most highly sulfonated the longest, as would be expected.

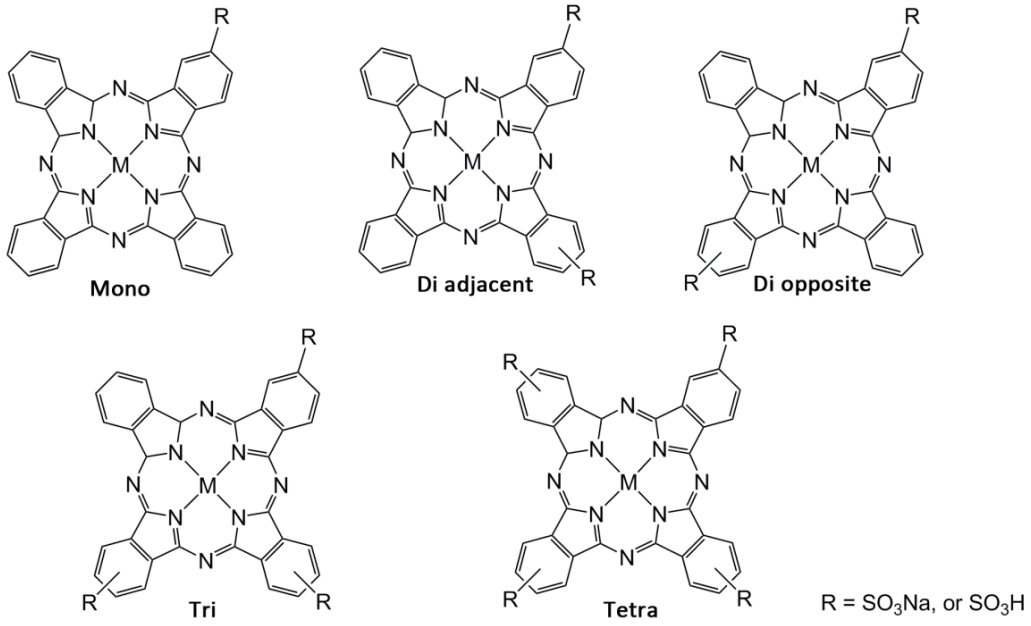

Figure 3.1.2 Mixture of sulfonated phthalocyanines by sulfonation of the macrocycle itself[7]

3.1.2 Polyethylene glycol substituted phthalocyanines

Poly(ethylene glycol) (PEG) substitution is a classical means for derivatisation as this is highly soluble in many and varied solvents and offers quite a flexible synthetic strategy. More importantly, PEG is generally inert offers excellent biocompatibility in biosystems, especially protein adsorption, and PEGylation has proved to be a successful and acceptable approach to drug delivery and therapeutic development.[8] Numerous phthalocyanines bearing PEG chains have been reported with various chain numbers and/or ethyleneglycol units. For some of them reported to be water-soluble, and various aggregation degrees in water.

The first described phthalocyanines (**Figure 3.1.3**) bearing PEG monomethyl ether chains form a series consisting of three octasubstituted unmetallated phthalocyanines, with two, eight, or fifteen ethylene glycol units.[9] These compounds are indeed highly aggregated but nevertheless water-soluble. Their classical synthetic route involves Williamson ether synthesis, followed by nitrile displacement of bromine by CuCN

and converting the phthalonitrile into desired phthalocyanines under an ammonia atmosphere.

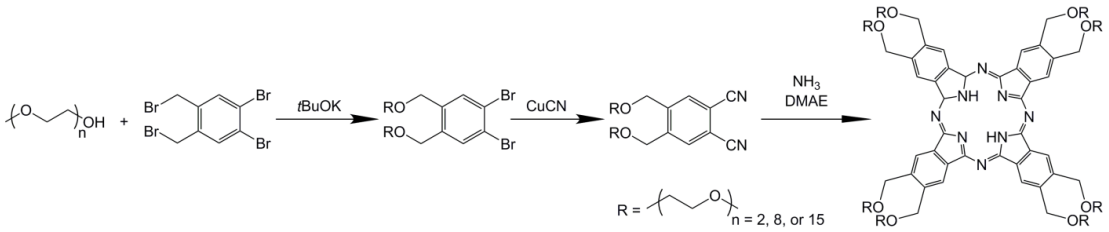

Figure 3.1.3 Synthesis of octasubstituted phthalocyanine[9]

By employing different number of PEG chains and/or various ethylene glycol units, the functionalised *Pcs* complexes can show tuneable structures with a range of properties. McKeown[10] and co-workers first reported *Pcs* substituted by four oligoethyleneoxy side chains that demonstrated both a columnar thermotropic mesophase and a lyotropic mesophase, **Figure 3.1.4**. The starting alcohols, triethylene glycol monomethyl ether and poly(ethyleneoxy) monomethyl ether (M_n = 350 g mol^{-1}) were reacted with 4-nitrophalonitrile via a base-catalyzed nitro-displacement reaction to afford the phthalonitrile precursors, followed by cyclotetramerisation to produce the desired dark green products using lithium pentoxide catalysis in refluxing pentanol. In subsequent studies, they also demonstrated variable liquid crystalline properties of tetra- or octa-PEG chains substituted *Pcs* with different average numbers of oxyethylene units.[11] They further termed these materials as *phthalocyanine-centered poly(oxyethylene)s*. Tuncel *et al*. reported that the presence of hydroxyl groups at the end of the chain can considerably enhance the water-solubility, and the position of the substitutions also has an effect.[12]

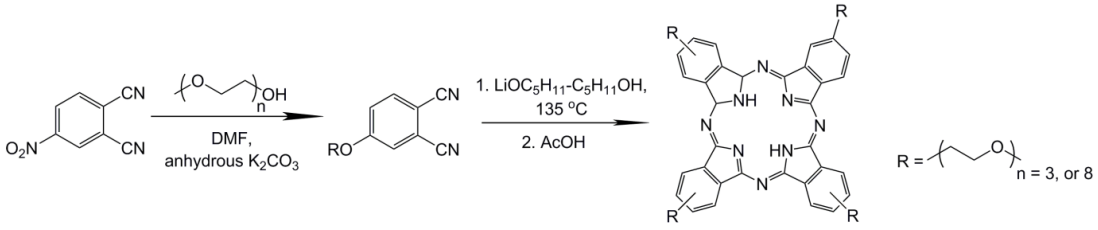

Figure 3.1.4 Synthetic route of *Pcs* substituted by only four methyl-terminated oligoethyleneoxy side-chains[10]

In the biomedical area, *Pcs* have been found to be a promising class of photosensitisers for photodynamic therapy (PDT) due to their high molecular absorption coefficients at higher wavelengths of the visible spectrum ($\varepsilon \approx 10^5$ $M^{-1}cm^{-1}$ at 640 – 710 nm), lack of dark toxicity, and chemical stability. However, due to their aggregation behaviour in aqueous media, these compounds have unfavourable intracellular localization. Therefore, incorporation of a tri- or tetravalent metal atom in the *Pc* core, such as aluminium (III) and silicon (IV), enables axial derivatization, which can improve the solubility in aqueous solution much more by enhanced steric shielding of the *Pc* core.[13, 14] Pc4 (**Figure 3.1.5**),[14-17] an axially substituted Pc that is known as one of the most effective *Pc*-based photosensitisers, localizes intracellularly in mitochondria and has been used in clinical trials.[18]

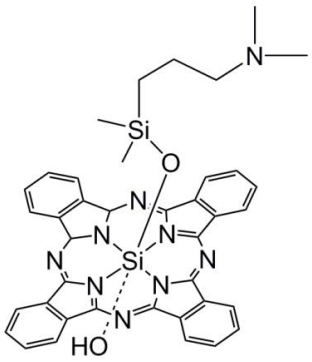

Figure 3.1.5 Structural Formula of Pc4

Highly water-soluble (> 5 mg mL^{-1}) $Si(PEG_{750})_2$*Pc* (**Figure 3.1.6**) was prepared by the substitution of axial chloride of unsubstituted *SiPc* with monomethoxy PEG_{750}.[19] The hydrophilic nature of the PEG chain is the key in providing the satisfactory water solubility as well as preventing the aggregation when substituted in the axial position.

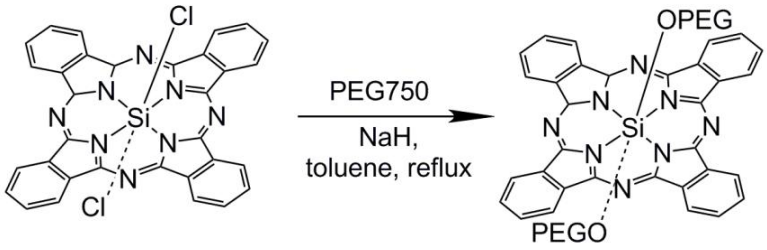

Figure 3.1.6 Synthetic route of axial substituted polyethylene glycol chain of *Si(IV)Pc*[19]

3.2 Results and discussion

3.2.1 Initial PEGylated copper phthalocyanine experiments

Copper phthalocyanines are commonly used in industry as a raw material for producing blue and green pigments. The initial functionalised *CuPc* derivatives were synthesised via an industrial procedure. The commercial available product, *CuPc*, was first treated with chlorosulfuric acid ($ClSO_3H$) and phosphorus trichloride (PCl_3), followed by addition of 2-(2-aminoethyoxy)ethanol yielding hydroxyl terminated *CuPc* derivatives, **Figure 3.2.1**. The final PEGylate *CuPc* complexes were obtained via DCC/EDC coupling reactions after preparation of mono-carboxylic acid terminated PEG monomethyl ether.

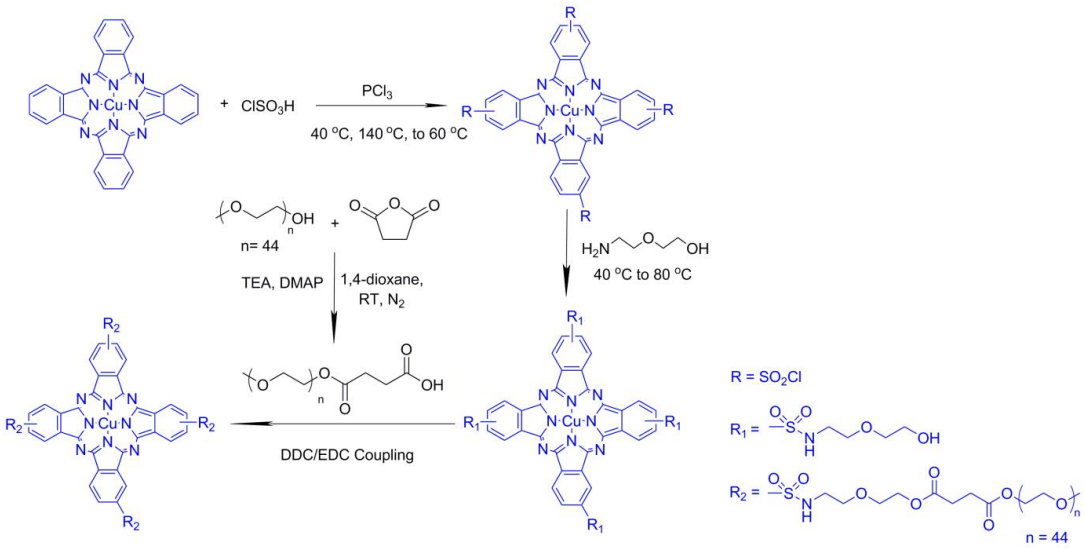

Figure 3.2.1 Synthetic strategy of PEGylated *CuPc* via DCC/EDC coupling reaction

The hydroxyl terminated *CuPc* intermediate has very low solubility in most organic solvents, which makes the isolated product difficult to purify as a tetra-substituted compound; therefore, the ^{1}H NMR analysis was conducted in CD_3OD with low concentration. However, due to the paramagnetic Cu(II) phthalocyanine complexes, the ^{1}H NMR spectra always give rise to complicating effects indicated by a wide chemical shift range and broadened signals, **Figure 3.2.2**, representing the protons on the aminoethyloxy ethanol arm.

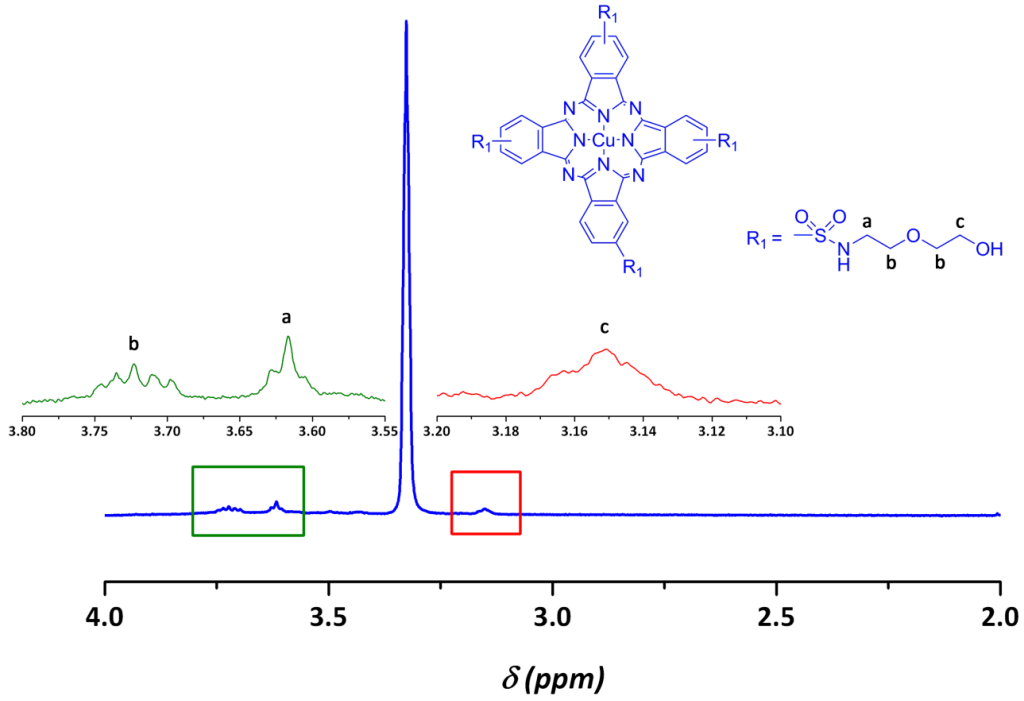

Figure 3.2.2 ^{1}H NMR analysis of hydroxyl terminated *CuPc* derivative

Following the synthesis of functionalised *CuPc*, mono-carboxylic acid terminated PEG monomethyl ether (HOOC-mPEG) was obtained by reacting mPEG (M_n = 2000 g mol^{-1}) with succinic anhydride in anhydrous 1,4-dioxane under nitrogen with addition of TEA and DMAP (**Figure 3.2.3**). The purified polymer was isolated as white powder after precipitation in petroleum ether.

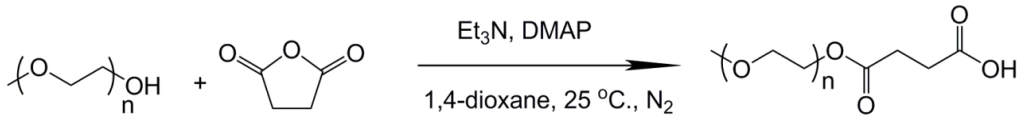

Figure 3.2.3 Reaction scheme of mono-carboxylic acid terminated PEG monomethyl ether

The mono-carboxylic acid terminated PEG monomethyl ether was analysed by MALDI-ToF-MS (**Figure 3.2.4**), and the expected mass increase of the addition of the ring-opening succinic anhydride to the PEG chain was observed. A number of distributions were observed, with predominant peaks corresponding to the sodiated functionalised PEG chain and smaller peaks contributed to the protonated derivative;

however, an minor distribution attributed to the sodiated unfunctionalised PEG chain was also noticed.

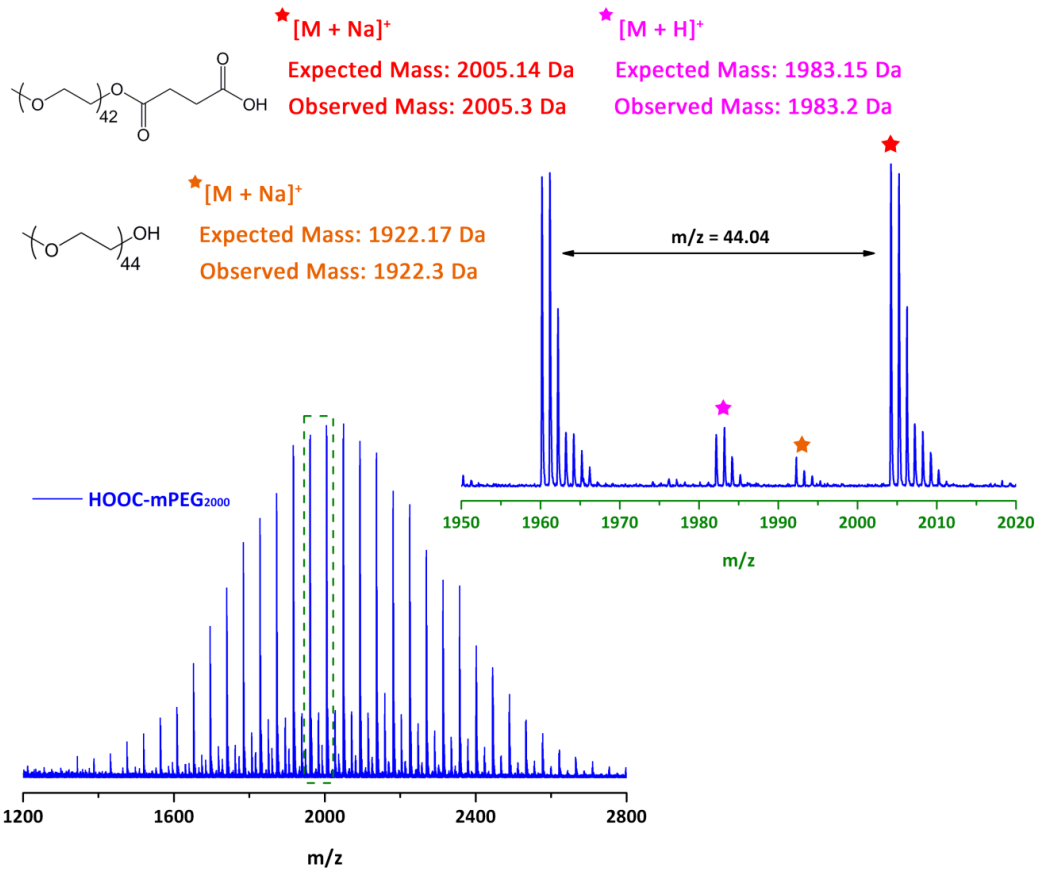

Figure 3.2.4 MALDI-ToF-MS analysis of monocarboxylic acid terminated $mPEG_{2000}$

The subsequent PEGylated *CuPc* complexes were prepared by using either dicyclohexylcarbodiimide (DCC) or *N*-(3-dimethylaminopropyl)-*N*′-ethylcarbodiimide hydrochloride **(**EDC) coupling agent, and 4-pyrrolidinopyridine (PYP) as a catalyst, **Figure 3.2.5**. Moreover, in order to optimise the coupling reaction, the effects of different amount of catalyst and different coupling agents used in the reaction were investigated.

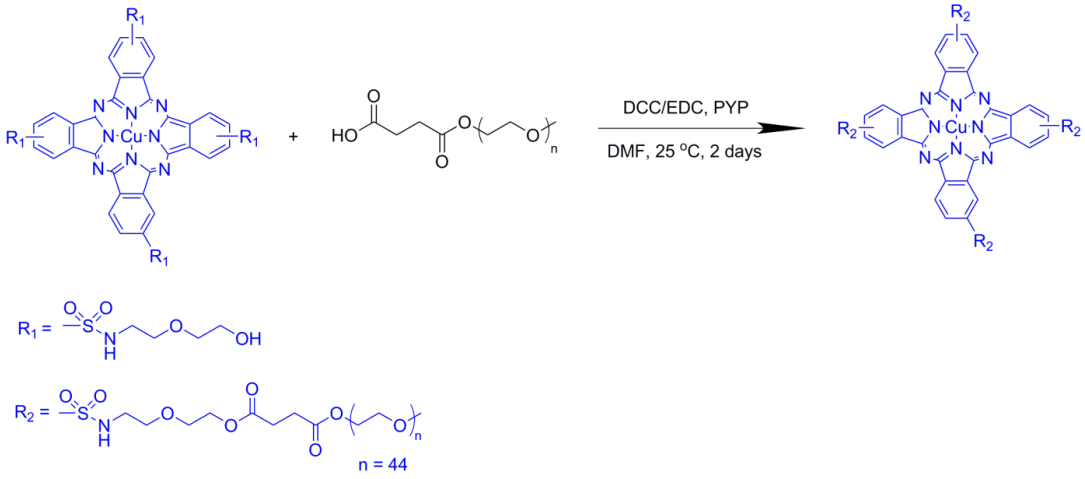

Figure 3.2.5 Reaction route of PEGylated *CuPc* via DCC/EDC coupling

The initial reaction was investigated by using DCC as a coupling agent with addition of different equivalents of PYP catalyst (relevant to the equivalent of *CuPc*) for two days. Samples were taken periodically and analysed by DMF-GPC equipped with UV detector (λ = 672 nm) to monitor the efficiency of the coupling reaction. It can be found that the reaction proceeded faster with lower amount of catalyst by comparing the same time period after GPC analysis, as shown in the chromatograms (**Figure 3.2.6**). It should also mention that there was little difference between two and eight hours, probably due to the presence of water in the reaction.

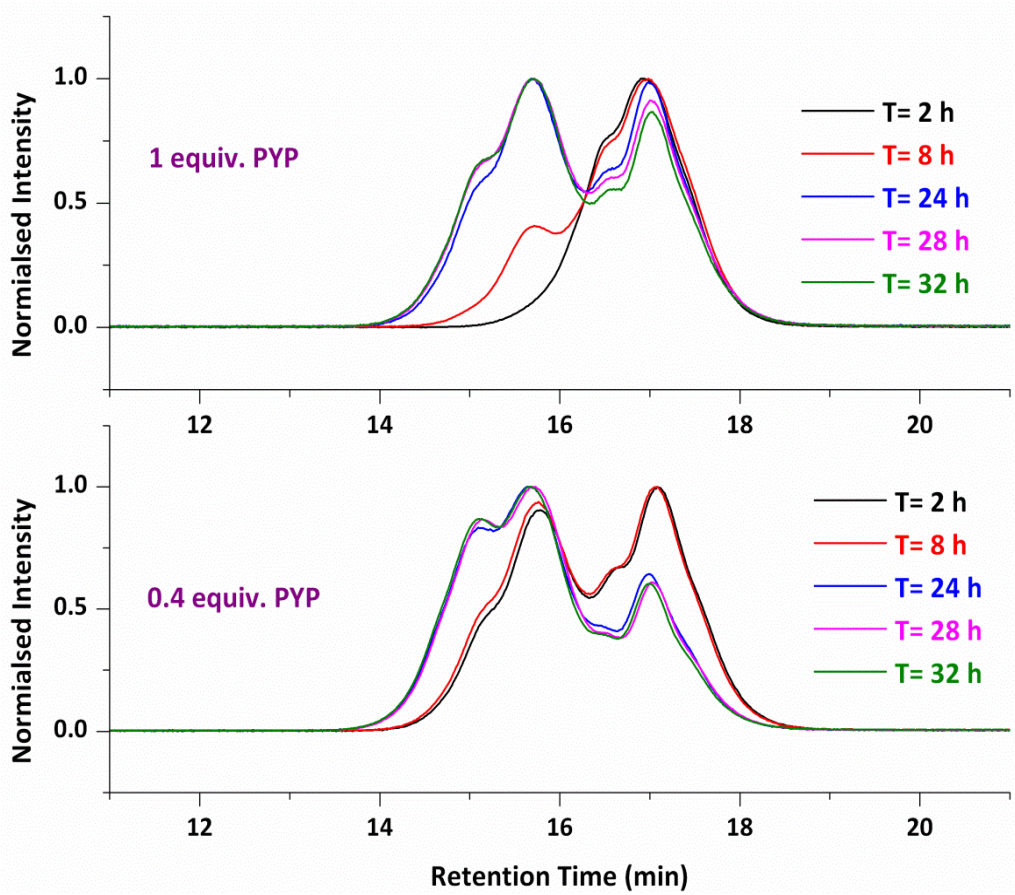

Figure 3.2.6 DMF-GPC analysis of PEGylated *CuPc* derivatives using different amounts of catalyst at different time periods by UV detection (λ = 672 nm)

Following DCC coupling with different amounts of catalyst, the reaction was further optimised by the use of EDC as a coupling agent with addition of 0.4 equivalent of catalyst (relevant to the amount of *CuPc*). It can be noticed that comparison with DCC coupling reaction at the same time period, the reaction was much more efficient with EDC such that the conjugation could be completed in 2 hours, analysed by DMF-GPC equipped with UV detector (λ = 672 nm), **Figure 3.2.7**.

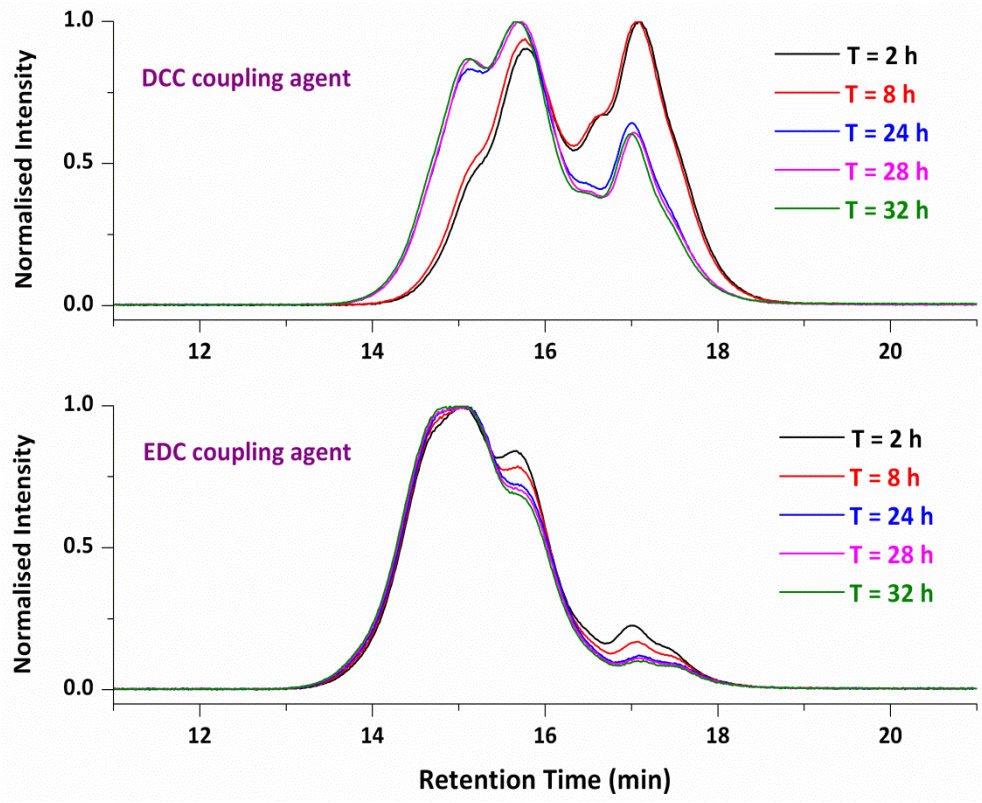

Figure 3.2.7 DMF-GPC analysis of PEGylated *CuPc* derivatives by comparison of different coupling agents by UV detector (λ = 672 nm)

The PEGylated *CuPc* was purified by precipitation in petroleum ether to yield blue powder. The final polymer and the starting materials, hydroxyl terminated *CuPc* (HO-*CuPc*) and mono-carboxylic acid functionalised PEG monomethyl ether (HOOC-mPEG), were analysed by DMF-GPC equipped with both RI and UV (λ = 672 nm) detectors, **Figure 3.2.8**. The chromatograms from both detectors showed that the shoulder peaks of the PEGylated *CuPc* indicate both starting materials left in the isolated polymer. The broad peaks also suggest the presence of mixture of substituted conjugation due to the uncompleted tetra-substituted starting material HO-*CuPc* revealed by broadening chromatogram obtained from the UV detector.

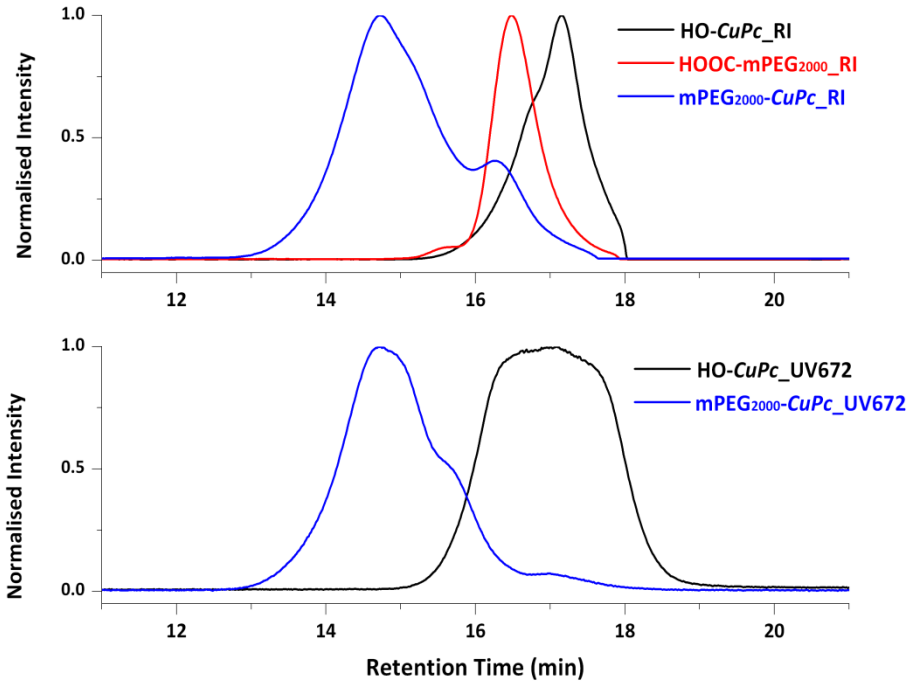

Figure 3.2.8 DMF-GPC analysis of purified PEGylated *CuPc* complex and both starting materials by RI and UV (λ = 672 nm) detectors

The UV-Vis analysis of PEGylated *CuPc* solution (**Figure 3.2.9**) shows an intense absorption at λ_{max} = 672 nm, indicating it is non-aggregated in DMF. However, the reduced and broad absorption with a blue shift of Q band at λ = 628 nm suggests that it is aggregated as dimer or oligomer in water. Moreover, the image shows that the functionalised *CuPc* after incorporated with PEG chain can be fully solubilised in water yielding bright blue solution in comparison with unsubstituted *CuPc* macrocycle in water.

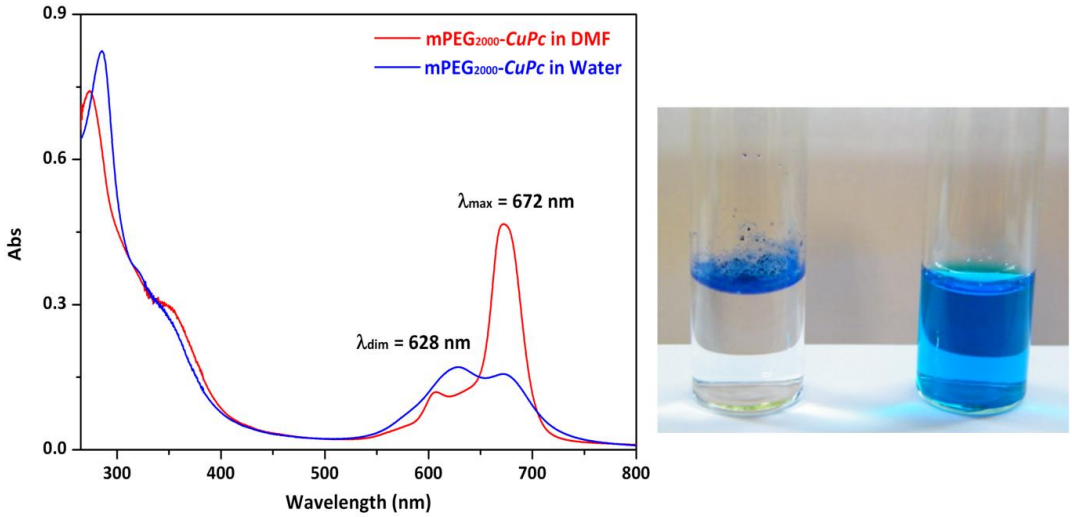

Figure 3.2.9 UV-Vis analysis of 0.2 mg mL^{-1} PEGylated *CuPc* solution in DMF and water, and the image showing 1 mg mL^{-1} *CuPc* (left) and PEGylated *CuPc* (right) in water.

It can be concluded that the initial experiments of PEGylated *CuPc* via coupling reactions can be optimised by using EDC as a coupling agent with addition of low amounts of catalyst. The final product shows high solubility in water and is non-aggregated in common organic solvents. However, the complex exist a mixture of substituted PEG chains and both of starting materials, which makes the product difficult to isolate giving rise to impure PEGylated *CuPc* species. Therefore, the method for preparation of fully functionalised *Pc* derivatives needs to be further investigated.

3.2.2 Design and synthesis of PEGylated (copper) phthalocyanines via a combination of Mitsunobu reaction and CuAAC "click" reaction

In order to optimise the PEGylation of phthalocyanines, the substituted macrocycles were prepared from 4,5-bis(4-hydroxyphenoxy)phthalonitrile (**Figure 3.2.10**, **6**) as a precursor according to Wőhrle *et al* in 1993.[20] The precursor was synthesised from the inexpensive commercially available 1,2-dichloro-1,2-benzenedicarboxylic acid (**1**) via anhydride (**2**), imide (**3**), diamide (**4**), and 4,5-dichloro-1,2-dicyanobenzene (**5**) with an overall yield of 30%.

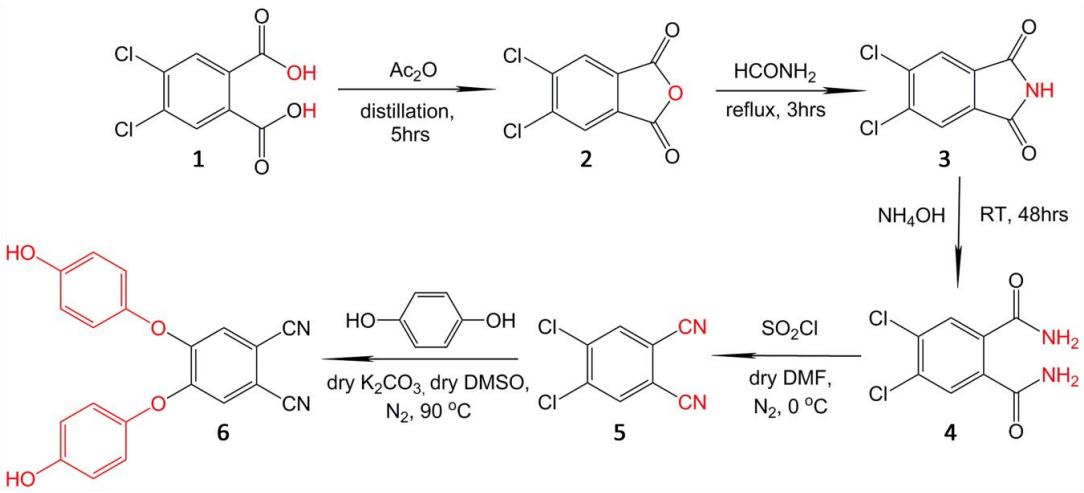

Figure 3.2.10 Reaction scheme of preparation of diphenyl phthalonitrile as a precursor to octa-substituted mPEG-(*Cu)Pcs*

Following the preparation of diphenyl phthalonitrile, we demonstrate a new approach for the synthesis of a series of symmetrically octa-substituted metal-free *Pcs* or *CuPcs* with different PEG chain lengths from average molecular weight 350 up to 2000 Da, **Figure 3.2.11**. The transformation of PEG to *Pcs* and *CuPcs* is achieved via the combination of Mitsunobu reaction[21, 22] and Cu(I)-catalysed azide-alkyne cycloaddition.[23-25] The Cu(I)-catalysed "click" reaction has been receiving increasing interest as a result of high yield, good selectivity, and excellent functional group tolerance. The resultant PEGylated *(Cu)Pc* complexes are highly soluble and non-aggregated in common organic solvents (CH_2Cl_2, THF, DMF, etc.), and also exhibit good solubility in water. More remarkably, the PEGylated *(Cu)Pcs* with different PEG chain lengths exhibit interesting tuneable thermal properties.

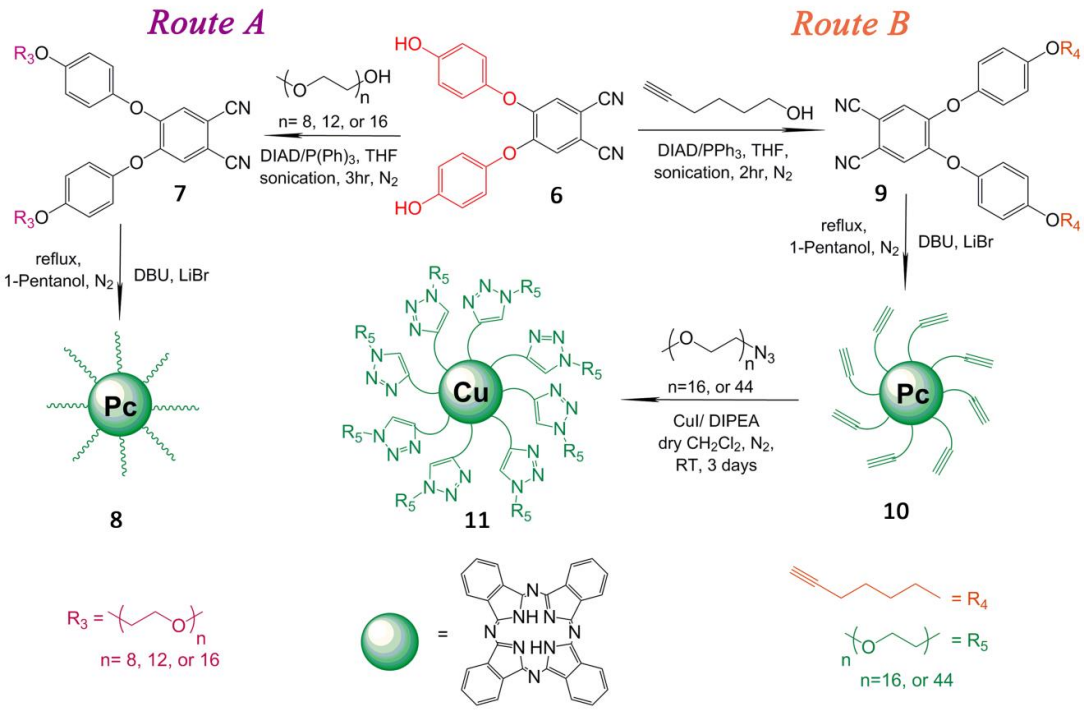

Figure 3.2.11 Preparation of both of octa-substituted metal free mPEG-*Pcs* (*Route A. Cyclotetramerisation*) and mPEG-*CuPcs* (*Route B. Click Chemistry*) with different PEG chain lengths.

3.2.2.1 Synthesis of octa-substituted mPEG-*Pcs* by Route A. Cyclotetramerisation

PEGylated phthalonitrile (**7**) with different chain lengths were directly prepared from diphenol phthalonitrile (**6**) by a Mitsunobu reaction with linear monomethyl ether PEG (average M_n = 350, 550, and 750 Da, **Figure 3.2.12**). The metal free mPEG-*Pcs* were synthesised by direct cyclotetramerisation, resulting in a deep green colour appearance of the polymer aqueous solution.

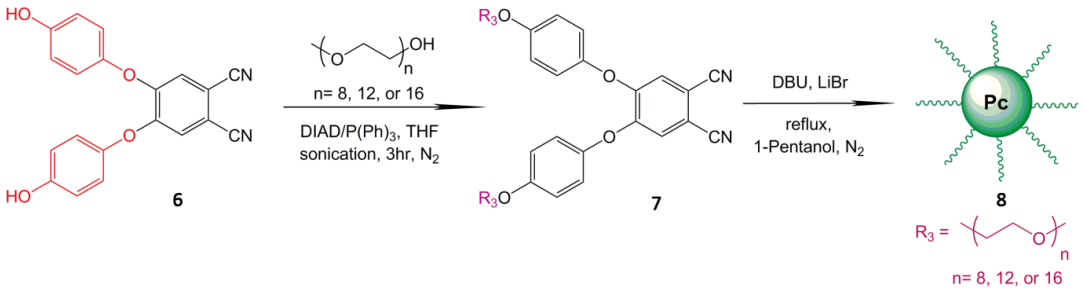

Figure 3.2.12 Preparation of both of octa-substituted metal free mPEG-*Pcs* via Route A. Cyclotetramerisation

Successful synthesis was confirmed by ^{1}H NMR of starting material $mPEG_{350}$, $mPEG_{350}$-phthalonitrile and purified $mPEG_{350}$-*Pc*, **Figure 3.2.13**. The hydroxyl proton of $mPEG_{350}$ at approximately δ 2.7 ppm disappeared after the Mitsunobu coupling, and was replaced with the appearance of chemical shift at approximately δ 7 ppm, corresponding to the protons on aromatic rings of $mPEG_{350}$-phthalonitrile, and also the well-resolved signals at δ 4.14 and 3.87 ppm represent the protons of the oxyethylene unit adjacent to the aromatic ring. After cyclotetramerisation, the protons at the non-peripheral position of *Pc* core are deshielded indicating a broad peak due to the intermolecular aggregation around δ 8.8 ppm (not shown here), and the protons on eight aromatic rings adjacent to the *Pc* core are slightly deshielded and separated between δ 7.5-6.8 ppm. The strongly shielding effect of the *Pc* ring current on the two internal protons is apparent from their chemical shift below δ -3.5 ppm (not shown). Moreover, this ring current produces a slight influence on the protons of oxyethylene subunit next to the aromatic rings, which are shifted to δ 4.17 and 3.90 ppm. The intense and large peak corresponding to the protons on the majority of the PEG side chains stay between δ 3.8-3.5 ppm. These NMR results clearly confirm a successful Mitsunobu coupling and cyclotetramerisation reaction to produce octa-substituted mPEG-*Pcs*.

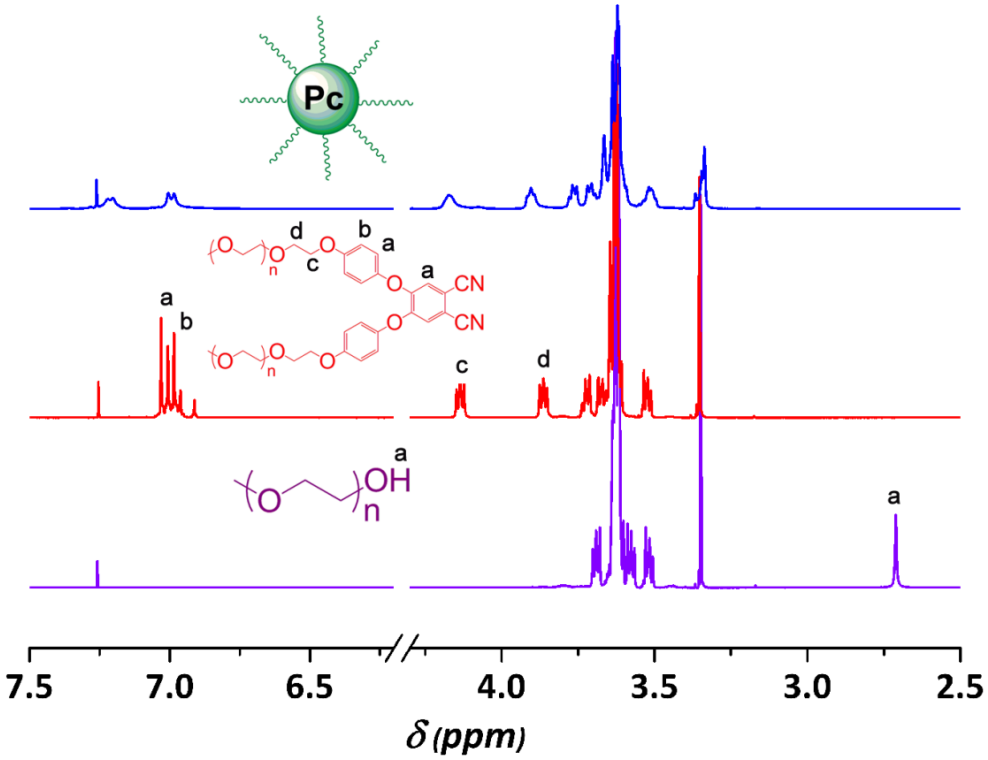

Figure 3.2.13 ^{1}H NMR of typical mPEG$_{350}$, mPEG$_{350}$-phthalonitrile, and purified mPEG$_{350}$-*Pc*

To further prove the efficiency of the route A method, we also explored the investigation of mPEG polymers with varied molecular weights, 550 and 750 Da. These *Pc*-centered poly(oxyethylene)s with different side chain lengths were purified, in each case, by Vivaspin 500 µl centrifugal filter before GPC analysis. As the chain length of the monomethyl ether PEG increases, there is an increase in hydrodynamic volume of three *Pc*-centered PEG polymers as expected **Figure 3.2.14**-(a). Impressively, the measured dispersities of these macromolecules are very narrow (PDI ≤ 1.1) indicating an efficient cyclotetramerised reaction and no obvious starting PEG chains were left following purification. Analysis via THF-GPC coupled with a photodiode array detector of *Pc*-centered poly(oxyethylene) with side chain of average molar mass 750 Da showed a strong absorption between 670 and 690 nm, the Q band, confirming the formation of the *Pc* core, **Figure 3.2.14**-(b). Furthermore, the split and intense Q band demonstrates metal-free *Pc* complex which is non-aggregated in THF. A similar UV-Vis spectra and longer elution time can be found from the images of mPEG$_{550}$-*Pc* and mPEG$_{350}$-*Pc*.

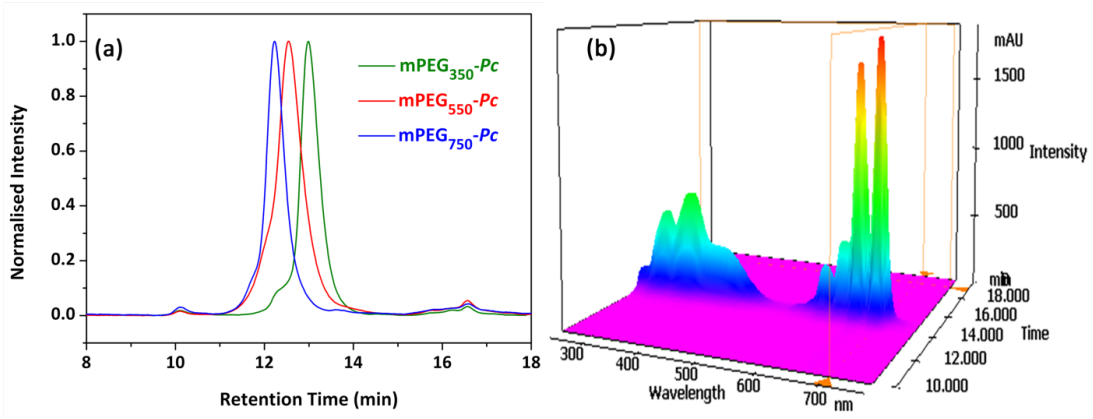

Figure 3.2.14 (a) THF-GPC (*mixed E Column*) chromatograms of mPEG-*Pcs* with different PEG chain lengths in by RI detector; (b) THF-GPC (*mixed D Column*) coupled PDA detector representing a 3D image of $mPEG_{750}$-*Pc*

3.2.2.2 Synthesis of octa-substituted mPEG-*CuPcs* by Route B. Click Chemistry

Route B (**Figure 3.2.15**) shows the synthetic pathway which combines a Mitsunobu reaction with CuAAC click reaction of the preparation of *CuPc*-centered poly(oxyethylene)s with different side chain lengths of average molar mass of 750 and 2000 Da. Alkyne-terminated phthalonitrile was prepared from diphenol phthalonitrile by coupling with commercially available 5-hexynl-1-ol, which is readily cyclotetramerised to form a "clickable" metal free *Pc*. The incorporation of multiple terminal alkyne moieties at peripheral positions of *Pc* provide good solubility in common organic solvents (such as CH_2Cl_2, $CHCl_3$, and THF) typically used in further click chemistry reactions.[26]

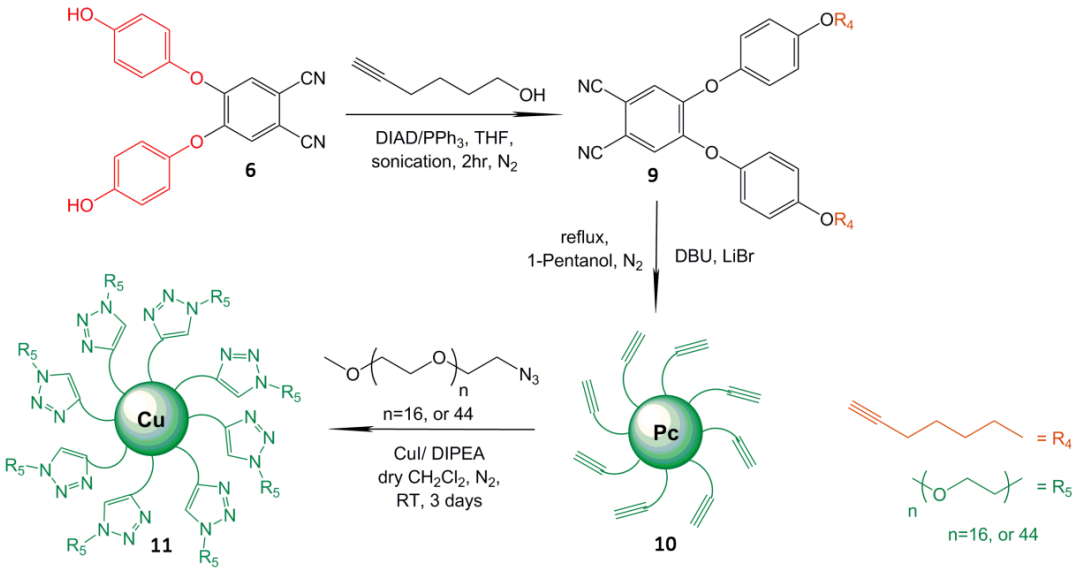

Figure 3.2.15 Preparation of both of octa-substituted mPEG-*CuPcs* via Route B. CuAAC click reaction

The synthesised octaalkynyl *Pc* (**10**) was characterised by UV-Vis spectroscopy, IR, NMR, MALDI-ToF, and THF-GPC analysis. The UV-Vis spectrum of the clickable *Pc* (ca. 2×10^{-6} M) in dichloromethane (DCM) indicates a B-band at approximately 342 nm, a split Q-band at 668 nm and 702 nm with the extinction coefficient $\varepsilon = 1.6\times10^{5}$ $M^{-1}cm^{-1}$, and the weak absorption bands at 607 nm and 640 nm are vibrational overtones of the Q-band, **Figure 3.2.16**-(a). IR spectra (**Figure 3.2.16**-b) show that the infrared absorption frequencies of $\nu_{C\equiv N}$ and $\nu_{C\text{-}H}$ from the alkyne groups of alkyne terminated phthalonitrile are sharp, at 2223 cm^{-1} and 3280 cm^{-1} respectively. The disappearance of the $\nu_{C\equiv N}$ vibrational frequency and the broad $\nu_{C\text{-}H}$ stretching from the alkyne groups also confirm the formation of the *Pc* macrocycle with multiple alkyne groups after cyclotetramerisation.

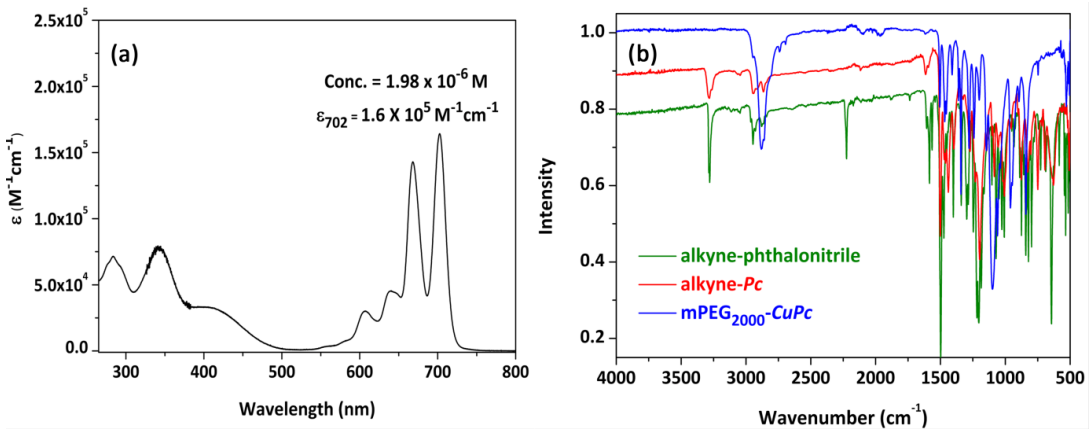

Figure 3.2.16 (a) UV-Vis spectrum of alkyne-terminated *Pc* (1.98 x 10^{-6} M) in DCM; (b) IR spectra of alkyne-terminated phthalonitrile, octaalkynyl *Pc*, and $mPEG_{2000}$-*CuPc*.

^{1}H NMR characterisation (**Figure 3.2.17**) of octaalkynyl *Pc* overlapped with starting compound 5-hexynl-1-ol and alkynyl phthalonitrile demonstrate that protons on aromatic rings appear between δ 7.05 ppm and δ 6.65 ppm, and the two protons on methylene adjacent to the phenol ring are shifted to δ 4.02 ppm after Mitsunobu coupling. The formation of *Pc* macrocycle has similar effect on the formation of *Pc*-centred poly(oxyethylene). The protons at non-peripheral position of *Pc* core and the protons at ortho position of the phenol rings which are close to the *Pc* core are strongly deshielded to δ 8.40 ppm and δ 7.27 ppm. However, the protons on the octaalkynyl chain only shift slightly due to the ring current.

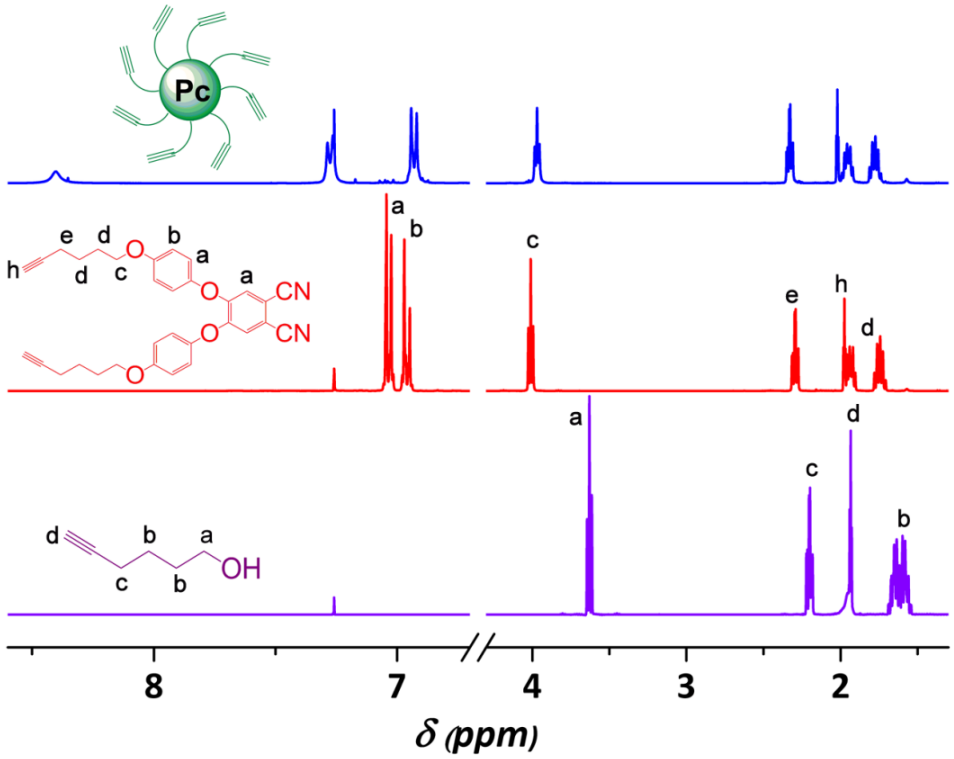

Figure 3.2.17 ^{1}H NMR characterisations of starting material 5-hexynl-1-ol, phthalonitrile-*Pc*, and product octaalkynl *Pc*

Following the formation of octaalkynyl terminated *Pc*, azide functionalised PEG monomethyl ether[27, 28] with different molecular weights (M_n = 750, and 2000 g mol^{-1}) was prepared from mesylation of the hydroxide end group of monodisperse PEG monomethyl ether, followed by azide substituion, **Figure 3.2.18**.

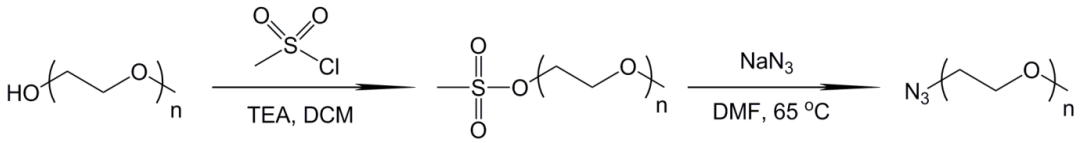

Figure 3.2.18 Synthesis of azido terminated PEG monomethyl ether

Quantification of end group substitution was achieved by both of ^{13}C NMR and MALDI-ToF-MS analysis. ^{13}C NMR analysis (**Figure 3.2.19**) of monodisperse PEG monomethyl ether (M_n = 750 g/mol) after mesylation and its following azide substitution showed that the signals corresponding to the end groups at δ 37.6 ppm (mesylate) and 50.6 ppm (methylene) carbons.

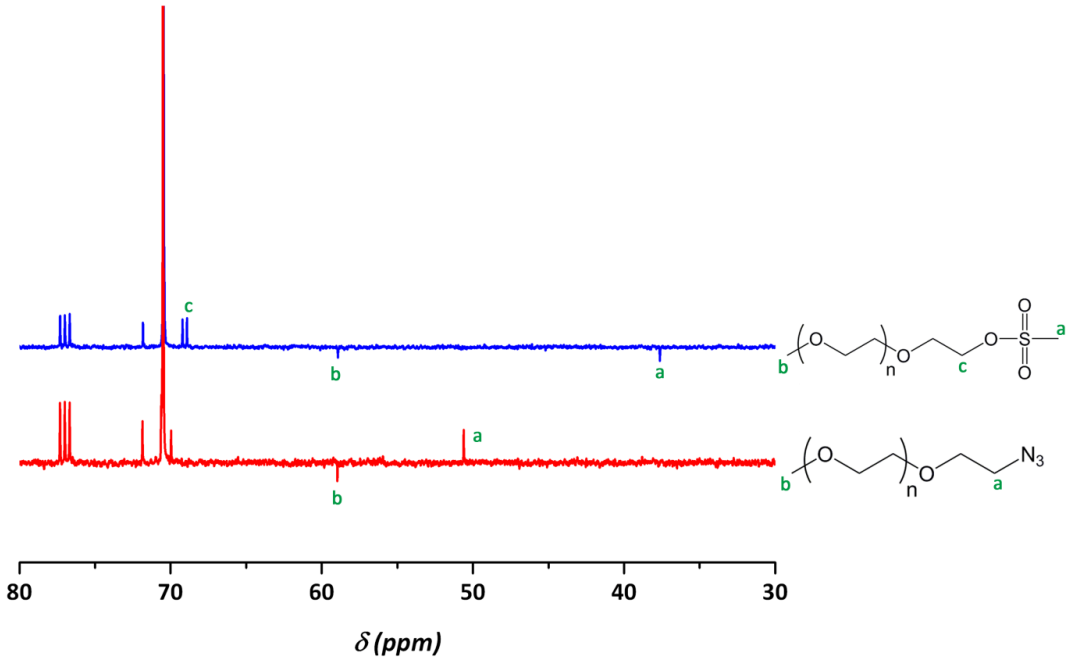

Figure 3.2.19 NMR showing the signals corresponding to the end groups of mesylated PEG monomethyl ether and azido teminated PEG monomethyl ether

Analysis of the functionalised monodisperse PEG monomethyl ether (M_n = 750 g/mol) by MALDI-ToF-MS (**Figure 3.2.20**) showed that in the case of either mesylation or subsequent azido substitution, a high degree of functionalisation was obtained. A clear shift is observed in the distribution with the corresponding mass increase expected upon mesylation of PEG chain. Moreover, the mass spectrum of the following azido displacement was observed as the major distribution. It can be also noticed that the minor distributions indicate fragmentation of the azide functionality via expulsion of N_2 (pink) and the formation of metastable ions (yellow) which is generated at some point during the ion flight path in the field free region between the ion source and detector.[29]

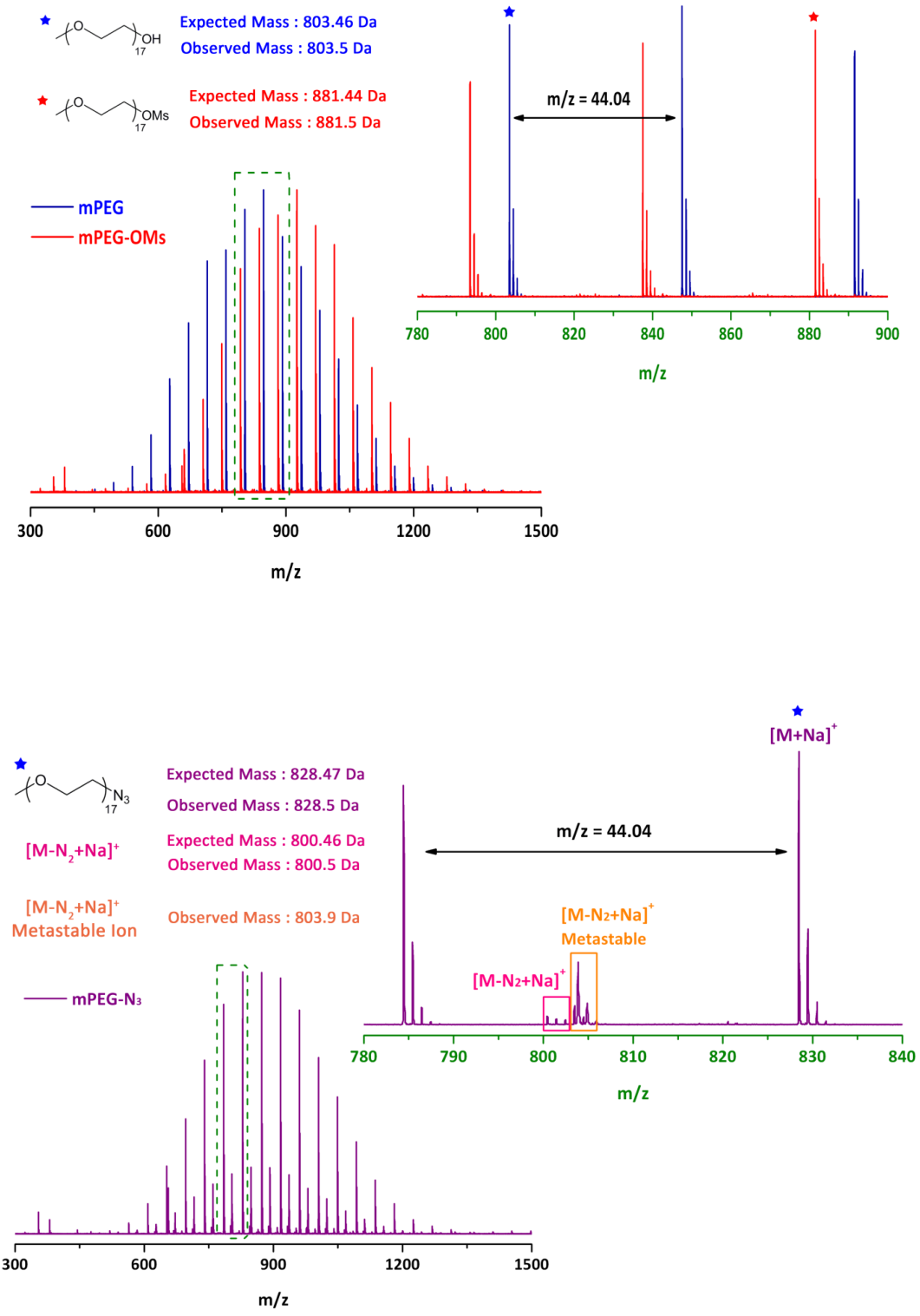

Figure 3.2.20 MALDI-ToF-MS analysis of mesylated PEG monomethyl ether and azido terminated PEG monomethyl ether

A longer PEG chain with average molar mass 2000 Da can also be incorporated into *Pc* core successfully by click chemistry. Cu(I)-based catalytic system in cycloaddition of octaalkynyl *Pc* and azido-$PEG_{750,\ 2000}$ enable the formation of *CuPc*-centred PEG under typical click conditions. A CuBr/TBTA catalytic system was initially investigated, with a reaction time of 7 days at ambient temperature required for the reaction to go to completion. However, it was found that metalation of alkyne-*Pc* (**10**) with Cu was incomplete, according to UV-Vis spectroscopy, probably due to the excellent-binding ability of TBTA with Cu(I).[30] Therefore, a combination of CuI/DIPEA catalyst was proved to be effective to provide desired product after 3 days in either THF or DCM.

The GPC traces (**Figure 3.2.21**-a) show that a decrease in elution time corresponding to molecular weight increases in comparison of $mPEG_{2000}$-*CuPc* with $mPEG_{750}$-*CuPc*. It is noted that low amount of high molecular weight polymers in presence of both mPEG-*CuPcs*; however, relatively narrow dispersities are still achieved (PDI ≤1.22). **Figure 3.2.21**-(b) represents a 3D image of $mPEG_{750}$-*CuPc* collected by THF-GPC coupled with PDA detector. In comparison with $mPEG_{750}$-*Pc* (**Figure 3.2.14**-b), the UV-Vis absorption combined with an elution time profile confirmed the formation of metalated mPEG-*CuPc*s, proved by an intense single Q-band at 682 nm, due to its higher symmetry than that of planar metal free *Pcs*.

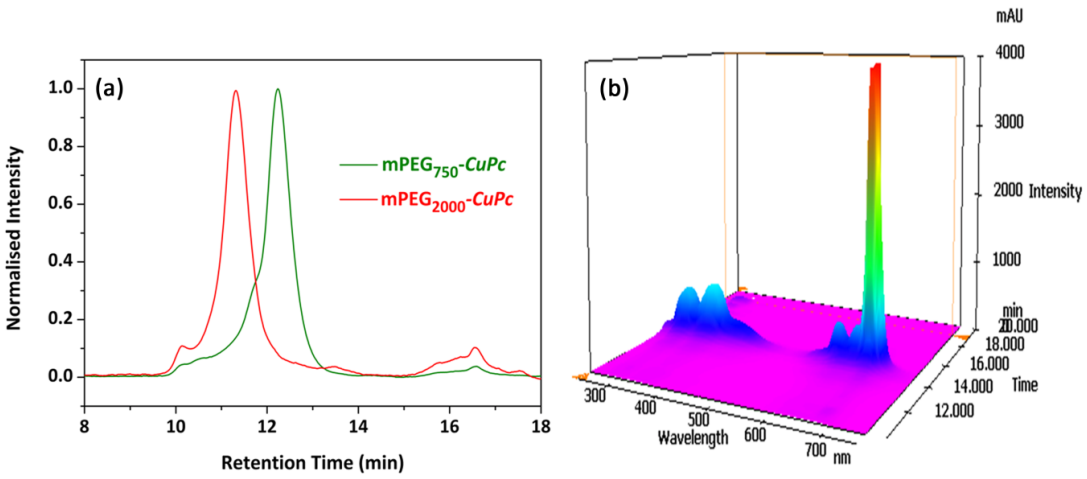

Figure 3.2.21 (a) THF-GPC (*mixed E Column*) chromatograms of mPEG-*CuPcs* by RI detector; (b) THF-GPC (*mixed D Column*) coupled PDA detector representing a 3D image of $mPEG_{750}$-*CuPc*

3.2.2.3 Aqueous solubility and thermal property of PEGylated *(Cu)Pcs*

It has been previously mentioned that all octa-substituted metal free *Pc* or *CuPc* with different chain lengths of PEG exhibit good solubility and are non-aggregating in common organic solvents. However, in water (**Figure 3.2.22**-a), it is noticed that a blue-shift of Q band (λ near 628 nm) appears in all polymers which is indicative of formation of aggregating complexes in solution due to exciton coupling between the oligomeric π systems. It is also found that, as expected, there is a decrease of UV-Vis absorption of *(Cu)Pc* core corresponding to an increase in the chain length of PEG. Moreover, it should be mentioned that the appearances of slight shoulder around 680 nm (dash line) in both of mPEG$_{750}$-*CuPc* and mPEG$_{2000}$-*CuPc*, which is the minor contribution from the monomeric species. Although UV-Vis spectra show the complex formation of these PEGylated *(Cu)Pcs*, they are still water soluble (**Figure 3.2.22**-b).

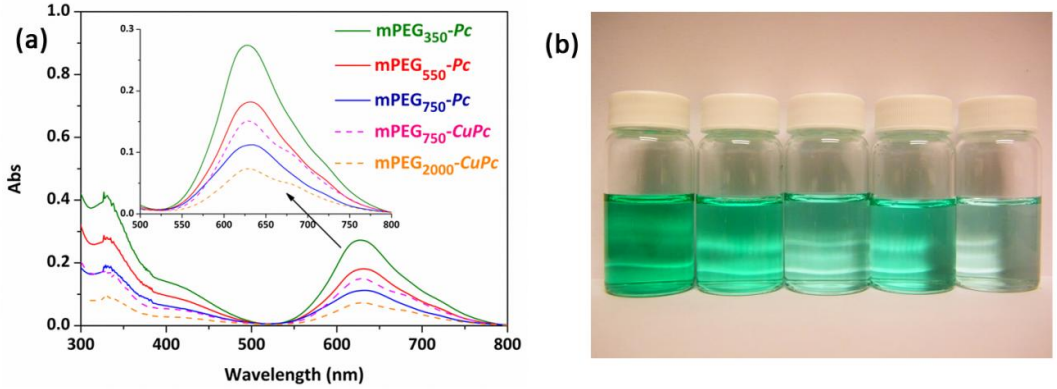

Figure 3.2.22 (a) UV-Vis spectra of a series of PEGylated *(Cu)Pc*: mPEG$_{350,\ 550,\ \text{and}\ 750}$-*Pc* (solid line); mPEG$_{750\ \text{and}\ 2000}$-*CuPc* (dash line) in distilled water at the same concentration (0.02 mg mL^{-1}); (b) image of aqueous solution of PEGylated *(Cu)Pc* species(from left to right): mPEG$_{350}$-*Pc*, mPEG$_{550}$-*Pc*, mPEG$_{750}$-*Pc*, mPEG$_{750}$-*CuPc*, and mPEG$_{2000}$-*CuPc*.

The thermal properties of a series of mPEG-*(Cu)Pc* polymers were analysed by DSC with three heating and cooling cycles from -100 ^{o}C to 120 ^{o}C at 10 K min^{-1}. In

general, it can be found that shorter PEG chains ($mPEG_{350}$, $mPEG_{550}$, and $mPEG_{750}$) after functionalisation with *Pc* or *CuPc* (**Figure 3.2.23**-a) exhibit more different thermal behaviours in comparison with the commercially available monomethyl ether PEGs (**Figure 3.2.23**-b).

The linear $mPEG_{350}$ shows two melting temperatures at T_m = -20 ^oC and -4 ^oC and with two corresponding exotherm peaks (T_c = -29 ^oC and -20 ^oC) in both cooling curves. However, after formation of octa-substituted $mPEG_{350}$-*Pc*, both T_m and T_c are not present with the appearance of a glass transition at $T_g \approx$ -57 ^oC in both heating and cooling cycles, indicating that the *Pc* ring has a strong impact on the crystallisation of the short PEG chain.

The $mPEG_{550}$-*Pc* does not show crystallisation in the cooling cycles but exhibits a glass transition at $T_g \approx$ -54 ^oC. The heating curves show a glass transition, an exothermal crystallisation and a melting peat at T_m = 14 ^oC. In contrast, the commercial $mPEG_{550}$ only exhibits a melting point and a crystalline temperature at approximately 19 ^oC and 6 ^oC respectively.

As for *Pc* substituted by octa-$mPEG_{750}$ chains, the sample presents a similar T_m = 29 ^oC as original $mPEG_{750}$ (T_m = 23 ^oC), and a considerably lower crystalline point T_c = -23 ^oC compared with T_c = 13 ^oC of $mPEG_{750}$. However, $mPEG_{750}$-*CuPc* has a quite different thermal behaviour from both of $mPEG_{750}$-*Pc* and $mPEG_{750}$ starting material and a similar heating and cooling transition with $mPEG_{550}$-*Pc*, showing no crystallisation temperature in cooling cycles, a glass transition ($T_g \approx$ -53 ^oC), a crystalline peak (T_c = -23 ^oC), an endothermic transition at approximately the same temperature. This difference probably can be explained by the presence of Cu in *Pc* ring, together with the introduction of short alkyl linkers and 1,2,3-triazole rings between $mPEG_{750}$ chain and *CuPc* core having a significant effect on the thermal properties of commercial $mPEG_{750}$.

As might have been expected, octa-substituted $mPEG_{2000}$-*CuPc* illustrates a similar melting temperature (T_m = 48 ^oC) in heating cycles and a slightly lower crystallisation (T_c = 15 ^oC) in cooling cycles, in comparison with the endothermic peak (T_m = 53 ^oC) and crystalline point (T_c = 27 ^oC) of starting $mPEG_{2000}$ polymer respectively.

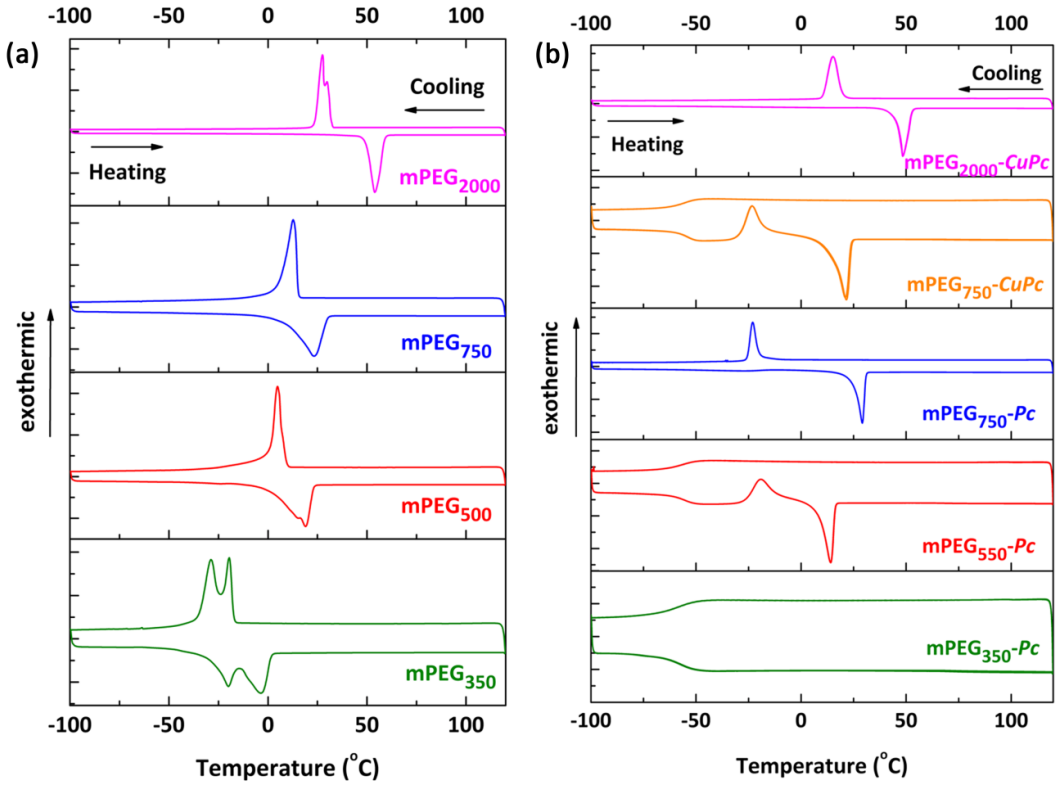

Figure 3.2.23 DSC traces of (a) starting materials from $mPEG_{350}$ to $mPEG_{2000}$, and (b) all mPEG-*(Cu)Pc* complexes under heating and cooling cycles between -100 ^{o}C to 120 ^{o}C at a rate of 10 K min^{-1}.

3.3 Conclusions

This chapter describes the preparation of PEGylation of *(Cu)Pcs* to achieve the dissolution of the macrocycle in water. PEGylated *CuPc* was initially prepared by DCC/EDC coupling reaction. The hydroxyl terminated *CuPc* derivative was synthesised in an industrial way, followed by reaction with monocarboxylic acid functionalised PEG monomethyl ether.

It shows that the reaction was much more efficient by using EDC as coupling agent. However, due to sulfonation of the macrocycle itself, the PEGylated *CuPc* derivatives exit a mixture of different numbers of substituted PEG chains as well as both of starting materials which are difficult to purify, according to the broadening peaks from DMF-GPC analysis. The products are non-aggregated in DMF and show the presence of dimeric complexes in water by UV-Vis analysis; however, the complexes still have good solubility in water resulting in bright blue solutions.

The synthetic strategy was subsequently modified by preparation of diphenol phthalonitrile as a precursor to a series of octa-substituted mPEG-*(Cu)Pcs* from average molar mass of 350, 550, 750, and up to 2000 by a combination of phenolic Mitsunobu reaction and CuAAC click chemistry.

The GPC results show that narrow dispersity single species products (PDI $\leq$ 1.2) can be achieved, and measurement from THF-GPC equipped with PDA detector shows the formation of desired products and to distinguish metal-free *Pc* polymer from the *CuPc* substituted species. All PEGylated *(Cu)Pc* polymers are highly soluble and non-aggregated in common organic solvents with a split intense Q band between 670 and 690 nm for mPEG-*Pc* polymers, and a single Q band at 682 nm for mPEG-*CuPc* complexes. The UV-Vis spectra of these polymers in water demonstrate that dimeric complexes are formed in all samples but a minor contribution of monomeric species can be found in octa-substituted mPEG-*CuPc* products. Finally, a DSC study shows that PEGylated *(Cu)Pcs* with shorter PEG chain exhibit more significant difference in thermal behaviours in comparison with commercial mPEGs; therefore, tuneable thermal properties can be achieved by incorporation of *(Cu)Pc* with different mPEG

chain lengths. This synthetic strategy expands the family of functionalised *Pc* with different polymers for various applications.

3.4 Experimental

Reagents and Conditions

Poly(ethylene oxide) monomethyl ether (mPEG, M_n = 350, 550, 750, and 2000 Da), 4,5-dichlorophthalic acid (99%, Sigma-Aldrich), hydroquinone (≥ 99%, Sigma-Aldrich), 5-hexynl-1-ol (96%, Sigma-Aldrich), NaN_3 (≥ 99.5%, Sigma-Aldrich), CuI (99.999% trace metals basis, Sigma-Aldrich), *N*,*N*-diisopropylethylamine (DIPEA, ≥ 99%, Sigma-Aldrich), LiBr (≥ 99%, Sigma-Aldrich), 1,8-diazabicyclo[5.4.0]undec-7-ene (DBU, 98%, Sigma-Aldrich), 1-pentanol (≥ 99%, Sigma-Aldrich), tetrahydrofuran (THF, anhydrous, ≥ 99.9%, Sigma-Aldrich), all the other reagents and solvents were obtained at the highest purity available from Sigma-Aldrich and used without further purification unless otherwise stated. TLC performed using pre-coated silica gel 60 F254 and developed in the solvent system indicated. Compounds were visualized by use of UV light (254 or 302 nm) or a basic solution (10 % w/w K_2CO_3 in water) of $KMnO_4$. Merck 60 (230 - 400 mesh) silica gel was used for column chromatography.

Instrumentals and analysis

Nuclear Magnetic Resonance

NMR spectra were obtained on Bruker DPX-300, Bruker DPX-400 and Bruker DRX-500 spectrometers. All chemical shifts are reported in ppm (δ) relative to tetramethylsilane, referenced to the chemical shifts of residual solvent resonance (^{1}H and ^{13}C). The following abbreviations were used to explain the multiplicities: s = singlet, d = doublet, dd = doublet of doublets, t = triplet, td = triplet of doublets, m = multiplet.

Gel Permeation Chromatography (GPC) Analysis

GPC analysis was performed based on solubility of the polymer or conjugated and on the available detectors of each system.

Dimethylformamide

GPC was performed on a Varian 390-LC MDS system equipped with a PL-AS RT/MT autosampler, a PL-gel 3 μm (50 x 7.5 mm) guard column, two PL-gel 5 μm (300 x 7.5 mm) mixed-D columns using DMF with 5 mM NH_3BF_4 at 50 ^oC as the eluent at a flow rate of 1.0 mL min^{-1}. The GPC system was equipped with ultraviolet and differential refractive index detectors. Narrow molecular weight PMMA standards (between 200 and 467,400 g mol^{-1}) were used to calibrate the SEC and data fitted with a 3rd order polynomial.

Tetrahydrofuran

THF (2% TEA) equipped with a differential refractive index and a Shimadzu SPD-M20A diode array detector, a PL-AS RT/MT autosampler, a PL-gel 3 μm (50 x 7.5 mm) guard column, 2 x PL-gel 5 μm (300 x 7.5 mm) mixed-D columns. The molar mass distributions of PEGylated *(Cu) Pcs* were measured on a SEC system equipped with a PL-gel 3 μm (50 x 7.5 mm) guard column 2 x PL-gel 3 μm (300 x 7.5 mm) mixed-E columns with DRI detector using 100% THF as eluent. Narrow molecular weight standards of both poly(MMA) (between 200 and 467,400 g mol^{-1}) and polystyrene (between 162 and 24,600 g mol^{-1}) were used to calibrate the SEC and data fitted with a 3rd order polynomial.

MALDI-ToF-MS Analysis

MALDI-ToF data was collected using a Bruker Ultraflex II MALDI-ToF spectrometer, equipped with a nitrogen laser delivering 2 ns laser pulses at 337 nm with positive ion ToF detection performed using an accelerating voltage of 25 kV. Samples were prepared by mixing α-cyano-4-hydroxycinnamic acid (CHCA) (20 μL of a 2 mg L^{-1} solution), sodium iodide (20 μL of a 1 mg L^{-1} solution), and the analyte solution (20 μL of a 2 mg L^{-1} solution), and then the resulting solution was spotted onto a ground steel MALDI plate and solvent removed prior to inserting into the vacuum chamber of the MALDI instrument.

Fourier Transform Infra-Red (FTIR) spectrometry

Infrared absorption spectra were recorder on a Bruker VECTOR-22 FTIR spectrometer using a Golden Gate diamond attenuated total reflection (ATR) cell.

Differential Scanning Calorimetry

DSC experiments were carried out on a Mettler Toledo DSC1-Star system under a flowing nitrogen atmosphere. For all experiments, polymer samples were approximately 10-20 mg, and loaded in the standard aluminium pans and then heated from -100 to 120 ^{o}C. The heating rate was 10 ^{o}C/min. The glass transition temperature (T_g) was determined as the midpoint value of glass transition curve.

Hydroxyl terminated copper phthalocyanine derivative (HOOC-*CuPc*)

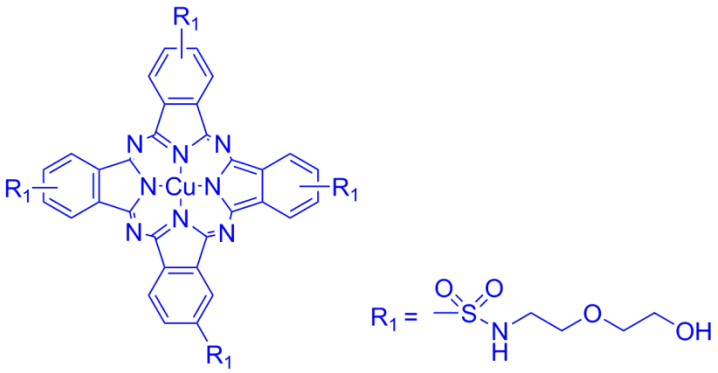

Copper phthalocyanine (5.76 g, 0.01 mol) was added in portions over 15-30 minutes to stirred chlorosulfonic acid (20 mL) keeping the temperature below 40 ^{o}C. The mixture was then heated to 140 ^{o}C over one hour and then stirred at this temperature for 6 hours. The mixture was cooled to 60 ^{o}C and PCl_3 (3.5 mL, 0.04 mol) was added dropwise to the reaction mixture over 30 minutes maintained 60 ^{o}C and left stirring overnight.

The mixture was cooled to ambient temperature and poured into a 1 L of water/ice mixture and the resultant precipitate was filtered off. The filter cake was washed with 400 ml of ice cold water and then dried overnight, followed by addition to 2-(2-aminoethyoxy) ethanol (0.09 mol, 10 mL) in 90 mL water. This was heated to 40 ^{o}C and stirred for 30 minutes, and then the mixture was heated to 80 ^{o}C and stirred for a further one hour and then allowed to cool. The pH of the reaction mixture was adjusted to pH 4 using HCl (~36%) and the resulting precipitate removed via

filtration and washed with water (500 mL). The filter cake was pulled dry and then dried in a vacuum oven (Yield: 80%).

IR (neat): ν = 3360 (OH), 1322 (SO_2) cm^{-1}.

^{1}H NMR (400.03 MHz, $CDCl_3$, 298 K): δ 3.72 (br, 4H, C*H*$_2$OC*H*$_2$), 3.62 (br, 2H, NHC*H*$_2$), and 3.15 (br, 2H, C*H*$_2$OH).

MALDI-ToF m/z: calcd for $C_{48}H_{52}CuN_{12}O_{16}S_4$ 1266.08 $[M+Na]^+$, observed 1266.5

Mono-carboxylic acid terminated PEG monomethyl ether

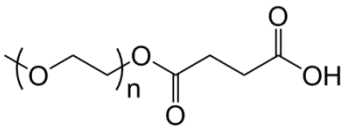

Poly(ethylene glycol) methyl ether (4 g, 2 mmol) was dissolved in anhydrous 1,4-dioxane (60 mL). Succinic anhydride (0.3 g, 3 mmol), 4-(dimethylamino) pyridine (DMAP) (0.37 g, 3 mmol) and triethylamine (TEA) (0.42 mL, 3 mmol) were added to the solution at ambient temperature. The reaction was then continued under stirring and a nitrogen atmosphere for 24 hours. The dioxane was removed under reduced pressure, and the residue was redissolved in chloroform. After filtration and concentration, the crude product was precipitated in cold diethyl ether. The final polymer was isolated as white powder (Yield: 83%).

IR (neat): ν = 2880 (CH_2), 1710 (COOH) cm^{-1}.

^{1}H NMR (400.03 MHz, $CDCl_3$, 298 K): δ 2.63 (m, 4H, OOCC_2*H*$_4$COOH), 3.36 (s, 3H, C*H*$_3$O), 3.63 (s, OC_2*H*$_4$), and 4.24 (m, 4H, OC_2*H*$_4$OOC).

MALDI-ToF m/z: calcd for $C_{89}H_{176}O_{46}$ 2005.14 [M+Na]+, observed 2005.3.

PEGylated CuPc via DCC/EDC coupling reaction

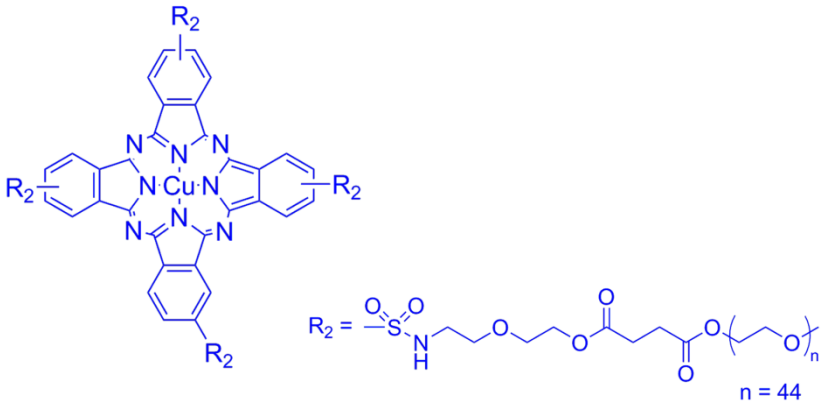

Hydroxyl-terminated copper phthalocyanine dye (0.2 g, 0.161 mmol) was dissolved in dry DMF (25 mL), followed by addition of mono-carboxylated PEG (1.31 g, 0.62 mmol) and DMAP (10 mg, 0.082 mmol) with stirring. Then, DCC (0.141g, 1.02 mmol) was added to reaction mixture at 0 ^{o}C and stirred for 5 min at this temperature. The mixture was reacted at 25 ^{o}C for 24 hours under nitrogen. The precipitated urea was then filtered off and DMF was removed by cold trap. The residue was redissolved in CH_2Cl_2 and any further precipitated urea was filtered. Subsequently, the solvent was removed under reduced pressure and the crude product was precipitated in excess amount of cold diethyl ether to obtain blue powder (Yield: 50%).

IR (neat): ν = ν = 2880 (CH_2), 1730 (COO ester) cm^{-1}.

5, 6-Dichloro-1,3-isobenzofurandione[20]

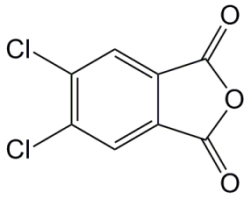

A suspension of 4, 5-dichlorophthalic acid (23.5 g, 0.1 mol) and Ac_2O (50 mL) was heated to slow reflux for 5 hours which allowed for the removal of AcOH by a slow distillation. After cooling, the precipitate was isolated by filtration and washed

intensively with petroleum ether (bp 40-60 ^{o}C). The white product was dried under vacuum (Yield: 70%).

Melting point: T_m = 185-187 ^{o}C (lit.)

IR (neat): ν = 1860, 1830, 1775 (C=O, anhydride), 1100 (C-O), 730, 715, 606 cm^{-1}.

^{1}H NMR (400.03 MHz, $CDCl_3$, 298 K): δ 8.11 (s, 2H); ^{13}C NMR (100.59 MHz, $CDCl_3$, 298 K): δ 160.65, 141.69, 130.25, and 127.41.

ESI-MS m/z: calcd for $C_8H_2Cl_2O_3$ 216.94 $[M+H]^+$, observed 217.00.

5, 6-Dichloro-1*H*-isoindole-1,3(2*H*)-dione[20]

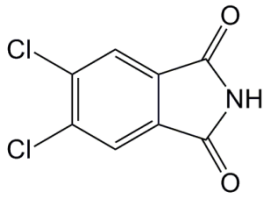

5, 6-Dichloro-1,3-isobenzofurandione (14.88 g, 0.069 mol) was heated under stirring in $HCONH_2$ (27 mL) for 3 hours under reflux. After cooling, the precipitate was isolated by filtration, washed with distilled water and dried in vacuum oven (60 ^{o}C) (Yield: 93%).

Melting point: T_m = 217-219 ^{o}C (lit.)

IR (neat): ν = 1770, 1718 (imide), 740, 701, 600 cm^{-1}.

^{1}H NMR (400.03 MHz, $CDCl_3$+DMSO, 298 K): δ 10.71 (br, 1H imide), 7.80 (s, 2H); ^{13}C NMR (100.59 MHz, $CDCl_3$+DMSO, 298 K): δ 167.01, 138.41, 132.00, and 125.03.

4, 5-Dichloro-1,2-benzenedicarboxamide[20]

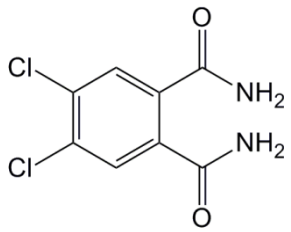

5, 6-Dichloro-1*H*-isoindole-1,3(2*H*)-dione (13.85 g, 0.064 mol) was stirred for 24 hours in 35% NH_4OH (300 mL); A further 100 mL NH_4OH was added and stirred continuously for 24 hours. The precipitate was isolated by filtration, washed with ice water and dried at 60 ^oC in a vacuum oven (Yield: 78%).

Melting point: T_m = 240 ^oC (dec.) (lit.)

IR (neat): ν = 3430, 3303, 3142 (N-H), 1687, 1656, 1609 (C=O, amide) cm^{-1}.

^1H NMR (400.03 MHz, DMSO-d_6, 298 K): δ 7.92 (s, 2H, NH_2), 7.75 (s, 2H), 7.54 (s, 2H, NH_2); ^{13}C NMR (100.59 MHz, DMSO-d_6, 298 K): δ 167.66, 136.6, 131.63, and 129.61.

ESI-MS m/z: calcd for $C_8H_6Cl_2N_2O_2$ 254.97 $[M+Na]^+$, observed 254.90.

4, 5-Dichloro-1,2-dicyanobenzene[20]

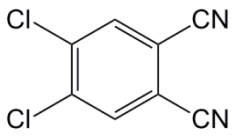

$SOCl_2$ (16 mL) was added dropwise to dry DMF (25 mL) at 0 ^oC under stirring and an atmosphere of nitrogen. After complete addition of $SOCl_2$, the solution was stirred at 0 ^oC for 2 h, followed by addition of dry 4,5-dichloro-1,2-benzenedicarboxamide (4.66 g, 0.02 mol). The mixture was stirred for 5 hrs at 0-5 ^oC, and then at ambient temperature overnight. The mixture was added to ice water. After filtration, the crude product was recrystallised from MeOH and dried in vacuum to give dark orange crystals (Yield: 59%).

Melting point: T_m = 180-184 ^oC (lit.)

IR (neat): ν = 3086, 3016 (C-H), 2238 (CN), 732, 684 cm^{-1}.

^{1}H NMR (400.03 MHz, $CDCl_3$, 298 K): δ 7.91 (s, 2H); ^{13}C NMR (100.59 MHz, $CDCl_3$, 298 K): δ 139.05 (2 x *C*Cl), 134.94 (2 x *C*H), 115.03 (2 x *C*CN), and 113.60 (2 x *C*N).

ESI-MS m/z: calcd for $C_8H_2Cl_2N_2$ 197.95 $[M+H]^+$, observed 197.0.

4,5-Bis(4-hydroxyphenoxy)phthalonitrile[20]

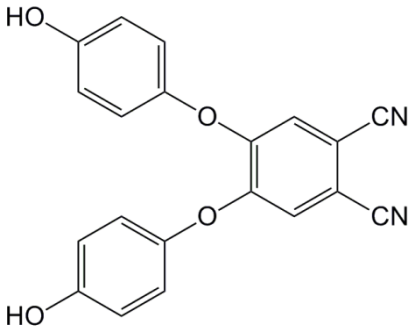

A mixture of hydroquinone (3.30 g 0.03 mol), dry fine powder K_2CO_3 (13.8 g 0.1 mol), and dry DMSO (75 mL) was stirred at ambient temperature under nitrogen for 30 min. 4,5-Dichloro-1,2-dicyanobenzene (1.97 g 0.01 mol) was then added and the reaction mixture was maintained at 90 ^{o}C with stirring for 12 h. After cooling to ambient temperature, the reaction mixture was poured into 1M HCl (250 mL) to induce precipitation. The precipitate was then filtered, washed with cold water, and redissolved in ethyl acetate. The resulting solution was washed with distilled water (3 x 100 mL) until the aqueous phase became neutral, dried with anhydrous $MgSO_4$, and the solvent removed under reduced pressure to obtain light tan colour solid. The solid was then powdered, and dispersed in CH_2Cl_2 (400 mL) with vigorous stirring. The precipitate was filtered to obtain the product (Yield: 74%).

IR (neat): ν = 3400 (O-H), 2238 (CN) cm^{-1}.

^{1}H NMR (400.03 MHz, DMSO-d_6, 298 K): δ 9.58 (s, 2H), 7.48 (s, 2H), 7.05-7.01 (m, 4H), 6.84-6.88 (m, 4H); ^{13}C NMR (100.59 MHz, DMSO-d_6, 298 K): δ 154.89, 151.97, 146.19, 122.01, 120.81, 116.57, 115.51 (2 x *C*CN), and 109.36 (2 x *C*N).

ESI-MS m/z: calcd for $C_{20}H_{12}N_2O_4$ 367.07 $[M+Na]^+$, observed 367.0.

Typical procedure for mPEG$_{350}$-phthalonitrile

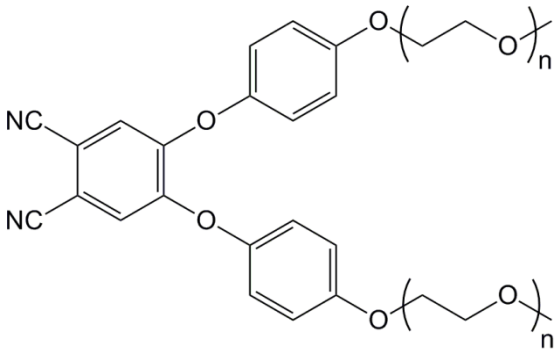

A mixture of mPEG$_{350}$ (0.734 g, 2.1 mmol), 4,5-Bis(4-hydroxyphenoxy)phthalonitrile (0.344 g 1 mmol), triphenyl phosphine (0.55 g 2.1 mmol) and a minimum amount of anhydrous THF (3 mL) was sonicated for 10 min at ambient temperature. Diisopropyl azodicarboxylate (DIAD) (0.42 mL 2.1 mmol) was added to the solution under N_2 dropwise via syringe with continuous stirring. The resulting solution was sonicated for 2 h under nitrogen. After concentration, the residue was precipitated in hexane (500 mL) with vigorous stirring, redissolved in distilled water followed by filtration, and then dialysed against distilled water using MWCO 1000 Da membrane for 2 days (as for mPEG$_{550}$-phthalonitrile or mPEG$_{750}$-phthalonitrile, the crude product was dialysed against water using MWCO 2000 Da membrane). The solution was lyophilised to yield the product as brown colour oil (Yield: 70%).

IR (neat): ν = 2869 (CH_2CH_2O), 2230 (CN) cm^{-1}.

^{1}H NMR (400.03 MHz, $CDCl_3$, 298 K): δ 7.04-7.01 (m, 6H), 6.99-6.97 (m, 4H), 4.14 (t, 4H, J = 5.02 Hz), 3.87 (t, 4H J = 4.77 Hz), 3.73 (m, 4H), 3.69-3.61 (m, 44H), 3.53 (m, 4H), 3.36 (s, 6H); ^{13}C NMR (100.59 MHz, $CDCl_3$, 298 K): δ 156.76, 152.38, 147.10, 121.41, 120.41, 116.27, 115.11 (2 x *C*CN), 109.63 (2 x *C*N), 71.87,70.80, 70.75, 69.61, 67.93, and 58.97.

Average $M_{n,\,NMR}$ = 1000 g mol^{-1}

Typical procedure for mPEG$_{350}$-Pc

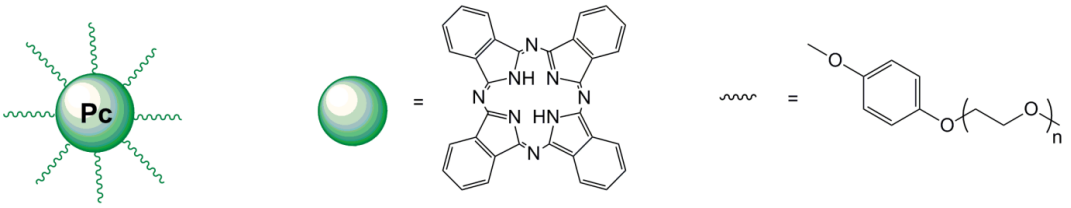

A mixture of mPEG$_{350}$-phthalonitrile (0.89 g, 8.54 mmol), DBU (0.13 mL, 8.54 mmol) and LiBr (7.4 mg, 0.854 mmol) in 1-pentanol (20 mL) were maintained at reflux under nitrogen for 40 hours. After cooling to ambient temperature, the solution was decanted and the residue dialysed against distilled water using MWCO2000 Da membrane for 3 days. The solution was lyophilised to yield the product as a greenish blue paste (Yield: 14%).

IR (neat): ν = 3291 (metal-free Pc N-H stretching), 2868 (CH_2CH_2O), 1018 cm^{-1} (ring vibration bands).

^{1}H NMR (400.03 MHz, $CDCl_3$, 298 K): δ 8.72 (br, 8H), 7.22-7.20 (br, d, 16H), 7.00-6.98 (br, d, 16H, J = 8.3 Hz), 4.17 (br, t, 16H), 3.91 (br, t, 16H, J = 4.5 Hz), 3.78-3.51 (br, 213H), 3.34 (br, s, 24H); ^{13}C NMR (100.59 MHz, $CDCl_3$, 298 K): δ 150.83, 146.53, 119.77, 115.72, 71.84, 70.78, 10.50, 69.83, 67.83, and 58.96.

Average $M_{n,\,NMR}$ = 4200 g mol^{-1}

4,5-Bis(4-hex-5-ynyloxy)phenoxy)phthalonitrile[26]

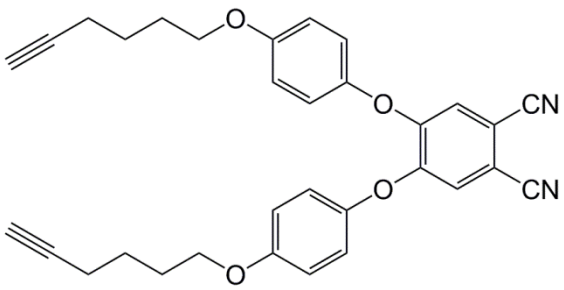

A solution of 5-hexynl-1-ol (0.23 mL 2.1 mmol), 4,5-Bis(4-hydroxyphenoxy)phthalonitrile (0.344 g 1 mmol), triphenyl phosphine (0.55 g 2.1

mmol) and a minimum amount of anhydrous THF (3 mL) was sonicated for 10 min at ambient temperature. Diisopropyl azodicarboxylate (DIAD) (0.42 mL 2.1 mmol) was added dropwise via syringe under N_2 to the stirring solution. The resulting solution was sonicated for 2 h under nitrogen. After concentration, the residue was left as a powder, and dispersed in hexane (500 mL) with vigorous stirring and filtered to obtain a light tan colour solid. The crude product was purified by column chromatography (100% DCM), afford white solid (Yield: 96%).

IR (neat): ν = 3280 (C-H), 2945, 2879, 2224 (CN) cm^{-1}.

^{1}H NMR (400.03 MHz, $CDCl_3$, 298 K): δ 7.06-7.02 (m, 6H), 6.98-6.94 (m, 4H), 4.01 (t, 4H, J = 6.1 Hz), 2.32-2.28 (dt, 4H, J = 2.51, 7.03 Hz), 1.98 (t, 2H, J = 2.6 Hz), 1.96-1.91 (m, 4H), 1.78-1.71 (m, 4H); ^{13}C NMR (100.59 MHz, $CDCl_3$, 298 K): δ 156.97, 152.45, 146.88, 121.48, 120.33, 116.06, 115.15 (2 x *C*CN), 109.57 (2 x *C*N), 83.95 (H*C*≡C), 68.70 (HC≡*C*), 67.78(*C*H_2O), 28.17, 24.96, and 18.1.

ESI-MS m/z: calcd for $C_{32}H_{28}N_2O_4$ 527.1 $[M+Na]^+$, observed 527.1

2,3,9,10,16,17,23,24-Octa(6-(triisopropylsilyl)hex-5-ynyloxy)phenoxy)phthalocyanine[26]

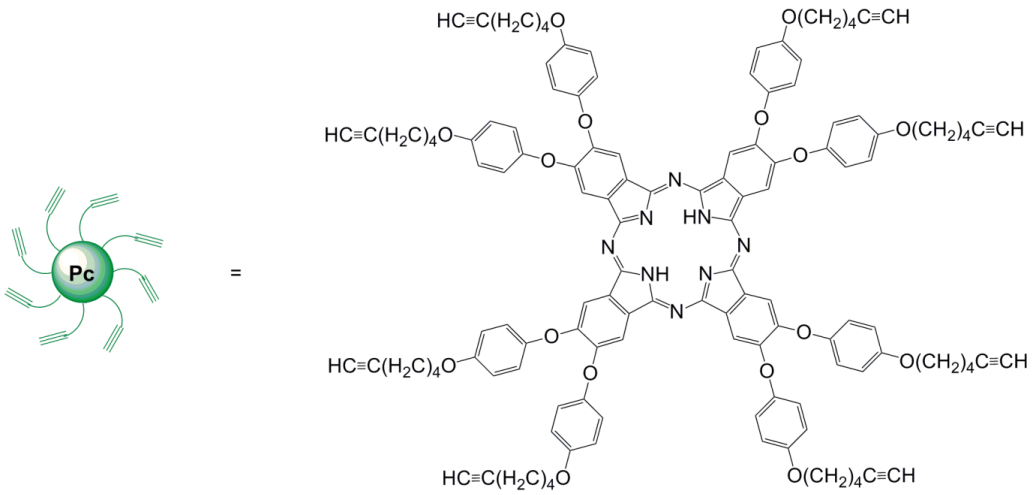

A mixture of 4,5-bis(4-hex-5-ynyloxy)phenoxy)phthalonitrile (0.845 g, 1.67 mmol), DBU (0.25 mL, 1.67 mmol) and LiBr (14.5 mg, 0.167 mmol) in 1-pentanol (30 mL) were maintained at reflux under nitrogen for 40 hours. After cooling to ambient temperature, the mixture was poured into 500 mL methanol. The dark green product was filtered and washed with methanol. The crude product was purified by flash chromatography on a silica column (SiO_2, 100% DCM) (Yield: 18%).

IR (neat): ν = 3284 (metal-free Pc N-H stretching), 2114 (C≡C), 1009 cm^{-1} (ring vibration bands).

^{1}H NMR (400.03 MHz, $CDCl_3$, 298 K): δ 8.40 (br, 8H), 7.29-7.26 (d, 16H, J = 8.8 Hz), 6.94-6.92 (d, 16H, J = 8.8 Hz), 3.99-3.96 (t, 16H, J = 6.3 Hz), 2.35-2.31 (dt, 16H, J = 2.6, 7 Hz), 2.03-2.02 (t, 8H, J = 2.6 Hz), 2.00-1.93 (m, 16H), 1.82-1.74 (m, 16H); ^{13}C NMR (100.59 MHz, $CDCl_3$, 298 K): δ 155.30, 150.82, 119.73, 115.50, 113.15, 68.76, 67.72, 28.51, 25.15, and 18.30.

MALDI-ToF m/z: calcd for $C_{128}H_{115}N_8O_{16}$ 2020.8 $[M+H]^+$, observed 2020.1.

Typical procedure for Azido-terminated PEG monomethyl ether (N_3-mPEG$_{750}$)

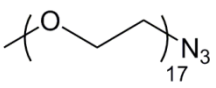

In a dry round-bottom flask, poly(ethylene glycol) methyl ether (average M_n = 750 g/mol, 7.5 g, 0.01 mol) was dissolved in dried DCM (150 mL). The solution was cooled to 0 ^oC in an ice bath before triethylamine (15.3 mL, 0.11 mol) and stirring for 15 min at 0 ^oC. Then, methanesulfonyl chloride (7.7 mL, 0.10 mol) was added dropwise at this temperature. After completion, the flask was removed from the ice bath and the reaction was warmed to room temperature over night. During this period, the reaction mixture slowly turned yellowish with precipitation. After filtration to remove the solid, the reaction mixture was washed successfully with 1 M HCl solution (3 x 100 mL), 1 M NaOH solution (3 x 100 mL), saturated $NaHCO_3$ (3 x 100 mL), and saturated brine solution (3 x 100 mL). The organic layer was dried over anhydrous $MgSO_4$, and concentrated under vacuum to afford PEG$_{750}$-OMs. The residue was redissolved in DMF (50 mL) with addition of NaN_3 (6.5 g, 0.1 mol) The

reaction was stirring at 65 ^{o}C overnight, following by cooled to ambient temperature and concentrated *in vacuo*. The residue was dissolved in water (200 mL) and then washed with DCM (2 x 100 mL). The organic layers were combined, washed with saturated brine (3 x 100 mL) and water (3 x 100 mL), and dried with anhydrous $MgSO_4$. After filtration and concentration, the product was dried overnight to afford monoazido PEG (Yield: 75%).

IR (neat): ν = 2867 (CH_2CH_2O), and 2101(N_3)

^{1}H NMR (400.03 MHz, $CDCl_3$, 298 K): δ 3.85 – 3.50 (m, C*H*$_2$O), 3.40-3.36 (s, 3H, OC*H*$_3$ end group, and t, 2H, C*H*$_2$N$_3$ end group); ^{13}C NMR (100.59 MHz, $CDCl_3$, 298 K): δ 71.87, 70.50, 69.96, 58.96, and 50.62.

MALDI-ToF m/z: calcd for $C_{35}H_{71}N_3O_{17}$ 828.47 $[M+Na]^+$, observed 828.5.

Typical procedure for CuAAC cycloaddition of Pc-alkyne with N_3-mPEG$_{2000}$

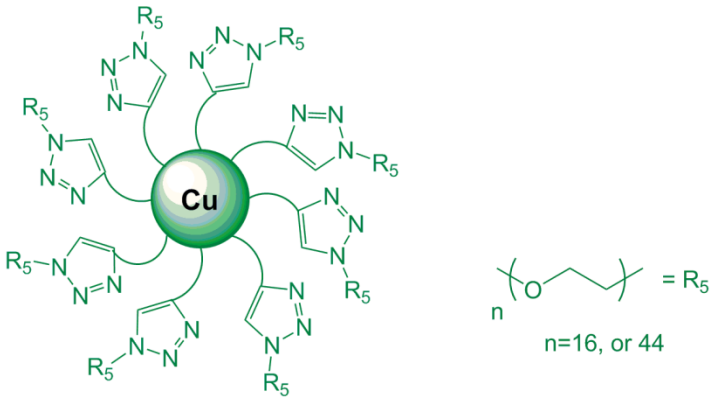

Pc-alkyne (0.025 g, 12.5 μmol, 1 equiv.) were charged in a Schlenk tube with 6 mL of dry DCM or THF. Subsequently, N_3-mPEG$_{2000}$ (0.2 g, 100 μmol, 8 equiv.) and DIPEA (17.2 μL, 100 μmol, 8 equiv.) were added. The Schlenk solution was subjected to 3 freeze-pump-thaw cycles and then cannulated under N_2 into a second Schlenk tube, previously evacuated and filled with N_2, containing CuI (3 mg, 14.8 μmol, 1.2 equiv.). The temperature was adjusted to 25 ℃. The reaction was carried out for 3 days. After reaction, the product was precipitated in diethyl ether, followed by filtration and dialysis using MWCO 2000 Da membrane in distilled water for 2

days. The solution was lyophilised to yield the product as a greenish blue powder (Yield: 70%).

3.5 References

1. F. Baumann, *U.S. Patent*, 1952, 2, 613, 128.
2. J. H. Weber and D. H. Busch, *Inorganic Chemistry*, 1965, **4**, 469-471.
3. G. Schneider, D. Wohrle, W. Spiller, J. Stark and G. Schulz-Ekloff, *Photochemistry and Photobiology*, 1994, **60**, 333-342.
4. M. Bressan, N. Celli, N. d'Alessandro, L. Liberatore, A. Morvillo and L. Tonucci, *Journal of Organometallic Chemistry*, 2000, **593–594**, 416-420.
5. H. Ali, R. Langlois, J. R. Wagner, N. Brasseur, B. Paquette and J. E. Van Lier, *Photochemistry and Photobiology*, 1988, **47**, 713-717.
6. J. Schofield and M. Asaf, *Journal of Chromatography A*, 1997, **770**, 345-348.
7. F. Dumoulin, M. Durmuş, V. Ahsen and T. Nyokong, *Coordination Chemistry Reviews*, 2010, **254**, 2792-2847.
8. P. Harder, M. Grunze, R. Dahint, G. M. Whitesides and P. E. Laibinis, *The Journal of Physical Chemistry B*, 1998, **102**, 426-436.
9. C. Piechocki and J. Simon, *Nouv. J. Chim.*, 1985, 159.
10. N. B. McKeown and J. Painter, *Journal of Materials Chemistry*, 1994, **4**, 1153-1156.
11. G. J. Clarkson, B. M. Hassan, D. R. Maloney and N. B. McKeown, *Macromolecules*, 1996, **29**, 1854-1856.
12. S. Tuncel, F. Dumoulin, J. Gailer, M. Sooriyaarachchi, D. Atilla, M. Durmus, D. Bouchu, H. Savoie, R. W. Boyle and V. Ahsen, *Dalton Transactions*, 2011, **40**, 4067-4079.
13. N. Brasseur, R. Ouellet, C. L. Madeleine and J. E. v. Lier, *British Journal of Cancer*, 1999, **80**.
14. J.-D. Huang, W.-P. Fong, E. Y. M. Chan, M. T. M. Choi, W.-K. Chan, M.-C. Chan and D. K. P. Ng, *Tetrahedron Letters*, 2003, **44**, 8029-8032.
15. X. Liang-yan, C. Song-mao and L. O. Nancy, *Oncogene*, 2001, **20**.

16. R. L. Morris, K. Azizuddin, M. Lam, J. Berlin, A.-L. Nieminen, M. E. Kenney, A. C. S. Samia, C. Burda and N. L. Oleinick, *Cancer Research*, 2003, **63**, 5194-5197.
17. C. M. Whitacre, D. K. Feyes, T. Satoh, J. Grossmann, J. W. Mulvihill, H. Mukhtar and N. L. Oleinick, *Clinical Cancer Research*, 2000, **6**, 2021-2027.
18. C. M. Allen, W. M. Sharman and J. E. Van Lier, *Journal of Porphyrins and Phthalocyanines*, 2001, **5**, 161-169.
19. J.-W. Hofman, F. van Zeeland, S. Turker, H. Talsma, S. A. G. Lambrechts, D. V. Sakharov, W. E. Hennink and C. F. van Nostrum, *Journal of Medicinal Chemistry*, 2007, **50**, 1485-1494.
20. M. E. Dieter Wöhrle , Kiyotaka Shigehara, Akira Yamada, *Synthesis*, 1993, **1993**, 194-196.
21. K. C. K. Swamy, N. N. B. Kumar, E. Balaraman and K. V. P. P. Kumar, *Chemical Reviews*, 2009, **109**, 2551-2651.
22. S. D. Lepore and Y. He, *Journal of Organic Chemistry*, 2003, **68**, 8261-8263.
23. G. Chen, L. Tao, G. Mantovani, V. Ladmiral, D. P. Burt, J. V. Macpherson and D. M. Haddleton, *Soft Matter*, 2007, **3**, 732-739.
24. J. Geng, J. Lindqvist, G. Mantovani and D. M. Haddleton, *Angewandte Chemie International Edition*, 2008, **47**, 4180-4183.
25. J. Geng, G. Mantovani, L. Tao, J. Nicolas, G. Chen, R. Wallis, D. A. Mitchell, B. R. G. Johnson, S. D. Evans and D. M. Haddleton, *Journal of the American Chemical Society*, 2007, **129**, 15156-15163.
26. X. Chen, J. Thomas, P. Gangopadhyay, R. A. Norwood, N. Peyghambarian and D. V. McGrath, *Journal of the American Chemical Society*, 2009, **131**, 13840-13843.
27. J. M. Ren, J. T. Wiltshire, A. Blencowe and G. G. Qiao, *Macromolecules*, 2011, **44**, 3189-3202.
28. Y. Li, M. D. Giles, S. Liu, B. A. Laurent, J. N. Hoskins, M. A. Cortez, S. G. Sreerama, B. C. Gibb and S. M. Grayson, *Chemical Communications*, 2011, **47**, 9036-9038.
29. Y. Li, J. N. Hoskins, S. G. Sreerama and S. M. Grayson, *Macromolecules*, 2010, **43**, 6225-6228.
30. T. R. Chan, R. Hilgraf, K. B. Sharpless and V. V. Fokin, *Organic Letters*, 2004, **6**, 2853-2855.

Chapter 4 Dual-Responsive Star-Shaped Poly(*N*,*N*-dimethylaminoethyl methacrylate) with Zinc Phthalocyanine Core and Its Quaternized Ammonium Salts

4.1 Introduction

4.1.1 Water-soluble phthalocyanines containing quaternized amines

Cationic groups obtained by the quaternization of aliphatic or aromatic nitrogen atoms have proven to be an efficient alternative to provide the water-solubility of phthalocyanines. The main synthetic pathway is the introduction of an amino group, which can be either formed prior to the formation of the phthalocyanine core, or introduced to a preformed macrocycle bearing suitable reactive groups. In most cases, the quaternization process always occurs on the phthalocyanine at the final step of the synthesis. Multi-methylation is probably the simplest way to achieve quaternization by methylating agents which are commonly used: methyl bromide/ iodide and dimethylsulfate.

Leznoff *et al*.[1] prepared the first cationic phthalocyanine bearing quaternized amines in 1989, **Figure 4.1.1**. Iodophthalonitrile was reacted with 3-*N,N'*-diethylaminoprop-1-yne, followed by reduction of the triple bond resulting in alkylaminophthalonitrile. The metal free or zinc metalated phthalocyanine was obtained from the corresponding diiminisoindoline product. The desired complexes were then prepared by quaternization with iodomethane. This first quaternized phthalocyanine was used for the comparison of their different properties with those anionic and neutral ones. Since then, a number of mono or disubstituted phthalonitrile bearing amino groups have been reported for formation of cationic water-soluble phthalocyanines, and a variety of central metals can be accommodated.

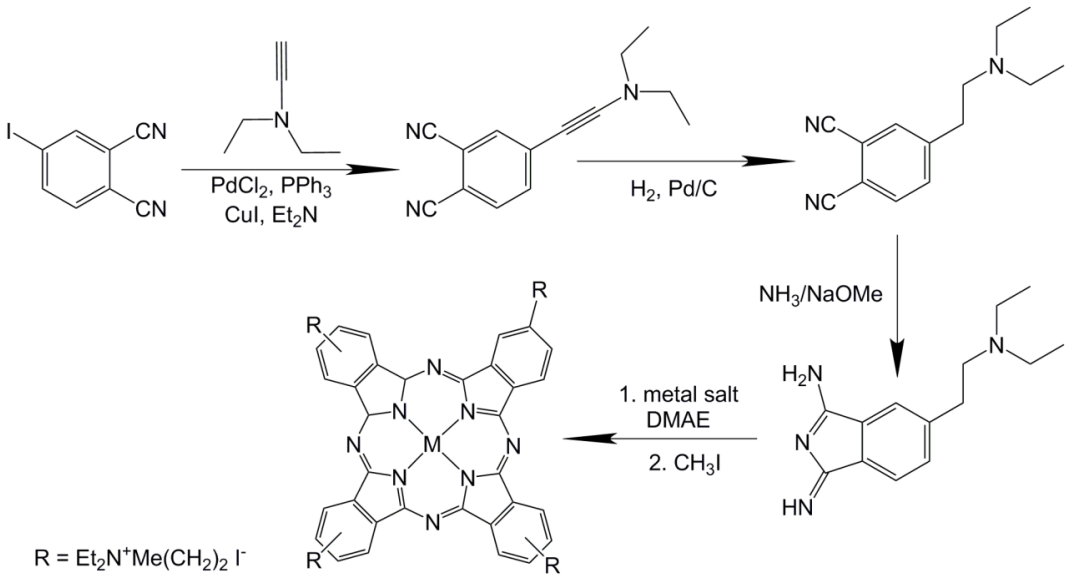

Figure 4.1.1 Synthetic route of the first cationic phthalocyanine bearing quaternized amines[1]

Several water soluble metal phthalocyanines bearing 12 tertiary amine groups,[2] **Figure 4.1.2**, enable the molecules to dissolve in number of organic solvents and water. Metallophthalocyanines were synthesised directly by cyclotetramerisation of the phthalonitrile derivative in the presence of anhydrous metal salt and *N*-donor base DBU in a high-boiling solvent. The electronic spectra of these metallophthalocyanines with dimethylamino substituents in water are sensitive to changes in pH of the solution. Solution studies indicated that the complexes were monomeric only in acidic medium (pH < 6) due to the repulsion of amino groups converted into cationic form. Impressively, a further investigation of a cationic Pd phthalocyanine obtained by full methylation of the twelve tertiary amines showed that the quaternized dye was absolutely non-aggregated in water and monomeric at all pH values.

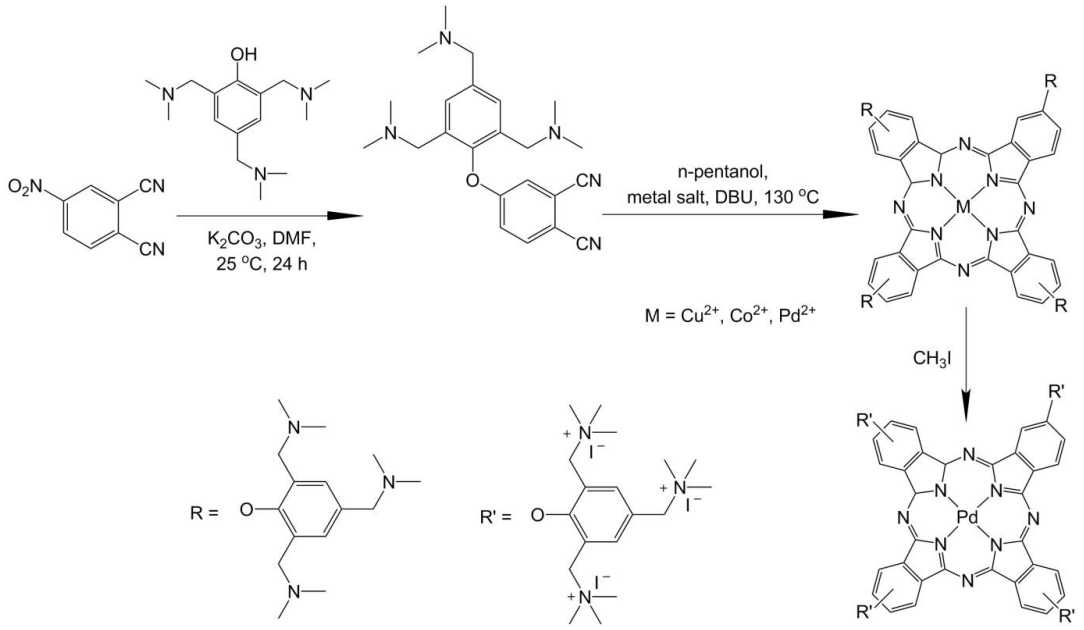

Figure 4.1.2 Synthesis of cationic phthalocyanine bearing twelve quaternized amino groups[2]

More complex synthetic pathways have been also developed, enlarging the number available water-soluble phthalocyanine derivatives. A synthetic route involved successive bromination and dinitrilation of aromatic compounds bearing protecting phthalimide as precursor is one of these strategies.[3] After cyclotetramerisation, the removal of the protecting group occurs on the phthalocyanine derivative resulting in the complex bearing four primary amine groups. The following quaternization step achieved on itself lead to the water-soluble product.

Quaternized aromatic nitrogen on tetra- or octapyridinium substituted phthalocyanine derivatives are expected to be water-soluble. However, due to the planar pyridinium aromatic rings being less bulky than the alkylated complexes, these compounds are generally more aggregated than cationic alkyl phthalocyanines bearing the same number of quaternized charges.[4]

Zwitterionic phthalocyanines existing simultaneously anionic and cationic charges are only reported in a few papers, and they are generally a result of the quaternization by propanesultone bearing a hidden sulfonate function, including the case of the tetrapyridino *ZnPc*,[5] of the Ge derivative[6] and of the $Si(OH)_2$ derivative,[7]

which are all combining four positive charges on the pyridine ring and four negative charges on sulfonate groups. These zwitterionic complexes were employed for the photocatalytic oxidation of 2-mercaptoethanol in aqueous alkaline solution under irradiation with visible light,[5, 6] which oxidise the thiolate to the sulfonic acid and sulfate.

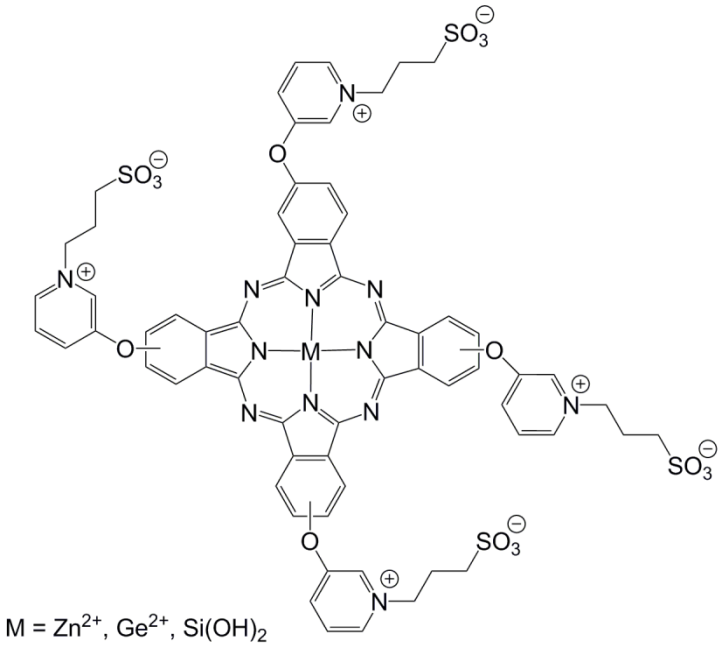

Figure 4.1.3 Zwitterionic phthalocyanines[5-7]

4.1.2 Polymerisation of tertiary amine (meth)acrylate monomers and their properties

Polymers that are responsive to applied stimulus are of great interest for their numerous applications in biological and medical fields. These "smart" materials can undergo conformational or phase changes in response to variations on solution temperature, pH, electrolyte concentration, intensity of light, or a combination of such environmental changes. In particular, of all the established stimulus-responsive systems, those tertiary amine monomers building blocks, as shown in **Figure 4.1.4**, have been shown to exhibit diverse aqueous solution behaviour, which lies in the fact that their corresponding homopolymers possess very different properties in water.

Well-defined homopolymers of 2-(dimethylamino)ethyl methacrylate (DMAEMA, **Figure 4.1.4**, **1**) were prepared under ATRP conditions,[8-11] and the reported cloud

points of PDMAEMA vary from 14 to 50 ^{o}C in pure water, depending on the degree of polymerisation.[12-15] In aqueous solutions of both linear and star-shaped PDMAEMA, the lower critical solution temperature (LCST) can be readily tuned between 25 to 80 ^{o}C by changing the pH of the solution, as well as the molecular weight and concentration of the polymer.[16] In comparison, homopolymers of 2-(diethylamino)ethyl methacrylate (DEAEMA, **Figure 4.1.4**, **4**) and 2-(di-isopropylamino)ethyl methacrylate (DiPAEMA, **Figure 4.1.4**, **5**) exhibit pH-responsive properties. At low pH, their homopolymers are soluble in water owing to the protonation of the tertiary amine pedant group but become hydrophobic at neutral to high pH when the amine groups are deprotonated. However, the unexpected transesterification of these three tertiary amine methacrylates (DMAEMA, DEAEMA, and DiPAEMA) during methanolic ATRP occurred at ambient temperature, which was observed for the first time by Bores-Azeau *et al.*;[17] thus, methanol should not be used as a (co)solvent for the ATRP of these three amine functional monomers.

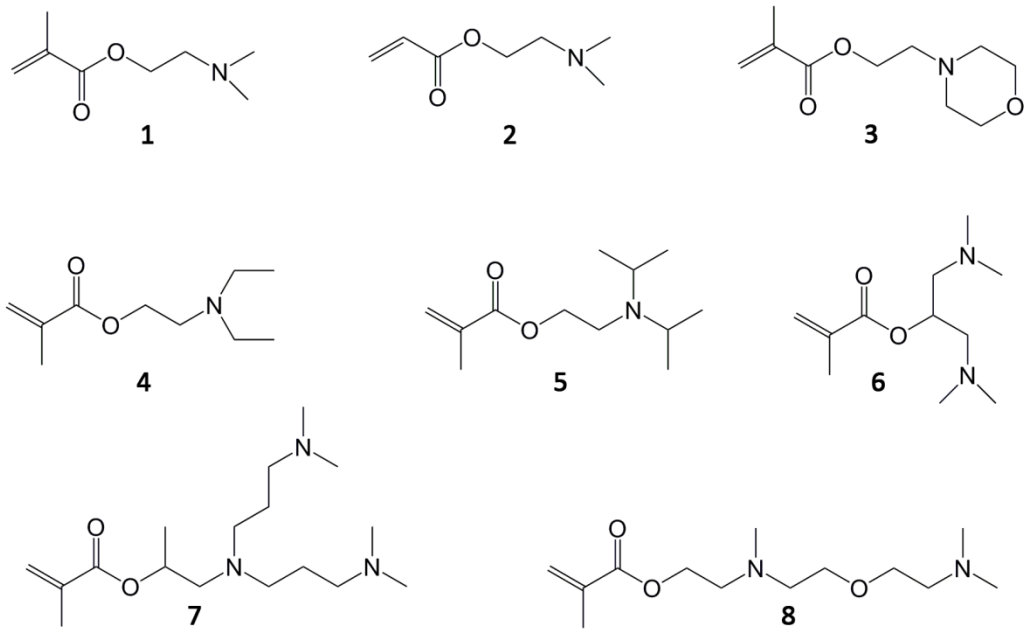

Figure 4.1.4 Structures of various commercial available and synthetic tertiary amine (meth)acrylate monomers

Moreover, the hydrolytic stability of DMAEMA and its corresponding homopolymers were investigated by Hennink group.[18] The study showed that the ester in DMAEMA is rather unstable towards hydrolysis at pH = 7.4 (37 ^{o}C, $t_{1/2}$ = 17 h). However, the ester groups in its polymer are quite insensitive toward hydrolysis, which might be explained by the low dielectric constant in the microenvironment of the polymer backbone. Similarly, ^{1}H and ^{13}C NMR analysis confirmed that the corresponding acrylate monomer (DMAEA , **Figure 4.1.4**, **2**) as well as its polymer (PDMAEA) were found to undergo a self-catalysed ester interchange reaction in methanol and to hydrolyse in aqueous solution by McCool *et al*.[19] A detailed study demonstrated by Monteiro *et al*.[20] illustrated that the degradation of well-defined PDMAEA prepared via RAFT (**Figure 4.1.5**) was independent of both the polymer molecular weight and solution pH, and it was consistent with a self-catalysed hydrolysis process without the need for an internal or external degradation trigger.

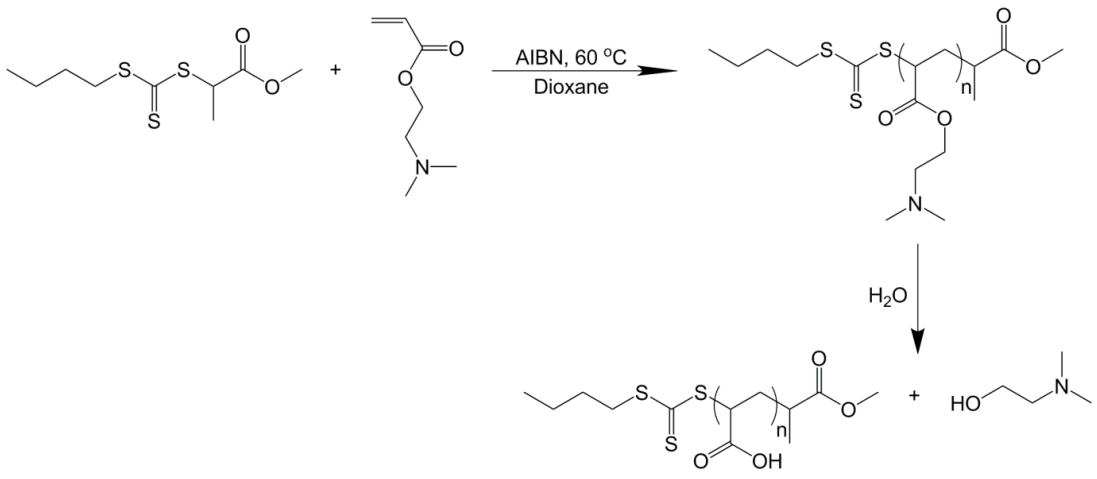

Figure 4.1.5 Polymerisation and self-catalysed hydrolysis of PDMAEA[20]

Homopolymers of 2-(*N*-morpholino)ethyl methacrylate (MEMA, **Figure 4.1.4**, **3**) by group transfer polymerisation (GTP) were explored by Armes and co-workers,[14] in a similar fashion to PDMAEMA, exhibited an LCST between 34 and 53 ^{o}C, again depending on the molecular weight. In addition, the MEMA homopolymers were particularly sensitive to the added electrolyte, with 'salting out' occurring at 20 ^{o}C with addition of 0.2 - 0.3 M Na_2SO_4. Last but not least, the synthesis, RAFT

(co)polymerisation and aqueous phase behaviour of new methacrylates containing two or three pendent tertiary amine functional groups (**Figure 4.1.4**, **6-8**) were described by Yu *et al*..[21] All three homopolymers were shown to possess an LCST ranging from ~ 22 ^{o}C to ~ 63 ^{o}C respectively. Additionally, they became hydrophobic and phase separated at high solution pH. Therefore, due to such different aqueous solution characteristics of tertiary amine containing polymers, the combinations of these monomers, as well as with other hydrophilic building blocks are able to form higher ordered structures, such as micelles and vesicles to environmental changes including such as solution pH, temperature, and electrolyte concentration.

It should also be noted that these water soluble polyamines are promising candidates for polymeric gene transfer agents. Hennink and co-workers have shown that DMAEMA based (co)polymers are able to bind plasmid DNA via electrostatic interactions, which are taken up by cells.[22, 23] The influence of polymer architecture and molecular weight of PDMAEMA polycations on the transfection efficiency and cell viability was studied by Müller group.[24] From the combined cytotoxicity and transfection data, they suggested that polymers with a branched architecture and an intermediate molecular weight could be the most promising candidates for efficient gene delivery.

4.1.3 Phthalocyanine-thermoresponsive polymer conjugates

Thermoresponsive polymers that respond to the changes in temperature belong to the class of stimuli-responsive materials. The polymers exhibit an LCST behaviour, whereby below its LCST the polymer is soluble in aqueous solution due to the extensive hydrogen bonding interaction with the surrounding water molecules and restricted intra- and intermolecular hydrogen bonding between polymer molecules, as represented in **Figure 4.1.6**. Upon heating, hydrogen bonding with water is disrupted, and intra- and intermolecular hydrophobic interactions dominate, which result in a transition in solubility.[25, 26]

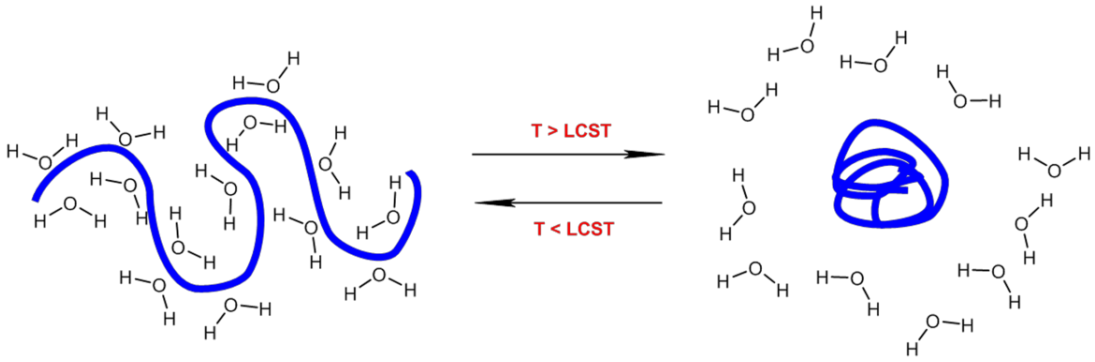

Figure 4.1.6 Schematic representation of polymer lower critical solution temperature

These polymers reported to have potential use in biomedical application including controlled drug delivery, bioseparations, filtrations, and DNA sequencing etc.[26, 27] Poly(*N*-isoprpylacrylamide) (PNIPAAM) is the most widely studied thermo-responsive polymer, which is able to undergo a reversible phase transition at ~ 32 ^{o}C. By incorporation of phthalocyanine derivatives with PNIPAAM (*ZnPc*-PNIPAAM, **Figure 4.1.7**) in the field of photocatalytic oxidation, the polymeric photocatalysts possessed both catalytic activity and thermoresponsive property by the degradation of Rhodamine B in presence of hydrogen peroxide under visible light, and facilitate the recycling the catalyst upon changing the temperature of the system.[28, 29] ATRP of NIPAAM was carried out in toluene at 70 ^{o}C using asymmetrically substituted *ZnPc*Br as initiator and CuBr/Me_6-TREN as the catalyst. A series of well-defined *ZnPc*-PNIPAAM with narrow PDI between 1.14 and 1.20 were obtained, which revealed the polymerisation was in a controlled process.

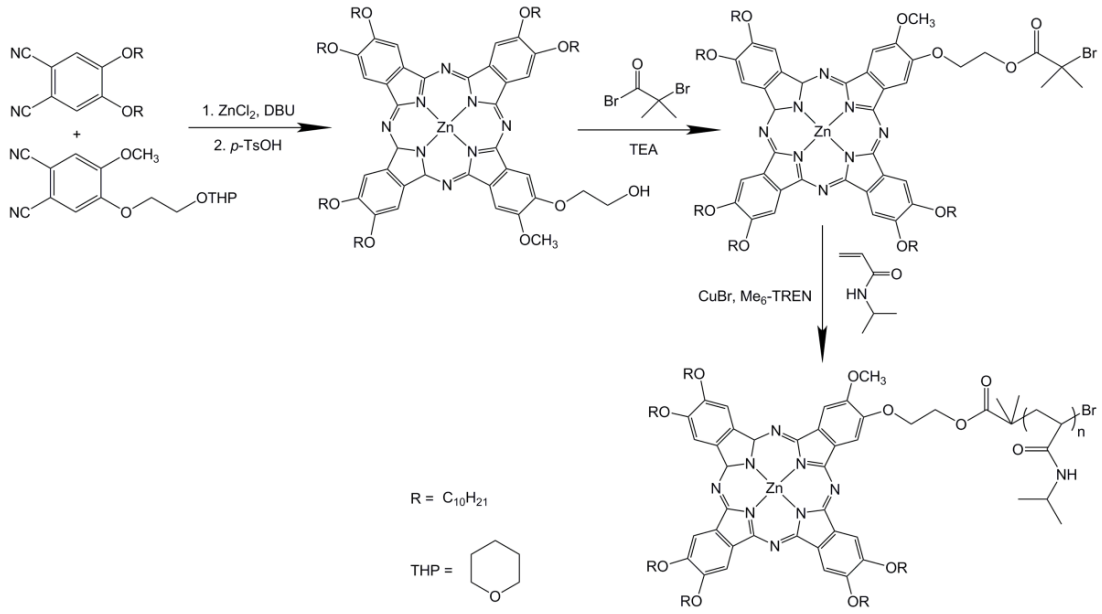

Figure 4.1.7 Synthetic route for the well-defined *ZnPc*-PNIPAAM via ATRP[28]

Thermoresponsive polymers derived from oligo(ethylene glycol)-based monomers, **Figure 4.1.8**, have been considered as attractive alternatives to PNIPAAM based on their use in various biologically relevant applications, which have recently been highlighted by Lutz.[30] Homopolymers of di(ethylene glycol)methyl ether methacrylate ($PMEO_2MA$) and tri(ethylene glycol)methyl ether methacrylate ($PMEO_3MA$) were synthesised by living anionic polymerisation and shown to exhibit the reversible cloud points at 26 and 52 ^{o}C, respectively.[31] Poly(oligo(ethylene glycol) methacrylates) (POEGMA) with longer side-chains ($OEGMA_{300}$ and $OEGMA_{475}$) were found to show transitions in the range 60 – 90 ^{o}C.[32, 33] Therefore, copolymers with various ratios of MEO_2MA and OEGMA exhibit tuneable thermal transitions between 26 and 90 ^{o}C.[34, 35]

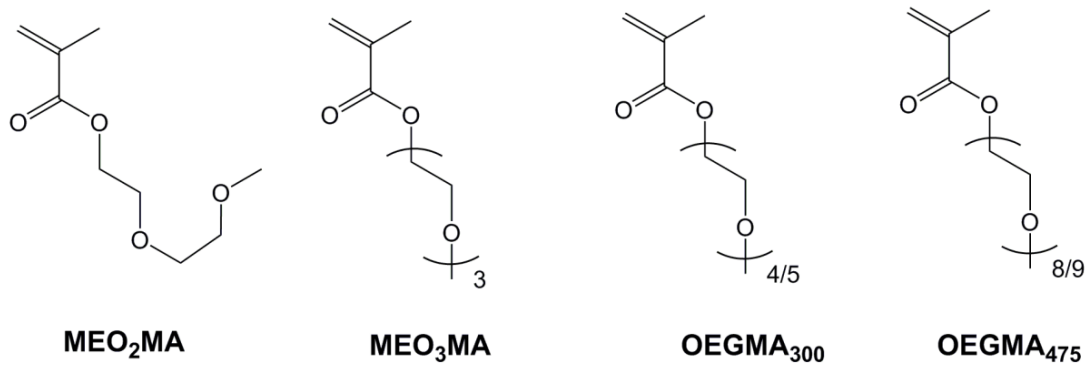

Figure 4.1.8 Molecular structures of oligo(ethylene glycol) methacrylates frequently used for synthesising thermoresponsive biocompatible polymers[30]

Recently, a multi-targeting drug nanocarrier for PDT has been successfully prepared by the conjugation of silicon(IV) phthalocyanine dichloride (*SiPc*Cl_2) to the thermoresponsive PEG-methacrylates based polymers, **Figure 4.1.9**, which were synthesised by RAFT polymerisation using 2-cyanoprop-2-yl α-dithionaphthalate (CPDN) as the RAFT agent and AIBN as the initiator.[36] The LCST of the *SiPc*-polymer can be readily controlled via changing the composition of the applied monomers, MEO_2MA, $OEGMA_{475}$, and 2-hydroxyethyl methacrylate (HEMA). The polymer forms micelles in aqueous solution and shows good potential as a drug carrier which can selectively retained in the cancer cells. Moreover, the incorporation of *SiPc* resulting in a good quantum yield makes the polymer considered as a good candidate for photodynamic therapy.

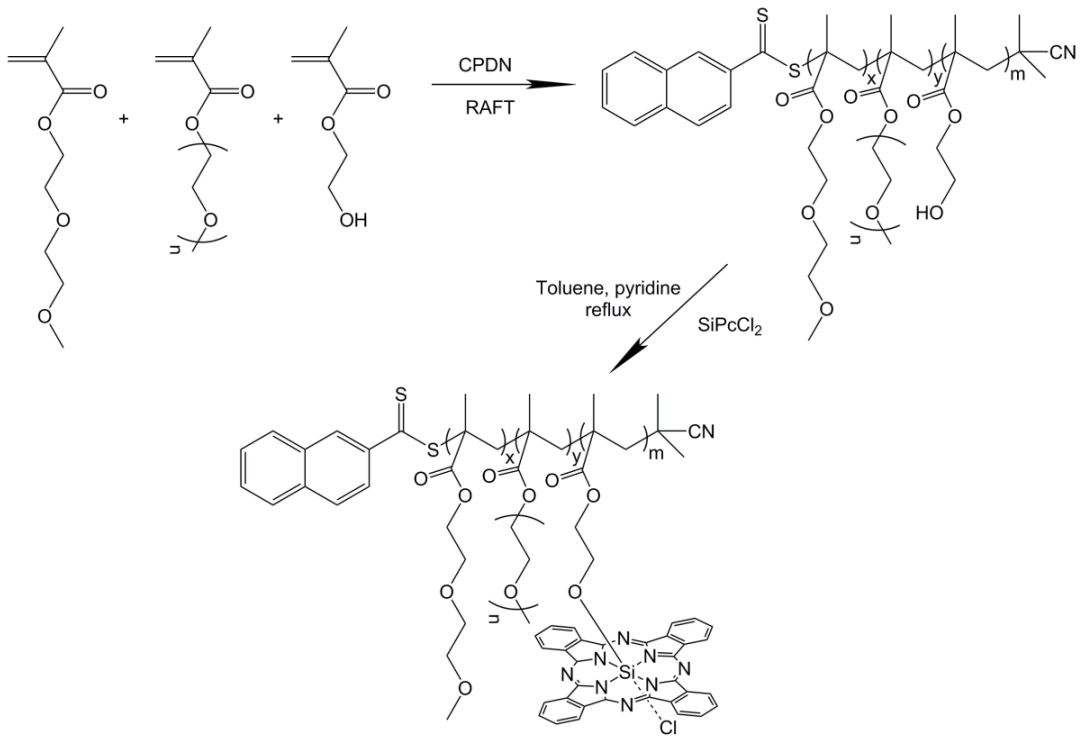

Figure 4.1.9 Synthesis of the thermoresponsive prepolymers via RAFT polymerisation and incorporation of *SiPc*Cl_2 to the prepolymer[36]

4.2 Results and discussion

Due to the adhesive and anti-bacterial effects of PDMAEMA previously investigated in our group,[10, 11, 37] dual-responsive star-shaped poly(*N*,*N*-dimethylaminoethyl methacrylate) with zinc phthalocyanine core (*ZnPc*-PDMAEMA) was first prepared by a core-first approach, **Figure 4.2.1**. As the synthetic strategies discussed in chapter 3, octaalkyne-substituted zinc phthalocyanine was synthesised from alkyne-terminated phthalonitrile by cyclotetramerisation with addition of $Zn(OAc)_2{\cdot}2H_2O$ to form the "clickable" *ZnPc*. The following star polymers were synthesised via a combination of ATRP and CuAAC click chemistry.

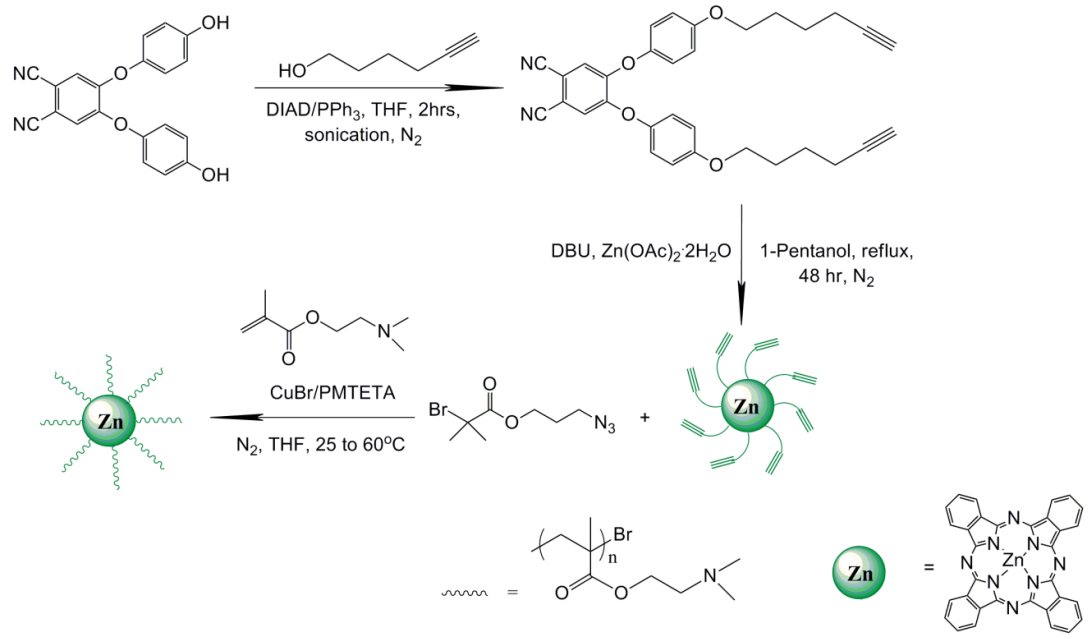

Figure 4.2.1 Synthetic strategies of star-shaped *ZnPc*-PDMAEMA

4.2.1 Synthesis of octaalkyne-substituted *ZnPc*

The hydrophobic zinc phthalocyanine core with octaalkyne-terminated groups was prepared as previously with addition of zinc salt. In contrast to the paramagnetism of Cu(II) compound, *ZnPc* could be successfully characterised by NMR spectroscopy with addition of 5% TFA in $CDCl_3$.

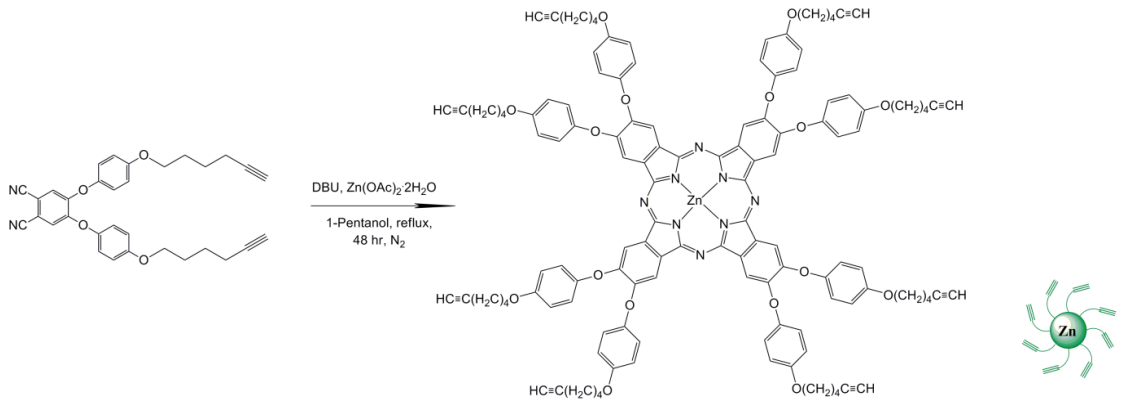

Figure 4.2.2 Synthesis of alkyne-terminated *ZnPc*

^{1}H NMR of *ZnPc*-alkyne, **Figure 4.2.3**, shows the similarity as that of metal-free *Pc*-alkyne. The protons at non-peripheral position of *ZnPc* ring are strongly deshielded indicating a broad peak due to the intermolecular aggregation around δ 8.7 ppm, and the separated doublet peaks between δ 7.2-7.0 ppm contribute to each of 16 protons on eight aromatic rings which are adjacent to the *ZnPc* core. The protons on the octaalkynl chain between δ 4.1-1.7 ppm show similar chemical shift and splitting patterns as that of *Pc*-alkyne compound.

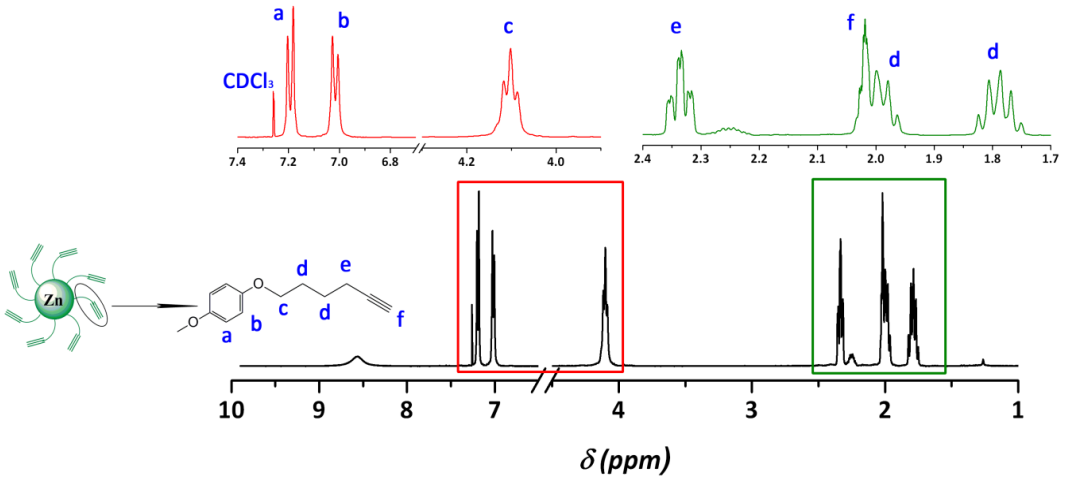

Figure 4.2.3 ^{1}H NMR characterisation of octaalkyne-terminated *ZnPc* in $CDCl_3$ with addition of 5 % TFA

To further prove the success of synthesised clickable *ZnPc*, the product was also characterised by UV-Vis spectroscopy, IR, THF-GPC, and MALDI-ToF analysis. **Figure 4.2.4**-(a) indicates the difference from metal-free *Pc* around Q-band of clickable *ZnPc* (ca.2.4 × 10^{-6} M) in DCM, showing a single absorption at 677 nm with extinction coefficient ε = 2.15 × 10^{5} $M^{-1}cm^{-1}$. The THF-GPC equipped with PDA detector represents a 3D image of *ZnPc*-alkyne, **Figure 4.2.4**-(b), illustrating the same UV-Vis absorption as the product in DCM combined with an elution time profile and rather narrow dispersity (PDI = 1.03), which indicates non-aggregation behaviour of the compound in THF and the formation of a single species.

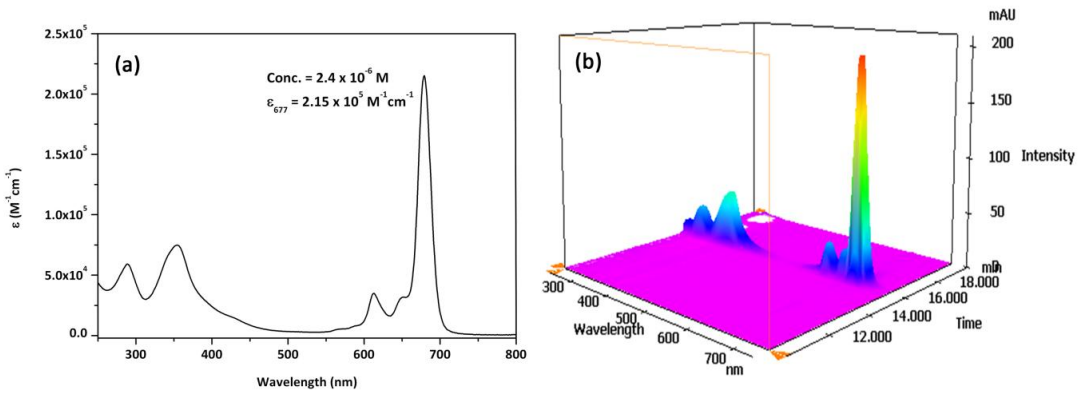

Figure 4.2.4 (a) UV-Vis spectrum of *ZnPc*-alkyne (2.4 x 10^{-6} M) in DCM; (b) THF-GPC equipped with PDA detector representing a 3D image of *ZnPc*-alkyne

IR spectra (**Figure 4.2.5**-a) show that the infrared absorption frequencies of $\nu_{C\equiv N}$ and ν_{C-H} from the nitrile and alkyne groups of alkyne terminated phthalonitrile are sharp, at 2223 cm^{-1} and 3280 cm^{-1} respectively. The disappearance of the $\nu_{C\equiv N}$ vibrational frequency and the broad ν_{C-H} stretching from the terminate alkyne groups also confirm the formation of the macrocycle with multiple alkyne groups after cyclotetramerisation. The MALDI-ToF-MS analysis in reflector mode is also one of the most valuable tools for characterisation of *ZnPc* related compounds, which provides a means to determine the molecular weight of the compound ion in $[M+H]^+$ form, **Figure 4.2.5**-(b).

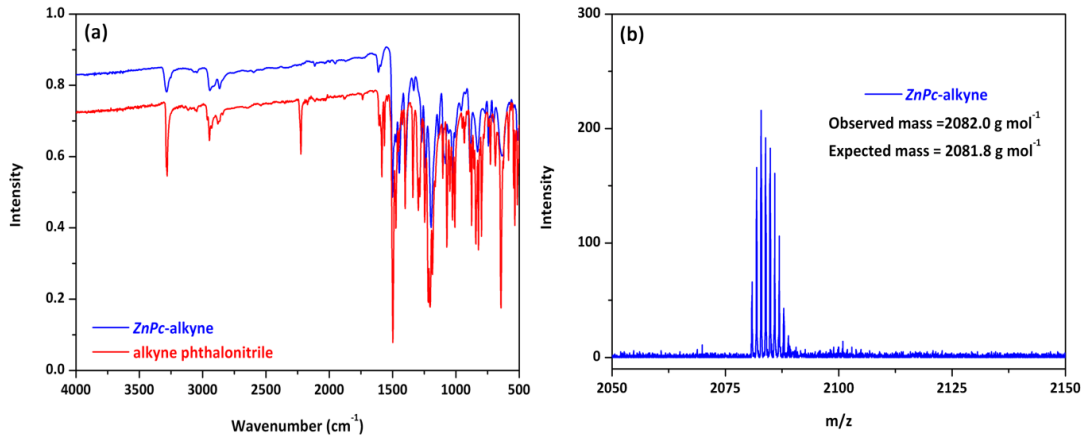

Figure 4.2.5 (a) IR spectra of starting material alkyne phthalonitrile and *ZnPc*-alkyne; (b) MALDI-ToF-MS analysis of *ZnPc*-alkyne using CHCA as matrix and NaI as ion source

4.2.2 Synthesis of star-shaped *ZnPc*-PDMAEMA via a combination of ATRP and CuAAC click chemistry

Azido terminated initiator was synthesised first before polymerisation of DMAEMA, as shown in **Figure 4.2.6**. The 3-azido-propan-1-ol intermediate were obtained by treatment of bromo-alcohol with NaN_3 in refluxing acetone/water mixture. Subsequent acylation with 2-bromoisobutyryl bromide and triethylamine gave the desired azido-ester initiators in reasonable yield (70%).

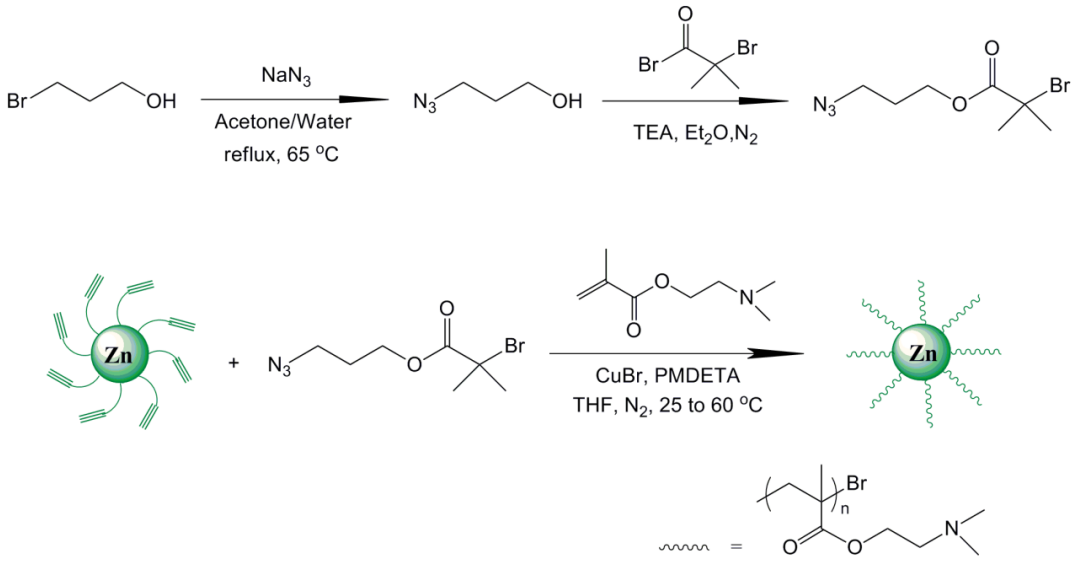

Figure 4.2.6 Synthetic protocols of azide initiator and star-shaped *ZnPc*-PDMAEMA via a combination of ATRP and CuAAC click chemistry

Synthesis of star-shaped *ZnPc*-PDMAEMA was carried out by core-first approach via a combination of ATRP and CuAAC click reaction. Initial attempts were performed by one-pot ATRP/CuAAC process, which has been developed as a novel synthetic tool for the preparation of functional molecular materials. The strategy involves polymerisation of DMAEMA using azido initiator together with *in situ* clicking to alkyne terminated *ZnPc* via sharing the CuBr/PMDETA catalytic system in THF at 60 ^{o}C. After 3 hours, the reaction was stopped and purified. The isolated green polymer was subjected to THF-GPC analysis. The chromatograms (**Figure 4.2.7**) represent the overlapped RI trace with UV signal for the polymer conjugated with *ZnPc* molecule. It can be observed that there is a second peak from the RI trace that has no UV-Vis absorption at λ = 677 nm, which indicates that the presence of small amount of linear azido-PDMAEMA impurity. Therefore, further purification needs to be employed when using this one-pot synthetic strategy.

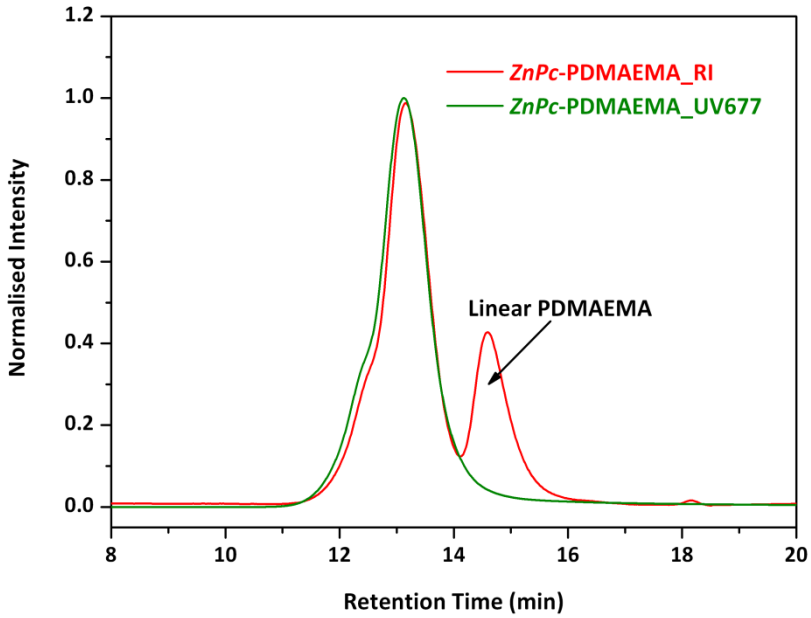

Figure 4.2.7 THF-GPC chromatograms (RI and UV λ=677 nm) of *ZnPc*-PDMAEMA by one-pot ATRP/CuAAC process

In order to improve the purity of *ZnPc*-PDMAEMA, the synthetic strategies have been slightly modified. The click reaction was carried out first overnight at ambient temperature, followed by addition of degassed DMAEMA via a degassed syringe. Then, the polymerisation was performed at 60 ^{o}C for 2 hours. ^{1}H NMR of purified *ZnPc*-PDMAEMA compared with that of *ZnPc*-alkyne shows the successful incorporation of *ZnPc* molecule, **Figure 4.2.8**. The aromatic protons adjacent to the *ZnPc* core become broader and stay between δ 7.2-6.9 ppm, and the two broad singlet peaks around δ 4.04 and 2.55 ppm are corresponding to each of the two ethyl protons close to ester and amino groups respectively. Compared to those polymers conjugated with *CuPc* core, the molecular weight of *ZnPc*-PDMAEMA can be estimated by ^{1}H NMR via comparing the integral of the aromatic protons at either δ 7.15 or 6.95 ppm to that of ethyl protons close to ester group around δ 4.04 ppm. Therefore, the molecular weight of *ZnPc*-PDMAEMA is calculated as $M_{n,NMR}$ = 38,000 g mol^{-1}, and the degree of polymerisation is estimated as DP_{NMR} = 27 per arm.

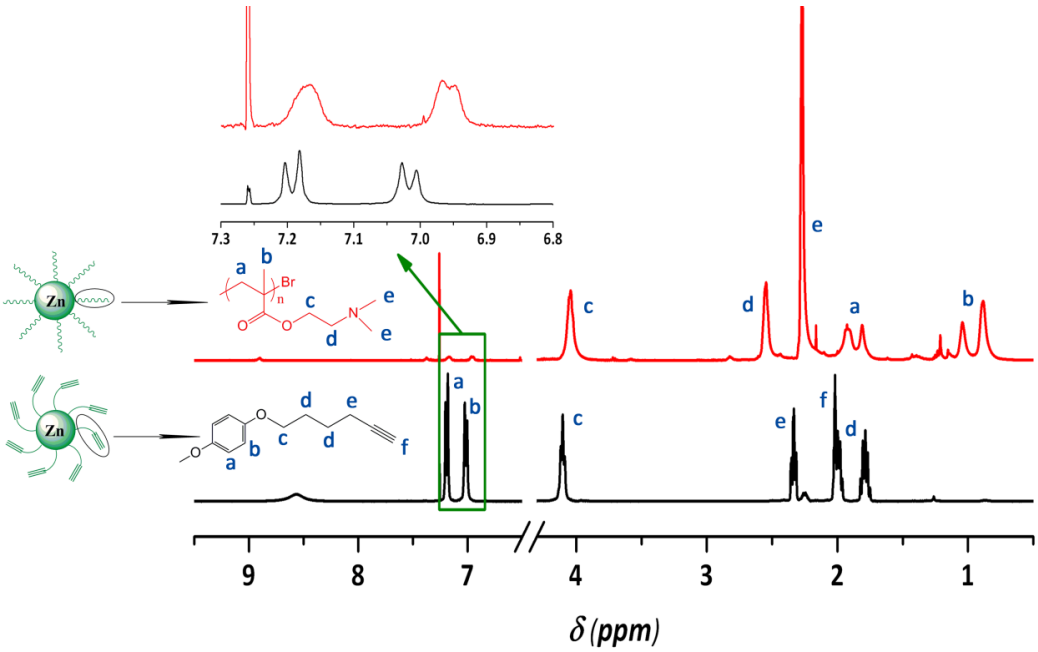

Figure 4.2.8 ^{1}H NMR characterisations of star-shaped *ZnPc*-PDMAEMA in $CDCl_3$ overlapped with that of *ZnPc*-alkyne in $CDCl_3$ with 5% TFA

The GPC traces (**Figure 4.2.9**-a) from the UV detector (λ= 677 nm) show that a slight decrease in elution time corresponding to molecular weight increases in comparison of the intermediate initiator *ZnPc*-Br with the starting material *ZnPc*-alkyne. Furthermore, the dispersity remains rather narrow after click reaction indicating the formation of the majority of single species. After polymerisation, there is a further decrease in elution time of *ZnPc*-PDMAEMA due to an obvious increase in hydrodynamic volume of the polymer, and there is no obvious starting *ZnPc*-alkyne or intermediate *ZnPc*-Br remaining in the polymer according to the UV detector. The GPC traces of purified *ZnPc*-PDMAEMA from both of RI and UV (λ= 677 nm) detectors are well-overlapped with each other, **Figure 4.2.9**-(b), and a relatively narrow dispersity still can be achieved (PDI = 1.19). It should be mentioned that no shoulder peak can be observed from the RI detector without UV-Vis absorption at 677 nm compared with the initial one-pot ATRP/CuAAC process, which indicates that all PDMAEMA should be successfully conjugated with the *ZnPc* core.

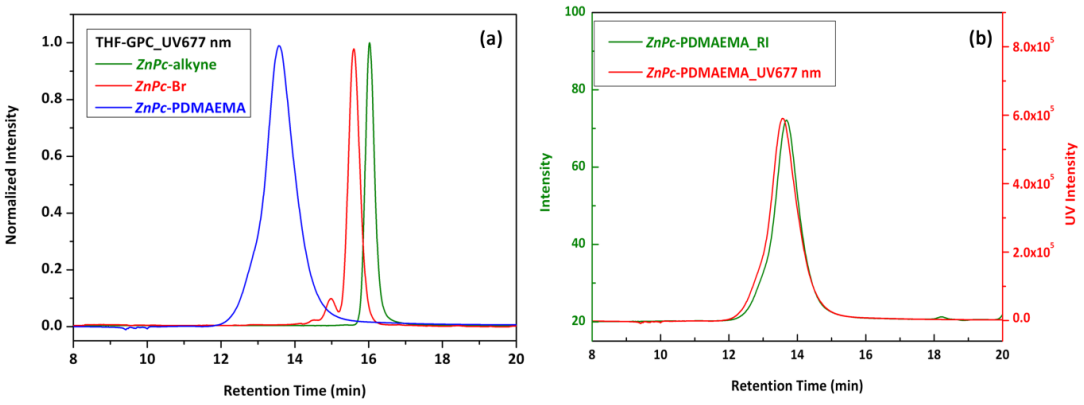

Figure 4.2.9 THF-GPC analysis of (a) starting material *ZnPc*-alkyne, intermediate *ZnPc*-Br, and purified *ZnPc*-PDMAEMA from UV detector (λ= 677 nm); (b) overlapped chromatograms of purified *ZnPc*-PDMAEMA from both of RI and UV (λ= 677 nm) detectors

The IR spectra (**Figure 4.2.10**-a) shows the infrared absorption frequencies of ν_{N3} and ν_{C-H} from the starting materials of azido initiator and alkyne terminated *ZnPc* are around 2100 cm^{-1} and 3280 cm^{-1} respectively. However, after reaction, the intense absorption frequencies from both of starting materials are totally disappeared, further indicating that the improved ATRP/CuAAC combination strategy has been completed and no azido terminated PDMAEMA can be observed. The 3D image from the PDA detector of THF-GPC illustrates the same UV-Vis spectrum but an earlier elution time compared with that of *ZnPc*-alkyne, **Figure 4.2.10**-(b), which suggests the incorporation of *ZnPc* compound into the polymer chain and non-aggregated property of *ZnPc*-PDMAEMA in THF.

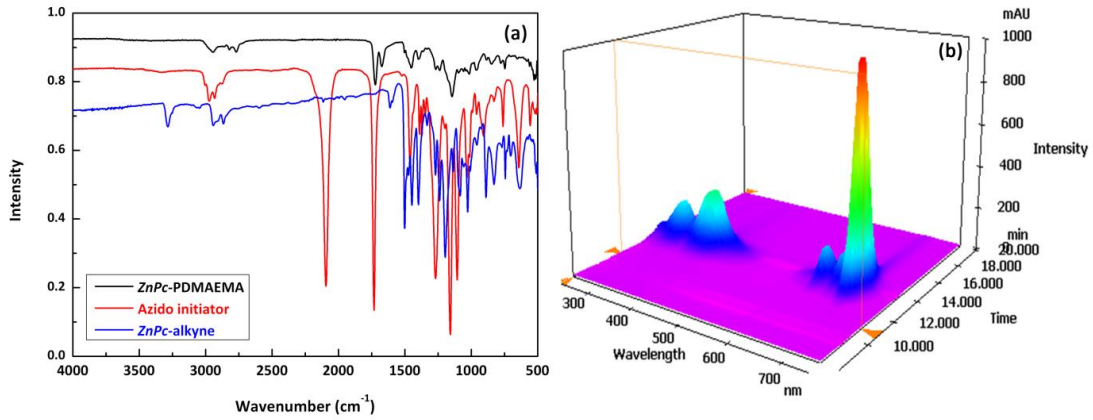

Figure 4.2.10 (a) IR spectra of starting material *ZnPc*-alkyne, azido initiator and purified polymer *ZnPc*-PDMAEMA; (b) 3D image of *ZnPc*-PDMAEMA from THF-GPC coupled with PDA detector

4.2.3 Universal calibration of star-shaped *ZnPc*-PDMAEMA

In order to investigate the polymeric structure of *ZnP*c-PDMAEMA, a viscosity detector was used in the GPC for measuring the specific viscosity of the polymer sample in solution which can converted to the intrinsic viscosity of the sample. The measurement of the intrinsic viscosity by GPC allows the calculation of accurate molecular weights of polymer via the Universal Calibration regardless of the chemistry of the calibration standards employed. Moreover, the GPC separation is based uppon the size of the polymer in solution which is the effective hydrodynamic volume proportional to the intrinsic viscosity and the molecular weight. Therefore, this technique should give a closer representation of the molecular weight of the polymer independent of chemistry and architecture.

In comparison with using the universal calibration to analyse star-shaped *ZnPc*-PDMAEMA, linear PDMAEMA and 8-armed sucrose-PDMAEMA was polymerised by free radical polymerisation (FRP) and ATRP respectively, **Figure 4.2.11**. A similar condition, CuBr/HMTETA with 20% equiv. of Cu(II)Br as catalytic system was used for ATRP of sucrose-PDMAEMA.

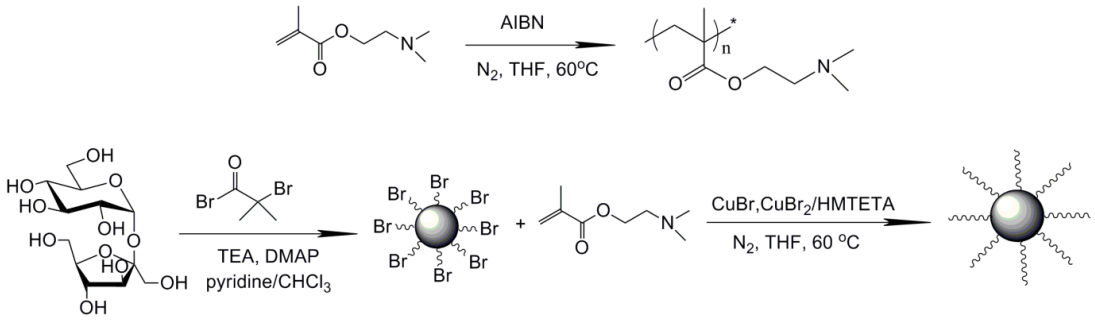

Figure 4.2.11 Synthesis of linear PDMAEMA by FRP, and 8-armed star PDMAEMA using sucrose initiator by ATRP

Furthermore, the use of viscometer allows the assessment of the Mark-Houwink plot according to Mark-Houwink equation which is the relationship between molecular weight and intrinsic viscosity, $[\eta] = KM^{\alpha}$. Therefore, plotting a log form log [η] against logM gives a straight line with intercept of logK and a slope of α, which are useful constant for a particular polymer-solvent system. The value of α indicates the information about the dynamic behaviour of the polymer molecules in solution in the range from 0.5 and 0.8 for most flexible polymers, with lower values indicating the 'hard sphere' model, and with the limiting value of 2.0 indicating the 'rigid rod' model.

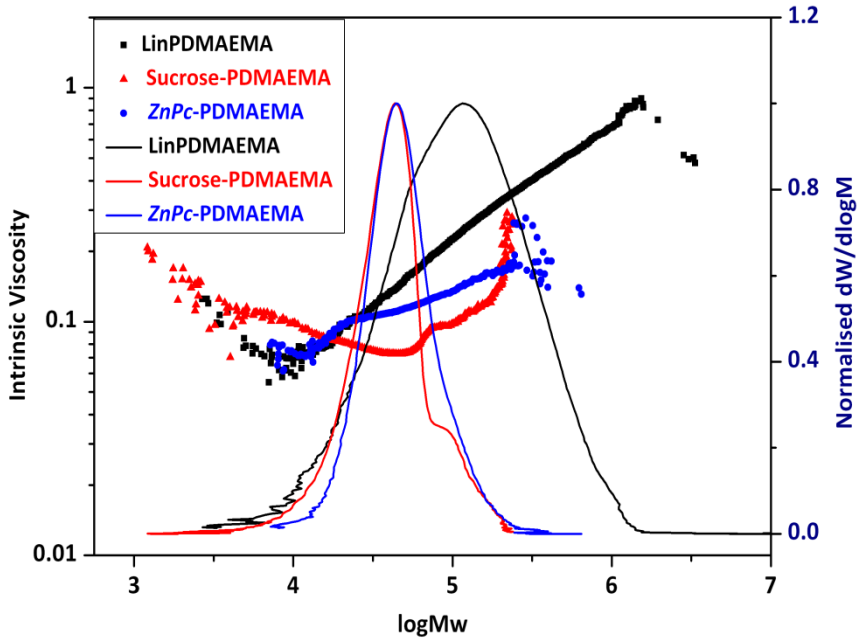

Figure 4.2.12 Overlapped Mark-Houwink plots and the molecular weight distributions calculated by universal calibration for linear PDMAEMA (black), sucrose-PDMAEMA (red), and *ZnPc*-PDMAEMA (blue)

Linear PDMAEMA (black) polymerised by FRP method provides a broader molecular weight distribution covering a wide range of polymer from low to high molecular weight. The Mark-Houwink plot shows that the intrinsic viscosity increases linearly with the increasing molecular weight of PDMAEMA in the main molecular weight region. It should be noticed that for all three polymers, the low molecular weight region, however, suggests less reliable information as the concentration of polymer is very low; therefore, the α value of the plot was calculated only from the main molecular weight distribution areas, **Figure 4.2.12**.

The 8-armed sucrose-PDMAEMA (red) shows a high molecular weight shoulder ascribed to star-star coupling even with 20% Cu(II)Br during the reaction. The Mark-Houwink plot represents an interesting trend in the single star region, where the intrinsic viscosity decreases slightly with an increase in molecular weight over the area. This is probably due to a rather narrow dispersity and few data points with similar intrinsic viscosity of star polymer produced. However, within the bimodal star-star coupling region, there is an obvious increase in the intrinsic viscosity across

the high molecular weight distribution, especially at the transition point from single star to aggregates.

The star-shaped *ZnPc*-PDMAEMA (blue) shows a similar molecular weight distribution region as that of sucrose-PDMAEMA, and it should be mentioned that there is no obvious star-star coupling can be observed. The Mark-Houwink plot exhibits the same gradient as that of linear PDMAEMA at low molecular weight, probably owing to the small amount of linear *ZnPc*-PDMAEMA present in the polymer sample. However, the intrinsic viscosity increases more uniformly over the remainder of the molecular weight distribution, indicating that no bimodal nature can be found in the Mark-Houwink plot.

	$M_{n,NMR}$	Conventional GPC		Universal Calibration			
		$M_{n,GPC}$	PDI	$M_{n,GPC}$	PDI	DP	α
LinPDMAEMA	---	40,300	2.20	59,700	2.8	380	0.5
Sucrose-PDMAEMA	39,300	30,000	1.09	34,400	1.56	26 *per arm*	0.12
ZnPc-PDMAEMA	38,000	24,800	1.19	38,900	1.4	28 *per arm*	0.24

Table 4.2.1 GPC results of linear PDMAEMA, star sucrose-PDMAEMA and *ZnPc*-PDMAEMA from both of conventional GPC and universal calibration using PMMA calibration standards

The summarised table reports the results from both conventional GPC calibration and universal calibration. It can be noted that a higher M_n, and PDI are usually obtained using the universal calibration than using the conventional calibration to analyse polymers. In comparison with $M_{n,NMR}$, the results are much closer to the one collected from the universal calibration. Furthermore, α value from each of Mark-Houwink plot, suggests the dynamic behaviour of polymer in solution. For linear PDMAEMA, α= 0.5 is indicative of theta solvent in which the polymer acts as a random coil. For both of star-shaped sucrose-PDMAEMA and *ZnPc*-PDMAEMA, α is much less than 0.5 revealing a more compact dense structure following the 'hard sphere' model. It should be mentioned that the value for sucrose-PDMAEMA is less reliable due to the disordered the Mark-Houwink plot; however, it still can be a suggestion of star-shaped PDMAEMA in solution.

4.2.4 Thermo-and pH-responsive star-shaped *ZnPc*-PDMAEMA

PDMAEMA is an example of a polymer that exhibits a LCST. However, the reported cloud point of PDMAEMA in the literature ranges from 14 to 50 ^{o}C in water, depending on the molecular weight. One of the attractive properties of PDMAEMA in aqueous solution is that the phase transitions and solubility changes can be easily tuned by changing pH due to the tertiary amine pedant group. Due to the considerable drop of pH during heating in the water and the effect of pH on the LCST behaviour,[16] in this study, the thermoresponsive behaviour of aqueous solutions of star-shaped *ZnPc*-PDMAEMA has been investigated in different buffer solution, which keeps the pH more constant over the whole temperature range with an increased ionic strength owing to the salt present in buffer solution.

The LCST analysis of star-shaped *ZnPc*-PDMAEMA and sucrose-PDMAEMA polymer solutions were conducted using Aglient Cary 60 UV-Vis spectrometer at a wavelength of 510 nm. The temperature of the sample cell was thermostatically controlled by an external superconstant temperature bath. The temperatures of each solution were equilibrated for 5 min before measurement. The LCST values of each polymer solution were defined as the temperature producing a 50% increase in optical absorbance.

A 1 mg mL^{-1} solution of the star-shaped *ZnPc*-PDMAEMA was freshly prepared from different buffer solution (pH = 10, borax/sodium hydroxide; pH = 9, borax/hydrochloric acid; pH = 8, borax/hydrochloric acid; pH = 7, phosphate/sodium hydroxide; ionic strength of all buffers in the order of 0.1 mol/L) and added to a cuvette for optical analysis. Each of the aqueous polymer solutions was heated to an appropriate temperature region at a rate of 1 ^{o}C min^{-1}, and the change in absorbance was recorded, **Figure 4.2.13**. It can be observed that there is a shift of phase boundary to lower temperature with increasing pH of the buffer solution.

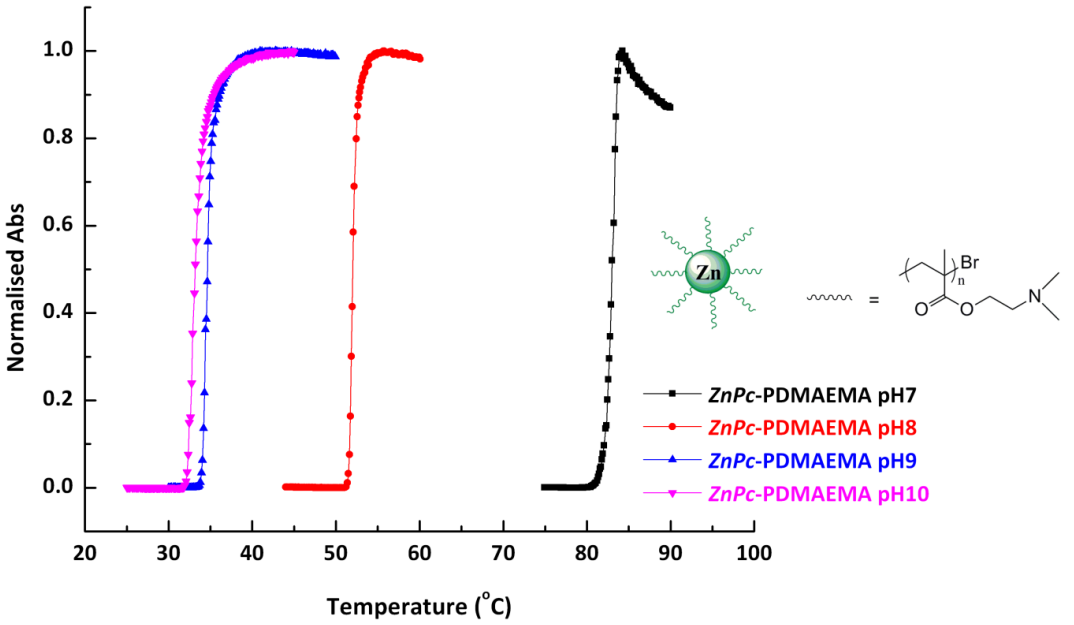

Figure 4.2.13 The cloud point analysis of *ZnPc*-PDMAEMA at varied pH by turbidimetry

The cloud point of sucrose-PDMAEMA with similar molecular weight as *ZnPc*-PDMAEMA was also measured using the same system. A 1 mg mL^{-1} solution of the star-shaped sucrose-PDMAEMA was freshly prepared from the same buffer solution. The polymer solution in varied pH was heated up in an appropriate temperature range at 1 ^{o}C min^{-1}, and the change in absorbance was recorded, **Figure 4.2.14**. A similar trend has been shown in comparison with *ZnPc*-PDMAEMA solution, the cloud point increases with decreasing pH of the aqueous solution.

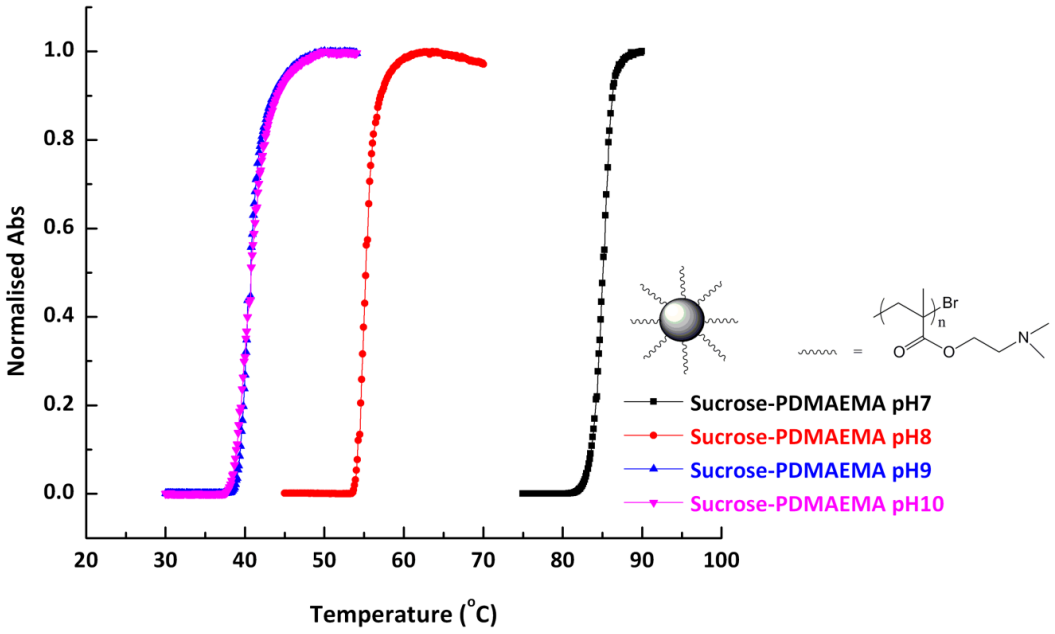

Figure 4.2.14 The cloud point analysis of sucrose-PDMAEMA at varied pH by turbidimetry

The cloud points at 1 mg ml^{-1} of both of star-shaped sucrose-PDMAEMA and *ZnPc*-PDMAEMA aqueous solution are presented in **Figure 4.2.15** in dependence of pH. It can be found that the LCSTs decreased dramatically for both sucrose-PDMAEMA and *ZnPc*-PDMAEMA from 85.2 to 40.9 ^{o}C and 82.9 to 33.2 ^{o}C respectively, with an increase in pH of the buffer solution, from pH 7 to pH 10. At higher pH (≥ 9), where the stars are almost uncharged, the cloud points exhibit a lower temperature. However, at decreasing pH (=7 or 8), the PDMAEMA stars get more and more charged, which is also reflected in the shift of the phase boundary to higher temperature as expected. It can be noticed that already at pH = 8, the cloud points are increased by more than 10 ^{o}C. Furthermore, this charging effect is even more pronounced at pH = 7, and the cloud points are increased up to more than 80 ^{o}C. It should be mentioned that with the similar molecular weights of both sucrose-PDMAEMA and *ZnPc*-PDMAEMA stars determined by either ^{1}H NMR or GPC universal calibration, the cloud points for *ZnPc*-PDMAEMA stars are generally lower than that of sucrose-PDMAEMA stars, especially at higher pH (≥ 9). This may be due to the effect of super hydrophobic core of *ZnPc* shifting the LCST to a lower temperature at each pH.

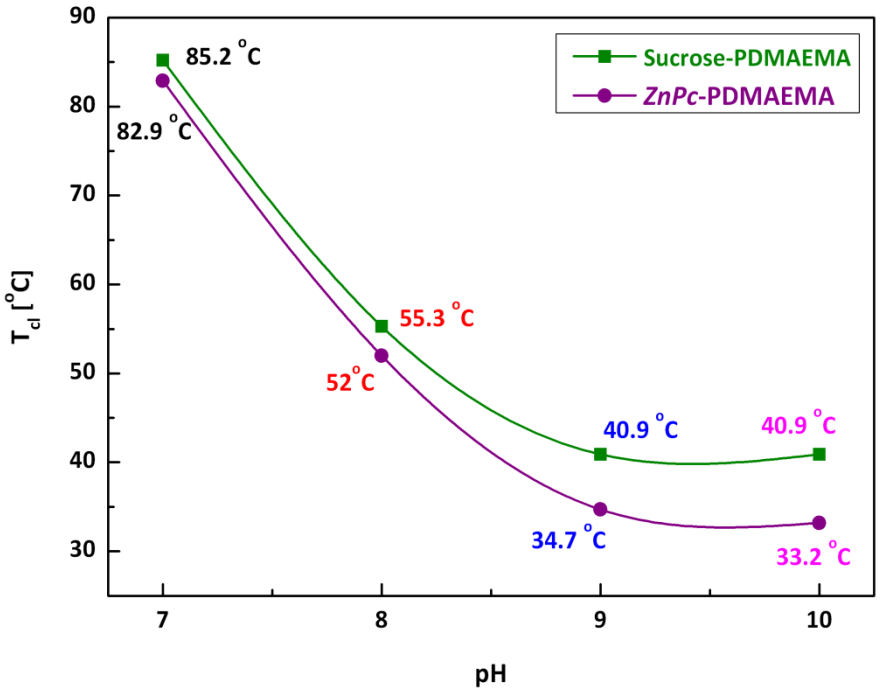

Figure 4.2.15 Cloud points T_{cl} at 1 mg mL^{-1} aqueous solution of both of star-shaped sucrose-PDMAEMA and *ZnPc*-PDMAEMA in dependence of pH

4.2.5 Quaternization of star-shaped *ZnPc*-PDMAEMA

Another interesting property of PDMAEMA is that it can be transformed from weak polyelectrolyte into strong polyelectrolyte by quaternization of the pendant amino group. Therefore, the *ZnPc*-PDMAEMA stars can be either quaternized with methyl iodide, leading to *ZnPc*-poly{[2-(methacryloyloxy)ethyl] trimethylammonium iodide (*ZnPc*-PMETAI), or converted to zwitterionic structures with 1,3-propanesultone, bringing about *ZnPc*-poly{[2-(methacryloyloxy)ehthyl]dimethyl(3-sulfopropyl)ammonium hydroxide} (*ZnPc*-PMEDSAH).

The *ZnPc* conjugated polyelectrolyte stars (*ZnPc*-PMETAI or *ZnPc*-PMEDSAH) were formed by the reaction of *ZnPc*-PDMAEMA with large excess of either methyl iodide or propanesultone in THF stirring overnight at ambient temperature, **Figure 4.2.16**.

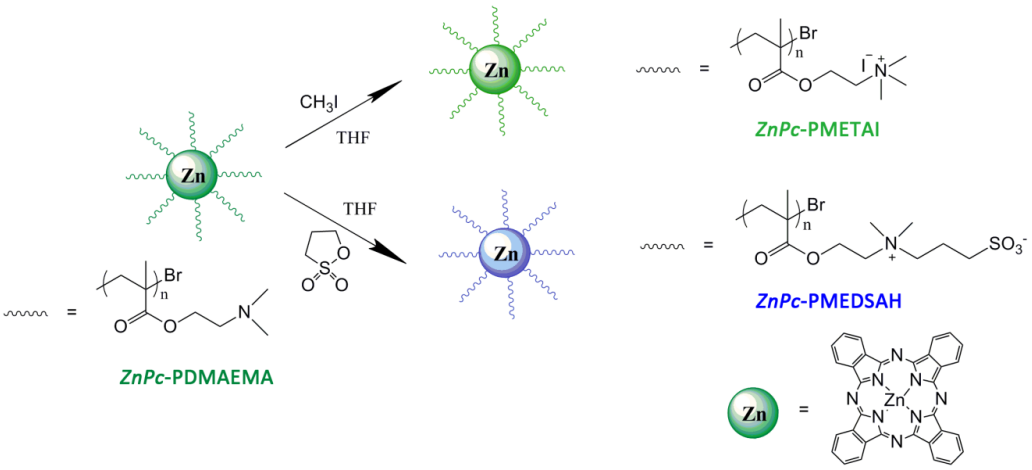

Figure 4.2.16 Synthetic routes of quaternization of star-shaped *ZnPc*-PDMAEMA

The completeness of quaternization is verified by NMR analysis, **Figure 4.2.17**. It should be mentioned that the super hydrophobic core *ZnPc* can be hardly detected in D_2O. However, the proton signals on pendant amino group of *ZnPc*-PDMAEMA can be observed. After quaternization with methyl iodide, there is a complete shift of the methyl protons on the amino group to the downfield for *ZnPc*-PMETAI stars. Similarly, after converted to zwitterionic structures, the proton signals on the pendant amino group are shifted to higher ppm values and the appearance of protons on the zwitterionic side-groups indicates the full quaternization.

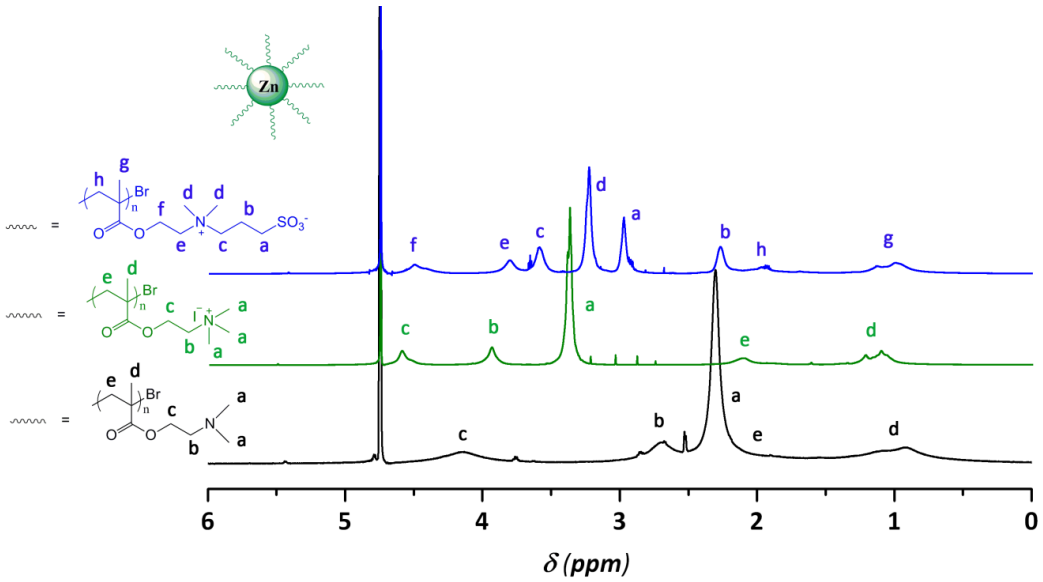

Figure 4.2.17 ^{1}H NMR of *ZnPc*-PDMAEMA star and quaternized *ZnPc*-PDMAEMA stars in D_2O.

The quaternized *ZnPc*-PDMAEMA stars were also analysed by appropriate GPC systems. Due to the solubility issue, *ZnPc*-PMEDSAH stars were only run by aqueous GPC. Its UV-Vis spectrum was performed prior to GPC analysis, **Figure 4.2.18**-(a), and shown a λ_{max} at 630 nm which is characteristic of dimerization of *ZnPc* related compounds in aqueous solution. However, a shoulder peak around 680 nm still can be observed, indicating the presence of the monomeric *ZnPc*-PMEDSAH stars in solution. The zwitterionic star was further analysed by aqueous GPC using a UV detector set at λ = 630 nm, **Figure 4.2.18**-(b). The well-overlapped chromatograms further proved the incorporation of *ZnPc* core into this zwitterionic star polymer. The tail at low molecular weight can also be noticed, maybe due to the interaction of the zwitterionic side-group with the GPC column.

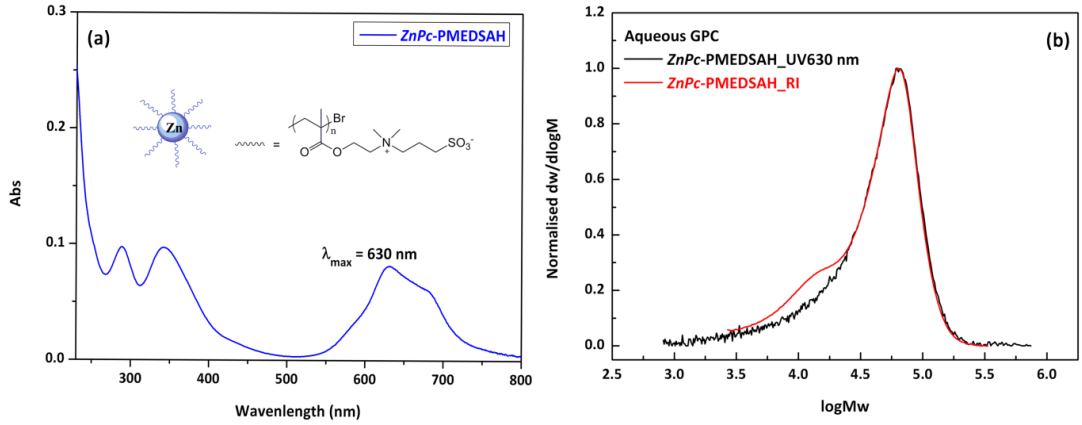

Figure 4.2.18 (a) UV-Vis analysis of *ZnPc*-PMEDSAH stars in water at 0.1 mg mL^{-1}; (b) aqueous GPC analysis of *ZnPc*-PMEDSAH stars by both of RI and UV (λ = 630 nm) detectors

Owing to the column used in aqueous GPC, the *ZnPc*-PMETAI star was found not to be eluted; therefore, DMF-GPC was used instead. The UV-Vis analysis of this strong polyelectrolyte at 0.1 mg mL^{-1} shows a single Q band around λ = 677 nm in DMF-GPC eluent (DMF with 5 mM NH_3BF_4), **Figure 4.2.19**-(a), revealing it is non-aggregated in DMF eluent. The overlapped chromatograms of *ZnPc*-PMETAI star analysed by DMF-GPC (**Figure 4.2.19**-b) represents the similar tail at low molecular weight as shown above (**Figure 4.2.18**-b), maybe due to the interaction of the strong polyelectrolyte star with the GPC column. Moreover, the broader UV-Vis signal obtained mainly owing to the highly diluted concentration of the sample used during analysis in comparison with that used in RI detection.

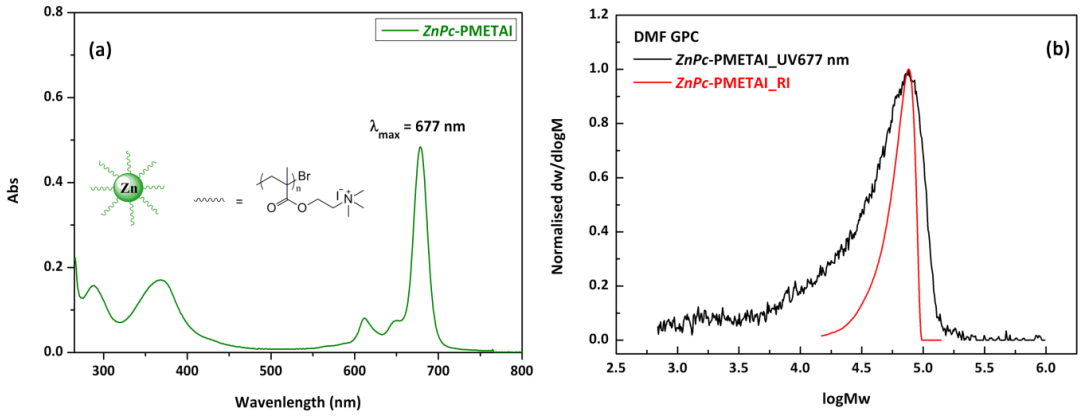

Figure 4.2.19 (a) UV-Vis analysis of *ZnPc*-PMETAI stars in DMF (GPC eluent with 5mM NH_3BF_4) at 0.1 mg mL^{-1}; (b) DMF GPC analysis of *ZnPc*-PMETAI stars by both of RI and UV (λ = 677 nm) detectors

4.2.6 Thermo-responsive zwitterionic *ZnPc*-PMEDSAH star polymer

Due to the zwitterionic *ZnPc*-PMEDSAH star polymer which processes both positive and negative charges on the same pendant group, UCST behaviour has been introduced into the *ZnPc* incorporated star. This unique property was induced by the extremely high dipole moment of the zwitterionic groups leading to reversible self-association of the polymer chains via strong inter- and intramolecular dipolar interactions.[27, 38]

The UCST analysis of both quaternized star solutions was conducted using Aglient Cary 60 UV-Vis spectrometer at a wavelength of 510 nm. The temperatures of solutions were cooled down to 0 ^oC and equilibrated for 5 min before measurement. The UCST values were defined as the temperature producing a 50% increase in optical absorbance. 40 mg mL^{-1} solutions of *ZnPc*-PMETAI and *ZnPc*-PMEDSAH were freshly prepared and heated up at 1 ^oC min^{-1}, the changes of the absorbance curves were recorded respectively. As shown in **Figure 4.2.20**, the absorbance curve of *ZnPc*-PMEDSAH star exhibits a sudden transition during heating and the UCST value is around 17 ^oC. At low temperature (T < UCST), the zwitterionic star is insoluble or sparingly soluble in water since the strong inter- and intra-chain associations of the quaternized ionic *N*,*N*-dimethylaminoethyl groups prevent the dissolution of the polymer. Therefore, the polyzwitterionic stars collapse together

from solution. At higher temperatures (T > UCST), however, the inter- and intramolecular interactions are weakened by the thermal energy, and allow the *ZnPc*-PMEDSAH star transformed from a compact coil conformation to an expanding shape. In comparison with the strong polyelectrolyte star, *ZnPc*-PMETAI, no obvious phase transition can be observed during heating process.

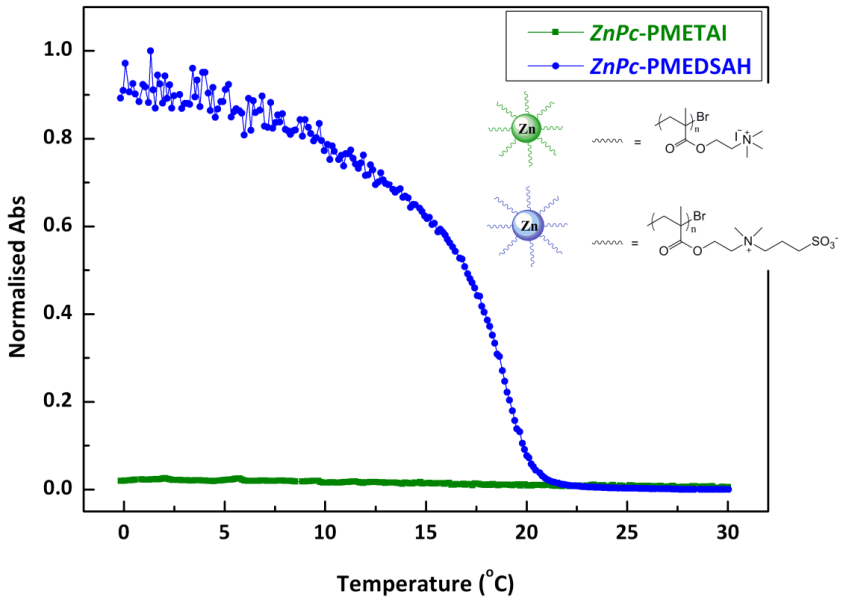

Figure 4.2.20 UCST behaviour of zwitterionic *ZnPc*-PMEDSAH star in comparison with *ZnPc*-PMETAI star by turbidimetry

4.2.7 Optical properties of *ZnPc*-PDMAEMA and quaternized *ZnPc*-PDMAEMA stars in aqueous solution

It has been previously mentioned that star-shaped *ZnPc*-PDMAEMA exhibits excellent solubility and is non-aggregated in a range of organic solvents, such as $CHCl_3$, THF, and DMF, etc. As for strong polyelectrolyte, *ZnPc*-PMETAI, it shows non-aggregated in DMF. However, in water (**Figure 4.2.21**), all the three star polymers represent different degree of aggregation analysed by UV-Vis spectroscopy. Severe band broadening and blue-shift of Q band (around λ = 630 nm) appear in all polymer solutions indicating the oligomerisation occurs. It still can be observed that the shoulder peaks at round λ = 680 nm contribute to the monomeric star polymers. At 0.1 mg mL^{-1}, *ZnPc*-PMETAI solution presents more monomeric stars than dimers, compared with *ZnPc*-PDMAEMA and *ZnPc*-PMEDSAH.

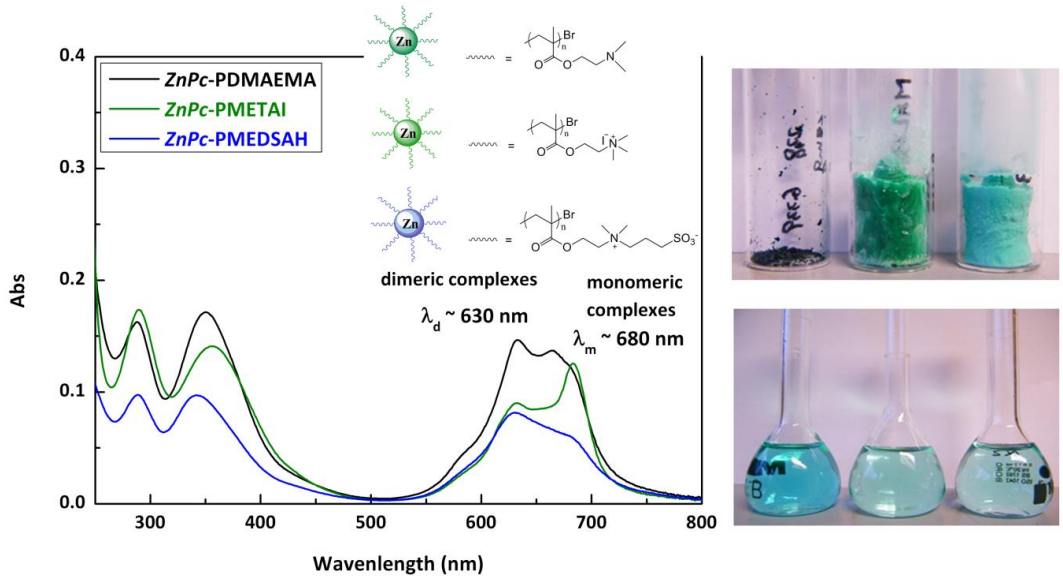

Figure 4.2.21 UV-Vis spectra of *ZnPc*-PDMAEMA and quaternized *ZnPc*-PDMAEMA stars in water at 0.1 mg mL^{-1}, and the images of *ZnPc*-PDMAEMA, *ZnPc*-PMETAI, and *ZnPc*-PMEDSAH products including their aqueous solution at 0.1 mg mL^{-1} (from left to right)

The aggregation behaviour of *Pc* related compounds is also concentration-dependant in aqueous solution. The UV-Vis spectra of *ZnPc*-PMETAI aqueous solution with increasing concentration is shown in **Figure 4.2.22**. It can be noticed that both dimeric and monomeric *ZnPc*-PMETAI stars are present in all aqueous solutions. At lower concentrations (≤ 0.1 mg mL^{-1}), the absorptions around λ = 680 nm are higher than those at λ = 630 nm, indicating that the monomeric stars are the dominated species in solution. However, the absorptions at λ = 630 nm are gradually increasing in comparison with those near λ = 680 nm at higher concentrations (≥ 0.5 mg mL^{-1}), revealing an increase in the amount of dimeric complexes.

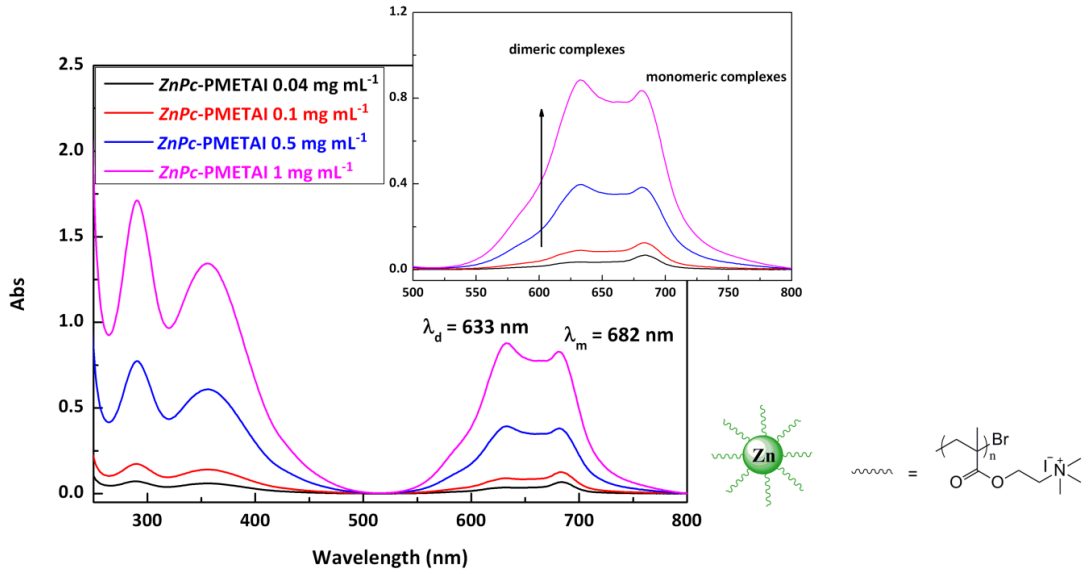

Figure 4.2.22 UV-Vis spectra of *ZnPc*-PMETAI star solutions with increasing concentration

4.3 Conclusions

A novel strategy for the synthesis of dual-responsive star-shaped PDMAEMA with *ZnPc* core has been developed. The process starts from the synthesis of clickable *ZnPc*, as shown in previous chapter, which is fully characterised by IR, ^{1}H NMR and MALDI-ToF-MS analysis. The resulting *ZnPc*-PDMAEMA conjugate was prepared according to 'core first' approach involving a modified combination of CuAAC click chemistry and ATRP via sharing the same CuBr/PMDETA catalyst. The star polymer can be clearly analysed by ^{1}H NMR with an indication of DP_{NMR} = 27 per arm. The well-overlapped chromatograms from RI and UV (λ = 677 nm) detectors of conventional GPC illustrates the incorporation of the *ZnPc* molecule, and a relatively narrow dispersity (PDI = 1.19) was achieved. Moreover, the molecular architecture was proved by performing universal calibration. The Mark-Houwink constant α = 0.24 reveals a branched shape of *ZnPc*-PDMAEMA, compared with the Mark-Houwink constants of linear PDMAEMA and 8-armed sucrose-PDMAEMA polymerised by FRP and ATRP respectively. The molecular weight generated by universal calibration is also in good agreement with that by ^{1}H NMR.

The phase transitions and solubility changes of PDMAEMA aqueous solutions can be easily tuned by changing pH due to the presence of tertiary amine pendant group. The cloud points of both of star-shaped sucrose- and *ZnPc*-PDMAEMA solution are decreasing with an increase in the pH of the buffer solution due to the charging effect on the amino side group. At lower pH (≤8), the polymer stars are more and more charged, which shift the phase boundary to a higher temperature. The LCSTs of both polymer solutions can be increased up to more than 80 ^{o}C at pH =7.

Furthermore, the weak star polyelectrolyte *ZnPc*-PDMAEMA was transformed into permanent strong polyelectrolyte by quaternized with either methyl iodide or 1,3-propane sultone. ^{1}H NMR analysis represents a completeness of quaternization for both star polymers. The polyzwitterionic *ZnPc*-PMEDSAH star exhibits a UCST transition around 17 ^{o}C in comparison with the *ZnPc*-PMETAI star, as the inter-and intra-chain associations of the quaternized ionic *N,N*-dimethylaminoethyl groups prevents the dissolution of the star polymer at lower temperature.

The UV-Vis analysis of *ZnPc*-PDMAEMA and quaternized *ZnPc*-PDMAEMA star solutions shows different degrees of aggregation in water. At same concentration, *ZnPc*-PMETAI star presents relatively more monomeric complexes in solution compared with the other two stars. The aggregation behaviour is also concentration-dependant. It was found that with increasing concentration of *ZnPc*-PMETAI solutions, the dimeric stars are becoming dominated species in water.

4.4 Experimental

Reagents and Conditions

Copper(I) bromide (Aldrich, 98%) was purified according to the method of Keller and Wycoff.[41] All reactions were carried out using standard Schlenk techniques under an inert atmosphere of nitrogen, unless otherwise stated. TLC performed using pre-coated silica gel 60 F254 and developed in the solvent system indicated. Compounds were visualized by use of UV light (254 or 302 nm) or a basic solution (10 % w/w K_2CO_3 in water) of $KMnO_4$. Merck 60 (230 - 400 mesh) silica gel was used for column chromatography.

Instrumentals and analysis

Nuclear Magnetic Resonance

NMR spectra were obtained on Bruker DPX-300, Bruker DPX-400 and Bruker DRX-500 spectrometers. All chemical shifts are reported in ppm (δ) relative to tetramethylsilane, referenced to the chemical shifts of residual solvent resonance (^1H and ^{13}C). The following abbreviations were used to explain the multiplicities: s = singlet, d = doublet, dd = doublet of doublets, t = triplet, td = triplet of doublets, m = multiplet.

Gel Permeation Chromatography (GPC) Analysis

GPC analysis was performed based on solubility of the polymer or conjugated and on the available detectors of each system.

Dimethylformamide

GPC was performed on a Varian 390-LC MDS system equipped with a PL-AS RT/MT autosampler, a PL-gel 3 μm (50 x 7.5 mm) guard column, two PL-gel 5 μm (300 x 7.5 mm) mixed-D columns using DMF with 5 mM NH_3BF_4 at 50 ^oC as the eluent at a flow rate of 1.0 mL min^{-1}. The GPC system was equipped with ultraviolet

and differential refractive index detectors. Narrow molecular weight PMMA standards (between 200 and 467,400 g mol^{-1}) were used to calibrate the SEC and data fitted with a 3rd order polynomial.

Tetrahydrofuran

GPC was performed on a Varian 390-LC MDS system equipped with a PL-AS RT/MT autosampler, a PL-gel 3 μm (50 x 7.5 mm) guard column, two PL-gel 5 μm (300 x 7.5 mm) mixed-D columns equipped with a differential refractive index and Shimadzu SPD-M20A diode array detectors, using THF with 2% TEA as the eluent with a flow rate of 1.0 mL min^{-1}. Narrow molecular weight standards of both poly(MMA) (between 200 and 467,400 g mol^{-1}) and polystyrene (between 162 and 24,600 g mol^{-1}) were used to calibrate the SEC and data fitted with a 3rd order polynomial.

Chloroform

GPC was performed on a Varian 390-LC MDS system equipped with a PL-AS RT/MT autosampler, a PL-gel 3 μm (50 x 7.5 mm) guard column, two PL-gel 5 μm (300 x 7.5 mm) mixed-D columns equipped with a differential refractive index detector, using $CHCl_3$ as the eluent with a flow rate of 1.0 mL min^{-1}. Narrow molecular weight standards of both poly(MMA) (between 200 and 467,400 g mol^{-1}) and polystyrene (between 162 and 24,600 g mol^{-1}) were used to calibrate the SEC and data fitted with a 3rd order polynomial.

Aqueous system

GPC was performed on a Varian 390-LC MDS system equipped with a PL-AS RT/MT autosampler, a PL aquagel-OH 8 μm (50 x 7.5 mm) guard column, two PL aquagel-OH 8 μm (300 x 7.5 mm) mixed-H columns equipped with ultraviolet and differential refractive index detectors, using pH 8.2 phosphate buffer as the eluent with a flow rate of 1.0 mL min^{-1}. Narrow molecular weight standard of PEG (between 110 and 458,500 g mol^{-1}) was used to calibrate the SEC and data fitted with a 3rd order polynomial.

MALDI-ToF-MS Analysis

MALDI-ToF data was collected using a Bruker Ultraflex II MALDI-ToF spectrometer, equipped with a nitrogen laser delivering 2 ns laser pulses at 337 nm

with positive ion ToF detection performed using an accelerating voltage of 25 kV. Samples were prepared by mixing α-cyano-4-hydroxycinnamic acid (CHCA) (20 μL of a 2 mg L^{-1} solution), sodium iodide (20 μL of a 1 mg L^{-1} solution), and the analyte solution (20 μL of a 2 mg L^{-1} solution), and then the resulting solution was spotted onto a ground steel MALDI plate and solvent removed prior to inserting into the vacuum chamber of the MALDI instrument.

Fourier Transform Infra-Red (FTIR) spectrometry

Infrared absorption spectra were recorder on a Bruker VECTOR-22 FTIR spectrometer using a Golden Gate diamond attenuated total reflection (ATR) cell.

Turbidimetry

The cloud point measurements were conducted using Aglient Cary 60 UV-Vis spectrometer at a wavelength of 510 nm. The temperature of the sample cell was thermostatically controlled by an external "superconstant" temperature bath. The temperatures of each solution were equilibrated for 5 min before measurement. Each of the aqueous polymer solution was heated up in an appropriate temperature region at a rate of 1 ^{o}C min^{-1}, and the LCST values were defined as the temperature producing a 50% increase in optical absorbance.

UV-Vis Spectroscopy

All UV-Vis absorption spectra were measured on a Perkin Elmer Lambda-35 UV/VIS spectrometer using 1 cm path length quartz cuvettes.

2,3,9,10,16,17,23,24-Octa(6-(triisopropylsilyl)hex-5-ynyloxy)phenoxy) zinc phthalocyanine

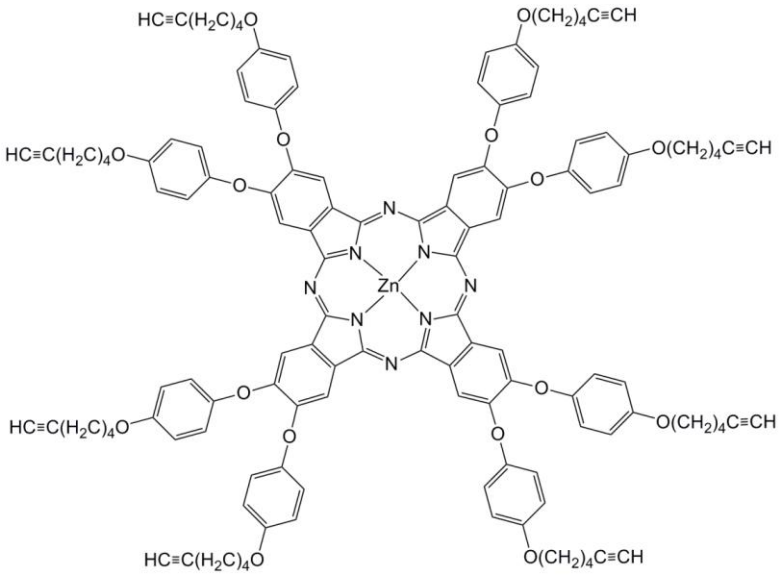

A mixture of 4,5-bis(4-hex-5-ynyloxy)phenoxy)phthalonitrile (0.77 g, 1.53 mmol), DBU (0.2 mL, 1.53 mmol) and $Zn(OAc)_2$ $2H_2O$ (16.7 mg, 0.763 mmol) in 1-pentanol (30 mL) were maintained at reflux under nitrogen for 40 hours. After cooling to ambient temperature, the mixture was poured into methanol. The dark green product was filtered and washed with methanol. The crude product was purified by silica column (SiO_2, DCM/THF = 10/0.1) (Yield: 20%).

IR (neat): ν = 3285 (alkyne C-H), 2114 (C≡C), 1009 cm^{-1} (ring vibration bands).

^{1}H NMR (400.03 MHz, $CDCl_3$, 298 K): δ 8.56 (br, 8H), 7.20-7.18 (d, 16H, J= 8.8Hz), 7.03-7.01 (d, 16H, J= 8.8Hz), 4.10 (t, 16H, J= 6.5 Hz), 2.36-2.32 (dt, 16H, J= 2.6 , 7 Hz), 2.03-1.96 (m, 24H), 1.83-1.75 (m, 16H); ^{13}C NMR (100.59 MHz, $CDCl_3$, 298 K): δ 155.30, 150.82, 119.73, 115.50, 113.15, 68.76, 67.72, 28.51, 25.15, and 18.30.

MALDI-ToF m/z: calcd for $C_{128}H_{112}N_8ZnO_{16}$ 2081.75 $[M+H]^+$, observed 2082.0

2-Bromo-2-methyl-propionic acid 3-azido-propyl ester[39]

3-Bromo-1-propanol (5.00 g, 36 mmol) and sodium azide (1.96 g, 64.7 mmol) were dissolved in a mixture of acetone (90 mL) and water (15 mL) and the resulting solution was refluxed overnight. Most of the acetone was then removed under reduced pressure, 50 mL of water was added and the mixture was extracted with diethyl ether (3 x 50 mL). The organic layers collected, and dried over anhydrous $MgSO_4$. After removal of the solvent under reduced pressure, the product was isolated as colourless oil (Yield: 70 %).

IR (neat): ν = 3331 (broad, OH), 2954, 2882, 2094, 1455, 1344, 1260, 1048, 956, 901, 633, 543, 531, 508 cm^{-1}.
^1H NMR (400.03 MHz, $CDCl_3$, 298 K): δ 3.76 (q, 2H, J 5.7 Hz), 3.45 (t, 2H, J= 6.5 Hz), 1.83 (quint, 2H, J= 6.3 Hz); ^{13}C NMR (100.59 MHz, $CDCl_3$, 298 K): δ 59.87 (*C*H_2OH), 48.45 (*C*H_2N_3), 31.40. ESI-MS m/z: calcd for $C_3H_7N_3O$ 124.05 $[M+Na]^+$, observed 124.0

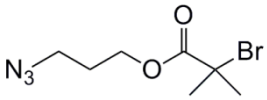

A solution of 3-azido-propan-1-ol (2.16 g, 21.3 mmol), DMAP (0.26 g, 2.13 mmol) and triethylamine (5.95 mL, 42.7 mol) in Et_2O (50 mL) was cooled to 0 ^oC, followed by slow addition of 2-bromo-2-methyl propionyl bromide (5.27 mL, 42.7 mmol). After stirring 1 h at 0 ^oC and overnight at ambient temperature the resulting white suspension was filtered and the pale yellow solution was washed with saturated $NaHCO_3$ aqueous solution (3 x 100 mL), water (3 x 100 mL) and dried with $MgSO_4$. After filtration the solvent was removed under reduced pressure and the yellow oily residue was purified by flash chromatography (SiO_2, petroleum ether/Et_2O = 20/1) (Yield: 70%).
IR (neat): ν = 2972, 2932, 2098, 1735 (C=O), 1462, 1273, 1162, 1108 cm^{-1}.

^{1}H NMR (400.03 MHz, $CDCl_3$, 298 K): δ 4.27 (t, 2H, J= 6.1 Hz), 3.44 (t, 2H, J= 6.7 Hz), 1.97 (m, 2H), 1.94 (s, 6H); ^{13}C NMR (100.59 MHz, $CDCl_3$, 298 K): δ 171.63 (*C*=O), 62.84 (*C*H_2O), 55.78, 48.14, 30.81, 28.08. ESI-MS m/z: calcd for $C_7H_{12}BrN_3O_2$ 272.00 $[M+Na]^+$, observed 272.0

Synthesis of octa-*O*-isobutyryl bromide-sucrose[40]

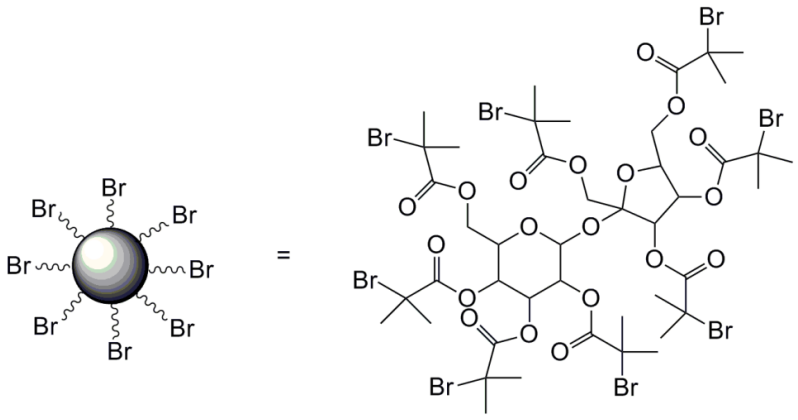

Octa-*O*-isobutyryl bromide-sucrose was synthesised by the slow addition of 2-bromoisobutyryl bromide (39.6 mL, 0.32 mol) to a suspension of sucrose (6.85 g, 0.02 mol) in anhydrous pyridine (150 mL) and $CHCl_3$ (70 mL). The mixture was stirred for 48 h under a dry atmosphere at ambient temperature. The solution was washed with ice cold water, 0.1 M NaOH (3 x 200 mL), and water (3 x 200 mL), prior to drying over anhydrous $MgSO_4$. The crude product was recrystallised from methanol/H_2O (3:1) to yield white crystals (Yield: 20%).

IR (neat): ν = 2978, 1740, 1140, 1100 cm^{-1}.

^{1}H NMR (400.03 MHz, $CDCl_3$, 298 K): δ 5.86 (d, 1H, H-1), 5.77 (d, 1H, H-3'), 5.74-5.64 (m, 2H, H-4', H-3), 5.39 (t, 1H, H-4) 5.15 (dd, 1H, H-2), 4.84 (d, 1H, H-1'), 4.71 (d, 1H, H-1'), 4.52-4.42 (m, 5H, H-6/6'), 4.17 (d, 1H), 2.02-1.86 (m, 48H, CH_3) ^{13}C NMR (100.59 MHz, $CDCl_3$, 298 K): δ 171.22-169.62 (C=O), 102.60, 88.68, 75.81, 73.65, 70.91, 70.68, 68.49, 68.23, 64.66, 61.92, 55.56-54.71, 50.77, 30.79-30.20.

MALDI-ToF m/z: calcd for $C_{44}H_{62}Br_8O_{19}$ 1556.72 $[M+Na]^+$, observed 1557.0

Star-shaped sucrose-PDMAEMA by ATRP

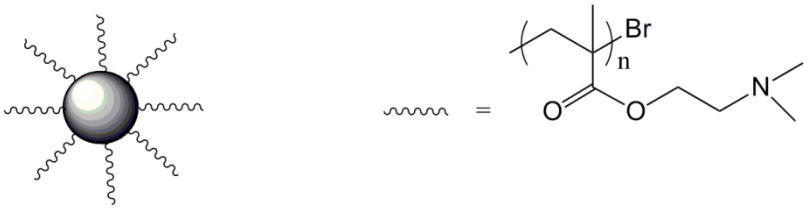

Sucrose initiator (66 mg, 43 μmol), HMTETA (94 μL, 0.344 mmol), DMAEMA (5.8 mL, 34.4 mmol) were charged in a Schlenk tube with 1 mL mesitylene as internal standard in anhydrous THF. The solution was subjected to three freeze-pump-thaw cycles and then cannulated under N_2 in a second Schlenk tube, previously evacuated and filled with N_2, containing CuBr (39.5 mg, 0.275 mmol) and $CuBr_2$ (15 mg, 68.8 μmol). The reaction was carried out at 60 ^oC for 2 hr. The solution was diluted with THF and passed through a basic aluminium oxide column to remove the copper catalyst. After concentration, the crude product was precipitated in hexane and the polymer was dried *in vacuo*. (Yield: 25 %) The linear PDMAEMA was synthesised by conventional radical polymerisation using AIBN as the initiator. AIBN (52 mg, 0.318 mmol), DMAEMA (2.14 mL, 12.7 mmol) was dissolved in of anhydrous THF, bubbled with nitrogen for 20 min to eliminate oxygen, and place in water bath at 60 ^oC for 30 min. The mixture was cooled to ambient temperature, precipitated in hexane, and dried *in vacuo* (Yield: 30 %).

^1H NMR (400.03 MHz, $CDCl_3$, 298 K): δ 4.04 (br, $COOCH_2$), 2.55 (br, CH_2N), 2.26 (s, $N(CH_3)_2$), 2.02-1.7 (br, $CH_2C(CH_3)$ polymer backbone), 1.14-0.75 (br, $CH_2C(CH_3)$ polymer backbone); ^{13}C NMR (100.59 MHz, $CDCl_3$, 298 K): δ 176.55, 63.00, 57.06, 54.20, 45.77, 16.71

Star-shaped *ZnPc*-PDMAEMA by combination of CuAAC click chemistry with ATRP

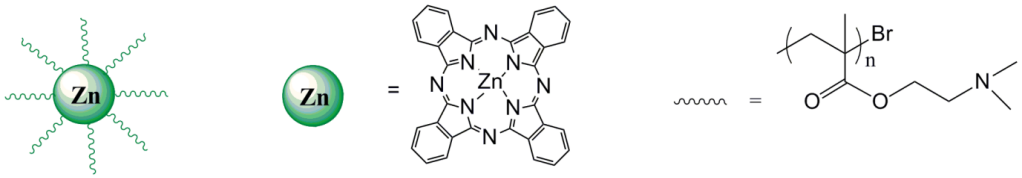

ZnPc-alkyne (0.042 g, 20.2 µmol, 1 equiv.) was charged in a Schlenk tube with 8 mL of anhydrous THF. Subsequently, N_3-Br (0.04 g, 161 µmol, 8 equiv.) and PMDETA (44 µL, 210 µmol, 10.4 equiv.) were added. The Schlenk solution was subjected to 3 freeze-pump-thaw cycles and then cannulated under N_2 into a second Schlenk tube, previously evacuated and filled with N_2, containing CuBr (23 mg, 161 µmol, 8 equiv.). The reaction was carried out at ambient temperature overnight. Then, DMAEMA (2.72 mL, 16.1 mmol) with 1 mL mesitylene as internal standard in dry THF (4 mL) was bubbled with N_2 for 15 min, prior to addition to the reaction mixture via a degassed syringe. The solution was bubbled with N_2 for another 20 min, followed by immersed in water bath at 60 ^{o}C for 1.5 h. The crude product was diluted with THF and passed through a basic aluminium oxide column to remove the copper catalyst. The polymer was concentrated, precipitated in hexane and dried *in vacuo* (Yield: 20%).

^{1}H NMR (400.03 MHz, $CDCl_3$, 298 K): δ 8.90 (br, 8H), 7.17 (br, 16H), 6.96 (br, 16H), 4.05 (br, COOCH_2), 2.55 (br, CH_2N), 2.27 (s, N(CH_3)$_2$), 2.00-1.71 (br, CH_2C(CH$_3$) polymer backbone), 1.10-0.8 (br, CH$_2$C(CH_3) polymer backbone); ^{13}C NMR (100.59 MHz, $CDCl_3$, 298 K): δ 177.26, 67.92, 62.85, 57.0, 54.09, 45.74, 18.50, 16.75

Quaternization of star-branched *ZnPc*-PDMAEMA

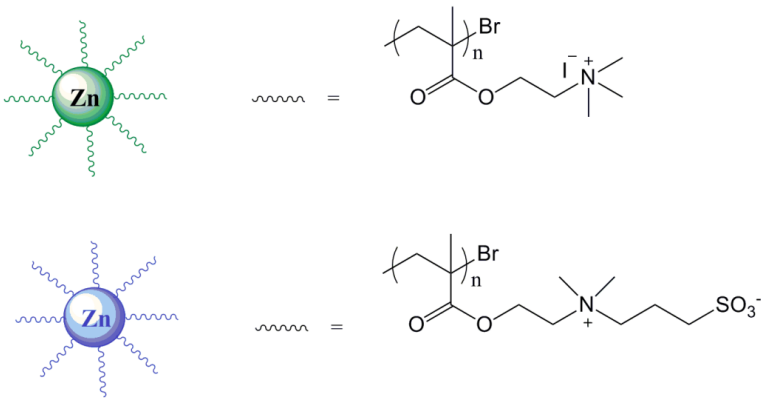

The pendant amino groups of star-branched *ZnPc*-PDMAEMA was quaternized with methyl iodide and 1,3-propanesultone respectively. *ZnPc*-PDMAEMA (0.154 g, 4.05 μmol) and a large excess of CH_3I (0.25 mL), or 1,3-propanesultone (0.65 g) was charged in separated round-bottom flask with 10 mL anhydrous THF. The mixture was kept stirring overnight at ambient temperature. The polymer was filtered, washed with THF and dialysis against distilled water for 2 days using MWCO 1000 Da membrane. The solution was lyophilised to yield the product as a green powder (Yield: 72%).

ZnPc-PMETAI: $M_{n,NMR}$ = 68,700 g mol^{-1}

ZnPc-PMEDSAH: $M_{n,NMR}$ = 64,300 g mol^{-1}

4.5 References

1. C. C. Leznoff, S. Vigh, P. I. Svirskaya, S. Greenberg, D. M. Drew, E. Ben-Hur and I. Rosenthal, *Photochemistry and Photobiology*, 1989, **49**, 279-284.
2. B. Ş. Sesalan, A. Koca and A. Gül, *Dyes and Pigments*, 2008, **79**, 259-264.
3. D. A. Fernández, L. E. Dicelio and J. Awruch, *Journal of Heterocyclic Chemistry*, 1995, **32**, 519-522.
4. N. Kuznetsova, D. Makarov, O. Yuzhakova, A. Strizhakov, Y. Roumbal, L. Ulanova, A. Krasnovsky and O. Kaliya, *Photochemical & Photobiological Sciences*, 2009, **8**, 1724-1733.
5. G. Schneider, D. Wohrle, W. Spiller, J. Stark and G. Schulz-Ekloff, *Photochemistry and Photobiology*, 1994, **60**, 333-342.
6. Ł. Łapok, G. Schnurpfeil, R. Gerdes, S. M. Gorun, O. Suvorova, G. S. Kudryavtseva and D. Wöhrle, *Journal of Porphyrins and Phthalocyanines*, 2009, **13**, 346-357.
7. M. Kaneko, H. Ueno, S. Masuda, K. Suzuki, H. Okimi, M. Hoshino, L. Lapok and D. Wöhrle, *Journal of Porphyrins and Phthalocyanines*, 2005, **09**, 667-680.
8. S. B. Lee, A. J. Russell and K. Matyjaszewski, *Biomacromolecules*, 2003, **4**, 1386-1393.
9. F. A. Plamper, A. Schmalz, E. Penott-Chang, M. Drechsler, A. Jusufi, M. Ballauff and A. H. E. Müller, *Macromolecules*, 2007, **40**, 5689-5697.
10. L.-A. B. Rawlinson, S. a. M. Ryan, G. Mantovani, J. A. Syrett, D. M. Haddleton and D. J. Brayden, *Biomacromolecules*, 2009, **11**, 443-453.
11. S. Keely, A. Rullay, C. Wilson, A. Carmichael, S. Carrington, A. Corfield, D. M. Haddleton and D. J. Brayden, *Pharm Res*, 2005, **22**, 38-49.
12. S. H. Cho, M. S. Jhon, S. H. Yuk and H. B. Lee, *Journal of Polymer Science Part B: Polymer Physics*, 1997, **35**, 595-598.
13. Q. Liu, Z. Yu and P. Ni, *Colloid Polym Sci*, 2004, **282**, 387-393.
14. V. Bütün, S. P. Armes and N. C. Billingham, *Polymer*, 2001, **42**, 5993-6008.
15. G. Burillo, E. Bucio, E. Arenas and G. P. Lopez, *Macromolecular Materials and Engineering*, 2007, **292**, 214-219.

16. F. A. Plamper, M. Ruppel, A. Schmalz, O. Borisov, M. Ballauff and A. H. E. Müller, *Macromolecules*, 2007, **40**, 8361-8366.
17. X. Bories-Azeau and S. P. Armes, *Macromolecules*, 2002, **35**, 10241-10243.
18. P. van de Wetering, N. J. Zuidam, M. J. van Steenbergen, O. A. G. J. van der Houwen, W. J. M. Underberg and W. E. Hennink, *Macromolecules*, 1998, **31**, 8063-8068.
19. M. B. McCool and E. Senogles, *European Polymer Journal*, 1989, **25**, 857-860.
20. N. P. Truong, Z. Jia, M. Burges, N. A. J. McMillan and M. J. Monteiro, *Biomacromolecules*, 2011, **12**, 1876-1882.
21. B. Yu and A. B. Lowe, *Journal of Polymer Science Part A: Polymer Chemistry*, 2009, **47**, 1877-1890.
22. W. N. E. van Dijk-Wolthuis, P. van de Wetering, W. L. J. Hinrichs, L. J. F. Hofmeyer, R. M. J. Liskamp, D. J. A. Crommelin and W. E. Hennink, *Bioconjugate Chemistry*, 1999, **10**, 687-692.
23. P. van de Wetering, J. Y. Cherng, H. Talsma, D. J. A. Crommelin and W. E. Hennink, *Journal of Controlled Release*, 1998, **53**, 145-153.
24. C. V. Synatschke, A. Schallon, V. Jérôme, R. Freitag and A. H. E. Müller, *Biomacromolecules*, 2011, **12**, 4247-4255.
25. S. Fujishige, K. Kubota and I. Ando, *The Journal of Physical Chemistry*, 1989, **93**, 3311-3313.
26. D. Roy, W. L. A. Brooks and B. S. Sumerlin, *Chemical Society Reviews*, 2013.
27. H.-i. Lee, J. Pietrasik, S. S. Sheiko and K. Matyjaszewski, *Progress in Polymer Science*, 2010, **35**, 24-44.
28. Z. Gao, X. Tao, Y. Cui, T. Satoh, T. Kakuchi and Q. Duan, *Polymer Chemistry*, 2011, **2**, 2590-2596.
29. Z. Gao, J. Liang, X. Tao, Y. Cui, T. Satoh, T. Kakuchi and Q. Duan, *Macromol. Res.*, 2012, **20**, 508-514.
30. J.-F. Lutz, *Advanced Materials*, 2011, **23**, 2237-2243.
31. S. Han, M. Hagiwara and T. Ishizone, *Macromolecules*, 2003, **36**, 8312-8319.
32. T. Ishizone, A. Seki, M. Hagiwara, S. Han, H. Yokoyama, A. Oyane, A. Deffieux and S. Carlotti, *Macromolecules*, 2008, **41**, 2963-2967.

33. J.-F. Lutz, *Journal of Polymer Science Part A: Polymer Chemistry*, 2008, **46**, 3459-3470.

34. J.-F. Lutz and A. Hoth, *Macromolecules*, 2005, **39**, 893-896.

35. J.-F. Lutz, K. Weichenhan, Ö. Akdemir and A. Hoth, *Macromolecules*, 2007, **40**, 2503-2508.

36. J. Li, W. Zhang, Z. Hu, X.-J. Jiang, T. Ngai, P.-C. Lo, W. Zhang and G. Chen, *Polymer Chemistry*, 2013, **4**, 782-788.

37. A. J. Limer, A. K. Rullay, V. S. Miguel, C. Peinado, S. Keely, E. Fitzpatrick, S. D. Carrington, D. Brayden and D. M. Haddleton, *Reactive and Functional Polymers*, 2006, **66**, 51-64.

38. O. Azzaroni, A. A. Brown and W. T. S. Huck, *Angewandte Chemie International Edition*, 2006, **45**, 1770-1774.

39. G. Mantovani, V. Ladmiral, L. Tao and D. M. Haddleton, *Chemical Communications*, 2005, 2089-2091.

40. M. H. Stenzel-Rosenbaum, T. P. Davis, V. Chen and A. G. Fane, *Macromolecules*, 2001, **34**, 5433-5438.

41. R. N. Keller and H. D. Wycoff, *Inorg. Synth.*, 1946, 1-4.

Chapter 5 Development of Water-Soluble Zinc Phthalocyanine Conjugated Poly(Galactose) via Arm-First Approach

5.1 Synthesis of carbohydrate substituted phthalocyanines for water-solubility

Carbohydrate units can be attached to macrocycles which will prevent phthalocyanine aggregation and increase solubility in water. Only a few examples of carbohydrate substituted phthalocyanines have been reported in literature since the first carbohydrate substituted phthalocyanine was prepared by Maillard *et al*. in 1989.[1] However, a significantly increasing interest for such compounds has been attracted since 2005, mainly on carbohydrate Zn(II) and Si(IV) phthalocyanine derivatives, probably due to their potentials for PDT applications. Most of these phthalocyanine derivatives have a symmetric substitution pattern and a few are asymmetrically substituted.

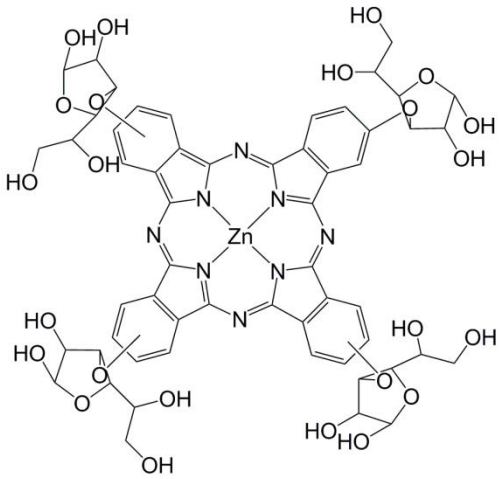

Figure 5.1.1 Structure of the first carbohydrate substituted phthalocyanine[1]

5.1.1 Symmetric substitution pattern

Most of the water-soluble carbohydrate substituted phthalocyanines are obtained from protected carbohydrate phthalonitriles. Following cyclotetramerisation, water-solubility is achieved only followed by removing of the protecting groups on the carbohydrate units, and also depends on the overall substitution pattern of the molecule.

Acetalated carbohydrates, 1,2:5,6-diisopropylidene-D-glucofuranose and 1,2:3,4-di-*O*-isopropylidene-α-D-galactopyranose, have been widely used to prepare the corresponding glycosylated phthalonitrile by nucleophilic aromatic substitution, **Figure 5.1.2**. A series of tetra- or mono-glycosylated zinc(II) phthalocyanines were synthesised from the protected phthalonitrile precursors (**Figure 5.1.2, 1-4**) by Choi *et al*., and the *in vitro* photodynamic activities of this class of photosensitisers were studied.[2] The desired phthalocyanines were difficult to characterise by NMR after acidic hydrolysis, due to the presence of the mixtures of isomers, particularly for tetra-substituted patterns owing to the possible promoted aggregation of the macrocycles through hydrogen bonding after deprotection.

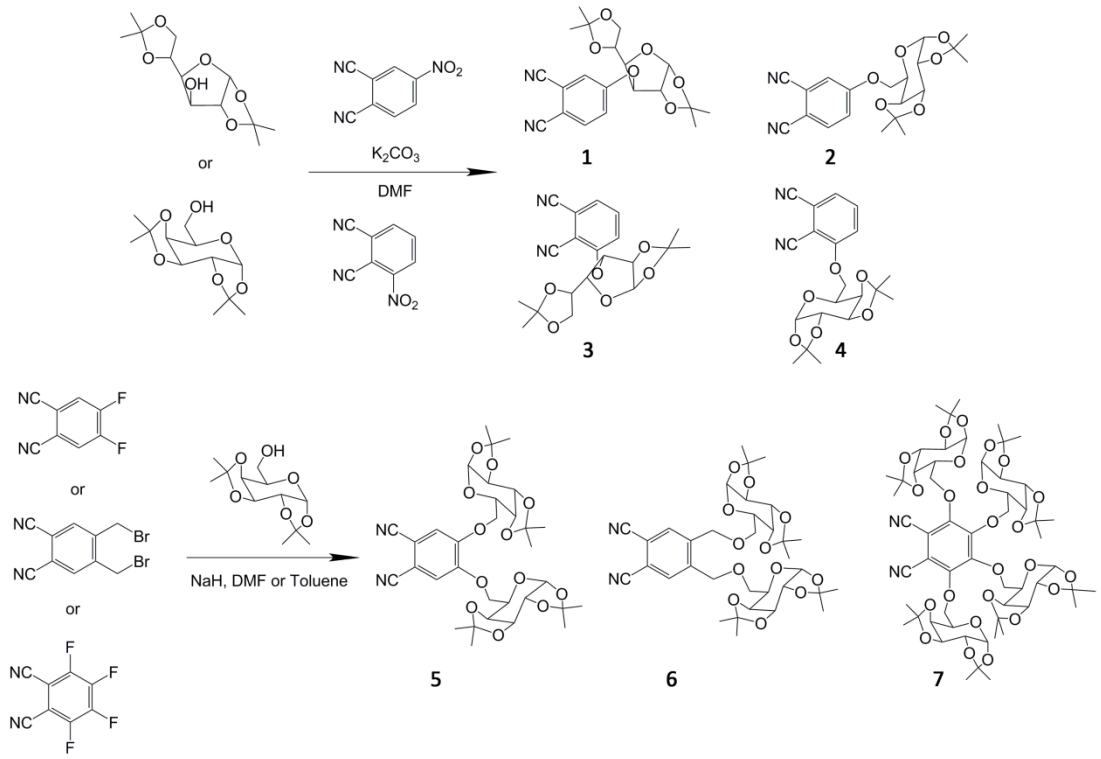

Figure 5.1.2 Acetal protected carbohydrate substituted phthalonitriles[2-5]

The preparation and characterisation of the first glucose substituted zinc phthalocyanines linked via the anomeric carbon through glycosidation method has been reported by Ziegler and co-workers.[6] This synthetic strategy is based on the cyclotetramerisation following by removal of the protecting groups (acetyl, benzoyl or benzyl) proved to be unsuccessful. Therefore, the method was further modified by removal the protecting groups from the glycosylated phthalonitriles prepared from a new glycosidation protocol developed by the same group.[7] The resulting phthalonitrile was directly converted into the a series of water-soluble *ZnPcs* peripherally tetra-glycosylated with D-glucopyranose, 1-thio-β-D-glucopyranose, β-D-galacopyranose, 1-thio-β-D-cello- and lactobiose in dimethylacetamide/n-butanol mixture (2/1, v/v) with dry zinc acetate at 100 ^{o}C.[8]

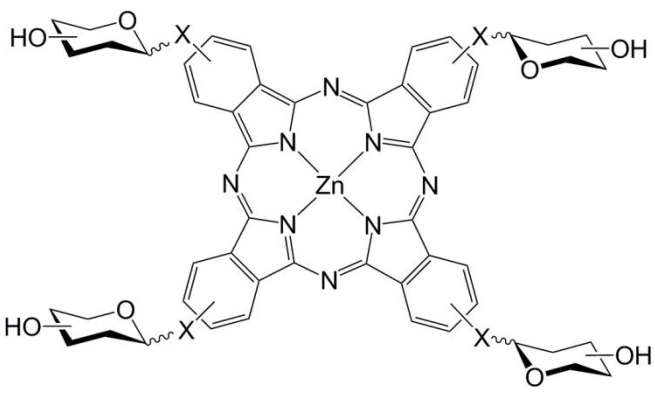

Figure 5.1.3 Anomerically tetra-glycosylated zinc(II) phthalocyanines. The glycosyl moieties represent glucose, galactose, cellobiose and lactose residues, X = O or S[6-8]

Recently, the synthesis of two similar octacarbohydrate substituted phthalocyanines, **Figure 5.1.4**, has been simultaneously published by Hanack and Torres respectively.[3, 5] These macrocycles were prepared from disubstituted phthalonitriles **5** and **6** (**Figure 5.1.2**) by reacting acetal protected galactose with 4,5-difluorophthalonitrile (nearly quantitatively) or 4,5-bis(bromomethyl) phthalonitrile (with low yields).

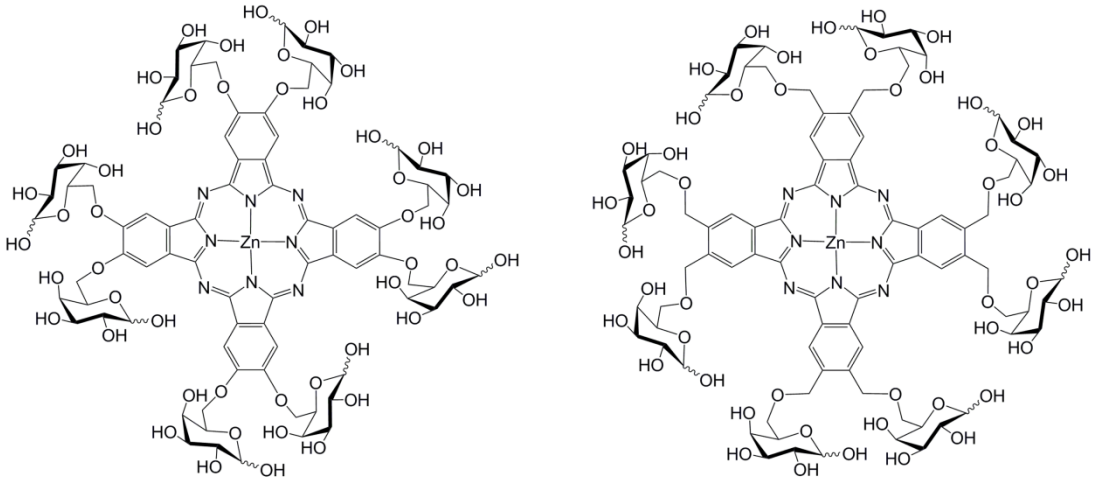

Figure 5.1.4 Structures of octagalactose substituted zinc phthalocyanines[3, 5]

5.1.2 Asymmetric substitution pattern

A few asymmetrically carbohydrate substituted phthalocyanines have been reported. Stable water solutions of *ZnPcs* using a covalent linkage to the β-cyclodextrin were first obtained by the Torres group.[9] The *ZnPc*-CD dyads (**Figure 5.1.5**, **1**) were prepared by statistical cross condensation of the unprotected cyclodextrin-phthalonitrile with an excess of phthalonitrile or 4,5-dibutoxyphthalonitrile, respectively, in the presence of zinc chloride. The CD moiety promotes good amphiphilic character to the new compounds. As far as the cyclodextrins and phthalocyanines were concerned, this family of compounds may be of interest as water-soluble photosensitisers for PDT, as well as for constructing supramolecular systems for molecular recognition, with potential applications in optical sensing.

A further novel water-soluble asymmetrical sugar-phthalocyanine (**Figure 5.1.5**, **2**) was prepared by the same group.[4] The synthetic strategy involved the preparation of glycophthalonitrile (**Figure 5.1.2**, **7**) by nucleophilic substitution of the four fluorine atoms of tetrafluorophthalonitrile by four protected galactose units. The expected AB_3-type phthalocyanine was then prepared by statistical cross-condensation of glycophthalonitrile with an excess of 1,2-dicyanobenzene, and converted into the water-soluble phthalocyanine derivative by acidic hydrolysis of the protecting acetals.

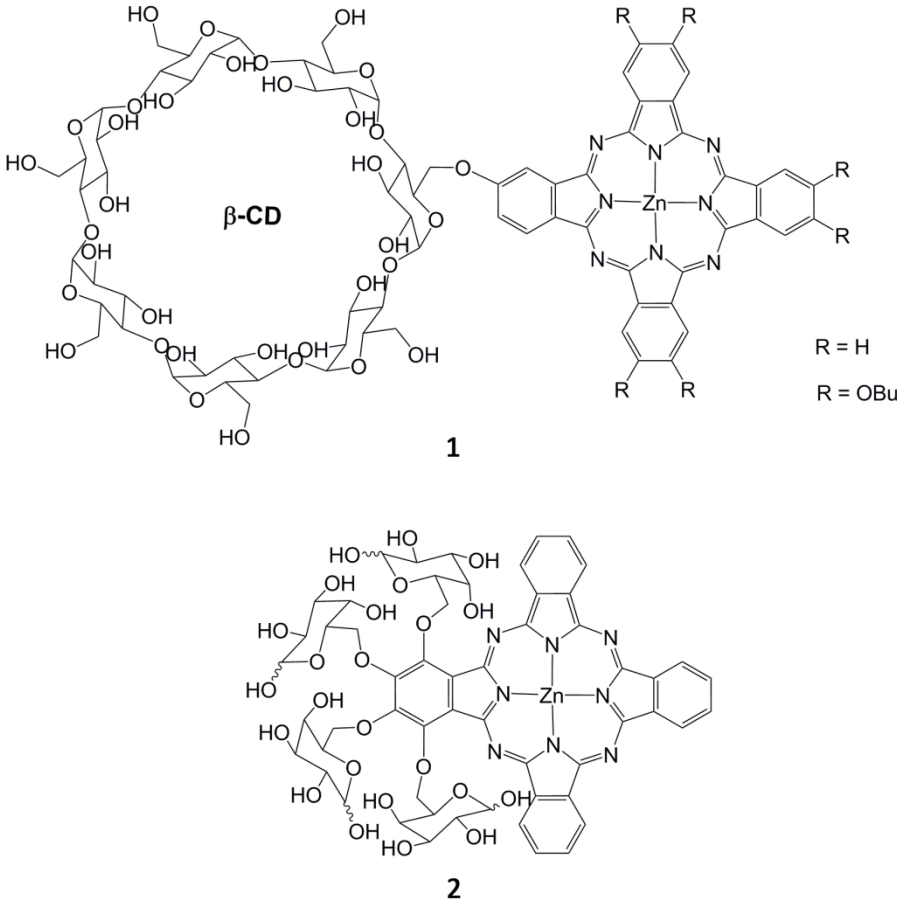

Figure 5.1.5 First example of β-cyclodextrin substituted *ZnPcs* (**1**) and asymmetric tetragalactose substituted phthalocyanine (**2**)[4, 9]

More recently, a series of glycosylated silicon(IV) and zinc(II) phthalocyanines have been synthesised and evaluated for their *in vitro* photodynamic activities by Ng and co-workers,[2, 10-12] due to their potential applications on PDT. The glucoconjugation may promote the uptake of photosensitisers through the glucose transporter proteins, which are over-expressed in a variety of human carcinomas.[13] Two novel glucoconjugated silicon(IV) phthalocyanines (**Figure 5.1.6**) were prepared with two axial 1,2:5,6-di-*O*-isopropylidene-α-D-glucofuranose substituents linked to the silicon centre through the tetraethylene glycol chain. The peripherally unsubstituted analogue was reported as a highly promising photosensitiser, which shows an extremely high *in vitro* photocytotoxicity and a highly selective subcellular localization property targeting the lysosomes.[10]

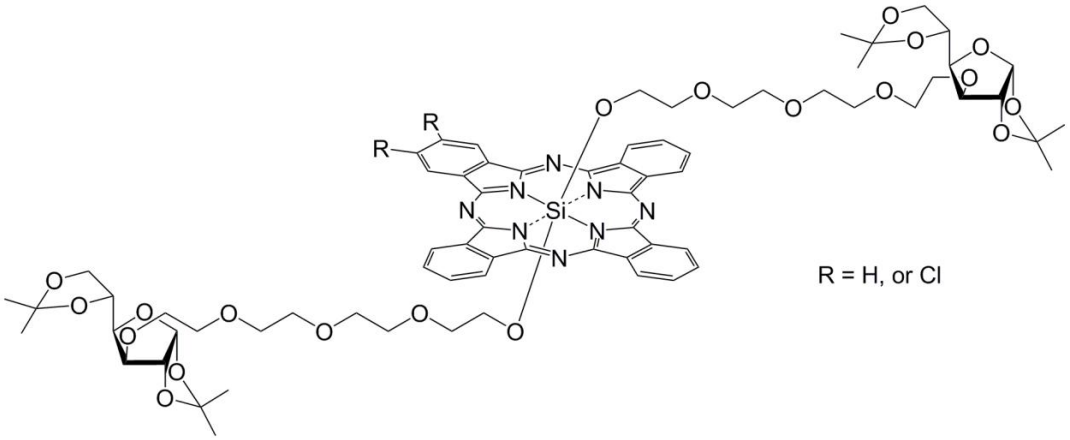

Figure 5.1.6 Structures of glucoconjugated silicon(IV) phthalocyanine and dichloro-substituted silicon(IV) phthalocyanine[10]

In a later report, the synthesis, characterisation, photophysical properties and *in vitro* photocytotoxicity of a new series of zinc(II) phthalocyanines substituted with two tetraethylene-glycol-linked glucose units at the α- or β-positions have been investigated by the same group.[14] The strategy used to prepare the di-α-substituted derivatives was shown in **Figure 5.1.7**. Treatment of tosylated sugar-substituted tetraethylene glycol with 2,3-dicyanohydroquinone resulted in the corresponding phthalonitrile. This kind of 1,4-disubstituted phthalocyanine was obtained by a typical mixed cyclisation reaction with phthalonitrile, and has been shown to possess desirable characteristics for PDT application according to their previous studies.[15, 16] Following the deprotection in TFA and water (9:1 v/v), the deprotected derivative *ZnPc*(α-Glu)$_2$ was afforded. The di-β-glucosylated analogue *ZnPc*(β-PGlu)$_2$ was prepared according to **Figure 5.1.8**. The 4,5-dibromocatechol was firstly treated with monotosylated tetraethylene glycol to afford the disubstituted product, which was further converted to the ditosylated derivative. Following nucleophilic substitution with protected glucose units and reaction with CuCN, the desired phthalocyanine was obtained again by a mixed cyclisation reaction with phthalonitrile without further deprotection. The *in vitro* photodynamic activities were evaluated and found that the di-α-substituted phthalocyanine has a great influence on the *in vitro* photocytotoxicity as compared with the di-β-substituted derivative. The protected di-α-substituted analogue was particularly potent and could be a promising photosensitiser for further investigation.

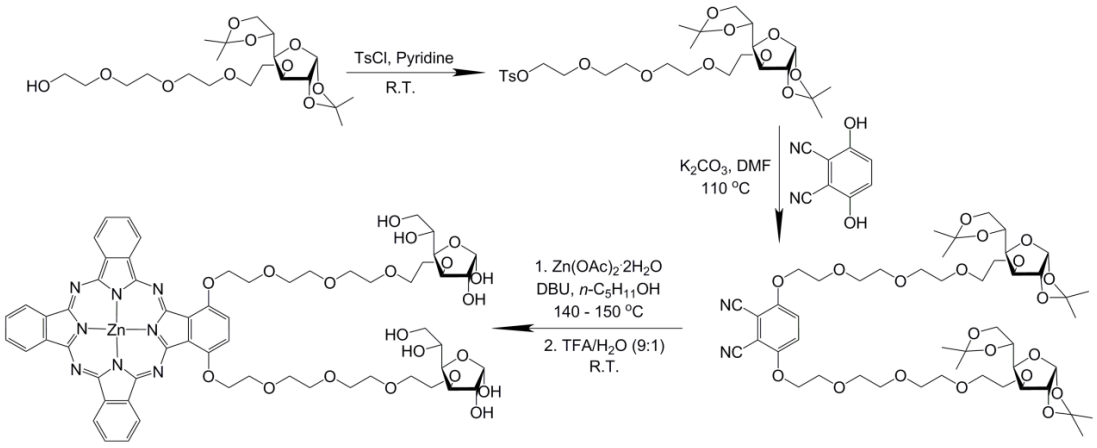

Figure 5.1.7 Synthesis of di-α-glucosylated zinc phthalocyanine[14]

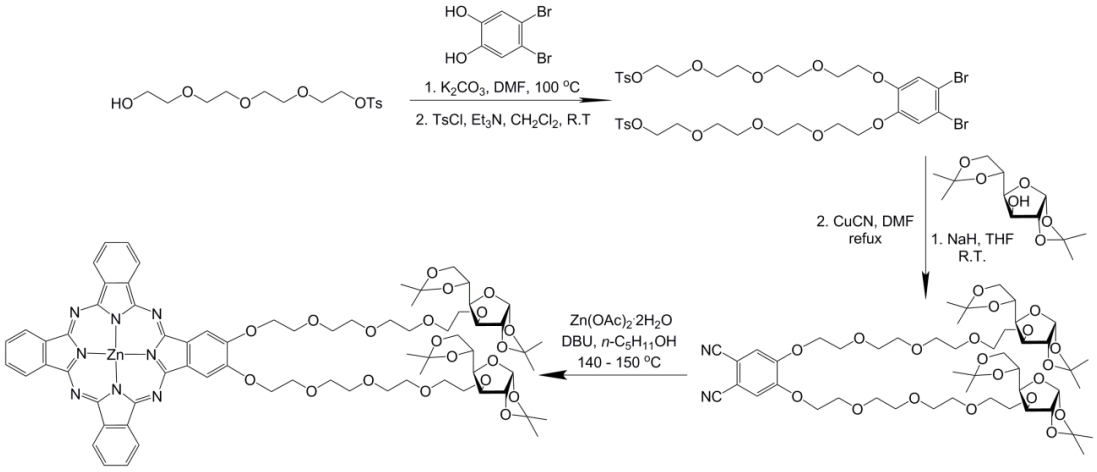

Figure 5.1.8 Synthesis of protected di-β-glucosylated zinc phthalocyanine[14]

5.2 Recent synthesis of glycopolymers

Glycopolymers with pendant saccharides exhibit specific interactions with lectins and have been successfully used for the multivalent presentation of carbohydrate ligands mimicking the cluster-glycoside effect.[17, 18] Therefore, the synthesis of carbohydrate-containing macromolecules, and their high affinities for proteins and molecular recognition abilities have been widely investigated by a number of groups.[19-22] Most synthetic glycopolymers were based on the polymerisation of carbohydrate-containing monomers. Alternatively, preformed polymer scaffolds

modified by saccharide-containing reagents were also proved to be an excellent synthetic route.[23] The combination of click chemistry and controlled radical polymerisation techniques have been most commonly employed for preparation of glycopolymers with well-controlled chain length, composition and architecture.

The preparation of well-defined glycopolymers via a combination of Cu-mediated living radical polymerisation and click reactions has been widely studied by Haddleton *et al*.[24-26] The synthesis of poly(alkynes) as polymeric scaffold were carried out by polymerisation of (trimethylsilyl)propargyl methacrylate (TMS-PMA), followed by removal of TMS group using TBAF in the presence of acetic acid, **Figure 5.2.1**.[24] Azide-functional sugars have been readily synthesised from unprotected sugars by one-pot synthetic route in appropriate solvent described by Shoda *et al*.[27] This approach was further modified to synthesise glycopolymers with mono, di-, and tri- saccharides by Gibson and co-workers.[28] Furthermore, well-defined mannose-functional polymers were demonstrated by the copper catalysed one-pot simultaneous CuAAC-LRP process via sharing a CuBr/iminopyridine catalytic system.[29]

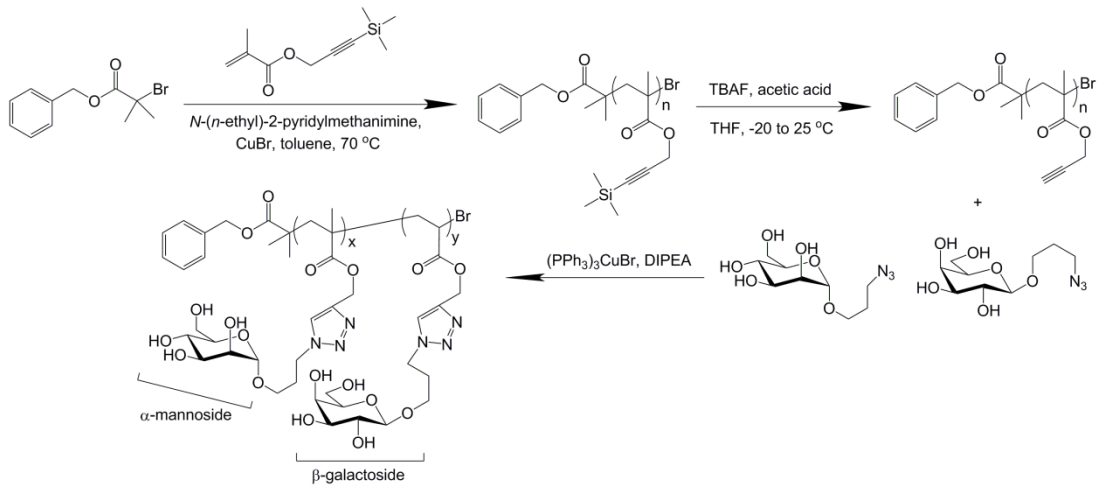

Figure 5.2.1 Synthesis of glycopolymers by combination of LRP and CuAAC reaction[24]

Recently, the new class of precision polymers with a high level of controlled architecture preserving both the monodisperse character and the defined monomer sequence were programmed and contributed to the understanding of complex biomedical-related processes.[30-33] The synthesis of sequence-defined monodisperse glycopolymer segments via solid-phase polymer synthesis was presented by Hartmann and co-workers for the first time.[34] Three dimer building blocks with the same chain length of sequence-defined poly(amidoamines) (PAMAMs) for solid-phase polymer synthesis carrying mono-, di, and tri-alkyne moieties were prepared, as shown in **Figure 5.2.2**, for further modification with mannose azides via 1,3-dipolar cycloaddition. After conjugation, the final glycopolymer segments were cleaved from the resin by acidic treatment with TFA in DCM leading to the final structures. The sequence-control and monodispersity of the products were confirmed by ESI-MS and RP-HPLC analysis, and their lectin binding affinity via inhibition studies were tested using Surface Plasmon Resonance (SPR), which indicated that the trivalent glycopolymer segment showed a strong increase in relative binding activity due to the optimal ligand spacing and chemical composition of the scaffold.

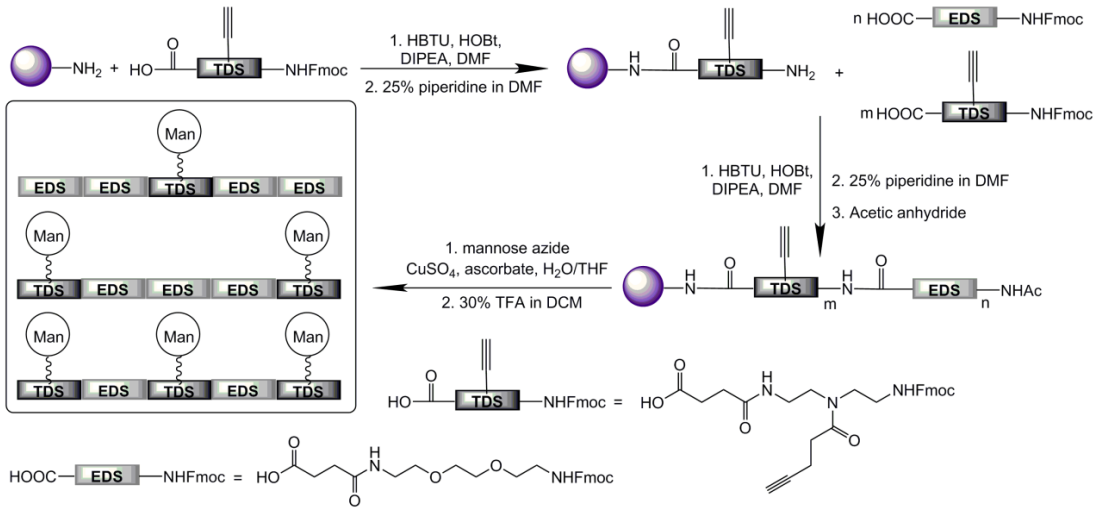

Figure 5.2.2 Schematic representation of solid-phase glycopolymer synthesis[34]

More recently, Haddleton and co-workers reported the precise control of the glycomonomer sequence along the polymer chain was achieved by SET-LRP.[26] Three different types of glycomonomer were prepared first by reacting 3-

azidopropylacrylate (APA) and alkylated mannose, glucose, and fucose via CuAAC reaction with $CuSO_4$ and sodium ascorbate in methanol/water mixture. The polymerization of mannose glycomonomer (ManA) was carried out in DMSO using Cu(0)/Cu(II), and Me_6-TREN as catalyst system at 25 ^oC, and the resulting high chain fidelity enabled for chain extension with glucose glycomonomer (GluA) and sequential fucose glycomonomer (FucA) up to six short blocks of glycopolymers (DP = 2 for each block). A similar approach was undertaken to prepare a thermo-responsive mannose-carrying sequence-controlled multi-block copolymer, **Figure 5.2.3**. SET-LRP of di(ethylene glycol) ethyl ether acrylate (DEGEEA) (DP = 6) was carried out under the same condition. After over 90% monomer conversion, ManA (DP = 3) was added and reached more than 95% conversion in 4.5 hours. The sequential addition cycle was continued until the polymer reached a hexablock structure. The obtained glycopolymers were further examined for their binding behaviour to dendritic cell-specific intercellular adhesion molecule-3-grabbing non-integrin (DC-SIGN) using SPR. As expected, stronger binding affinity for DC-SIGN was observed for the polymers with higher mannose content.

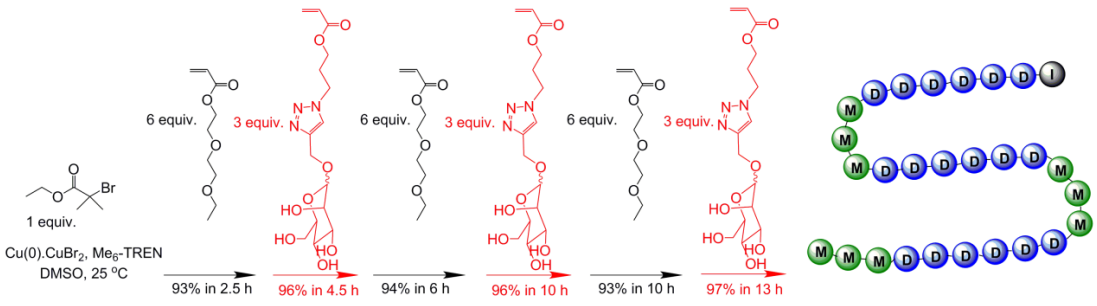

Figure 5.2.3 Schematic representation of the synthesis of sequence-controlled multiblock glycopolymers by iterative addition of DEGEEA and mannose glycomonomer at defined time[26]

5.3 Results and discussion

Owing to the desired water-solubility and high affinities for proteins and molecular recognition abilities of carbohydrate-containing macromolecules, in comparison with previous chapter, star-shaped poly(galactose)-*ZnPc* conjugates (*ZnPc*-P(Galactose)) were prepared by an arm-first approach. The protected galactose oligomer (Oligo(pGalactose)) arm was synthesised by SET-LRP with well-controlled molecular weight and high end-group fidelity. After substitution of bromide with azide, the CuAAC click reaction was carried out resulting in the protected poly(galactose) with *ZnPc* conjugated stars (*ZnPc*-P(pGalactose)), followed by deprotection of acetal groups to yield star-shaped *ZnPc*-P(Galacotse) with α/β anomers, **Figure 5.3.1**.

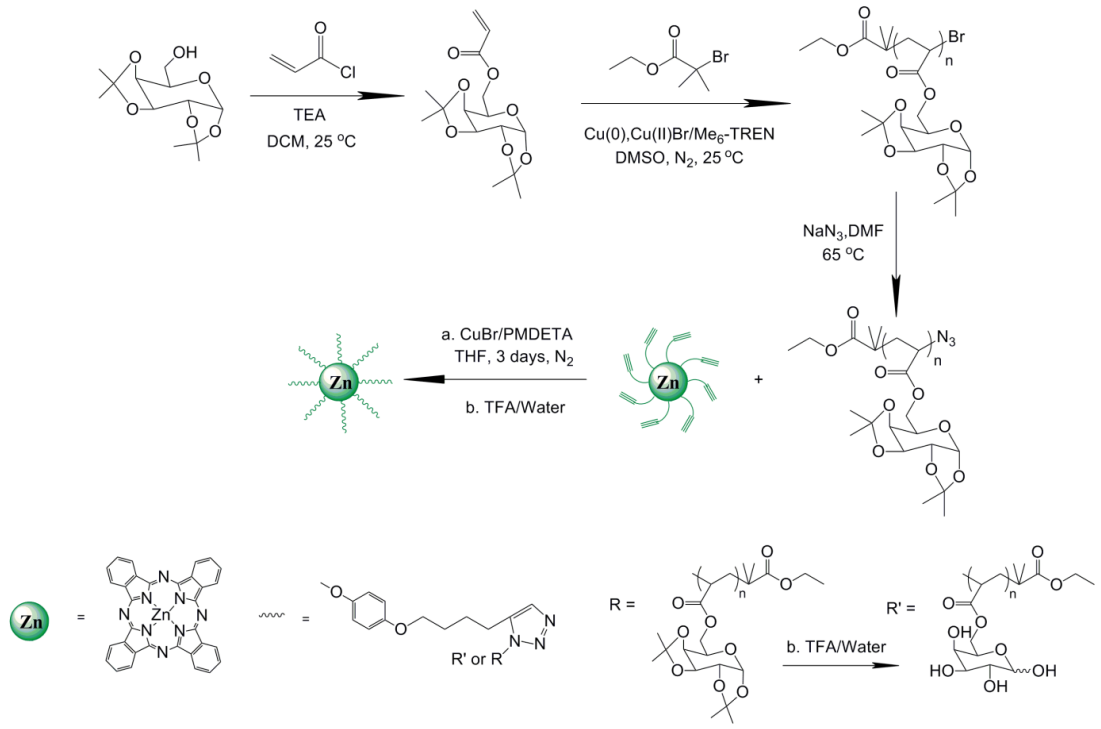

Figure 5.3.1 Summarised synthetic route of star-shaped *ZnPc*-P(Galactose)

5.3.1 Synthesis of protected poly(galactose) by SET-LRP

The protected galactose acrylate monomer was prepared from acylation of commercially available acetal protected galactose with acryloyl chloride, with addition of triethyl amine giving the desired acrylate monomer in good yield (60%).

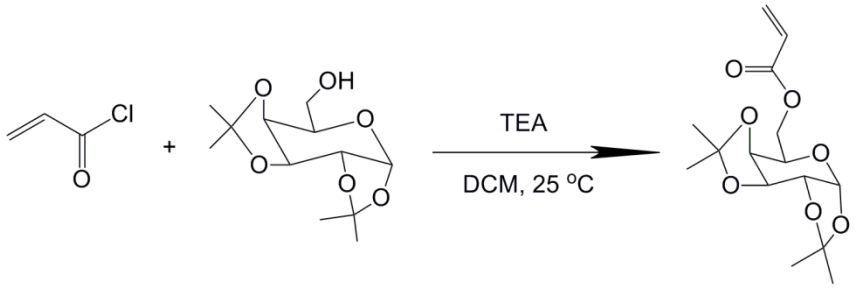

Figure 5.3.2 Reaction scheme of protected galactose acrylate monomer

Following flash chromatography, the product was isolated as white powder. ^{1}H NMR analysis of the synthesised monomer allowed all peaks to be assigned clearly, **Figure 5.3.3**. The protons on vinyl group are between δ 6.5 and 5.8 ppm. Moreover, the protons on the galactose ring are well-separated, and the proton on H-1 position is most deshielded. Their corresponding carbons are also well-defined in **Figure 5.3.4**.

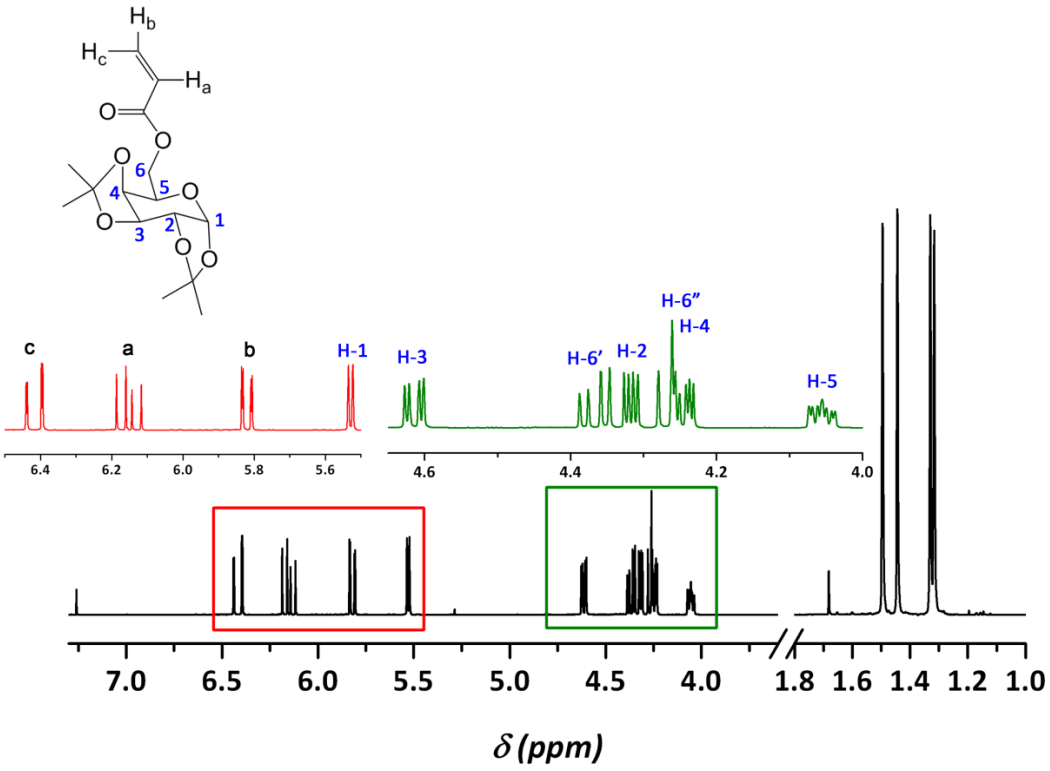

Figure 5.3.3 ^{1}H NMR analysis of acetal group protected galactose acrylate

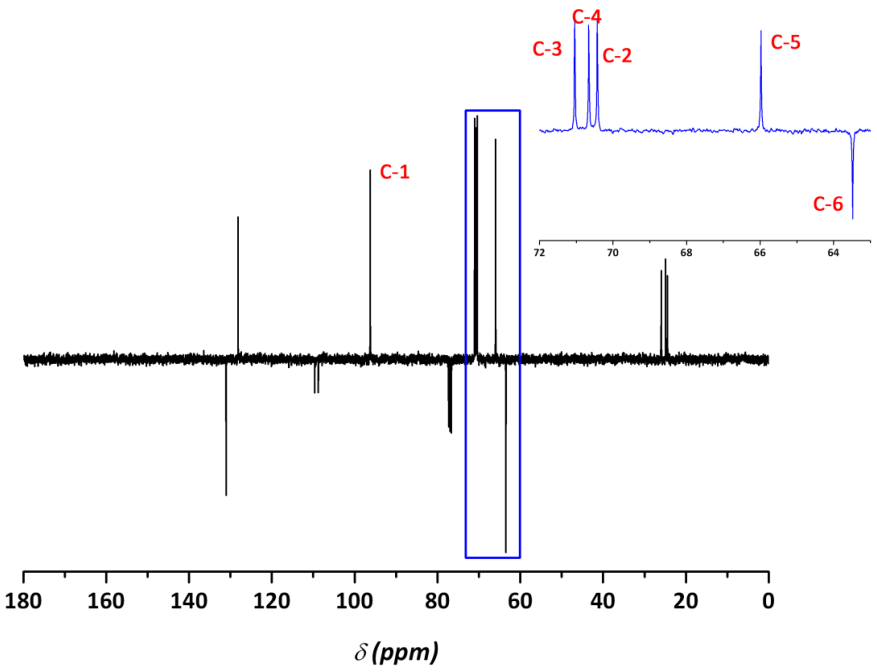

Figure 5.3.4 ^{13}C NMR analysis of acetal group protected galactose acrylate

SET-LRP with Cu(0) was utilised as to polymerise the protected galactose acrylate monomer, which possesses a number of attractive features. The process is mediated by Cu(0) as an activator, and requires polar/coordiniating solvents and active ligands to facilitate disproportionation of Cu(I) and to stablise [$L_xCu(II)X_2$] respectively. Under these conditions, the polymerisation shows high end-group fidelity until high monomer conversions, resulting in polymers with narrow dispersity and increased livingness/control. The initial polymerisation was carried out as previously reported protocol,[35] using Cu(0) wire, ethyl-2-bromoisobutyrate as the initiator, and sub-stoichiometric amounts of Cu(II)Br and Me_6-TREN relative to initiator (0.05 and 0.18 eq. respectively), **Figure 5.3.5**. The reaction was deoxygenated via bubbling with N_2 for 30 min and allowed to proceed overnight so as to achive full monomer conversion.

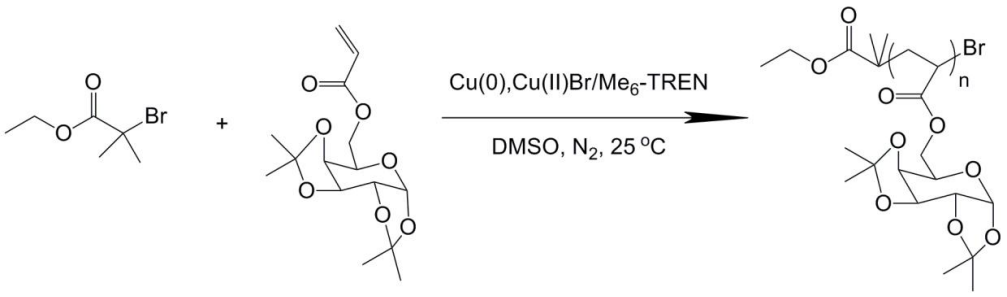

Figure 5.3.5 Synthesis of protected galactose oligomer by SET-LRP

One of the most valuable tools for end group identification of polymers is MALDI-ToF-MS analysis, which contains information about *n*-mer's end group; therefore, as long as the mass of the individual signal can be precisely determined, the mass of end groups can be calculated. However, the MALDI-ToF analysis of the protected galactose oligomer revealed two main distributions, **Figure 5.3.6**. The main distribution with higher intensity was attributed to the desired oligomer chain with retained bromide end-group. The lower intensity distribution was contributed to the termination by radical transfer to the ligand resulting in 'dead' oligomer chains. Recently, the importance of ligand mediated termination events has been investigated in our group.[36] It was found that two modes of termination can be

observed in presence of higher amounts of Me_6-TREN (≥ 0.18 eq.), either by radical chain transfer to Me_6-TREN, or due to ligand quaternization at the ω-chain end.

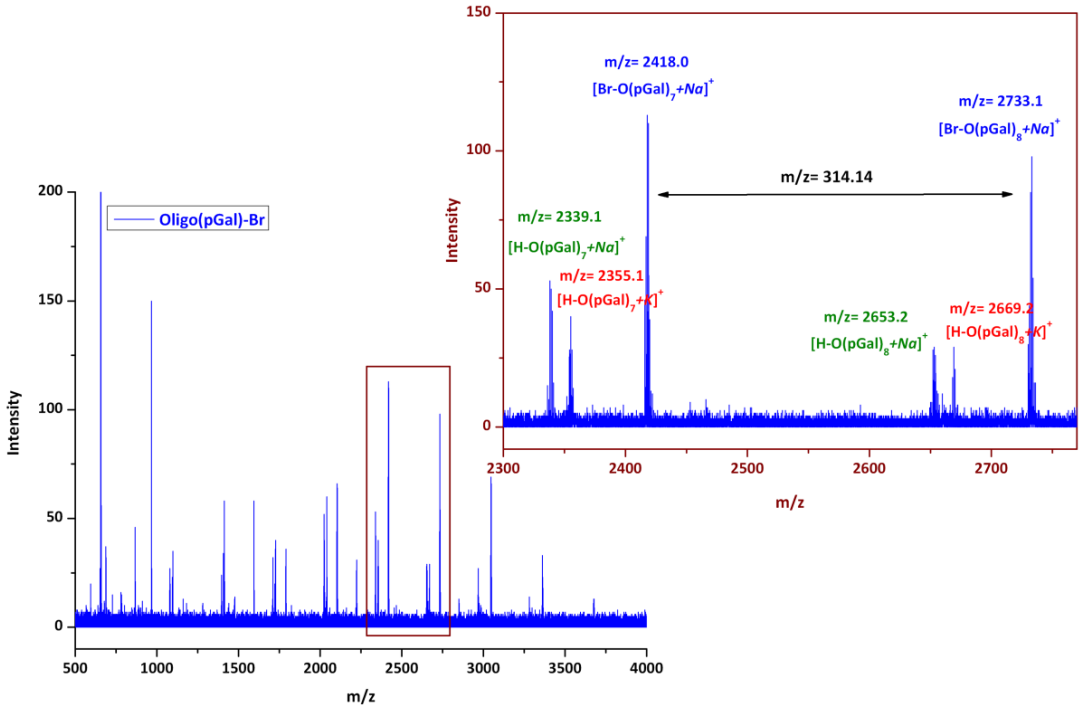

Figure 5.3.6 MALDI-ToF analysis of initial SET-LRP of protected galactose acrylate showing the distributions of desired oligomer with retained end-group functionality and the terminated polymer chain

Therefore, optimum polymerisation conditions were obtained when the amount of Me_6-TREN was reduced (0.12 eq.), as quaternization was eliminated and termination by chain transfer was significant reduced.[36] MALDI-ToF-MS analysis of the protected oligomer from optimum conditions shows only one distribution of peaks, which was ascribed to the protected galactose oligomer with the desired ω-chain end, and the undesired termination by chain transfer can be significantly suppressed, **Figure 5.3.7**. Through this approach, very high end group fidelity, which is important for either in situ chain extension or post-functionalisation of ω-chain end, can be achieved.

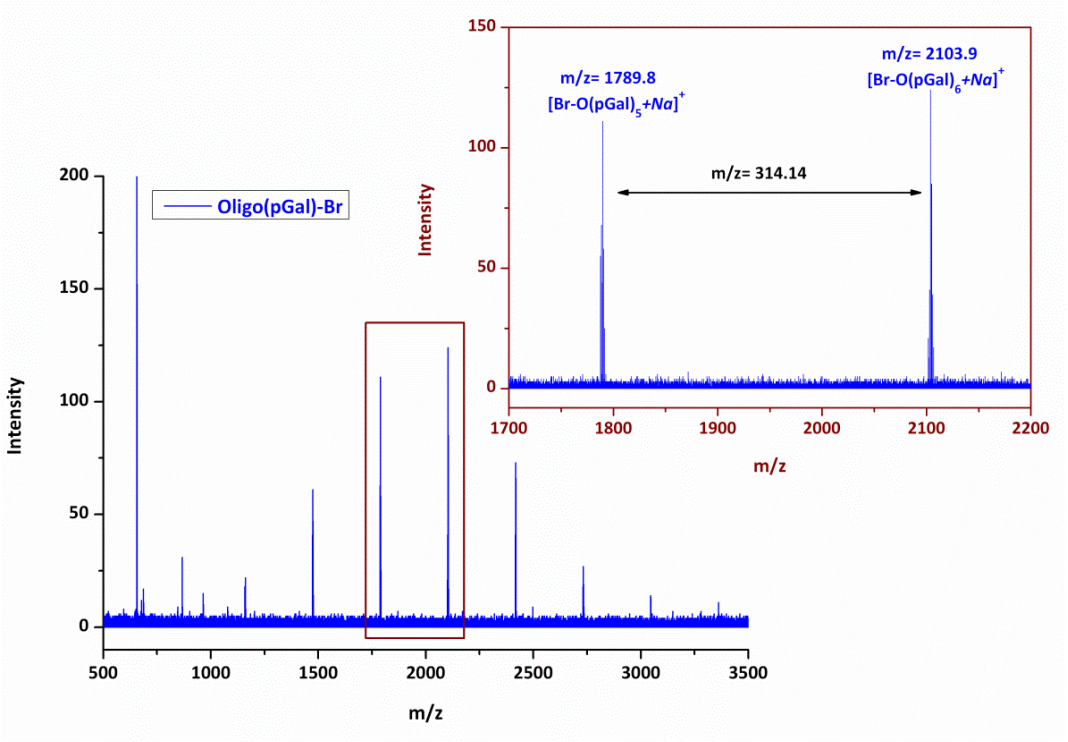

Figure 5.3.7 MALDI-ToF analysis of protected galactose oligomer under optimum polymerisation conditions

The protected galactose oligomer was further analysed by ^{1}H NMR, **Figure 5.3.8**. The protons are most deshielded around δ 5.4 and 4.6 ppm representing the protons on H-1 and H-3 positions of the galactose cyclic ring respectively. The protons on the initiator can be also well-resolved as shown. Therefore, the molecular weight of the oligomer can be estimated by ^{1}H NMR via comparing the integral of the two methyl protons of initiator at δ 1.13 ppm to that of the H-1 proton on the galactose ring around δ 5.4 ppm. Following the integration, the molecular weight of protected galactose oligomer is calculated as $M_{n,\ NMR}$ = 1800 g mol^{-1}, and the degree of the polymerisation is estimated as DP_{NMR} = 5.

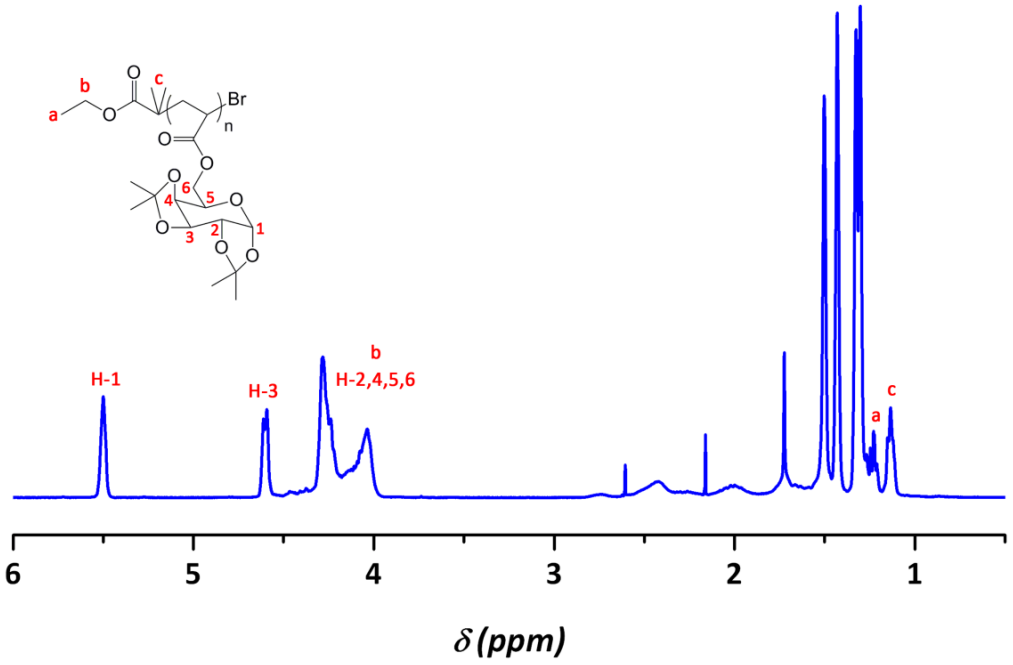

Figure 5.3.8 ^{1}H NMR analysis of protected galactose oligomer in $CDCl_3$

5.3.2 Post-functionalisation of protected galactose oligomer

Due to the achievement of very high ω-chain end of the protected galactose oligomer, the post-functionalisation was readily carried out by displacement of bromide end-group with sodium azide to give the protected galactose oligomer with azido-chain end. The reaction was performed in DMF at 65 ^{o}C overnight, **Figure 5.3.9**.

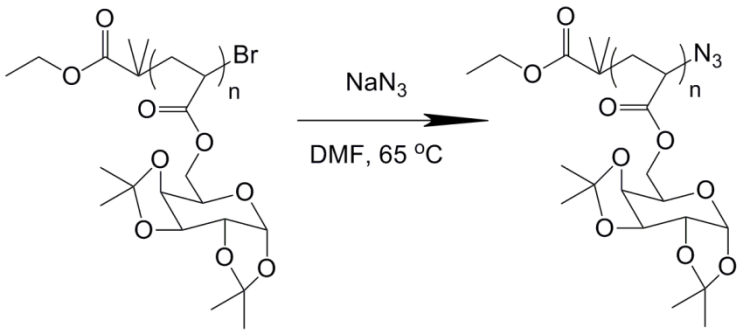

Figure 5.3.9 Reaction scheme of post-functionalisation of protected galactose oligomer with sodium azide

THF-GPC analysis of bromide functionalised protected galactose oligomer shows the molecular weight distribution, **Figure 5.3.10**-(a), shifted towards slightly lower molecular weight after the nucleophilic substitution with sodium azide, and narrow dispersity has been retained (PDI $\leq$ 1.13). The IR spectra illustrate the appearance of ν_{N_3} vibrational frequency at around 2110 cm^{-1}, further demonstrating the successful displacement of the azido group at the chain end, **Figure 5.3.10**-(b).

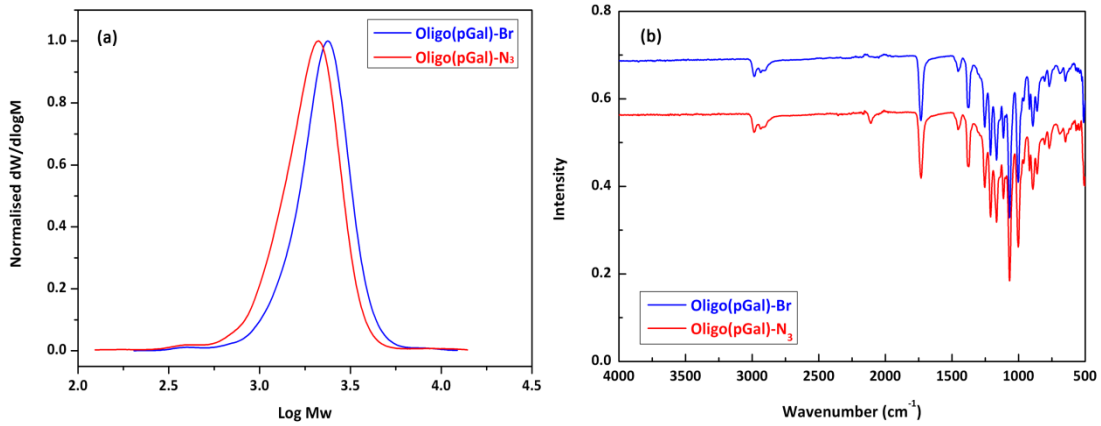

Figure 5.3.10 (a) Molecular weight distributions of bromide and azide functionalised protected galactose oligomers by THF-GPC; (b) IR spectra of bromide and azide functionalised protected galactose oligomers

MALDI-ToF-MS analysis of the azido-chain end functionalised protected galactose oligomer (**Figure 5.3.11**) showed a clean shifted distribution corresponding to the expected masses of the functionalised oligomer. No trace of the original bromo-end oligomer was observed, suggesting an efficient nucleophilic substitution.

It can be noticed that the mass spectra obtained indicates fragmentation of the azide functionality with the expulsion of N_2 ($[N_3\text{-}O(pGal)_6 - N_2 + Na]^+$ in green) giving rise to ions 28 mass units less than the mass of the *n*-mer during the matrix-assisted laser desorption ionization.[37, 38] Moreover, another distribution was observed in addition to the [M – 28] ions which has a mass loss less than 28 mass units (in purple), exhibiting the formation of metastable ions. As reported by Li *et al.*,[39] the metastable ions were formed when a parent ion generated during laser desorption fragments at some point during the flight path in the field free region between the ion

source and detector.[40] In reflector mode, ions are decelerated partway through their flight path and then reaccelerated in a different direction by a "mirror" towards a second detector to provide enhanced resolution. The metastable ions formed before arriving at the mirror will undergo a different deceleration, reacceleration than their parent ion; thus, the mass for these metastable ions (purple) will be some intermediate value between that of the parent ion (red) and the fragmented ion (green).

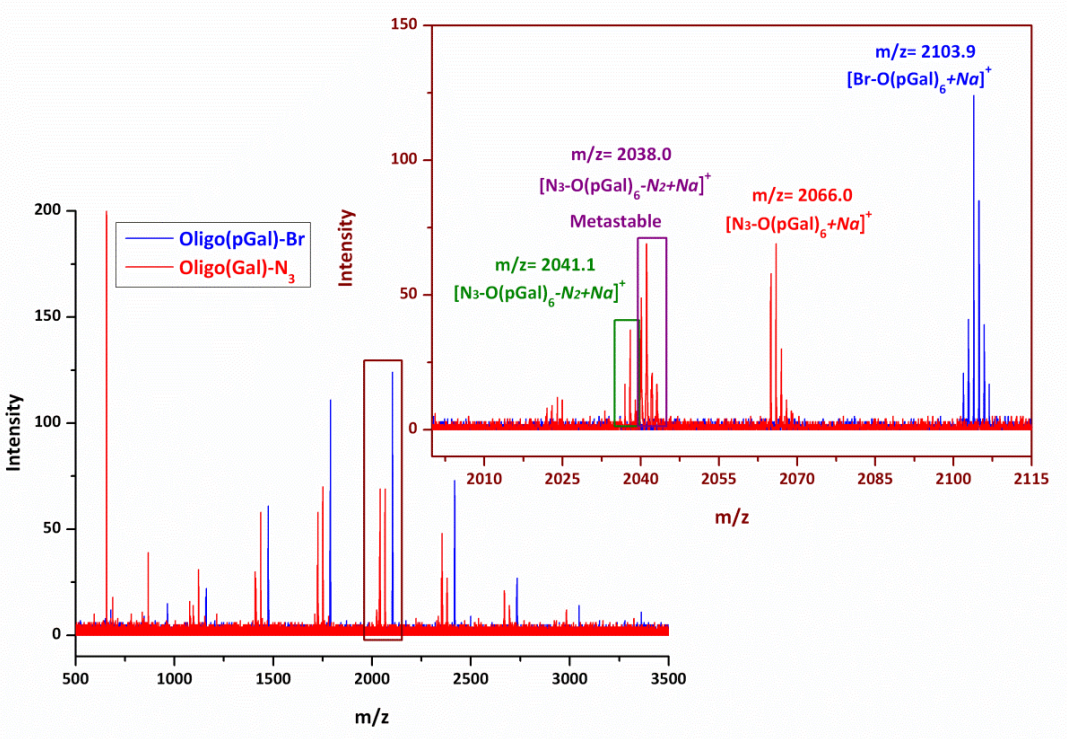

Figure 5.3.11 MALDI-ToF-MS analysis of the overlaid molecular weight distributions of protected galactose oligomers with bromo- and azido-chain ends as well as a zoom of the DP = 6 region

5.3.3 Synthesis of *ZnPc*-P(pGalactose) conjugates by CuAAC click chemistry

Following successful displacement of the bromo-end group with azide, star-shaped acetal protected galactose polymer with *ZnPc* conjugates [*ZnPc*-P(pGalactose)] were prepared via CuAAC click chemistry using previous synthesised *ZnPc*-alkyne, **Figure 5.3.11**. The reaction was carried out using a CuBr/PMDETA catalyst for 3

days to achieve a complete reaction. The crude product was isolated via passing through a basic aluminium oxide column, followed by precipitation in petroluem ether to yield greenish blue fine powder.

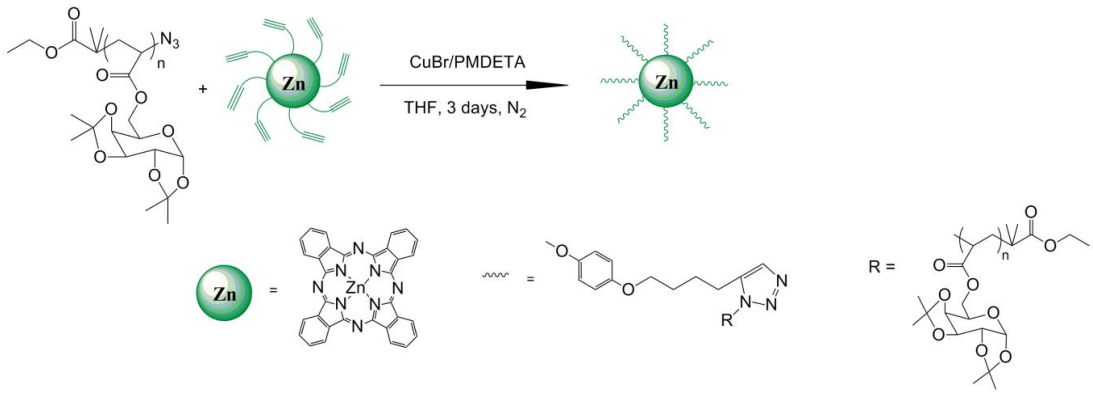

Figure 5.3.12 Reaction scheme of *ZnPc*-P(pGalactose) star conjugates by CuAAC cycloaddition

The desired product was confirmed by ^{1}H NMR in $CDCl_3$ in addition of traces of pyridine-d_5 to prevent aggregation, **Figure 5.3.13**. The protons at non-peripheral position of *ZnPc* ring are strongly deshielded around δ 9 ppm, and the appearance and the integration of broad peak at δ 7.7 ppm represents the protons on 1,2,3-triazole ring due to complete reaction. The molecular weight of *ZnPc*-P(pGalactose) conjugates can be calculated via comparing the integral of aromatic protons adjacent to *ZnPc* ring between δ 7.1 and 6.9 ppm to that of the H-1 proton on the protected galactose cyclic ring staying at δ 5.5 ppm. According to this approach, the molecular weight is estimated as $M_{n,\,NMR}$ = 19,200 g mol^{-1}, and the degree of polymerisation, by ^{1}H NMR, is approximately DP_{NMR} = 6 per arm.

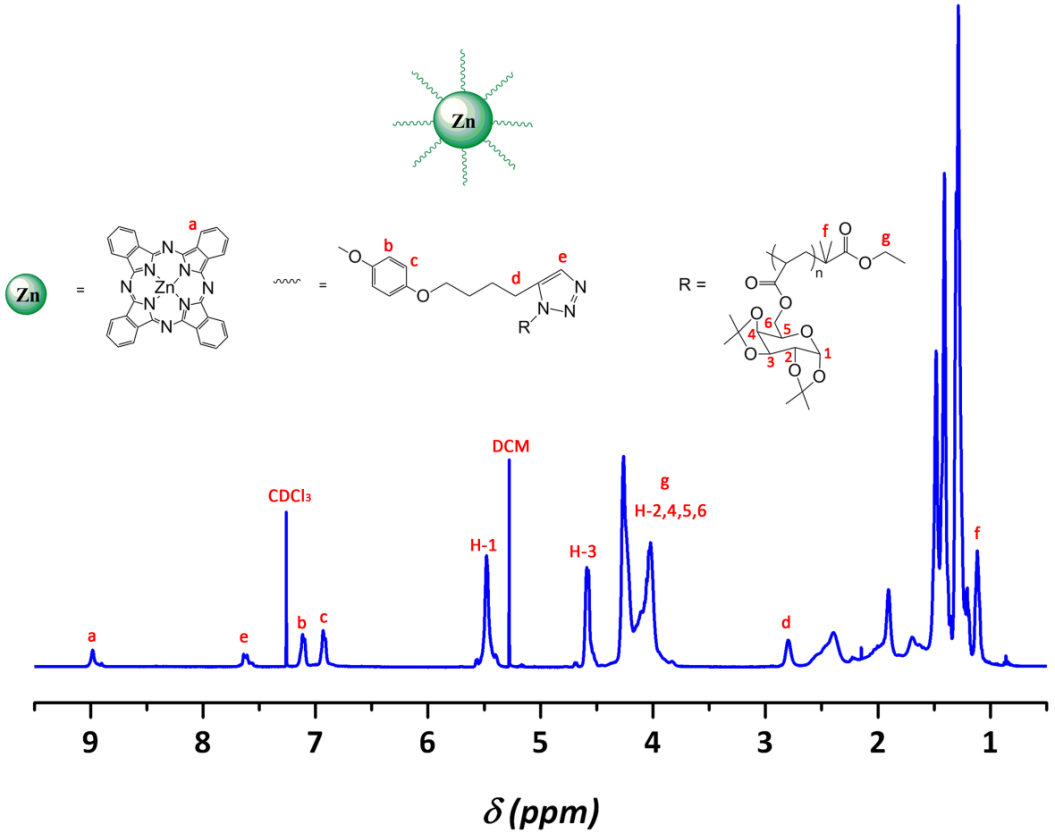

Figure 5.3.13 ^{1}H NMR analysis of *ZnPc*-P(pGalacotse) in $CDCl_3$ with traces of pyridine-d_5

Following characterisation by ^{1}H NMR, the *ZnPc*-P(pGalactose) conjugation was analysed THF-GPC and IR, further proving the efficiency of the click process. The chromatograms, **Figure 5.3.14**-(a) collected from UV detector (λ = 677 nm) of THF-GPC suggest full consumption of starting material *ZnPc*-alkyne; moreover, narrow dispersity was achieved (PDI = 1.03) after reaction and overlaid well with the chromatogram obtained from the RI detector. The 3D image (**Figure 5.3.14**-b) collected from PDA detector exhibits the full UV-Vis spectrum of *ZnPc*-P(pGalactose) conjugation together with its indicative retention time of *ZnPc* chromophore incorporated with protected galactose oligomers. Furthermore, the intense UV-Vis absorption of Q band at λ = 677 nm indicates that the conjugate is non-aggregated in THF.

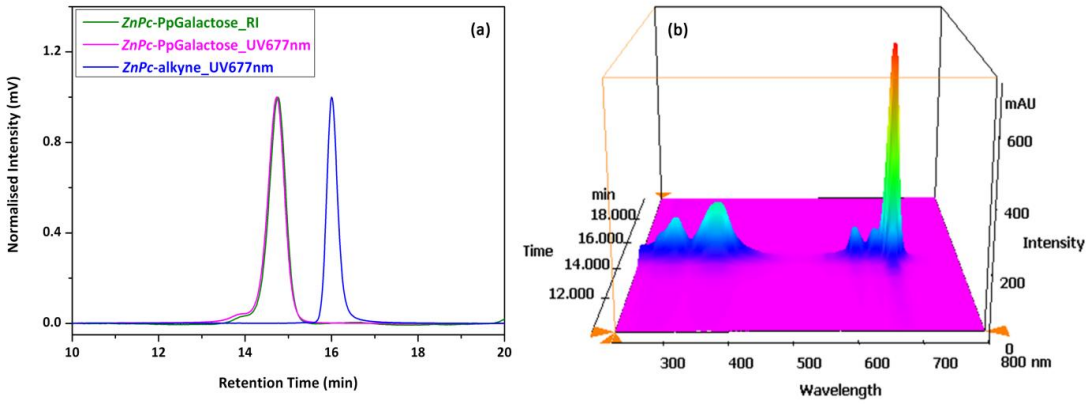

Figure 5.3.14 (a) THF-GPC analysis of starting material *ZnPc*-alkyne by UV detector (λ = 677 nm), and *ZnPc*-P(pGalactose) conjugates by both RI and UV (λ = 677 nm) detectors; (b) 3D image of *ZnPc*-P(pGalactose) conjugates collected from THF-GPC equipped with a PDA detector

The THF-GPC chromatograms from RI detector (**Figure 5.3.15**-a) represent an entire shift towards earlier retention time suggesting an increase in hydrodynamic volume after reaction, and no obvious acetal protected galactose oligomer traces can be observed. The IR spectra illustrates that the infrared absorption frequencies of ν_{N3}= 2100 and ν_{C-H}= 3280 cm^{-1} are from the starting materials of azido-end group of oligomers and terminate alkyne of *ZnPc*-alkyne respectively, **Figure 5.3.15**-(b). The thorough disappearance of both the vibrational frequencies also reveals the complete reaction.

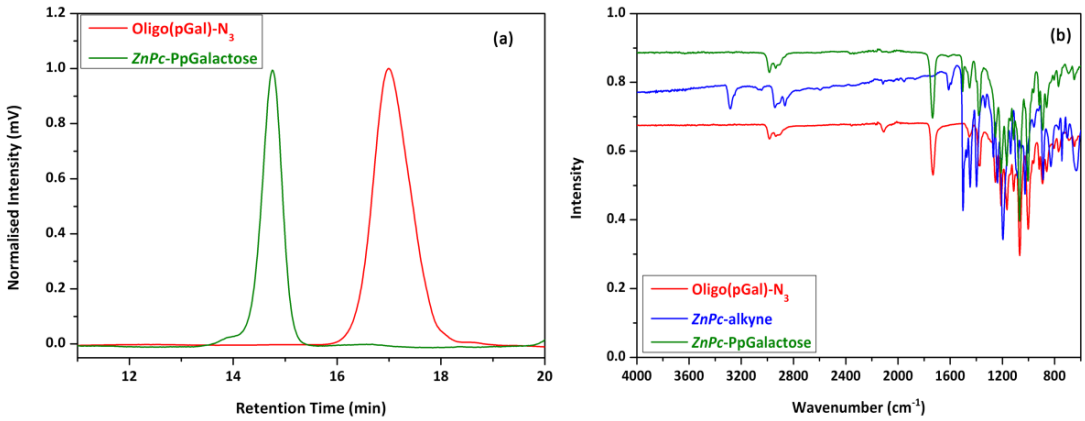

Figure 5.3.15 (a) THF-GPC chromatograms of starting material of protected galactose oligomer with azido-end group and purified *ZnPc*-P(pGalactose) conjugates by RI detector; (b) IR spectra of both starting materials of protected galactose oligomer with azido-end group and alkyne terminated *ZnPc*, and purified *ZnPc*-P(pGalactose) conjugates after click reaction

5.3.4 UV-Vis absorption and fluorescence property of *ZnPc*-P(pGalactose) conjugate

The UV-Vis and fluorescence spectra of the protected galactose oligomer conjugated *ZnPc* were measured in DMF, **Figure 5.3.16**. The compound gave a typical UV-Vis spectrum for non-aggregated phthalocyanines representing an intense and sharp Q band in the red visible region around λ_{max} = 678 nm. The solvent, DMF, probably acts as a coordinating solvent, binding axially to the zinc(II) macrocycle and reducing their tendency for aggregation. The fluorescence spectrum of the conjugate solution was measured by excitation at λ_{ex} = 610 nm exhibiting a fluorescence emission at λ_{em} = 693 nm, which probably makes *ZnPc*-P(pGalactose) conjugate can be a candidate of photosensitizer for photodynamic cancer therapy.

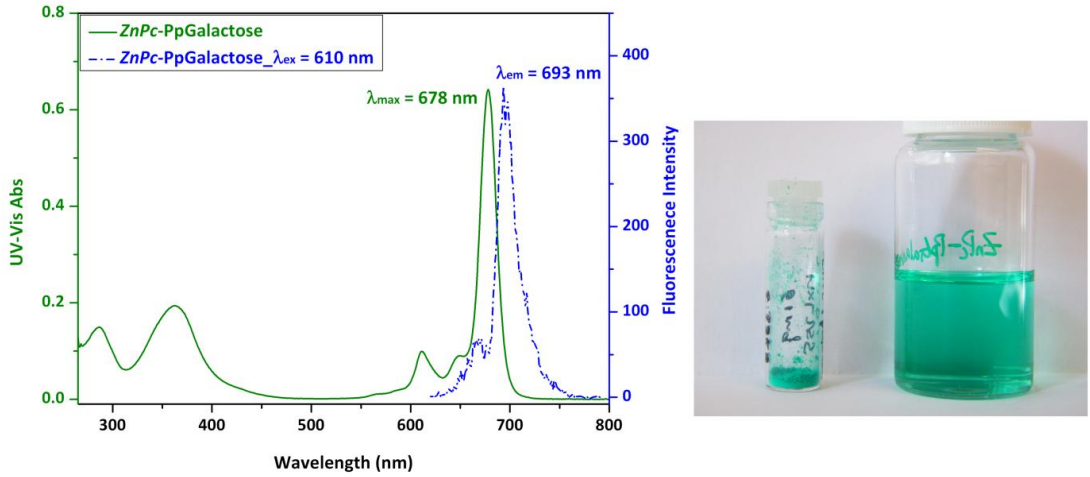

Figure 5.3.16 UV-Vis spectrum of *ZnPc*-P(pGalactose) in DMF (0.04 mg mL^{-1}) and fluorescence spectrum *ZnPc*-P(pGalactose) in DMF (0.1 mg mL^{-1}) excited at λ_{ex} = 610 nm; the image of *ZnPc*-P(pGalactose) powder and 0.1 mg mL^{-1} *ZnPc*-P(pGalactose) in DMF

5.3.5 Deprotection of star-shaped *ZnPc*-P(pGalactose) conjugates

The deprotection of the star-shaped *ZnPc*-P(pGalactose) conjugation was carried out by hydrolysing the isopropylidene-protected galactose functionality under acidic conditions (**Figure 5.3.17**), a mixture of TFA/H_2O (9/1, v/v) was added for 1 hour, in order to yield water-soluble poly(galactose) conjugated *ZnPc* macrocycle. The TFA was removed under reduced pressure, and the crude product was dialysed against water for 2 days followed by lyophilisation to yield greenish blue powder.

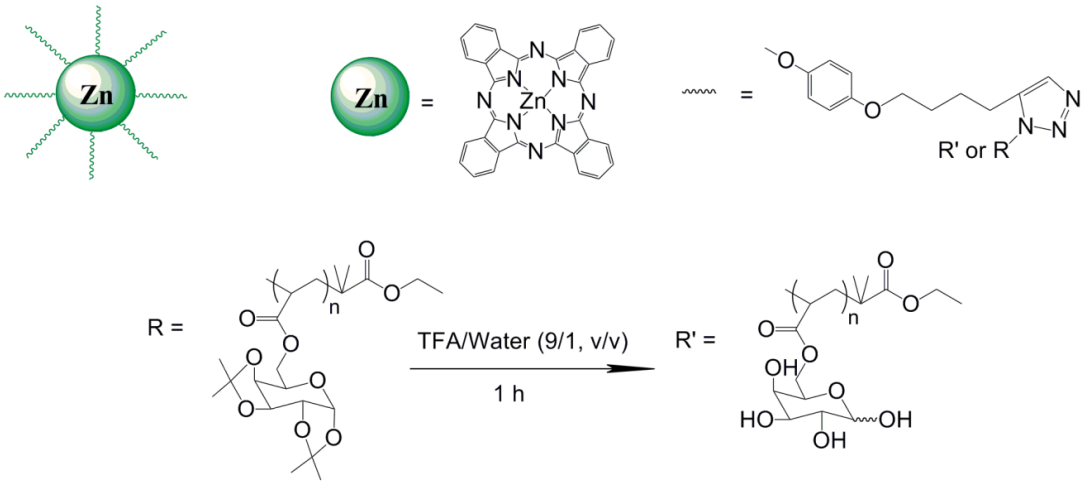

Figure 5.3.17 Synthetic route for deprotection of *ZnPc*-P(pGalactose) conjugation

Successful deprotection was confirmed by ^{1}H NMR analysis in DMSO-d_6 in addition of a trace of pyridine-d_5 to prevent intermolecular aggregation (**Figure 5.3.18**). The disappearance of the isopropylidene CH_3 protons at δ 1.2-1.48 ppm proves the deprotection of the carbohydrate moieties. The resonances of the anomeric OH protons appear between δ 6.57 and 6.17 ppm as broad singlets (these signals disappeared when D_2O was used), and the ratio of α/β anomers is approximately 6/5 according to integration. The multiplets at δ 5.5-3.2 ppm are assigned to the resonances of carbohydrate units; while the eight non-peripheral protons on *ZnPc* ring stay at downfield as a broad singlet at δ 8.9 ppm. Moreover, the eight protons from the individual 1,2,3-triazole ring and the protons on the aromatic rings remain at δ 7.98 ppm and δ 7.25-705 ppm respectively.

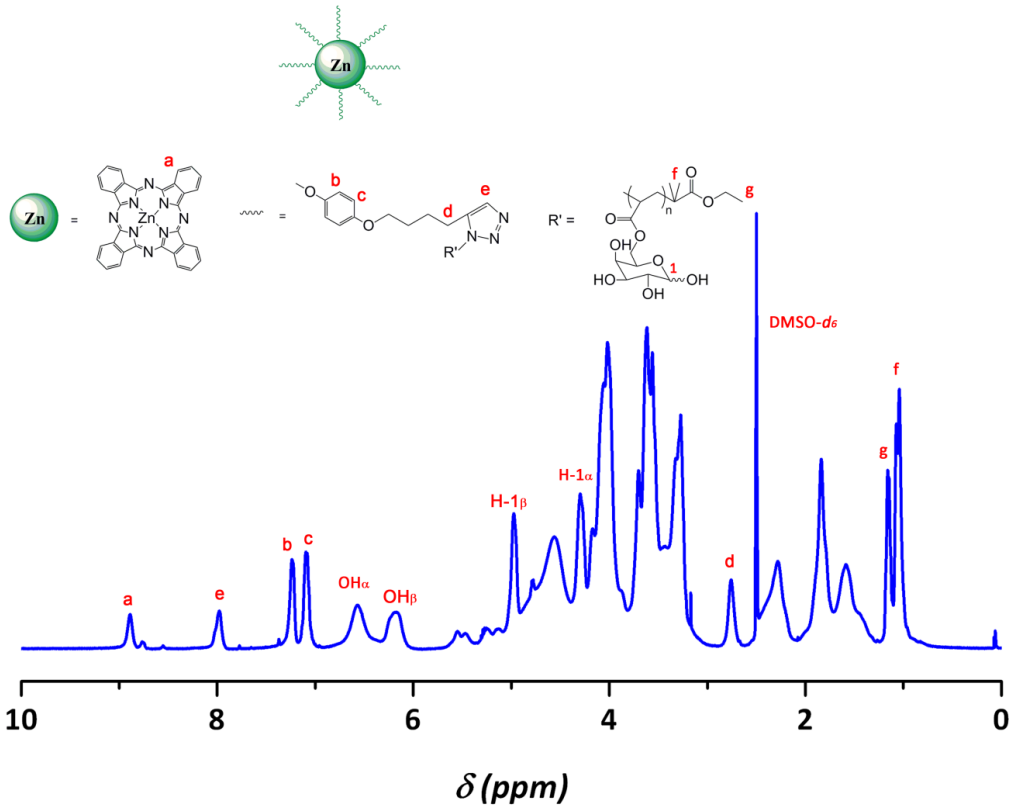

Figure 5.3.18 ^{1}H NMR spectrum of *ZnPc*-P(Galactose) conjugation in DMSO-d_6 with a trace of pyridine-d_5

The IR spectra illustrates the comparison between the protected and deprotected star *ZnPc*-P(pGalactose) and *ZnPc*-P(Galactose) conjugates. After deprotection, the appearance of a broad –OH stretching is clearly around 3400 cm^{-1}, as well as the disappearance of a large number of the C-O stretches between 1000 and 1300 cm^{-1}, **Figure 5.3.19**.

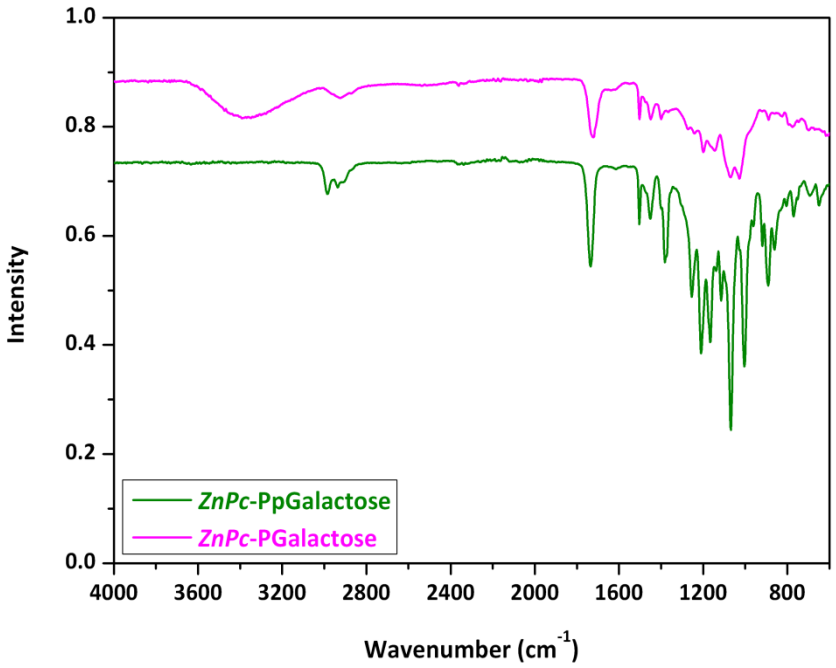

Figure 5.3.19 IR spectra of *ZnPc*-P(pGalactose) conjugate before and after deprotection

Both of the protected *ZnPc*-P(pGalactose) and deprotected *ZnPc*-P(Galactose) conjugates were further analysed by DMF-GPC, which is equipped a PolarGel-L column running better for polar solvent and more hydrophilic polymers. The image (**Figure 5.3.20**) represents the overlaid UV-Vis (λ = 678 nm) chromatograms of *ZnPc*-P(pGalactose) before and after deprotection, revealing an insignificant influence on the retention time, probably due to the minimum effect on the change of hydrodynamic volume after deprotection of the star *ZnPc*-P(pGalactose) conjugate.

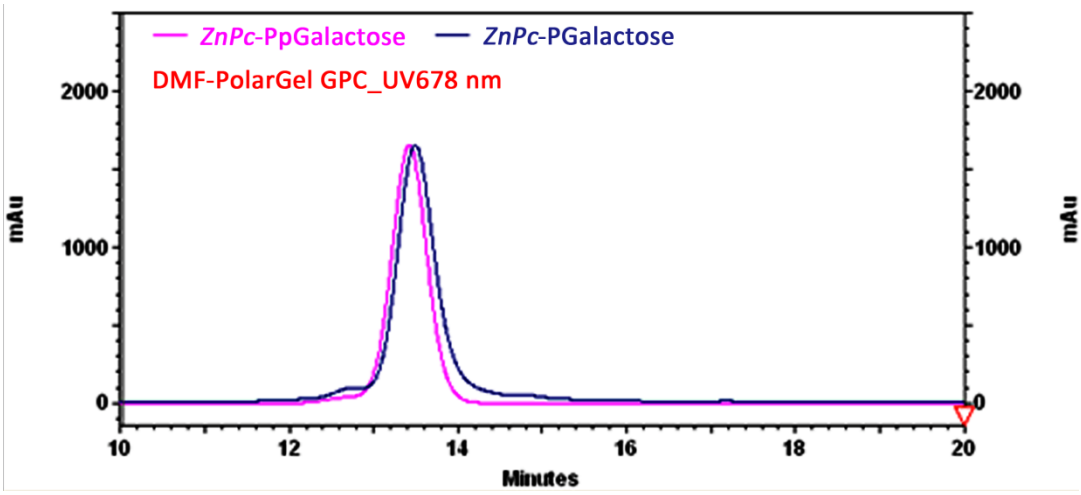

Figure 5.3.20 DMF-GPC analysis of protected *ZnPc*-P(pGalactose) and deprotected *ZnPc*-P(Galactose) conjugates using PDA detector with extracted wavelength at λ = 678 nm

However, the results obtained from the RI detector exhibits a shoulder peak at approximately 14.8 minutes retention time from the tail of peak, **Figure 5.3.21**. According to a previous investigation, there was neither obvious protected galactose arms left in the system after the click process, nor decomposition of the *ZnPc* macrocycle, as reported under acidic condition in the literature. Therefore, the reason for the formation of this shoulder peak in RI chromatogram was further analysed by a multi-detector view from the GPC software.

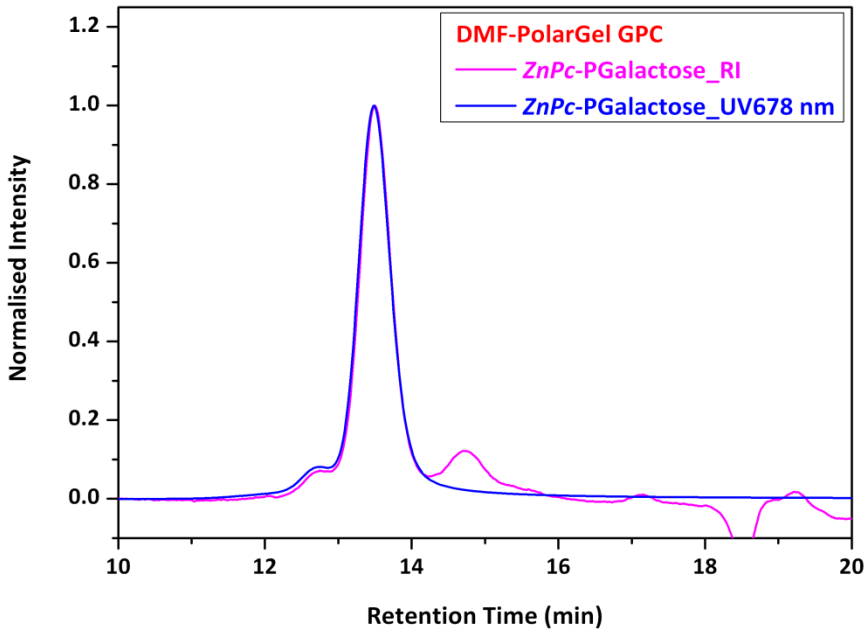

Figure 5.3.21 DMF-GPC analysis of star *ZnPc*-P(Galactose) conjugate by both RI and UV (λ = 678 nm) detectors

As shown in multi-view image, **Figure 5.3.22**-(a), the retention time was set at t = 14.8 min where the shoulder peak eluted from the RI detector, and the wavelength was set at λ = 678 nm where the *ZnPc* macrocycle absorbance is easily distinguished. Therefore, the chromatogram of *ZnPc*-P(Galactose) (**Figure 5.3.22**-b) represents a narrow distribution at λ = 678 nm with slight tail at t = 14.8 min retention time. The corresponding UV-Vis spectrum at t = 14.8 min retention time illustrates a characteristic and non-aggregated absorption for phthalocyanines, **Figure 5.3.22**-(c). Hence, it can be concluded that the shoulder peak at t = 14.8 min retention time from RI detector shows the UV-Vis spectrum of *ZnPc*-P(Galactose) conjugate, and this is probably due to the interaction between the star polymer and the column due to the presence of highly dense hydroxyl groups from the galactose moieties.

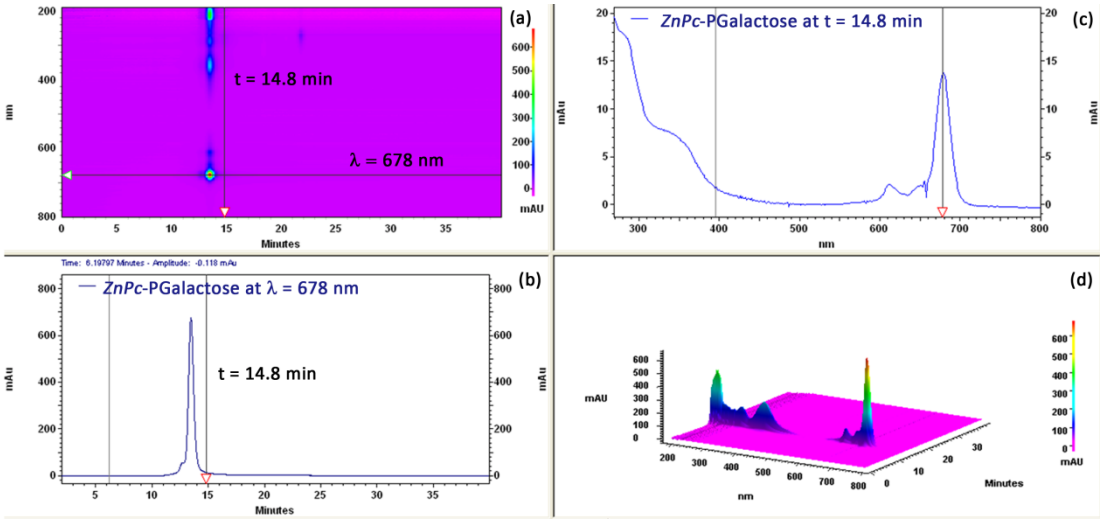

Figure 5.3.22 Multi-view image from the DMF-GPC equipped with PDA detector: (a) chromatograms of *ZnPc*-P(Galactose) with x axial as retention time (min), y axial as intensity (mAU), and z axial as wavelength (nm); (b) GPC chromatogram of *ZnPc*-P(Galactose) extracted from λ = 678 nm; (c) UV-Vis spectrum of *ZnPc*-P(Galactose) at t = 14.8 min retention time; (d) 3D image of *ZnPc*-P(Galactose) chromatogram UV-Vis spectrum of *ZnPc*-P(Galactose) at t = 14.8 min retention time

5.3.6 UV-Vis absorption and fluorescence properties of *ZnPc*-P(Galactose) conjugates

Following analysis by DMF-PolarGel GPC, the optical properties of star *ZnPc*-P(Galactose) conjugate were further analysed by UV-Vis and flourescence spectroscopy, **Figure 5.3.23**. The UV-Vis spectrum of 0.04 mg mL^{-1} polymer solution in DMF show an intense single Q band at λ_{max} = 679 nm with good agreement of the result obtained from the PDA detector of DMF-GPC, and its sharp fluorescence emission band is approximately at λ_{em} = 695 nm via excitation at λ_{ex} = 610 nm. However, the absorption is significantly reduced and becoming broad in aqueous solution as expected, suggesting dimerization occurs; therefore, no fluorescence emission could be observed. The picture exhibits the greenish blue polymer after lyophilisation, and slightly colour difference when dissolution in DMF and water respectively.

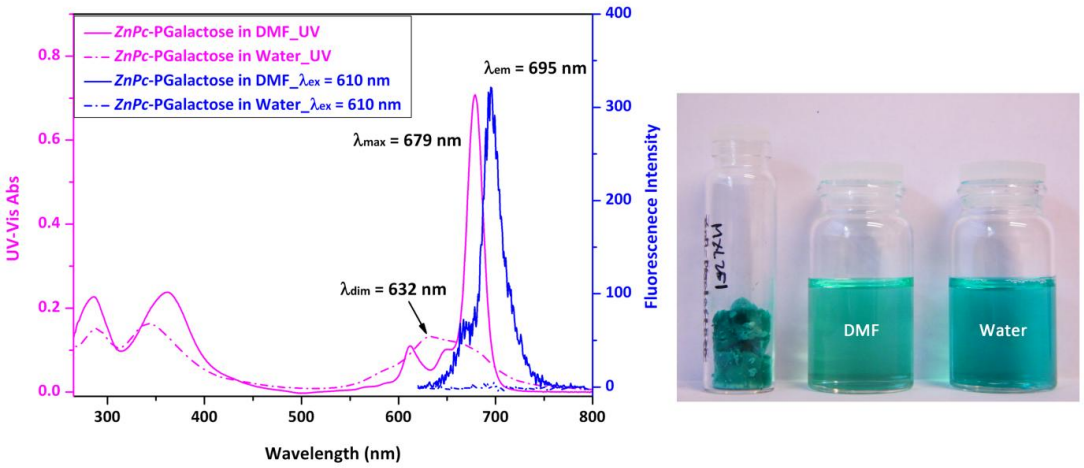

Figure 5.3.23 UV-Vis spectra of 0.04 mg mL^{-1} *ZnPc*-P(Galactose) in DMF and water respectively and fluorescence spectra 0.1 mg mL^{-1} *ZnPc*-P(Galactose) in DMF and water respectively excited at λ_{ex} = 610 nm; the image of *ZnPc*-P(Galactose) after lyophilisation and 0.1 mg mL^{-1} *ZnPc*-P(Galactose) in DMF and water respectively (left to right)

5.4 Conclusions

This work has involved the successful synthesis of novel water-soluble *ZnPc* conjugated poly(galactose) via a arm-first approach. The strategy began with the preparation of the arm, protected galactose oligomer, which was obtained under SET-LRP conditions. The optimum polymerisation conditions were obtained when the amount of Me_6-TREN was reduced (0.12 eq.). The resulting protected oligomer was shown to achieve perfect bromo end group fidelity by MALDI-ToF MS analysis. The molecular weight of the oligomer was clearly estimated by ^{1}H NMR ($M_{n,\,NMR}$ = 1800 g mol^{-1}, DP_{NMR} = 5), and a narrow dispersity was achieved according to GPC analysis.

Following post-functionalisation with sodium azide, the MALDI-ToF MS analysis has shown a clear shift on molecular weight distribution indicating the azido-chain end. Additionally, another two distributions suggested the presence of the fragmentation of azide functionality via expulsion of N_2, as well as the formation of metastable ions. The molecular weight of azido-terminated protected galactose

oligomer slightly decreased and the dispersity remained narrow, which were confirmed by THF-GPC analysis.

Previously synthesised octaalkyne terminated *ZnPc* was successfully conjugated with protected galactose oligomer by CuAAC click reaction. The efficient conjugation was confirmed via integrating the protons on triazole groups by ^{1}H NMR characterisation with an indicative of star shape. Furthermore, well-overlapped chromatograms from RI and UV detectors of THF-GPC illustrated the incorporation of *ZnPc* chromophore, and no starting materials were observed. UV-Vis analysis of the conjugated polymer suggested non-aggregation in DMF with an intense Q band at 678 nm, and fluorescent emission at 693 nm was also detected by excitation at 610 nm, which probably makes *ZnPc*-P(pGalactose) conjugate could be a candidate of photosensitizer for photodynamic cancer therapy.

Following the deprotection of acetal groups, water-soluble star-shaped poly(galactose) conjugated *ZnPc* was achieved. NMR and IR analysis confirmed the successful deprotection by appearance the hydroxyl groups on the sugar moieties. Moreover, DMF-PolarGel GPC analysis represented *ZnPc* chromophore and narrow PDI remained throughout. The *ZnPc*-P(Galactose) conjugation was non-aggregated in DMF with fluorescence emission at λ_{em} = 695 nm via excitation at λ_{ex} = 610 nm. However, the significantly reduced and broad absorption in aqueous solution suggested that dimerisation occurs, and no fluorescence was observed.

5.5 Experimental

Reagents and Conditions

Copper wire (diameter = 1.25 mm) was activated by washing in 35% hydrochloric acid for 15 min, and exhaustively rinsed with MilliQ water and dried under nitrogen. All the other reagents and solvents were obtained at the highest purity available from Sigma-Aldrich and used without further purification unless otherwise stated. All reactions were carried out using standard Schlenk techniques under an inert atmosphere of nitrogen, unless otherwise stated. TLC performed using pre-coated silica gel 60 F254 and developed in the solvent system indicated. Compounds were visualized by use of UV light (254 or 302 nm) or a basic solution (10 % w/w K_2CO_3 in water) of $KMnO_4$. Merck 60 (230 - 400 mesh) silica gel was used for column chromatography.

Instrumentals and analysis

Gel Permeation Chromatography (GPC) Analysis

GPC analysis was performed based on solubility of the polymer or conjugated and on the available detectors of each system.

Dimethylformamide

GPC was performed on a Varian 390-LC MDS system equipped with a PL-AS RT/MT autosampler, a PL-gel 3 μm (50 x 7.5 mm) guard column, two PL-gel 5 μm (300 x 7.5 mm) mixed-D columns using DMF with 5 mM NH_3BF_4 at 50 ^oC as the eluent at a flow rate of 1.0 mL min^{-1}. The GPC system was equipped with ultraviolet and differential refractive index detectors. Narrow molecular weight PMMA standards (between 200 and 467,400 g mol^{-1}) were used to calibrate the SEC and data fitted with a 3rd order polynomial.

Tetrahydrofuran

GPC was performed on a Varian 390-LC MDS system equipped with a PL-AS RT/MT autosampler, a PL-gel 3 μm (50 x 7.5 mm) guard column, two PL-gel 5 μm

(300 x 7.5 mm) mixed-D columns equipped with a differential refractive index and Shimadzu SPD-M20A diode array detectors, using THF with 2% TEA as the eluent with a flow rate of 1.0 mL min^{-1}. Narrow molecular weight standards of both poly(MMA) (between 200 and 467,400 g mol^{-1}) and polystyrene (between 162 and 24,600 g mol^{-1}) were used to calibrate the SEC and data fitted with a 3rd order polynomial.

MALDI-ToF-MS Analysis

MALDI-ToF data was collected using a Bruker Ultraflex II MALDI-ToF spectrometer, equipped with a nitrogen laser delivering 2 ns laser pulses at 337 nm with positive ion ToF detection performed using an accelerating voltage of 25 kV. Samples were prepared by mixing α-cyano-4-hydroxycinnamic acid (CHCA) (20 μL of a 2 mg L^{-1} solution), sodium iodide (20 μL of a 1 mg L^{-1} solution), and the analyte solution (20 μL of a 2 mg L^{-1} solution), and then the resulting solution was spotted onto a ground steel MALDI plate and solvent removed prior to inserting into the vacuum chamber of the MALDI instrument.

Fourier Transform Infra-Red (FTIR) spectrometry

Infrared absorption spectra were recorder on a Bruker VECTOR-22 FTIR spectrometer using a Golden Gate diamond attenuated total reflection (ATR) cell.

UV-Vis Spectroscopy

All UV-Vis absorption spectra were measured on a Perkin Elmer Lambda-35 UV/VIS spectrometer using 1 cm path length quartz cuvettes.

1,2:3,4-Di-*O*-isopropylidene-6-*O*-acryloyl-a-d-galactopyranose[41]

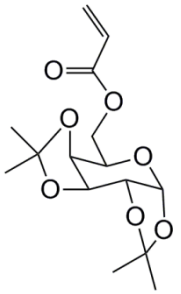

To a solution of 1,2:3,4-di-*O*-isopropylidene-α-D-galactopyranose (3.2 g, 12.3 mmol, 1 equiv.) in dichloromethane (50 mL), triethylamine (5.14 ml, 36.9 mmol, 3 equiv.) and acryloyl chloride (1.5 ml, 18.4 mmol, 1.5 equiv.) were added at 0 ^{o}C stirring for 30 min. The mixture was stirred overnight at ambient temperature. The resulting solution was then diluted with 50 mL DCM, washed with saturated $NaHCO_3$ (3 x 100 mL) and water (3 x 100 mL), and dried with anhydrous $MgSO_4$. After filtration and concentration, the crude product was obtained as syrup which was purified by flash column chromatography (SiO_2, petroleum ether/ethyl acetate = 9/2 v/v). (Yield: 65%)

IR (neat): ν = 2989, 2928, 1725, 1633 cm^{-1}.

^{1}H NMR (400.03 MHz, $CDCl_3$, 298 K): δ 6.42 (dd, 1H, J= 17.3, 1.5 Hz), 6.15 (dd, 1H, J= 17.3 10.5 Hz), 5.82 (dd, 1H, J= 10.3, 1.5), 5.53 (d, 1H, H-1, J= 5 Hz),4.61 (dd, 1H, H-3, J= 8, 2.5 Hz), 4.37 (m, 1H, H-6'), 4.32 (dd, 1H, H-2, J= 5, 2.5 Hz), 4.25 (m, 2H, H-4 and H-6''), 4.06 (ddd, 1H, H-5, J= 7.4, 5, 1.9), 1.5 (s, 3H), 1.44 (s, 3H), 1.32 (d, 6H, J= 5.3 Hz); ^{13}C NMR (100.59 MHz, $CDCl_3$, 298 K): δ 173.48, 131.04, 128.16, 109.63, 108.76, 96.26 (C-1), 71.04 (C-3), 70.66 (C-4), 70.43 (C-2), 65.98 (C-5), 63.48 (C-6), 25.95, 25.92, 24.92, 24.45

ESI-MS m/z: calcd for $C_{15}H_{22}O_7$ 337.13 $[M+Na]^+$, observed 337.1

Poly(1,2:3,4-Di-*O*-isopropylidene-6-*O*-acryloyl-a-d-galactopyranose) by SET-LRP

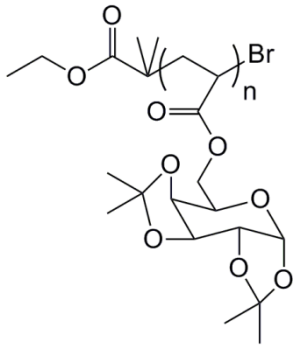

1,2:3,4-Di-*O*-isopropylidene-6-*O*-acryloyl-a-d-galactopyranose (0.786 g, 2.5 mmol, 5 equiv.), DMSO (5 mL), EBiB (73.3 µL, 0.5 mmol, 1 equiv.), Me_6-TREN (16 µL, 0.06 mmol, 0.12 equiv.), $CuBr_2$ (5.6 mg, 0.025 mmol, 0.05 equiv.) and a magnetic stir bar were charged to a Schlenk fitted with a rubber septum and the mixture was degassed by purging nitrogen for 30 min. Copper wire (3 cm) was activated by immersing in conc. HCl for 15 min, thoroughly rinsed with water and acetone then dried. The pre-activated copper wire was carefully added in to the degassed mixture under a nitrogen blanket. The Schlenk tube was then resealed and polymerised at ambient temperature overnight to achieve full conversion. The reaction mixture was diluted with acetone and passed over an aluminium oxide column to remove metal salts. After concentration, the crude product was dialysis against water for two days using MWCO 1000 Da membrane, and the precipitate was lyophilised to yield white powder (Yield: 97%).

IR (neat): ν = 2983, 2928, 1733, 1454 cm^{-1}.

^{1}H NMR (400.03 MHz, $CDCl_3$, 298 K): δ 5.5 (br, H-1), 4.6 (br, H-3), 4.29 (br, H-2, H-6', H-6'', H-4), 4.03 (br, H-5), 2.42-2.03 (br, polymer backbone), 1.5, 1.43, 1.32, 1.3 (s, acetal protons); ^{13}C NMR (100.59 MHz, $CDCl_3$, 298 K): δ 174.38, 109.35, 108.61, 96.16, 70.65, 65.61, 63.47, 41.00, 25.95, 24.96, 24.43

M_n (GPC, THF) = 2000 g mol^{-1}; PDI = 1.12

Azido-poly-(1,2:3,4-Di-*O*-isopropylidene-6-*O*-acryloyl-a-d-galactopyranose)

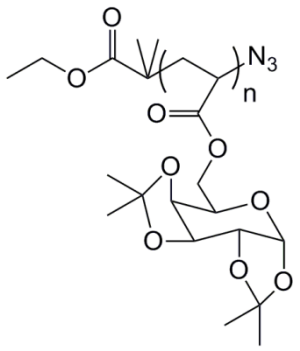

Protected galactose polymer (0.625 g, 0.3 mmol, 1 equiv.), and NaN_3 (0.195, 3 mmol, 10 equiv.) were stirring in 10 mL anhydrous DMF at 65 ^oC overnight. After cooling to ambient temperature, 50 mL DCM was added to the mixture, and washed with brine (3 x 100 mL) and water (3 x 100 mL). The organic layer was dried with anhydrous $MgSO_4$. After filtration and concentration, the yellow oil was dialysis against water for two days using MWCO 1000 Da membrane, the precipitate was lyophilised to yield light yellow powder (Yield: 90%).

IR (neat): ν = 2983, 2109, 1733, 1454 cm^{-1}.

^1H NMR (400.03 MHz, $CDCl_3$, 298 K): δ 5.5 (br, H-1), 4.6 (br, H-3), 4.29 (br, H-2, H-6', H-6'', H-4), 4.03 (br, H-5), 2.42-1.70 (br, polymer backbone), 1.5, 1.43, 1.32, 1.3 (s, acetal protons) ; ^{13}C NMR (100.59 MHz, $CDCl_3$, 298 K): δ 174.11, 109.38, 108.61, 96.16, 70.66, 65.73, 63.47, 41.20, 25.93, 24.92, 24.41

M_n (GPC, THF) = 1600 g mol^{-1}; PDI = 1.13

Star-shaped *ZnPc*-P(pGalactose) by CuAAC click chemistry

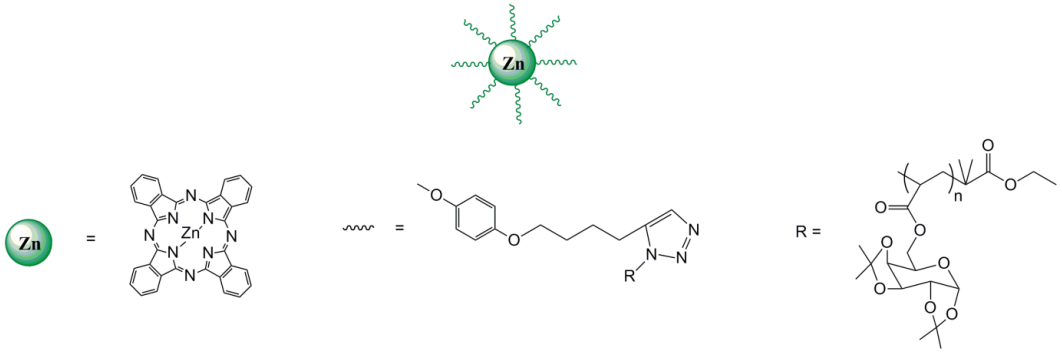

ZnPc-alkyne (0.025 g, 12 µmol, 1 equiv.), N_3-O(pGalactose) (0.192, 96 µmol, 8 equiv.) and PMDETA (26 µL, 0.125 mmol, 10.4 equiv.) were charged in a Schlenk tube with 8 mL of anhydrous THF. The Schlenk tube solution was subjected to 3 freeze-pump-thaw cycles and then cannulated under N_2 into a second Schlenk tube, previously evacuated and filled with N_2, containing CuBr (13.8 mg, 96 µmol, 8 equiv.). The reaction was carried out at ambient temperature for 3 days. The reaction mixture was diluted with THF and passed through a short aluminium oxide column to remove copper salt. After concentration, the crude product was precipitated in 500 mL petroleum ether to yield green powder (Yield: 70%).

IR (neat): ν = 2983, 1733, 1502 cm^{-1}.

^{1}H NMR (400.03 MHz, $CDCl_3$ + pyridine-d_5, 298 K):δ 7.12 (br, protons on aromatic ring), 6.95(br, protons on aromatic ring), 5.49 (br, H-1), 4.58 (br, H-3), 4.26-4.03 (br, H-2, H-6', H-6'', H-4, H-5), 2.42-1.70 (br, polymer backbone), 1.49-1.3 (br, acetal protons) ; ^{13}C NMR (100.59 MHz, $CDCl_3$ + pyridine-d_5, 298 K): δ 174.11, 109.36, 108.61, 96.11, 70.66, 65.53, 63.45, 40.95, 25.94, 24.95, 24.40

M_n (GPC, DMF) = 9900 g mol^{-1}; PDI = 1.03

Deprotection of *ZnPc*-P(pGalactose)

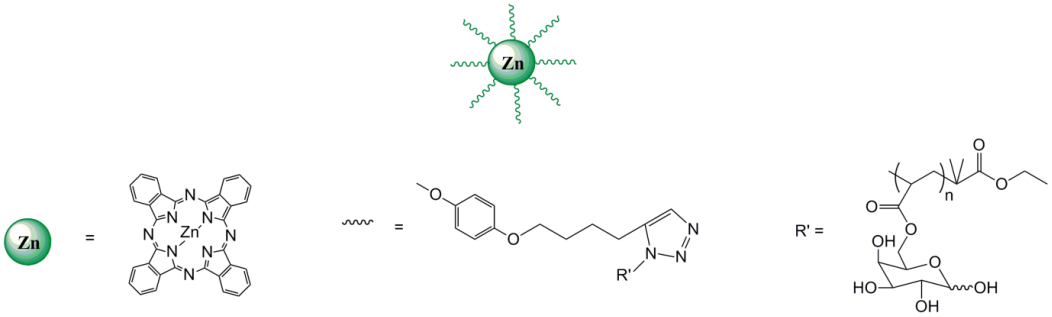

ZnPc-P(pGalactose) (0.11 g, 6.1 μmol) was dissolved in a 9:1 (v/v) mixture of trifluoroacetic acid and water (11 mL) for 4 h at ambient temperature. The acid was removed under reduced pressure, and the crude product was dissolved back to water. The solution was dialysis against water for two days, and lyophilised to yield green powder (Yield: 85%).

IR (neat): ν = 3371 (OH, br), 2922, 1727 cm^{-1}.

^{1}H NMR (400.03 MHz, DMSO-d_6 + pyridine-d_5, 298 K): δ 8.89 (br, 8H), 7.98 (br, 8H), 7.27-7.08 (br, 32H), 6.57 (br, anomeric -OH_α), 6.17 (br, anomeric -OH_β), 4.98-3.27 (m, carbohydrate protons), 2.28-1.58 (m, protons on polymer backbone), 1.16-1.04 (m, CH_3 on initiator); ^{13}C NMR (100.59 MHz, DMSO-d_6 + pyridine-d_5, 298 K): δ 175.34, 102.24, 97.83, 95.84, 93.13, 89.71, 82.91, 82.06, 77.72, 76.41, 73.49, 72.31, 69.44, 68.94, 67.93, 64.39, 28.96, 25.54.

M_n (GPC, DMF) = 10,900 g mol^{-1}; PDI = 1.11

5.6 References

1. P. Maillard, S. Gaspard, J. L. Guerquin-Kern and M. Momenteau, *Journal of the American Chemical Society*, 1989, **111**, 9125-9127.
2. C.-F. Choi, J.-D. Huang, P.-C. Lo, W.-P. Fong and D. K. P. Ng, *Organic & Biomolecular Chemistry*, 2008, **6**, 2173-2181.
3. Z. Iqbal, M. Hanack and T. Ziegler, *Tetrahedron Letters*, 2009, **50**, 873-875.
4. A. O. Ribeiro, J. P. C. Tomé, M. G. P. M. S. Neves, A. C. Tomé, J. A. S. Cavaleiro, Y. Iamamoto and T. Torres, *Tetrahedron Letters*, 2006, **47**, 9177-9180.
5. A. R. M. Soares, J. P. C. Tomé, M. G. P. M. S. Neves, A. C. Tomé, J. A. S. Cavaleiro and T. Torres, *Carbohydrate Research*, 2009, **344**, 507-510.
6. X. Alvarez-Mico, M. J. F. Calvete, M. Hanack and T. Ziegler, *Tetrahedron Letters*, 2006, **47**, 3283-3286.
7. X. Álvarez-Micó, M. J. F. Calvete, M. Hanack and T. Ziegler, *Carbohydrate Research*, 2007, **342**, 440-447.
8. X. Álvarez-Micó, M. J. F. Calvete, M. Hanack and T. Ziegler, *Synthesis*, 2007, **2007**, 2186-2192.
9. A. O. Ribeiro, J. P. C. Tomé, M. G. P. M. S. Neves, A. C. Tomé, J. A. S. Cavaleiro, O. A. Serra and T. Torres, *Tetrahedron Letters*, 2006, **47**, 6129-6132.
10. P.-C. Lo, C. M. H. Chan, J.-Y. Liu, W.-P. Fong and D. K. P. Ng, *Journal of Medicinal Chemistry*, 2007, **50**, 2100-2107.
11. P.-C. Lo, S. C. H. Leung, E. Y. M. Chan, W.-P. Fong, W.-H. Ko and D. K. P. Ng, *Photodiagnosis and Photodynamic Therapy*, 2007, **4**, 117-123.
12. P.-C. Lo, W.-P. Fong and D. K. P. Ng, *ChemMedChem*, 2008, **3**, 1110-1117.
13. R. E. Airley and A. Mobasheri, *Chemotherapy*, 2007, **53**, 233-256.
14. J.-Y. Liu, P.-C. Lo, W.-P. Fong and D. K. P. Ng, *Organic & Biomolecular Chemistry*, 2009, **7**, 1583-1591.
15. J.-Y. Liu, X.-J. Jiang, W.-P. Fong and D. K. P. Ng, *Organic & Biomolecular Chemistry*, 2008, **6**, 4560-4566.
16. J.-Y. Liu, P.-C. Lo, X.-J. Jiang, W.-P. Fong and D. K. P. Ng, *Dalton Transactions*, 2009, **0**, 4129-4135.

17. J. J. Lundquist and E. J. Toone, *Chemical Reviews*, 2002, **102**, 555-578.
18. B. Voit and D. Appelhans, *Macromolecular Chemistry and Physics*, 2010, **211**, 727-735.
19. V. Ladmiral, E. Melia and D. M. Haddleton, *European Polymer Journal*, 2004, **40**, 431-449.
20. S. R. S. Ting, G. Chen and M. H. Stenzel, *Polymer Chemistry*, 2010, **1**, 1392-1412.
21. C. R. Becer, *Macromolecular Rapid Communications*, 2012, **33**, 742-752.
22. L. L. Kiessling and J. C. Grim, *Chemical Society Reviews*, 2013, **42**, 4476-4491.
23. S. Slavin, J. Burns, D. M. Haddleton and C. R. Becer, *European Polymer Journal*, 2011, **47**, 435-446.
24. V. Ladmiral, G. Mantovani, G. J. Clarkson, S. Cauet, J. L. Irwin and D. M. Haddleton, *Journal of the American Chemical Society*, 2006, **128**, 4823-4830.
25. J. Geng, G. Mantovani, L. Tao, J. Nicolas, G. Chen, R. Wallis, D. A. Mitchell, B. R. G. Johnson, S. D. Evans and D. M. Haddleton, *Journal of the American Chemical Society*, 2007, **129**, 15156-15163.
26. Q. Zhang, J. Collins, A. Anastasaki, R. Wallis, D. A. Mitchell, C. R. Becer and D. M. Haddleton, *Angewandte Chemie*, 2013, **125**, 4531-4535.
27. T. Tanaka, H. Nagai, M. Noguchi, A. Kobayashi and S.-i. Shoda, *Chemical Communications*, 2009, **0**, 3378-3379.
28. N. Vinson, Y. Gou, C. R. Becer, D. M. Haddleton and M. I. Gibson, *Polymer Chemistry*, 2011, **2**, 107-113.
29. J. Geng, J. Lindqvist, G. Mantovani and D. M. Haddleton, *Angewandte Chemie*, 2008, **120**, 4248-4251.
30. H. G. Börner, *Macromolecular Rapid Communications*, 2011, **32**, 115-126.
31. J.-F. Lutz, *Polymer Chemistry*, 2010, **1**, 55-62.
32. L. Hartmann and H. G. Börner, *Advanced Materials*, 2009, **21**, 3425-3431.
33. D. Schaffert, N. Badgujar and E. Wagner, *Organic Letters*, 2011, **13**, 1586-1589.
34. D. Ponader, F. Wojcik, F. Beceren-Braun, J. Dernedde and L. Hartmann, *Biomacromolecules*, 2012, **13**, 1845-1852.
35. A. H. Soeriyadi, C. Boyer, F. Nyström, P. B. Zetterlund and M. R. Whittaker, *Journal of the American Chemical Society*, 2011, **133**, 11128-11131.

36. A. Anastasaki, C. Waldron, P. Wilson, R. McHale and D. M. Haddleton, *Polymer Chemistry*, 2013, **4**, 2672-2675.

37. K. Matyjaszewski, Y. Nakagawa and S. G. Gaynor, *Macromolecular Rapid Communications*, 1997, **18**, 1057-1066.

38. J. Raynaud, C. Absalon, Y. Gnanou and D. Taton, *Journal of the American Chemical Society*, 2009, **131**, 3201-3209.

39. Y. Li, J. N. Hoskins, S. G. Sreerama and S. M. Grayson, *Macromolecules*, 2010, **43**, 6225-6228.

40. B. Spengler, D. Kirsch, R. Kaufmann and R. J. Cotter, *Rapid Communications in Mass Spectrometry*, 1991, **5**, 198-202.

41. S. C. Abeylath and E. Turos, *Carbohydrate Polymers*, 2007, **70**, 32-37.

Appendix

Teeth Whitening Evaluation

In vitro teeth whitening studies were investigated by using water-soluble PEGylated *(Cu)Pcs* synthesised via a combination of Mitsunobu reaction and CuAAC click reaction in chapter 2. Human extracted anterior teeth obtained for research purposes were mounted in acrylic resin blocks. The enamel surfaces were cleaned with a prophylaxis paste to remove any extrinsic stain, following by placing in human whole saliva for 2 h to allow an *in vitro* salivary pellicle forming. The teeth were rinsed with a small amount of water, and the original colour of the teeth was measured by a colorimeter in the CIELAB mode which provides representation for the perception of colour stimuli, defined as a three-dimensional colour space by the Commission International De l'Echairage (CIE) in 1976. The three axes are L*, a*, and b*, where L* represents a measure of the lightness of the object and a* and b* represent the colour on the red (+) – green (-) and yellow (+) – blue (-) axes respectively.[1] Five separate measurements were taken on the surface of each teeth, and the mean value, b*(o), was calculated.

Five PEGylated *(Cu)Pcs* solutions ($mPEG_{350}$-*Pc*, $mPEG_{550}$-*Pc*, $mPEG_{750}$-*Pc*, $mPEG_{750}$-*CuPc*, and $mPEG_{2000}$-*CuPc*) were prepared at a concentration of 0.005% (w/w) in deionised water. The teeth were dipped in an appropriate aqueous solution for 1 minute and the colour of the teeth after treatment was remeasured as described above; therefore, the mean value, b*(t), was calculated. The yellow-blue shift (Δb*) in tooth colour is important for perceptual tooth whitening and can be calculated as $\Delta b^* = b^*(t) - b^*(o)$.

In this study, the colour changes of a total number of ten teeth were measured, and the bar chart (**Figure S.1**) shows the differences of the tristimulus values (ΔL*, Δa*, and Δb*) for each treatment. It can be found that the yellowness of the teeth was significantly reduced after treated with $mPEG_{750}$-*CuPc* aqueous solution compared to the other four treatments, and the green hue and darkness of the teeth were also

severely enhanced. Therefore, the effects of other phthalocyanines containing polymer solutions synthesised in this thesis need to be investigated, and the problem of increasing the green hue and darkness of the teeth using phthalocyanines need to be overcome in the future.

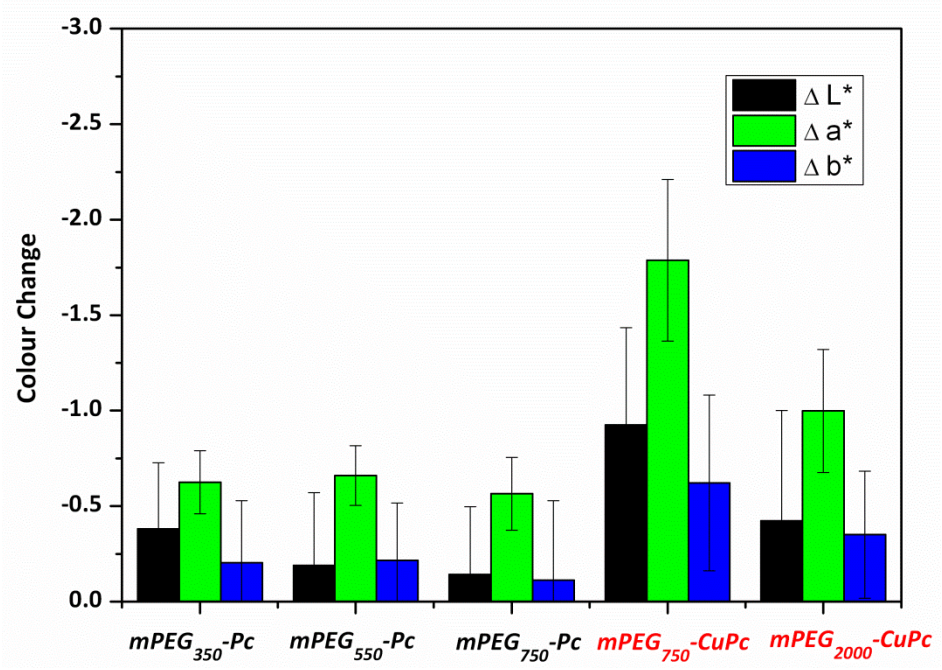

Figure S.1 Colour shifts of the teeth after treated with each PEGylated *(Cu)Pcs* aqueous solutions (0.005%, w/w)

References

1. A. Joiner, *Journal of Dentistry*, 2004, **32**, 3-12.